GLUCOSE AND FRUCTOSE METABOLISM AND TRANSPORT DURING PIG PREGNANCY

A Dissertation

by

AVERY CHRISTINE KRAMER

Submitted to the Graduate and Professional School of
Texas A&M University
in partial fulfillment of the requirements for the degree of

DOCTOR OF PHILOSOPHY

Chair of Committee,	Gregory A. Johnson
Committee Members,	Fuller W. Bazer
	Robert C. Burghardt
	Guoyao Wu
Head of Department,	Todd O'Hara

December 2021

Major Subject: Biomedical Sciences

ABSTRACT

The swine industry experiences high rates of embryonic/fetal loss and there is considerable variation of birthweight between piglets within a litter. These outcomes negatively impact the swine industry's overall efficiency and profitably. It is hypothesized that insufficient placental development and endometrial support during pregnancy are direct causes of the high rates of embryonic/fetal loss within this industry. This study examined how glucose and fructose are transported and metabolized at the uterine placental interface to support growth and development of the placenta and embryo/fetus.

Conceptuses from day 16 of pregnancy were incubated with either ^{14}C-glucose or ^{14}C-frucose and amounts of radiolabeled CO_2 released from the conceptuses were measured to determine the oxidation rates of glucose and fructose. Glucose and fructose were both actively metabolized by the conceptuses, with glucose being metabolized to a greater extend then fructose in that in the presence of glucose and fructose, glucose was preferentially metabolized over fructose. Endometrial and placental expression for the glucose transporters *SLC2A1*, *SLC2A2*, *SLC2A3*, and *SLC2A4* were determined. *SLC2A1* mRNA and protein was the most abundant glucose transporter in the endometrium and expressed in the uterine luminal epithelium (LE) of pregnant gilts compared to cyclic gilts. *SLC2A4* mRNA was also expressed in the uterine LE of pregnant gilts. On day 15 of pregnancy, the conceptus trophectoderm weakly expressed *SLC2A2* mRNA, while *SLC2A3* mRNA was abundant in the trophectoderm/chorion throughout pregnancy.

Proliferating and migrating cells switch metabolism from oxidative phosphorylation to aerobic glycolysis to enhance the production of glycolytic intermediates for utilization of the branching pathways of glycolysis. One of the branching pathways of glycolysis is the Pentose Phosphate Pathway (PPP). Lactate concentrations with in the uterine lumen increase from day 13 to 15 and 17 of pregnancy. Conceptus trophectoderm cells express the enzyme G6PDH mRNA and protein, with highest levels of mRNA and protein on days 13 and 15 of pregnancy, respectively, G6PDH protein then decreases sharply on day 16 of pregnancy. Carbons derived from glucose, but not fructose entered into the PPP with maximum levels of utilization on day 15 of pregnancy. These results establish the molecular components for hexose sugar transport from the maternal vasculature and into conceptus tissues, glucose and fructose can be directly metabolized by conceptus trophectoderm cells, and conceptus trophectoderm cells metabolize glucose via the pentose phosphate pathway.

ACKNOWLEDGEMENTS

I would like to thank my committee chair, Dr. Greg Johnson, for his guidance, mentorship, and support throughout the course of this research. I would also like to thank my committee members, Drs. Fuller Bazer, Robert Burghardt, and Guoyao Wu, for sharing their knowledge and continued guidance in helping me develop in to a scientist throughout my doctoral program.

I would also like to thank my family and friends who have provided continual encouragement and support throughout the many years of school.

CONTRIBUTORS AND FUNDING SOURCES

All work conducted for this dissertation was supported by Drs. Gregory A. Johnson, Fuller W. Bazer, Robert C. Burghardt, and Guoyao Wu.

This work was also supported by fellow members of the laboratory, Dr. Heewon Seo and Bryan McLendon.

Funding Source

This work was also made possible in part by the National Research Initiative Competitive Grants from the USDA National Institute of Food and Agriculture under Grant Number 2018-67015-28093 and 2020-67015-31136. Its contents are solely the responsibility of the authors and do not necessarily represent the official vies of the USDA.

TABLE OF CONTENTS

Page

LIST OF FIGURES

Page

LIST OF TABLES

Page

CHAPTER I

INTRODUCTION

Embryonic/fetal mortality is a major cause of economic loss within the swine industry. Sows will typically ovulate between 20 and 30 oocytes, but only 9 to 15 piglets will be delivered at term. This is a result of embryonic and/or fetal losses during two main time points during pregnancy. The first major period of pregnancy loss occurs during the peri-implantation period around Days 14-25 and the second is later in pregnancy around Days 50-70. During both of these periods of pregnancy the placenta is undergoing major growth and development requiring an abundance of nutrients to support the growing conceptuses (embryos and associated placental membranes) and the extensive folding of the uterine-placental interface, respectively. In order to support this rapid growth and development, the uterus secretes histotroph (a combination of nutrients such as sugars, amino acids, hormones, and enzymes) into the uterine lumen for utilization by the conceptus. The hexose sugars glucose and fructose are known to increase within the uterine lumen during the peri-implantation period (Zavy et al., 1982).

During the peri-implantation period, the elongating conceptus trophectoderm cells are undergoing hypertrophy and proliferation in order for elongation to occur, and alterations in early embryonic/placental development are most noticeable during this time (Geisert et al., 1982a). If there is insufficient elongation of the conceptus trophectoderm, placental development will be directly affected leading to potentially detrimental alterations of the uterine/placental interface (Vallet and Freking, 2007). These alterations

can be linked to intrauterine growth restriction (IUGR) creating large variation in the birthweights of piglets from a single litter (Widdowson, 1971). The low birthweight piglets are usually one-half to one-third the size of their largest littermates and the decreased bodyweight has been correlated with a reduction in the survival and growth of the IUGR piglets, resulting in increased costs to producers (Ritacco et al., 1997; Tilley et al., 2007). There is evidence showing that alterations of the maternal diet can improve fetal survivability and result in more uniform birthweights in the litter. It is important to further our understanding of nutrient transport and metabolism in the conceptus trophectoderm and uterine endometrium of pregnant pigs to further improve placental development and birth weight of piglets (De Vos et al., 2014; Wu et al., 2013).

The hexose sugars, glucose and fructose, are abundant within the porcine endometrium and conceptus (embryo/fetus and associated placental membranes), with fructose being the most abundant of the two. Glucose and fructose are detected in the uterine flushings of pregnant gilts as early as day 12 of pregnancy and fructose is also found in greater quantities than glucose in the allantoic fluid and fetal blood (Aherne et al., 1969; Zavy et al., 1982). Glucose is the main energy source used by the placenta and fetus, while fructose plays a more minor role in energy metabolism. It was previously thought that fructose was unable to be metabolized, but it has been determined that glucose and fructose are able to enter and be utilized by metabolic pathways in similar ways (Scott et al., 1967). However, the pig placenta oxidizes fructose at 20% the rate of glucose, suggesting that glucose is the primary energy source of the pig placenta (Pere, 1995; Randall, 1977). Fructose can be used as a substrate for a number of metabolic pathways

supporting conceptus development and growth; including biosynthesis of nucleic acids, glycosaminoglycans, and phospholipids (White et al., 1982). More recent *in vitro* studies have observed that porcine trophectoderm cells are able to utilize fructose via the hexosamine biosynthetic pathway for synthesis of hyaluronic acid and stimulate mechanistic target of rapamycin (mTOR) cell signaling (Kim et al., 2012).

The long-term goal of this research is to determine the roles of glucose and fructose in placental and fetal development in pigs, and determine how they influence fetal survival and birth weight. The short-term goal of the research described in this dissertation were to: 1) localize hexose sugar transporters endometria and placentae; 2) determine the metabolism of glucose and fructose by the conceptus trophectoderm; and 3) determine the utilization of glucose and fructose by the pentose phosphate pathway for production of ribose-5-phosphate for use in nucleotide synthesis.

Our hypothesis was that glucose and fructose are transported from the maternal vasculature, secreted into the uterine lumen, and transported into the conceptus trophectoderm. During the peri-implantation period when the conceptus trophectoderm cells are free floating, dependent on nutrients from the endometrium, and undergoing elongation, the conceptuses are within a hypoxic environment. This hypoxic environment causes a metabolic switch from oxidative phosphorylation to glycolytic metabolism providing biosynthetic intermediates for the synthesis of ribose, amino acids, nucleotides, and fatty acids for conceptus growth.

CHAPTER II

LITERATURE REVIEW

Uterine and Placental Histoarchitectures

During embryo development, the uterine wall differentiates from the Mullerian ducts into two distinct compartments, the myometrium and endometrium (Mossman, 1974). The myometrium is composed of two layers of smooth muscle cells making up the inner circular and outer longitudinal layers, with vasculature throughout. In contrast, the endometrium is an epitheliomesenchymal organ. The endometrium is composed of the luminal epithelium (LE), glandular epithelium (GE), and the stroma. The LE is a simple columnar epithelium that lines the uterine cavity or lumen and is supported by a basement membrane that is adjacent to the underlying stroma. Projecting down from the LE and into the stroma is the GE. The GE lines long, branched, and coiled tubular glands, which form a lumen that empty secretions into the uterine lumen and eventually into areolae (Cooke et al., 1997). Areolae are pockets of chorionic epithelium (CE) that form cavities over the mouths of the endometrial glands for the uptake of histotroph and contain specialized microvasculature (Friess et al., 1981). Deep to the chorion is the allantoic stroma in both the areolar and inter-areolar areas. The allantoic stroma contains fibroblasts and cells of the vasculature and deep to the allantoic stroma is the allantoic epithelium, lining the allantoic sac.

Following apposition, on Days 13 to 15 of pregnancy, the chorioallantois closest to the openings of the uterine glands begins to reach over the openings and develop

cavities, or areolae. The appearance of the areolae begins as small white discs, but grows quickly to cover the mouths of the glands between Days 18 and 30 of pregnancy (Friess et al., 1981). The uterine glands secrete histotroph, which contains a variety of macromolecules, specifically sugars; amino acids, hormones, and transcription factors, to support the growth and development of the conceptus throughout pregnancy. The epithelial cells composing the areolae are tall columnar cells. Histotroph fills the areolae and is transported across the placenta, and into the placental circulation, by fluid phase pinocytosis (Renegar et al., 1982; Song et al., 2010).

Estrous Cycle

The estrous cycle in pigs is approximately 21 days, ranging between days 18 to 24. Pigs are a polytocous species and spontaneous ovulators, ovulating 15-30 oocytes in one estrous period (Soede et al., 2011). Estrus, or standing heat, is the beginning of the cycle which lasts 40 to 60 hours and ovulation occurs about 40 hours after the onset of estrus. At the beginning of the estrous cycle, estrogen levels are high and progesterone levels are low. Following rupture of the oocytes, there is extensive reorganization and reformation of ovarian tissues ultimately forming fully functional corpus lutea (CL) and increasing the circulating levels of progesterone with peak concentrations by Days 8 to 9 after ovulation. This increase in progesterone primes the uterus to prepare for pregnancy. However, if pregnancy is not established, prostaglandin F_{2a} (PGF) is released in a pulsatile manner from the uterine luminal epithelium as a result of pituitary oxytocin binding to the oxytocin receptor in the LE on days 15 and 16 of the estrous cycle. PGF released by the LE travels

through the uterine-ovarian vein to the ovary causing structural and functional regression of the CL, thereby decreasing progesterone levels (Spencer et al., 2004). As a result of the decreased levels of progesterone, progesterone no longer has inhibitory effects over estrogens actions which allows for ovulation to occur again, with peak levels of estrogen about two days before ovulation (Soede et al., 2011).

Pregnancy

In pigs, mating occurs during estrus and ovulation occurs approximately 40 hours after the onset of estrus. Twenty-four hours after fertilization the 1-cell fertilized ovum is cleaved to form a 2-cell embryo and remains in the oviduct for 48 to 56 hours post fertilization and enters the uterus at the 4- to 8-cell stage. The embryo reaches the blastocyst stage by day 5, which is an important stage of embryonic development because the pluripotent blastomeres begin to differentiate into the inner cell mass (ICM) and trophectoderm. This differentiation of the two cell lines eventually results in development of the embryo/fetus proper and the placental chorion. However, the blastocysts must "hatch" from the zona pellucida before development can occur. The blastocysts (0.5 to 1 mm spheres) hatch from the zona pellucida on days 6 to 7, increasing in size by day 10 (2-6 mm) before undergoing a rapid morphological transition called elongation. The rapid process of elongation from a spherical to a filamentous form occurs between days 10 and 12 of pregnancy. These blastocysts transition from large spherical (10 to 15 mm) to then tubular (15 mm by 50 mm) and finally to filamentous (1 mm by 100-200 mm) forms by day 11 of pregnancy. As the spherical blastocysts elongate into a tubular shape, the

trophoblast cells and endoderm cells migrate toward the ICM creating a dense band of cells called the elongation zone. Following formation of the elongation zone, the conceptus continues to elongate, elongating from 100 to 200 mm to 800 to 1,000 mm in length by day 16 of pregnancy (Geisert et al., 1982b; Mattson et al., 1990). This phase of growth is due to hyperplasia and proliferation of the cells when each conceptus has increased its total surface area to maximize the area of contact between the trophectoderm and the uterine LE, which will provide greater nutrient exchange and ensure that estrogens secreted by the conceptus inhibit luteolysis.

Once the blastocyst hatches from the zona pellucida, gastrulation, or formation of the three germ layers begins. Gastrulation is an important process of development and is responsible for the beginning of organogenesis, as well as directionality of the developing embryo. In porcine embryos, gastrulation and elongation occur simultaneously (Oestrup et al., 2009). First, the blastocyst differentiates into the hypoblast, or the primitive endoderm, and the epiblast. Together, these are known as the bilaminar disc. The bilaminar disc determines the dorsal/ventral axis because the primitive endoderm is ventral to the blastocyst cavity and directly against the trophectoderm, while the epiblast is dorsal to the blastocyst cavity (Muhr and Ackerman, 2021). By day 9 of pregnancy, Rauber's layer or the trophectoderm cells covering the embryonic disc gradually degrades, exposing the epiblast to the uterine environment and forming the embryonic disc (Oestrup et al., 2009). The embryonic disc then differentiates into the three germ cell layers known as the endoderm, mesoderm, and ectoderm. The mesoderm and endoderm begin to form by day 11 of pregnancy, and the remaining epiblast cells differentiate into neural and

ectoderm cells (Tam et al., 1993). The definitive endoderm replaces the epiblast cells with the underlying hypoblast, while the mesodermal cells act as an intermediate mesenchymal cell layer and arrange themselves between the endoderm and ectoderm (Oestrup et al., 2009). Fusion of the extra-embryonic mesoderm with the primitive endoderm, ectoderm, and trophectoderm results in formation of the yolk sac, amnion, and chorion, respectively (Blomberg et al., 2008; Oestrup et al., 2009; Perry, 1981).

Maternal Recognition of Pregnancy

In the pig, the conceptus trophectoderm secretes estrogen, which has been proposed to be the pregnancy recognition signal in pigs (Bazer and Thatcher, 1977). On days 11 and 12 of pregnancy the porcine conceptus secretes estrogens, which redirect prostaglandin F2-alpha (PGF) secretion by the uterine endometrium away from the uterine vasculature and into the uterine lumen where it is sequestered and/or metabolized, thereby preventing luteolysis. Whereas in a normal estrous cycle, without the influence of conceptus secreted estrogen, PGF would be secreted into the uterine vasculature resulting in luteolysis of the CL. Maintenance of the CL is essential because it is responsible for the production of progesterone, which is also known as the hormone of pregnancy. Progesterone regulates uterine functions required for conceptus development, implantation, placentation, and maintenance of pregnancy. The theory of estrogen-induced maternal recognition of pregnancy in pigs has been based on these observations. Recently, however, this theory of maternal recognition has been challenged. Meyer et al., (2019) targeted the aromatase (CYP19A1) gene utilizing CRISPR/Cas9 genome editing

technology ablating conceptus derived estrogen, estrogen was observed to be nonessential for pre-implanting conceptus development, conceptus elongation, or early CL maintenance. Estrogen was, however, essential for maintenance of pregnancy past day 30, when ablation of estrogen appeared to disrupt a number of biological pathways (Meyer et al., 2019). These studies suggest that conceptus synthesized estrogen alone may not be the only signal involved in maternal recognition of pregnancy in pigs.

Progesterone and Estrogen Receptors in the Endometrium

Estrogen derived from the conceptus trophectoderm and progesterone from the CL mediate their effects on the endometrium though their respective steroid receptors. Expression of these receptors are spatially and temporally regulated throughout the estrous cycle and early pregnancy. This allows for controlled regulation of downstream targets to prepare the endometrium for another cycle or for the maintenance of a successful pregnancy. On day 5 of the estrous cycle the progesterone receptor (PGR) protein is localized to the uterine LE, GE, stromal cells, and myometrium, and expression is maintained through day 11 (Geisert et al., 1994; Steinhauser et al., 2017a). The PGR are no longer present in the LE or the superficial GE after Day 11, but remain in the deep glands, stroma, and myometrium through day 17 of the estrous cycle. The PGR protein is localized to the uterine LE, GE, stroma, and myometrium on day 9 of pregnancy. This expression is maintained in the GE, stroma, and myometrium through day 17 of pregnancy. The deep GE have stronger immunostaining than the superficial GE, while there is no expression of PGR protein within the LE between days 11 and 17 of pregnancy.

By day 25 of pregnancy PGR protein is expressed by the stromal cells and myometrium, and is only present in the GE near the areolae. Expression of the PGR protein by the stromal cells and myometrium remains the same from day 25 to 40 of pregnancy, but the expression of PGR protein in the GE decreases during this period and continues to decrease throughout day 85 of gestation (Steinhauser et al., 2017a).

The estrogen receptor (ESR1) protein is expressed in the uterine LE and GE on days 0 to 12 of the estrous cycle and pregnancy, and expression decreases in the LE and GE between days 5 and 10 of gestation. The ESR1 protein then increases between days 12 and 15 of pregnancy (Geisert et al., 1993). Expression of ER protein is highest in the stroma on day 0, but decreases by day 5, and either remains low throughout pregnancy or increases by day 18 of the estrous cycle. The deep GE continue to express ER protein through day 71 of pregnancy and ER are observed in the myometrium between days 10 and 32 of pregnancy (Knapczyk-Stwora et al., 2011).

Implantation

Implantation is a complex process and only occurs if there is developmental synchrony between the receptive uterus and the conceptus (Burghardt et al., 2002). If there is synchrony between the receptive uterus and the developing conceptus an implantation cascade begins. The phases of the implantation cascade are defined as: (1) shedding of the zona pellucida; (2) elongation of the conceptus trophectoderm; (3) pre-contact and orientation of the conceptus trophectoderm to the uterine LE; (4) apposition of the trophectoderm to the LE; (5) adhesion of the apical surface of the trophectoderm to the

apical surface of the uterine LE; and (6) development of interdigitating microvilli between the trophectoderm and LE (Bazer and Johnson, 2014; Johnson et al., 2009). In the pig, the implantation cascade is different from humans or rodents because porcine conceptuses are non-invasive and instead there is a prolonged pre-attachment period where the conceptus undergoes orientation, apposition, and adhesion. This prolonged pre-attachment period is considered part of the peri-implantation period of pregnancy. During the peri-implantation period, the conceptus trophectoderm and the uterine LE become adhesion competent to initiate the adhesion cascade initiating the window of receptivity. The window of receptivity is coordinated with the actions of progesterone and estrogen to locally produce growth factors, cell surface glycoproteins, cytokines, cell surface adhesion molecules, and extracellular matrix (ECM) proteins (Johnson et al., 2009). Progesterone is important for initiating the adhesion cascade, because it down-regulates the expression of the progesterone receptor in the LE of pigs after day 10 of pregnancy, just before the uterine endometrium becomes receptive for implantation (Geisert et al., 1994; Steinhauser et al., 2017a). Down regulation of the progesterone receptor corresponds with the progesterone-induced down regulation of anti-adhesive mucin 1 (MUC1) in the glycocalyx of the uterine LE (Bowen et al., 1996). MUC1 sterically inhibits the attachment of the conceptus trophectoderm and removal of MUC1 exposes low affinity carbohydrate ligand binding molecules like selectins and galectins, which potentially aid in attachment of the conceptus to the uterine LE. Therefore, the loss of MUC1 is required for the implantation process to begin. The smaller carbohydrate molecules initially provide low stability contact and then are replaced by a more stable and extensive collection of adhesive interactions between

integrins and extracellular matrix (ECM) proteins that are then maintained throughout pregnancy (Burghardt et al., 1997; Burghardt et al., 2002; Lessey, 2002). Integrins are transmembrane glycoprotein receptors that are composed of α and β subunits that are non-covalently bound and are involved in many cell adhesion cascades (Albelda and Buck, 1990; Giancotti and Ruoslahti, 1999; Kling et al., 1992). In the pig, the apical surface of the LE express integrins capable of binding to Arg-Gly-ASP (RGD) and non RGD amino acid sequence-containing ECM molecules, which can then link to other potential integrin receptors on the apical surface of the conceptus trophectoderm for more stable attachment (Johnson et al., 2014). One of the leading candidate molecules for attachment of the conceptus trophectoderm to the LE is secreted phosphoprotein 1 [SPP1, also known as osteopontin (OPN)] along with its integrin receptors to induce stable adhesion, cytoskeletal reorganization, and transduce signals though a multitude of signaling intermediates (Bazer et al., 2012; Burghardt et al., 2009). SPP1 is a ligand for integrin receptors and interacts with the αvβ1, αvβ3, αvβ5, and α4β1 integrin receptors (Johnson et al., 2014). On day 13 of pregnancy, conceptus secreted estrogen induces the expression of SPP1 in discrete regions of the uterine LE next to the implanting conceptus trophectoderm. By day 20 of pregnancy, SPP1 is expressed in the entire uterine LE when firm adhesion of the LE and conceptus trophectoderm occurs, and SPP1 remains high through the remainder of pregnancy (Garlow et al., 2002; White et al., 2005). *In vitro*, SPP1 binding to its integrin receptors has been observed to promote attachment of uterine LE cells to trophectoderm cells, and stimulate trophectoderm migration (Erikson et al., 2009). In addition, *in vivo* studies have observed large immunoreactive aggregates of

integrin αv (ITGVA) at the uterine-placental interface at day 20 of pregnancy, suggesting that integrins are forming aggerates in response to SPP1 binding to form focal adhesions important for cell attachment during implantation (Erikson et al., 2009).

Placentation

Pigs have a diffuse, epitheliochorial type placenta. This type of placentation is characterized by a superficial, non-invasive placentation where there is simple apposition of the endometrial and chorionic epithelia and the uterine LE remains intact (Edwards et al.,1955). Epitheliochorial type placentas are less intimate than other types of placentation because the uterine LE and chorionic epithelium remain intact (Amoroso, 1955). As a result, there is a significant barrier for the transfer of nutrients from the maternal uterine vasculature to the placental vasculature. Therefore, nutrients in the uterine vasculature must pass through the maternal endothelium, uterine stroma, uterine LE, chorionic epithelium, allantoic epithelium, and the endothelium of the allantois in order to reach the developing fetus.

Following apposition, on days 13 to 15 of pregnancy the chorioallantois closest to the openings of the uterine glands will begin to reach over the openings and develop a dome shaped structure, or areola. The appearance of the areolae begins as small white discs, but grows quickly to cover the mouths of the glands by day 18 to 30 of pregnancy (Friess et al., 1981). The uterine glands secrete histotroph, which contains a variety of macromolecules, particularly proteins, to support the growth and development of the conceptus throughout pregnancy. The epithelial cells composing the areolae are tall

columnar cells. Histotroph fills the areola and is transported across the placental and into the fetal circulation, by fluid phase pinocytosis (Renegar et al., 1982; Song et al., 2010).

As the conceptuses are undergoing elongation, they are also migrating along the uterine horn in order to establish their own segment of uterine endometrium for implantation/placentation. The conceptus trophectoderm stretches outwards along the uterine horn until it contacts another conceptus, so that there is minimal overlap between conceptus tissues. The portions of trophectoderm that contact one another become necrotic. By day 24 of pregnancy, attachment between the uterine LE and the trophectoderm is completed. By day 25 of pregnancy, the two adhered endometrial and placental tissues begin to fold to increase the surface area for nutrient transport, and as pregnancy progresses, the folding becomes more extensive (Friess et al., 1980; Seo et al., 2020b; Vallet and Freking, 2007). While the conceptuses are migrating and attaching to the uterine LE, they are primarily supported by histotroph, while later on in pregnancy is supported by histotroph and hemotroph, which is the transport of nutrients from the maternal blood to the placental blood that occurs in the non-areolar regions. As fold formation increases, the placental and uterine capillaries directly underneath the epithelia become closer together, decreasing the distance between the maternal and placental blood vessels to maximize hemotrophic support (Dantzer, 1985; Friess et al., 1980; Seo et al., 2020b). The distance between the two adherent epithelia and the capillaries can be reduced to as little as 2 microns (Friess et al., 1980). The capillaries from the maternal and fetal vasculature are positioned so that cross-countercurrent exchange of nutrients can occur across the two adherent sides of the epithelia. Meaning, if the fetal side of the placenta is

considered “up” the maternal blood will enter at the tops of the placental folds and exit at the bottom of the folds. The maternal side will then be considered “down” and the placental blood will enter at the bottoms of the folds and exit at the top of the folds (Leiser and Dantzer, 1988). The arrangement of this cross-countercurrent exchange allows for maximized nutrient transport across the uterine-placental interface.

Between days 18 to 30 of pregnancy the chorion and allantois rapidly expand and fuse together between days 30 to 60 of pregnancy. During this period, the placenta grows exponentially up until day 70 of pregnancy, when placental development is complete (Knight et al., 1977). While the placenta is completely developed, angiogenesis of the placental will continue until parturition, when in the last 40 days of pregnancy there is exponential growth of the fetus (Knight et al., 1977; Ullrey et al., 1965).

Fetal Growth

The fetal organs first begin to develop on days 15 to 30 of pregnancy from the three germ layers known as the endoderm, mesoderm, and ectoderm. Throughout development, the organs expand in weight and size, however this timing is organ dependent. For example, the lungs and spleen increase exponentially in weight from days 51 to 93, while the heart, brain, and liver expand in weight from days 51 to 114 (Ullrey et al., 1965). Fetal bones begin to calcify around day 30 of pregnancy. Interestingly, if fetuses are not viable prior to day 30 of pregnancy, before bone calcification, they will be reabsorbed by the uterus. However, if this occurs past day 30, the fetus will become a mummified stillborn. During the last third of pregnancy, total fetal weight increases

significantly requiring an increase of nutrient transport across the placenta (McPherson et al., 2004; Ullrey et al., 1965).

Allantoic and Amniotic Fluid

The allantoic cavity develops as an evagination from the hindgut which is an absorptive epithelium, specifically the endoderm and mesoderm, and expands rapidly between days 18 to 30 of pregnancy (Steven, 1975). Between days 30 and 60 of pregnancy the chorion and allantois fuse (Knight et al., 1977). The allantoic cavity was initially suggested to serve as a reservoir for fetal excretion, however this is not the case (Bremer, 1916; Davies, 1952). The allantoic fluid is of maternal origin and comes from water transported into the allantoic cavity by the surrounding allantoic epithelium. This fluid is a hypotonic solution composed of sugars, proteins, electrolytes, and water serving as a nutrient reservoir for the developing fetuses (Wu et al., 1995). Transport of these nutrients across the allantoic epithelium is an active process and is especially important for pigs because they have a true epitheliochorial placenta. Allantoic fluid volume and composition changes throughout pregnancy to serve several purposes. First, the allantoic fluid volume expands the chorioallantoic membranes aiding conceptus apposition with the uterine endometrium. The allantoic fluid volume then decreases until day 45, then again increases until day 58, and then decreases until parturition (Goldstein et al., 1980; Knight et al., 1977; Wislocki and Dempsey, 1946). Total amounts of glucose and fructose increase in the allantoic fluid as volumes increase, suggesting that these sugars may be sodium dependent as is the transport of water into the allantoic cavity.

The amnion is a fluid-filled sac directly surrounding the embryo/fetus. Similar to the allantoic fluid, amniotic fluid changes throughout gestation to meet the needs of the developing fetus. In addition, the amniotic fluid provides an aquatic environment allowing the fetus to develop symmetrically without pressure points that would lead to abnormal development (Patten, 1948). Suspension in the amnion also protects the developing fetus in the case of trauma or mechanical injury to the maternal abdomen. The amniotic fluid is also a source of nutrients for the fetus, containing proteins, electrolytes, and sugars that the fetus will drink up (Bazer et al., 2012).

Glucose and Fructose in Pregnancy

Glucose and fructose increase in the uterine lumen of pigs during pregnancy (Zavy et al., 1982). However, in general, fructose is found in higher concentrations in the fetal blood and fetal fluids in species with epitheliochorial or synepitheliochorial placentae when compared to glucose concentrations (Cole and Hitchcock, 1946; Huggett et al., 1951; Shelley, 1960; Shelley and Dawes, 1962). This is likely due to the fact that epitheliochorial placentas have little to no glycogen and have limited gluconeogenesis in the placenta and embryos/fetuses of these species (Bacon and Bell, 1948; Fowden et al., 1997). Total recoverable glucose increases from day 12 to days 16 and 18 of pregnancy, and the enzyme glucose phosphate isomerase (GPI) that converts glucose-6-phosphate into fructose-6-phosphate is present in the endometrial tissues of pigs (Zavy et al., 1982). Therefore, glucose can directly serve as an energy source for the developing conceptus. In the sheep, it has been observed that intravenous administration of glucose stimulates a

rapid increase in glucose followed by a delayed increase of fructose in the fetal blood. When glucose was injected into the umbilical vein of the fetus glucose levels increased in the maternal blood and hyperfructosemia occurred in the fetus, indicating that glucose is able to go from the conceptus vasculature and into the maternal blood, but fructose derived from glucose is unable to be transported to the maternal blood. Therefore, the placenta is likely responsible for the conversion of glucose to fructose. Fructose is also continuously produced by the placenta regardless of the glucose concentration in the maternal and fetal blood (Alexander et al., 1955; Battaglia and Meschia, 1981). These results have also been confirmed in the pig placenta, where researchers utilized radiolabeled glucose and demonstrated the conversion of glucose into fructose (White et al., 1979b; White et al., 1982). Interestingly, results showed that while glucose could be converted into fructose, fructose could not be converted into glucose.

The role of fructose has been largely ignored by those who investigate the metabolism of hexose sugars due to a number of studies indicating that fructose is not metabolized via glycolysis or the TCA cycle (Abrams, 1979; Battaglia and Meschia, 1981; Bell and Ehrhardt, 2002; Meznarich et al., 1987). However, in the fetal pig fructose can be utilized for the synthesis of nucleic acids and the generation of reducing agents, such as NADPH H+ (White et al., 1982). Fructose and glucose are similar when entering metabolic pathways to be used for synthesis of phospholipids and neutral lipids in the brain, liver, kidney, heart, and adipose tissue of fetal lambs (Scott et al., 1967) . These studies provide evidence that fructose can be metabolized, counter to previous findings. Aherne et al. determined that fructose is the main hexose sugar in the amniotic fluid and

allantoic fluid, however fructose decreases in the allantoic fluid as glucose increases between days 82 and 112 of gestation (Aherne et al., 1969). Interestingly, fructose is rapidly cleared from piglets 24 hours postpartum, suggesting that neonatal pigs are unable to utilize fructose as an energy source. If piglets are not given glucose within 30 hours they will not survive, indicating piglets have a limited ability to metabolize fructose via glycolysis to produce pyruvate (Goodwin, 1956; Steele et al., 1971).

Recent studies with porcine trophectoderm cells have determined that fructose is actively involved in stimulating cell proliferation and mRNA translation through activation of mechanistic target of rapamycin (MTOR) signaling (Wang et al. 2015a and 2015b). Furthermore, fructose can be metabolized by the hexosamine biosynthetic pathway and is responsible for the synthesis of glycosaminoglycans, specifically hyaluronic acid (Kim et al., 2012). Fructose has been shown to be similar or more stimulatory than glucose at stimulating cell proliferation (Gingras et al., 2004). However, glucose in human trophoblast cells can also stimulate proliferation through MTOR signaling (Wen et al., 2005). There is evidence that, in addition to glucose, fructose is able to be utilized for nucleotide synthesis, via the pentose phosphate pathway (PPP). The PPP is responsible for the generation of reducing equivalents, such as NADPH, to be used to reduce biosynthetic reactions within a cell and produce ribose-5-phosphate for use in nucleotides. White et al., (1982) determined that fetal pigs are able to utilize fructose for the synthesis of nucleic acids and reducing equivalents (White et al., 1982). The pig placenta is able to oxidize fructose at roughly 20% the rate of glucose, suggesting that glucose may be the main source for metabolic energy (Pere, 1995; Randall, 1977). Lactate

is also present in the plasma of fetal pigs and in the umbilical vein and artery, with concentrations of lactate higher in the umbilical vein compared to the umbilical artery. The high lactate concentrations indicate that lactate is likely produced from glucose and fructose due to aerobic metabolism (Pere, 1995).

Hexose Sugar Transport

Sugars are one of the most important organic compounds utilized by cells and serve five main purposes in most organisms: 1) they are sources of carbon skeletons; 2) they support signal transduction; 3) they support molecule transport; 4) they are drivers of osmotic processes; and 5) they are sequestered for transient energy storage (Chen et al., 2015). Sugars can be taken up from the environment, or can be synthesized within specialized cells. Regardless of how the sugars are acquired, there must be transport mechanisms in place to transport hydrophilic molecules across a hydrophobic membrane. The study of sugar transport across the cell membrane began with Cori's studies on the absorption of sugar in the intestines. These studies provided the first evidence for catalyzed transport, showing that different sugars are absorbed at different rates, displaying that the transporters could become saturated, and that there is competition between glucose and galactose (Cori, 1925, 1926). Years following this discovery, Sistroma (1958) observed that sugars could be transported against a concentration gradient and this discovery led investigators to study how active transport is energetically achieved (Sistrom, 1958). To address this question, Crane proposed the sodium/glucose transporter hypothesis where the sodium concentration gradient is an important driving factor. This

gradient is maintained by sodium/potassium pumps, providing the first evidence for an active transport mechanism for sugars (Crane, 1965). In 1965, Fox and Kennedy purified the first plasma membrane protein that facilitates transport, M (membrane) protein, a component of the β-galactoside transport system in *Esherichia coli* (Fox and Kennedy, 1965). Later, in 1970, a proton co-transporter mechanism for eukaryotic cells was discovered (Komor and Tanner, 1971). Collectively, these findings are the foundation to our understanding of sugar transport across plasma membranes.

In order for hexose sugars to be transported across a plasma membrane, there must be a transporter protein present. Transport of the hexose sugars occurs by one of three mechanisms. The first mechanism is through the use of a sugar concentration gradient, which is facilitated by members of the facilitated diffusion symporters or GLUT family (gene name: solute carrier family 2A; *SLC2A*) integral membrane proteins (Bell et al., 1993). The second mechanism functions as a sodium/glucose symporter, coupling glucose with sodium for transport that depends on the sodium potassium ATPase pump to maintain a sodium gradient to drive glucose transport into the cell. This is facilitated by membranes of the sodium-glucose transport family (SGLT; gene name *SLC5A*). Lastly, there are the SWEETs (Sugars Will Eventually be Exported Transporters) (Feng and Frommer, 2015). The mechanism for this SWEETs not been fully defined, as these transporters are a relatively new discovery, but they may function as uniporters (Chen et al., 2015).

The mammalian facilitative glucose transporter (GLUT) family of proteins is a member of the Major Facilitator Superfamily (MFS) of transport proteins, also called the uniporter-symporter-antiporter family (Baldwin, 1993; Griffith et al., 1992; Henderson,

1969). The MFS superfamily of proteins can be characterized by having a single polypeptide that can transport small molecules and this is an energy independent process (Pao et al., 1998). The GLUT family consists of 14 members (GLUT1-12, H+/myo-inositol transporter [HMIT], GLUT14; SLC2A1-14). All 14 members are composed of ~500 amino acids and have a homologous 12-transmembrane domain structure which creates a pore within the plasma membrane (Bell et al., 1993). Even though the GLUT family members all have similar structures the kinetic characteristics, specificity of substrates, regulation, and cell or tissue localization all vary greatly. The GLUT family can be further subdivided into three classes based on their structural similarities. Class I GLUTs are considered the traditional GLUTs and consist of GLUT1-4 and GLUT14; Class II consists of the fructose transporters GLUT 5, 7, 9, and 11; Class III comprises GLUT 6, 8, 10, 12, and HMIT1. The subdivision of these GLUTs is based on the similarities of their protein sequences and not based on their transport capabilities (Heimberg et al., 1995). One similarity of all these GLUTs, not including HMIT1, is they all have the capacity to transport either glucose, or fructose, or both sugars (Thorens and Mueckler, 2010).

The sodium-glucose transporter family (SGLT; gene name *SLC5A*) belongs to the large sodium-solute symporter family and is responsible for active sodium-coupled uptake of glucose, as well as being involved in glucose sensing (Cura and Carruthers, 2012). The SGLTs serve as high-affinity transporters and are able to transport glucose against a concentration gradient. This family consists of 12 members that transport sugars, iodine, myo-inositol, choline, and short-chain fatty acids. All members of the SGLTs contain 580-

718 amino acids coding for 60-80 kDa proteins and contain a 14 transmembrane alpha helical domain (Quick et al., 2003; Wright et al., 2011). Overall, the mechanism whereby the different sodium symporters transport glucose are the same, but the specific mechanisms vary. SGLT1 couples the transport of one glucose molecule with two sodium molecules, whereas SGLT2 couples one glucose molecule with one sodium molecule. Differences in the mechanisms between the different SGLTs may explain the differences observed in rates of transport.

Little is currently known about the recently discovered SWEETs and only one SWEET gene has been identified in animals and humans, while plants have approximately 20 (Deng and Yan, 2015). The SWEETs are the smallest of the glucose transporters and have a seven transmembrane domain (Feng and Frommer, 2015). In mammals, SWEETs mediate glucose transport and have a broad expression pattern, suggesting that the role of these transporters is important in animal and human physiology. However, our understanding of the mechanism of action of these transporters is limited. Based on the limited knowledge we have, the SWEET transporters are able to mediate both cellular uptake and efflux, and they have an extracellular N terminus, and a long cytosolic C-terminus that has multiple phosphorylation sites (Tao et al., 2015). The SWEETs have a relatively low affinity, but high capacity, for sugars and it is hypothesized that these transporters are specialized for high turnover rates, instead of efficiently moving low amounts of sugars (Chen et al., 2015).

Glucose Transporters

SLC2A1/GLUT1

GLUT1 is a 492 amino acid protein and was the first glucose transporter to be isolated and cloned, making it one of the most well studied of the GLUT family (Mueckler and Thorens, 2013). GLUT1 is responsible for basal levels of glucose uptake into cells and transports glucose with a Km = 3 mM. In addition to transporting glucose, GLUT1 can transport glucosamine, galactose, and mannose.

GLUT1 was first observed in human erythrocytes and since its discovery it has been observed throughout the body in many species and it is upregulated in many cancers (Nishimura and Naito, 2005). In humans, *SLC2A1* mRNA is most highly expressed in the placenta, compared to any other tissue. GLUT1 is expressed in both the apical and basal membranes of endothelial cells, cytotrophoblasts, and syncytiotrophoblasts (Jansson et al., 1993; Korgun et al., 2005). GLUT1 is also observed in the oocytes of mice and cattle through the blastocyst stage, specifically in the inner cell mass and the trophectoderm cells. Homozygous knockout of *SLC2A1* is embryonic lethal in mice (Aghayan et al., 1992; Augustin et al., 2001). GLUT1 protein is expressed in the LE, stroma, and decidua of the endometria of mice and rats (Frolova et al., 2009; Korgun et al., 2005).

One of the most predominant glucose transporter protein isoforms found in the sheep placenta is GLUT1, while GLUT3 is the other. *SLC2A1* mRNA and protein increase with gestational age (Currie et al., 1997). *SLC2A1* mRNA is abundant in the LE and GE of the endometrium during early pregnancy and SLC2A1 protein follows a similar pattern, but is also expressed in the trophectoderm and embryonic endoderm. Progesterone

upregulates *SLC2A1* mRNA. In sheep, interferon tau enhances the effects of progesterone to upregulate *SLC2A1* mRNA and protein in the uterine LE and superficial GE (Gao et al., 2009b).

SLC2A2/GLUT2

GLUT2 was first characterized in the livers of humans and rats (James et al., 1988; Kayano et al., 1988). GLUT2 has a low affinity for glucose, with a Km ~17mM. In addition to transporting glucose, it can also transport fructose, mannose, glucosamine, and galactose across the basolateral and/or apical surface of cells. Across species, GLUT2 protein is mainly located in the epithelial cells of the proximal tubules, pancreatic β-cells, enterocytes, and hepatocytes. The human placenta and uterus do not express *SLC2A2* mRNA, however it is highly expressed in the liver, kidneys, and small intestine (Nishimura and Naito, 2005; von Wolff et al., 2003). GLUT2 is expressed in mouse and cow trophectoderm cells (Aghayan et al., 1992; Augustin et al., 2001; Frolova and Moley, 2011b).

SLC2A3/GLUT3

The *SLC2A3* gene encoding GLUT3 was first identified in human fetal skeletal muscle cells and shares ~64% sequence identity to *SLC2A1* (Kayano et al., 1988). GLUT3 has a higher affinity, or lower Km value of 1.5 mM, and a higher transport rate for glucose then other Class I glucose proteins (Manolescu et al., 2007). This may be due to the fact that GLUT3 is the primary mediator for glucose uptake in neurons and is expressed in

cells that require rapid transport and high amounts of glucose (Leino et al., 1997). GLUT3 is also expressed in other cell types, such as mouse sperm flagellum (Urner and Sakkas, 1999) and preimplantation mouse embryos (Pantaleon et al., 1997). In addition, homozygous knockouts of *SLC2A3* are embryonic lethal at the neurulation stage, while heterozygous knockouts survive but are growth restricted later in gestation (Ganguly et al., 2007). The human placenta has been reported to have low to non-detectable expression of *SLC2A3* mRNA during late pregnancy, while during early pregnancy GLUT3 is expressed at higher levels within the extravillous trophoblast cells during invasion prior to direct contact with maternal blood (Brown et al., 2011; Hahn et al., 2001; Jansson et al., 1993). In sheep, the conceptus trophectoderm and embryonic endoderm express *SLC2A3* mRNA during early pregnancy; however, expression in later pregnancy has not been studied (Gao et al., 2009b).

SLC2A4/GLUT4

GLUT4 was first identified in rat adipocytes (James et al., 1988). Glut4 is most predominantly expressed in adipocytes, cardiomyocytes, and skeletal muscle, but is found in some other tissues including the uterus and placenta (Nishimura and Naito, 2005; Thorens and Mueckler, 2010). GLUT4 is often called the insulin-receptor glucose transporter because under basal insulin conditions GLUT4 primarily resides in intracellular membrane compartments. In response to an increase in blood glucose and circulating insulin, GLUT4 is translocated from the intracellular compartment to the plasma membrane where it can actively transport glucose (Huang and Czech, 2007).

Expression of *SLC2A4* mRNA is low in the endometrium of humans, mice, and rats when comparing expression levels to other GLUTs (Frolova and Moley, 2011c; Korgun et al., 2001). In sheep, *SLC2A4* mRNA is expressed at low levels in most cell types of the endometrium, while SLC2A4 protein is expressed in the uterine LE, GE, and trophectoderm. *SLC2A4* is not regulated by progesterone, while interferon tau appears to have suppressive effects on *SLC2A4* mRNA during early pregnancy (Gao et al., 2009b).

SLC2A5/GLUT5

GLUT5 was first identified in the human small intestine (Kayano et al., 1990). GLUT5 has a high specificity for fructose (Km = 6mM), transporting only fructose across the apical membrane of the small intestine (Douard and Ferraris, 2008). *SLC2A5* mRNA is expressed in the small intestines, bone marrow, kidneys, and testes of humans (Nishimura and Naito, 2005; von Wolff et al., 2003). Some species, such as mice, cattle, humans, and pigs, have high expression of *SLC2A5* in their sperm (Angulo et al., 1998; Burant et al., 1992; Sancho et al., 2007). During pregnancy, endometrial expression of *SLC2A5* is higher on days 11 to 13 compared to cyclic gilts, and increases in the endometrium between days 25 and 28 of pregnancy. The placenta also expresses *SLC2A5* mRNA and maintains this expression from days 30 to 85 of pregnancy. Administration of exogenous progesterone increased expression of *SLC2A5* in the uterine LE and GE (Steinhauser et al., 2017a).

SLC2A8/GLUT8

GLUT8 has a high affinity for glucose (Km ~2 mM) and can transport fructose and galactose. GLUT 8 is mainly expressed in the testis, muscle, adipose tissue, liver, placenta, and brain (Ibberson et al., 2000; Nishimura and Naito, 2005). In some cells, GLUT8 is only expressed in intracellular compartments, however, GLUT8 also has an N-terminal dileucine motif that is involved in mediating endocytosis from the plasma membrane (Ibberson et al., 2000; Lisinski et al., 2001). This transporter is also thought to be localized in endosomes, lysosomes, and endoplasmic reticulum (Augustin et al., 2005; DeBosch et al., 2014; Ibberson et al., 2000). The ovarian hormones, estrogen and progesterone, have been shown to upregulate *SLC2A8* expression in the brain (Harrell et al., 2014). In the mouse, GLUT8 protein localizes to the endometrium during implantation and decidualization of the uterine stroma, localizing to both the apical and basolateral surfaces of the LE and GE (Kim and Moley, 2009). In pigs, SLC2A8 protein is first detected on day 13 and expression is maintained through day 30 of pregnancy, when expression transitions from the LE to the tall columnar cells at the top of the folds of the chorion by day 50 of gestation. Expression of SLC2A8 is present at day13 of pregnancy and decreases in the uterine GE from day 20 to 25, and was detectable at only low levels through day 85 of pregnancy. The conceptus trophectoderm cells also expressed SLC2A8 on day 15 of pregnancy. Administration of exogenous progesterone also increased expression of SLC2A8 in the endometrium, while exogenous estrogen decreased overall expression of SLC2A8 (Steinhauser et al., 2016).

Overview of Metabolism

Metabolism is a complex network of biochemical reactions that take place during a cell's life and are essential for survival. These reactions include both the synthesis and degradation of complex macromolecules, as well as in energy production. Cells maintaining cellular homeostasis are metabolically distinct from cells undergoing proliferation and differentiation. Proliferating cells alter their metabolic activity to maintain adequate levels of energy stores to support survival and produce an abundance of biosynthetic intermediates to allow for cellular growth and proliferation. While these metabolic pathways are diverse in terms of their end products, these pathways are closely linked as a result of shared fuel inputs, for example glucose, as well as a dependence on the products from one pathway to feed into and support an alternative pathway as a precursor (Judge and Dodd, 2020; Mulukutla et al., 2016; O'Neill et al., 2016).

Glycolytic Metabolism in Hypoxia

Oxygen is an essential molecule for cell survival and drives the TCA cycle and oxidative phosphorylation for energy production, whereas hypoxia supports enhanced glycolysis. Hypoxia occurs when oxygen concentrations are lower than normal and is defined as less than 2% oxygen (Bertout et al., 2008). Hypoxia inducible factor 1 (HIF-1) is a transcriptional activator that regulates oxygen homeostasis (Semenza, 2001). Under hypoxic conditions, when oxidative phosphorylation is inhibited, low levels of ATP are produced decreasing the ATP/AMP ratio, thereby reducing the allosteric inhibition of ATP on the glycolytic enzyme phosphofructokinase (PFK) (Henderson, 1969). When activated,

PFK uses ATP to produce fructose-1,6-bisphosphate promoting flux through glycolysis. Under normoxic conditions, ATP inhibits pyruvate kinase when energy levels are high to reduce the rate of glycolysis; however, under hypoxic conditions, the decrease in energy levels reduces the inhibition of pyruvate kinase, increasing the generation of pyruvate, and therefore lactate. Fructose-1,6-bisphosphate also activates pyruvate kinase and is able to promote complete flux through glycolysis. While hypoxic conditions upregulate the glycolytic pathway, HIF transcription factors also stimulate upregulation of glycolytic enzymes and glucose transporters. This increases the availability of glucose for utilization by glycolysis, and upregulation of the glycolytic enzymes increases glucose flux through the pathway, thereby maintaining cellular energy levels. Once oxygen levels are restored to physiological levels, oxidative phosphorylation is typically restored in these cells (Bartrons and Caro, 2007). Tumor and immune cells are often in hypoxic environments and adapt to these metabolically restrictive microenvironments by enhancing glycolysis. Tumor cells are often poorly vascularized and outgrow their vascular supply due to rapid proliferation. It has also been shown that hypoxia promotes the invasiveness and metastasis of tumor cells (Harris, 2002). Immune cells develop in hypoxic environments and are recruited to sites of inflammation that often have limited oxygen availability (McNamee et al., 2013). In order for these cells to survive and perform their functions in environments with limited oxygen availability, these cells have adapted to utilizing enhanced glycolysis over oxidative phosphorylation (Bertout et al., 2008; Farina et al., 2020; Harris, 2002; Kierans and Taylor, 2021; McNamee et al., 2013).

Glycolysis

All cells require an energy source to maintain cellular homeostasis and maintenance. Cellular maintenance and homeostasis are energy consuming processes that are nonspontaneous; including protein turnover, DNA repair, basal transcription and translation, cytoskeletal dynamics, and vesicle trafficking. In addition to maintaining homeostasis, cells that are proliferating and/or migrating have additional energy demands for cellular division and growth. Therefore, proliferating and migrating cells have higher energy requirements and utilize these energy resources for the production of biosynthetic building blocks such as nucleotides, amino acids, and fatty acids. A main cellular energy and carbon source is glucose, which can be metabolized to pyruvate via glycolysis and oxidatively metabolized to CO2 in the tricarboxylic acid (TCA) cycle and oxidative phosphorylation to generate large amounts of adenosine triphosphate (ATP). The enzymes for the glycolytic pathway are located within the cytosomal fraction of cells. In 1924, Otto Warburg first observed that cancer cells utilize more glucose than normal control cells, and glucose is metabolized through glycolysis, resulting in high levels of lactate even in the presence of oxygen (Warburg, 1956; Warburg et al., 1927). This phenomenon is called aerobic glycolysis, where glucose is converted into lactate even in the presence of oxygen, which would otherwise support glucose catabolism via the TCA cycle and oxidative phosphorylation. Aerobic glycolysis is not exclusive to cancer cells, rapidly proliferating cells, such as immune cells, also utilize this mechanism. For example, it has been reported that human lymphocytes (Hedeskov, 1968), mouse lymphocytes (Wang et al., 1976), and rat thymocytes (Brand, 1985; Hume et al., 1978) increase uptake of glucose and lactate

excretion. In addition, non-transformed cells undergoing proliferation exhibit high rates of aerobic glycolysis, such as in the case of mouse fibroblasts where they increase their rate of glucose uptake and lactate production during the first part of logarithmic growth (Munyon and Merchant, 1959). Together, these studies suggest that aerobic glycolysis is utilized by actively proliferating cells.

Glycolysis is an inefficient way to generate ATP, generating only 2 ATP per glucose molecule via anaerobic glycolysis and 4 ATP per glucose molecule via aerobic glycolysis, when compared to complete oxidation of glucose via oxidative phosphorylation resulting in 36 ATP per glucose molecule. Although aerobic glycolysis is an inefficient way to produce ATP, it results in faster ATP production and is preferentially used in order to meet the high demands of proliferating and dividing cells (Pfeiffer et al., 2001). This is due to the fact that there are only ten reaction steps that take place during aerobic glycolysis, and cells are able to produce ATP and accumulate glycolytic intermediates more quickly compared to cells utilizing mitochondrial oxidative phosphorylation. While ATP produced via aerobic glycolysis is important for cellular function, aerobic glycolysis plays a more important role in proliferating cells in the utilization of nutrients for the production of biosynthetic precursors and to facilitate accumulation of cellular biomass. This is because generation of new daughter cells requires replication of all cellular contents. Glucose has the ability to provide all of the precursors required for production of these macromolecules. Therefore, the main role of glycolysis in proliferating cells is to maintain the production of glycolytic intermediates to support biosynthesis (Hume and Weidemann, 1979; Vander Heiden et al., 2010).

Glycolysis can be divided into three distinct phases (1) the energy investment phase or priming phase; (2) the splitting phase; and (3) the energy-generation phase. In the first phase, or the energy investment phase, glucose is phosphorylated to glucose-6-phosphate by hexokinase or glucokinase and this reaction is an irreversible reaction that is dependent on ATP and Mg^{2+}. The second phase is the splitting phase, where six carbon fructose 1,6-bisphosphate is split into two three-carbon compounds, glyceraldehyde-3-phosphate and dihydroxyacetone phosphate by the enzyme aldolase. The conversion of glyceraldehyde-3-phosphate to dihydroxyacetone phosphate is reversible and is catalyzed by the enzyme phosphotriose isomerase. Following this phase, one molecule of glucose is utilized to produce two molecules of glyceraldehyde 3-phosphate. Finally, there is the energy generation phase. This phase converts glyceraldehyde 3-phosphate to 1,3-bisphosphoglycerate by the enzyme glyceraldehyde 3-phosphate dehydrogenase and this step is important because it is involved in the formation of NADH2. When there is an active TCA cycle and oxidative phosphorylation, NADH goes through the electron transport chain where six ATPs are synthesized. In addition, 1,3-bisphosphoglycerate is considered a high-energy compound because the enzyme phosphoglycerate kinase will convert 1,3-bisphosphoglycerate to 3-phosphoglycerate, and during this conversion, ATP is also synthesized. Then 3-phosphoglycerate is converted to 2-phosphoglycerate, which is then reduced to phosphoenolpyruvate by the enzyme enolase. Finally, phosphoenolpyruvate is catalyzed by the enzyme pyruvate kinase to pyruvate and transfers the phosphate from phosphoenolpyruvate to ADP resulting in the formation of ATP (Akram, 2013).

The end product of glycolysis, pyruvate, has three major fates in mammalian cells: (1) conversion to lactate by lactate dehydrogenase (LDH); (2) conversion to alanine via alanine aminotransferase with the concomitant conversion of glutamine to alpha-ketoglutarate; or (3) conversion to acetyl-CoA within the mitochondria by the pyruvate dehydrogenase (PDH) complex to enter into the TCA cycle. In proliferating cells, the majority of the glucose is converted into lactate, and lactate production has been associated with anaerobic respiration in response to hypoxic environments leading to intracellular acidification. In stimulated human glioma cells, lactate production accounted for ~93% of glucose uptake (DeBerardinis et al., 2007). The generation of lactate plays an important role in glycolysis, where conversion of pyruvate to lactate by LDH leads to the regeneration of NAD+. Regeneration of NAD+ allows for glycolysis to be maintained through maintenance of the NAD+/NADH redox balance. This regeneration is required for continued flux through glycolysis because NAD+ is required for conversion of glyceraldehyde-3-phosphate to 1,3-bisphosphoglycerate, which allows glycolysis to proceed in the absence of ATP supplied from oxidative phosphorylation. NAD+ is also essential for nucleotide and amino acid biosynthesis, suggesting that lactate production may allow for greater glucose flux through glycolysis as well as greater incorporation into metabolites through efficient regeneration of NAD+.

In addition to directing pyruvate towards the production of lactate and the Krebs cycle, glycolytic flux is also diverted into the Pentose Phosphate Pathway (PPP), hexosamine biosynthetic pathway, glycerol phosphate and serineneogenesis/one carbon metabolism. The flux into these different pathways are dependent on the cellular and

biosynthetic needs of the cells, as the cells control the flux partly through allosteric regulation of key enzymes of glycolysis.

TCA Cycle

The TCA cycle is also known as the Krebs cycle, or the citric acid cycle, and is a major metabolic pathway used by non-proliferating cells that takes place within the mitochondrial matrix. This is because the TCA cycle and oxidative phosphorylation are efficient ways to generate ATP for cells whose primary requirements are energy and survival. The TCA cycle can receive a multitude of inputs, with the most noteworthy being glucose derived pyruvate or fatty acids derived from acetyl Coenzyme A (acetyl-CoA). Glutamine is also an important amino acid utilized by the TCA cycle and is directly converted into the TCA cycle intermediate alpha-ketoglutarate. Two major products produced by the TCA cycle are NADH and FADH2 that are able to transfer electrons to the electron transport chain, supporting oxidative phosphorylation for the production of ATP. This process provides cells with basal needs to maintain cellular homeostasis. The TCA cycle is also able to respond to growth signals by the cell diverting TCA cycle intermediates for the production of amino acids and lipids (O'Neill et al., 2016).

Pentose Phosphate Pathway

The Pentose Phosphate Pathway (PPP) is an important branching pathway of glycolysis which branches off after the first step of glycolysis, consuming the intermediate glucose-6-phosphate to generate fructose-6-phosphate and glyceraldehyde-3-phosphate

through the oxidative and nonoxidative branches of the PPP. The PPP is responsible for the production of NADPH and ribose-5-phosphate (R5P), and these two metabolites are essential for proliferation and survival of cells. NADPH is important for the synthesis of non-essential amino acids, fatty acids, sterols, and nucleotides (Patra and Hay, 2014; Wamelink et al., 2008). In addition, NADPH is a scavenger of reactive oxygen species, playing an important role in cellular antioxidant defense (Yen et al., 2020). R5P is a nucleotide building block involved in nucleotide synthesis.

The PPP has two branches: the oxidative branch and the non-oxidative branch which are both located within the cytosol of the cell. The oxidative branch has three irreversible reactions and generates NADPH and ribonucleotides. In the first reaction, glucose-6-phosphate is catalyzed to 6-phosphogluconolactone and yields NADPH by glucose 6-phosphate dehydrogenase (G6PDH). G6PDH is the rate-limiting enzyme of the oxidative PPP and determines the flux of glucose-6-phosphate into the pathway. 6-phosphogluconolactone is then hydrolyzed by phosphogluconolactonase (6PGL) to produce 6-phosphogluconate by the enzyme 6-phosphogluconate dehydrogenase (6PGD) yielding a second NADPH and ribulose-5-phosphate (Ru5P), which can then be converted to R5P. The non-oxidative branch consists of a series of reversible reactions that recruit additional glycolytic intermediates, such as fructose-6-phosphate and glyceraldehyde-3-phosphate. Interestingly, the oxidative branch of the PPP is the largest contributor of cytosolic NADPH (Eggleston and Krebs, 1974).

The enzymes of the PPP are able to allosterically regulate their own catalytic products and other metabolites (Eggleston and Krebs, 1974). In addition to this, the non-

oxidative branch is reversible, which allows the PPP to adapt to the metabolic needs of the cell. For example, in rapidly proliferating cells the majority of the pentose phosphates that are incorporated into DNA are derived from the PPP (Rais et al., 1999). Thus, the PPP is the pathway for generation of pentose phosphates from G6P in the oxidative branch and utilizing F6P and G3P in the non-oxidative branch (Boros et al., 1998a; Boros et al., 1998b). In cancer cells, it has also been observed that there is an increase in enzymatic activity, specifically G6PDH, which increases utilization of the oxidative branch increasing production of NADPH and R5P in proliferating cells (Kuehne et al., 2015; Patra and Hay, 2014; Riganti et al., 2012). In contrast, cells maintaining cellular homeostasis modify the PPP to increase the oxidative branch and direct the nonoxidative branch to resynthesizing F6P from pentose phosphate, which then replenishes G6P for use by the oxidative branch. Therefore, the PPP adapts to meet the cellular demands of the cells.

Glucose-6-Phosphate Dehydrogenase (G6PDH)

Glucose-6-Phosphate dehydrogenase (G6PDH) catalyzes the rate limiting step in the oxidative branch of the PPP, which brings G6P into the PPP. This first reaction generates the first molecule of NADPH, and, therefore, the expression and activity of G6PDH is tightly regulated by the cells. The G6PD gene encodes for a 514 amino acid protein subunit and forms a homodimer that is enzymatically active (Persico et al., 1986). In addition, the dimer can further dimerize forming a homotetramer that is also enzymatically active (Cohen and Rosemeyer, 1969). G6PDH can also exist as a monomer, but this is an inactive form. Each G6PDH subunit has one molecule of tightly bound

NADP, along with additional binding sites for NADP and G6P substrates (Au et al., 2000). Many normal metabolizing tissues express relatively high levels of G6PDH, including; the liver, mammary and adrenal glands, and adipose tissue (Hilf et al., 1975; Okano et al., 1965; Park et al., 2005; Rudack et al., 1971). There is also evidence that G6PDH expression is relatively high in tumor cells likely due to the regulation of this enzyme (Jonas et al., 1992). Regulation of G6PDH enzymatic activity is mainly modulated by the ratio of NADP+/NADPH, where NADPH negatively regulates G6PDH activity and NADP+ is required for G6PDH activity (Au et al., 2000). Due to this regulation, it makes sense that cancer cells that have high consumption rates of NADPH also have high expression of this G6PDH (Ayala et al., 1991).

Summary

The pig has a diffuse, epitheliochorial placenta type, which supports the growth and development of individual fetuses following conceptus elongation and implantation. The elongation process requires extensive remodeling of the blastocyst in order to transform from a spherical to a tubular, and finally a filamentous form. The later part elongation overlaps with the attachment phase of the trophectoderm to the uterine LE, and in pigs the porcine trophectoderm does not invade into the uterine LE. During the period of elongation, the porcine trophectoderm is also secreting estrogen, which is the pregnancy recognition signal in pigs, maintains the CL and progesterone production, and as a result pregnancy is maintained. To support placental growth and development, the placental

utilizes histotrophic and hemotrophic support, which is a combination of amino acids, sugars, proteins, cytokines, and hormones.

Sugars, such as glucose and fructose, are essential for the growth, development, and maintenance of cells, especially cells undergoing proliferation and differentiation, such as the conceptus trophectoderm. Hexose sugars are transported by either the facilitated diffusion symporters of the GLUT family or in a sodium-dependent manner by SGLT family transporters. These transporters are expressed throughout the body and localize to different cell types depending on the physiological function of the cells. GLUT1, GLUT3, and SGLT1 are the hexose transporters which have been studied the most within the reproductive tract during pregnancy and have been shown to be regulated by estrogen and progesterone.

Glucose and fructose have been found within the uterine flushings, fetal blood, amniotic fluid, and allantoic fluid during pregnancy, with concentrations of fructose being significantly higher than that of glucose. The roles of glucose and fructose have not been fully elucidated; however, our hypothesis is that these hexose sugars are being transported from the maternal blood and into the placenta and fetal blood to then be utilized by the conceptus trophectoderm to provide nucleotide building blocks to support growth and development. The studies described in this dissertation were aimed at determining the transport mechanism and metabolism of glucose and fructose.

CHAPTER III

STEROIDS REGULATE SLC2A1 AND SLC2A3 TO DELIVER GLUCOSE INTO TROPHECTODERM FOR METABOLISM VIA GLYCOLYSIS[*]

Introduction

In pigs, the majority of embryonic/fetal mortality occurs during two periods of pregnancy (Bazer and Johnson, 2014). The first period of embryonic mortality occurs between Days 14 and 25 of gestation when free-floating conceptuses (embryos and associated placental membranes) undergo implantation and early stages of placentation. The second period of fetal mortality is between Days 50 and 70 when the uterine-placental interface undergoes extensive folding and develops mature areolae to maximize hemotrophic and histotrophic support for the conceptuses. During both of these periods, the conceptuses require significant energy substrates, including the hexose sugars glucose and fructose. Abundances of glucose and fructose increase in the uterine lumen of pigs during the peri-implantation period (Zavy et al., 1982).

Glucose is an abundant hexose sugar that is transported into endometrial and placental tissues for use as a major energy substrate for growth and development of conceptuses (Pere, 2003; White et al., 1979a). There is minimal gluconeogenesis in the placentae and embryos/fetuses of pigs (Fowden et al., 1997). Therefore, in early pregnancy, glucose from maternal blood must be

---

[*] Kramer, A.C., Steinhauser, C.B., Gao, H., Seo, H., McLendon, B.A., Burghardt, R.C., Wu, G., Bazer, F.W., and Johnson, G.A. (2020). Steroids Regulate SLC2A1 and SLC2A3 to Deliver Glucose Into Trophectoderm for Metabolism via Glycolysis. Endocrinology *161*. By permission of Oxford University Press.

transported into the uterine lumen where it can be accessed by the free-floating conceptus and transported across the trophectoderm. Glucose is present, but fructose is the most abundant hexose sugar in porcine conceptuses (Goodwin, 1956). The presence of fructose in conceptuses is unique to species with epitheliochorial or synepitheliochorial placentae, indicating that fructose may be important for growth and development of fetuses supported by these types of placentae (Goodwin, 1956). Fructose plays a minor role as an energy source or substrate for the pentose shunt pathway in the placenta and fetus, because fructose is oxidized to CO_2 at only ~20% the rate of glucose (Meznarich et al., 1987). However, fructose can be used as a substrate in a number of metabolic pathways that could support conceptus development, including biosynthesis of glycosaminoglycans, phospholipids, and nucleic acids (White et al., 1982). As implantation and placentation progress during pregnancy, the adherence of the uterine luminal epithelium (LE) to the placental chorion creates the uterine-placental interface of the epitheliochorial pig placenta, a substantial tissue barrier that nutrients must traverse to reach the fetal-placental vasculature (Dantzer, 1984, 1985).

Glucose can be transported by either facilitated diffusion transporters of the solute carrier 2A (SLC2A; GLUT) family or sodium-dependent transporters of the solute carrier 5A (SLC5A; SGLT) family. In pigs, concentrations of glucose in fetal blood are 40-70% lower than concentrations of glucose in maternal blood, creating a concentration gradient to transport glucose (Pere, 1995; Randall, 1977). Therefore, this study focused on the SLC2A family of glucose transporters. There are 14 members of the SLC2A family (SLC2A1-14) responsible for transporting glucose in addition to multiple other sugars. Individual members of the family have differing affinities for glucose; some are regulated by insulin or steroid hormones, and all have distinct tissue-specific expression (Augustin, 2010). SLC2A1 is ubiquitously expressed

throughout the body and is responsible for basal glucose uptake into cells. SLC2A2 is a low affinity, high capacity glucose transporter often found in the basal plasma membrane of transporting epithelia. SLC2A3 is a high affinity, high capacity glucose transporter found in tissues such as the brain where glucose needs to be transported rapidly and in large quantities. SLC2A4 is an insulin-sensitive glucose transporter mostly found in skeletal muscle and adipose tissues (Olson and Pessin, 1996; Zhao and Keating, 2007).

The transporters, SLC2A1, SLC2A3, and SLC2A4, have been localized to endometrial or conceptus tissues of humans, mice, and sheep. SLC2A1 has been localized to the placental syncytiotrophoblasts of humans, and uterine LE, glandular epithelium (GE), and stromal cells of humans and mice (Frolova and Moley, 2011c; Jansson et al., 1993; von Wolff et al., 2003; Yamaguchi et al., 1996). SLC2A1 protein has also been detected in the endometrial LE and GE of sheep during the estrous cycle and early pregnancy, as well as ovine conceptus trophectoderm (Gao et al., 2009b). SLC2A2 has not been detected in endometria (Gao et al., 2009c; von Wolff et al., 2003). SLC2A3 has been detected in the stroma and decidua of human and mouse endometria in addition to the placenta (Brown et al., 2011; Hahn et al., 2001; Yamaguchi et al., 1996). SLC2A3 mRNA is expressed in the trophectoderm of sheep as early as Day 14 of pregnancy, but there is no detectable expression in the endometrium through Day 20 (Gao et al., 2009c). SLC2A4 has been detected in LE, GE and stromal cells of human and mouse endometria, as well as sheep endometrial LE and GE throughout the estrous cycle and early pregnancy (Frolova and Moley, 2011c; von Wolff et al., 2003; Yamaguchi et al., 1996).

Glucose transport from mother to conceptus can be influenced by several factors, including utero-placental blood flow, concentration gradients, surface area for exchange, placental metabolism, transporter expression, maternal hormones, and placental hormones. The true

epitheliochorial placenta of the pig represents a significant barrier to nutrient transport because nutrients must traverse multiple cell layers between the maternal and fetal microvasculatures (Dantzer, 1985). This barrier to nutrient transport is overcome by folding of the adhered interface, comprised of the maternal uterine LE and placental trophectoderm/chorion and underlying connective tissue, to increase surface area. Nutrient transport is also facilitated by accessory structures known as areolae. Areolae develop as invaginations of the chorioallantois, over the openings of uterine glands to transport secretions from uterine GE to the vasculature of the conceptus (Dantzer, 1984; Friess et al., 1981).

Expression of SLC2A1 protein in sheep is upregulated by progesterone (P4) in the uterine LE, but P4 does not affect expression of SLC2A4 protein (Gao et al., 2009b). Additionally, estrogen (E2) treatment increases glucose uptake and the expression of SLC2A1 protein in uteri of rats (24, 25). SLC2A1 protein is also up-regulated in the endometrial stroma of mice by P4 (Frolova et al., 2009).

Glucose and fructose increase in abundance in the uterine lumen of pigs during the peri-implantation period of pregnancy. However, it is not known if glucose and fructose are actively metabolized by porcine conceptuses. Further, while the glucose transporters, SLC2A1, SLC2A2, SLC2A3, and SLC2A4, have been studied in the endometrial and placental tissues of non-pregnant and early pregnant humans, mice, and sheep, there is no information regarding the temporal and cell-specific expression of these transporters in porcine endometria and placentae throughout pregnancy nor regulation of their expression by steroid hormones. Therefore, this study aimed to: (1) utilize isotope-labeled glucose and fructose to determine if elongating pig conceptuses metabolize glucose and fructose; and (2) quantify temporal and cell-specific changes in glucose transporters throughout the estrous cycle and pregnancy in the pig, and (3) determine whether

expression of glucose transporters is regulated by E2 and/or P4, two important hormones of pregnancy.

Materials and Methods

Animals and Tissue Collection

Sexually mature, 8-month-old crossbred gilts were observed daily for estrus (Day 0) and exhibited at least two estrous cycles of normal duration (18 to 21 days) before being used in these studies. All experimental and surgical procedures were in compliance with the Guide for Care and Use of Agricultural Animals in Teaching and Research, and approved by the Institutional Animal Care and Use Committee of Texas A&M University.

To evaluate oxidation of glucose and fructose, conceptuses on Day 14 (n = 4 litters) and Day 16 (n = 4 litters) of pregnancy were collected by flushing the uterine lumen with 40 ml physiological saline. The isolated conceptus tissues were washed three times with oxygenated (95% O_2 - 5% CO_2) Krebs-Henseleit Bicarbonate (KHB) buffer (pH 7.4) containing 20 mM HEPES (pH 7.4) and 1 mM glutamate, and then used immediately in the experiments.

To evaluate the effects of pregnancy on expression of SLC2A1 mRNA and protein, and *SLC2A2*, *SLC2A3* and *SLC2A4* mRNAs in endometria and placentae, gilts were assigned randomly to either cyclic or pregnant status. Gilts in the pregnant group were bred naturally to boars with proven fertility. Cyclic gilts were euthanized and then ovariohysterectomized on either Day 5, 9, 11, 12, 13, 15 or 17 of the estrous cycle, while pregnant gilts were euthanized and then ovariohysterectomized on either Day 9, 11, 12, 13, 15, 17, 20, 25, 30, 35, 40, 50, 60, or 85 of pregnancy (n = 3 or 4 gilts/day/status). The lumen of each uterine horn from Days 9 through 17 of the estrous cycle and pregnancy were flushed with 20 ml physiological saline. Pregnancy was

confirmed in the mated gilts by the presence of morphologically normal conceptuses. Tissue sections (uterus or uterus with attached placenta ~1 cm thick) from the middle of each uterine horn of all hysterectomized gilts were fixed in fresh 4% paraformaldehyde in PBS (pH 7.2) and embedded in Paraplast-Plus (Oxford Laboratory, St. Louis, MO) or snap frozen in Tissue-Tek OCT compound (Miles, Oneata, NY). Additionally, endometrium was physically dissected from the myometrium, snap-frozen in liquid nitrogen, and stored at -80°C for RNA extraction. Chorioallantoic tissue was physically dissected from endometrium and frozen in a similar manner.

Progesterone and Estrogen Models

To evaluate effects of E2 and E2-induced pseudopregnancy on expression of *SLC2A1*, *SLC2A2, SLC2A3,* and *SLC2A4* mRNAs in endometria, gilts were detected in estrus (Day 0) and assigned randomly to receive daily intramuscular injections of either estradiol benzoate (E2 in corn oil (E2); n = 4) or corn oil alone (CO; n = 4) on Days 11, 12, 13, and 14 of the estrous cycle to induce pseudopregnancy (Joyce et al., 2007). All gilts were euthanized and then ovariohysterectomized on Day 15. Endometrial tissues were collected as previously described.

To evaluate effects of long-term treatment with P4 on expression of *SLC2A1*, *SLC2A2, SLC2A3* and *SLC2A4* mRNAs in endometria, gilts were ovariectomized on Day 12 of the estrous cycle and assigned randomly to receive daily intramuscular injections of either CO (4 ml) or P4 (200 mg in 4 ml CO) on Days 12 through 39 post-estrus (n = 3/treatment) (Waugh and Wales, 1993). All gilts were hysterectomized on Day 40 post-estrus and endometrial tissues collected as previously described.

Concentrations of Glucose in Uterine Flushings

Uterine flushings were clarified by centrifugation at 3000 x g for 15 min at 4°C, and the supernatants aliquoted and stored at –80°C. Uterine flushings (0.5 ml) were deproteinized with an equal volume of 1.5 M $HClO_4$ followed by addition of 0.25 ml of 2 M K_2CO_3. Extracts were analyzed for glucose using a fluorometric method utilizing hexokinase and glucose-6-phosphate dehydrogenase as described previously (Steinhauser et al., 2016).

Oxidation of glucose and fructose in pig conceptuses

To evaluate oxidation of glucose and fructose, conceptus tissues (20 mg) were placed in polypropylene test tubes and incubated with either [U-^{14}C]glucose (0.033 μCi/ml; American Radiolabeled Chemicals Inc., St. Louis, MO) or [U-^{14}C]fructose (0.033 μCi/ml) in 1 ml of KHB buffer containing unlabeled glucose and/or fructose as follows: 1)[U-^{14}C]glucose + 4 mM glucose; 2) [U-^{14}C]fructose + 4 mM fructose; 3) [U-^{14}C]glucose + 4 mM glucose and fructose; or 4) [U-^{14}C]fructose + 4 mM glucose and fructose. After incubation for 2 h at 37°C, 0.2 ml of soluene (Perkin-Elmer, USA) was injected through the rubber cap into a suspended cup inside the tube, and 0.2 ml of 1.5 M $HClO_4$ acid was injected into the medium to liberate $^{14}CO_2$. Following the 1 h incubation, the suspended cups were transferred to scintillation vials containing 5 ml of cocktail. Radioactivity of $^{14}CO_2$ produced from oxidation of glucose and fructose by conceptus tissue were measured using liquid scintillation spectrometry (Perkin-Elmer, USA) (Kim et al., 2012).

RNA Extraction, cDNA Synthesis, and Primer Design

Total RNA was extracted from endometrial and chorioallantoic tissue samples using Trizol reagent (Life Technologies, Carlsbad, CA) according to the manufacturer's recommendations.

First strand cDNA was synthesized using a Superscript III First Strand Kit (Life Technologies, Carlsbad, CA) according to the manufacturer's instructions. First strand cDNA was diluted 10x for the qPCR reaction. Primers for qPCR and *in situ* hybridization were designed using NCBI Genbank sequences and Primer-BLAST (http://www.ncbi.nlm.nih.gov/). Primers were submitted to BLAST to confirm specificity against the known porcine genome. Primer information is summarized in Table 1.

Gene Name	Method	Gene ID	Sequence	Product Length
SLC2A1	qPCR	XM_005665507.1	F: 5'-TCCTTTACCCACATCCCACG-3' R: 5'-AAGGCAAGTGTCTAGGCAGG-3'	82
SLC2A1	ISH	X17058	F: 5'-TGGCCTTCATATCTGCTGTG-3' R: 5'-AACAGCTCCAGGATGGTGAC-3'	484
SLC2A2	qPCR	NM_001097417.1	F: 5'-CCCTGCTGCTTTAGCAATGG-3' R: 5'-TAAGGTCCACAGAAGTCCGC-3'	96
SLC2A3	qPCR	XM_003355585.3	F: 5'-ATCTTGGTATGGCCACTCGG-3' R: 5'-GCAAGGCAATCCACTAAGGC-3'	130
SLC2A3	ISH	NM_001009770.1	F: 5'-CCACACATGAGCCGTAAATG-3' R: 5'-TGAAGAGCCCAGTCTCCACT-3'	477
SLC2A4	qPCR	NM_001128433.1	F: 5'-GAGAGCCAGTTCTCTCCACC-3' R: 5'-CTCCACCCTGGAAGTAACGG-3'	88
SLC2A4	ISH	NM_001128433.1	F: 5'-CAACAGATAGGCTCCGAAGA-3' R: 5'-CACGTACATGGGCACCAG	465
ACTB	qPCR	XM_003124280.3	F: 5'-TCCCTGGAGAAGAGCTACGA-3' R: 5'-TGTTGGCGTAGAGGTCCTTC-3'	187
HPRT1	qPCR	DQ845175	F: 5'-GGACTTGAATCATGTTTGTG-3' R: 5'-CAGATGTTTCCAAACTCAAC-3'	91
SDHA	qPCR	DQ845177	F: 5'-CTACAAGGGGCAGGTTCTGA-3' R: 5'-AAGACAACGAGGTCCAGGAG-3'	141
TBP	qPCR	DQ845178	F: 5'-AACAGTTCAGTAGTTATGAGCCAGA-3' R: 5'-AGATGTTCTCAAACGCTTCG-3'	153
TUBA1B	qPCR	NM_001044544.1	F: 5'-GCTGCCAATAACTATGCCCG-3' R: 5'-ACCAAGAAGCCCTGAAGACC-3'	116

Table 1. **Primer information for SLC2A genes**

Quantitative PCR

Quantitative PCR assays were performed using PerfeCta SYBR Green Mastermix (Quanta Biosciences, Gaithersburg, MD) in 10 µl reactions with 2.5 mM of each specific primer, on a

Roche 480 Lightcycler (Roche) with approximately 60 ng cDNA per reaction. The PCR program began with 5 min at 95°C followed by 40 cycles of 95°C denaturation for 10 sec and 60°C annealing/extension for 30 sec. A melt curve was produced with every run to verify a single gene-specific peak. Standard curves using pooled cDNA with 2-fold serial dilutions were run to determine primer efficiencies. All primer correlation coefficients were greater than 0.95 and efficiencies were 95-102%. The geometric mean of *TATA-binding protein (TBP)*, *succinate dehydrogenase complex subunit A flavoprotein (SDHA),* and *beta actin (ACTB)* was used to normalize endometrial tissue, while the geometric mean of *TBP, hypoxanthine phosphoribosyl transferase 1 (HPRT1),* and *tubulin alpha 1B (TUBA1B)* was used to normalize chorioallantoic tissue (Kim et al., 2012). The $2^{-\Delta\Delta Ct}$ method was used to normalize data, and fold-changes were subjected to statistical analyses.

In situ Hybridization Analyses

Cell-specific expression of mRNAs in sections of porcine endometria and placentae were determined by radioactive *in situ* hybridization analyses as described previously (32). Briefly, partial cDNAs for porcine *SLC2A1, SLC2A2, SLC2A3* and *SLC2A4* mRNAs were cloned beginning with PCR amplification of total RNA from Day 15 pregnant porcine endometrial tissues using specific primers (Supplementary Table 1 (31)). PCR amplification was conducted as follows: 1) 95°C for 5 min; 2) 95°C for 45 sec, 60°C for 30 sec, and 72°C for 1 min for 35 cycles; and 3) 72°C for 10 min. The partial cDNAs of the correct predicted size were cloned into a pCRII plasmid using a T/A Cloning Kit (Life Technologies) and the sequence of each verified using an ABI PRISM Dye Terminator Cycle Sequencing Kit and ABI PRISM automated DNA sequencer (Applied Biosystems).

Radiolabeled antisense or sense cRNA probes were generated by *in vitro* transcription using linearized plasmid templates, RNA polymerases, and [α-^{35}S]-UTP. Deparaffinized, rehydrated, and deproteinated uterine tissue sections (5 μm thick) were hybridized with radiolabeled antisense or sense cRNA probes. After hybridization, washing, and ribonuclease A digestion, slides were dipped in NTB-2 liquid photographic emulsion (Kodak, Rochester, NY), and exposed at 4°C for 7 to 10 days. Slides were developed in Kodak D-19 developer, counterstained with Harris modified hematoxylin (Fisher Scientific, Fairlawn, NJ), dehydrated through a graded series of alcohol to CitriSolv (Fisher Scientific) and coverslips were affixed with Permount (Fisher Scientific). Slides were evaluated using an Axioplan 2 microscope (Carl Zeiss, Thornwood, NY) interfaced with an Axioplan HR digital camera and Axiovision 4.3 software. Digital images of representative fields were recorded under brightfield or darkfield illumination and plates for each figure were assembled using Adobe Photoshop (version 6.0, Adobe Systems Inc., San Jose, CA).

Immunofluorescence Analysis

Frozen sections of uterus or uterine-placental interface (10 μm) were fixed in methanol at -20°C for 20 min and washed in PBS. These sections were then blocked in 10% normal goat serum diluted in antibody dilution buffer for 1 h at room temperature. Rabbit anti-SLC2A1 IgG (1:100; Thermo Scientific, MA, USA; PA5-16793; RRID:AB_10986893) (32) was added and incubated overnight at 4°C in a humidified chamber. Normal rabbit IgG (Sigma-Aldrich, St. Louis, MO; I5006) was substituted for primary antibody and served as a negative control. We were unable to find antibodies that cross-reacted with the porcine SLC2A2, SLC2A3 or SLC2A4 proteins. Tissue sections were then washed three times for 5 min/wash in PBS. Goat anti-rabbit IgG Alexa 488

(Life Technologies, Grand Island, NY; 1:250) was added and incubated for 1 h at room temperature (34). Tissue sections were then washed three times for 5 min/wash in PBS. Slides were counterstained with Prolong Gold Antifade reagent containing DAPI (Life Technologies) and coverslipped. Images were taken using an Axioplan 2 microscope (Carl Zeiss, Thornwood, NY) interfaced with an Axioplan HR digital camera.

Statistical Analyses

Data for concentrations of glucose were analyzed for effects of day, pregnancy status (cyclic or pregnant), and their interaction using a 2-way ANOVA via the General Linear Models (GLM) procedures of the Statistical Analysis System (SAS Institute, Cary, NC).

Data for $^{14}CO_2$ produced by Day 14 and Day 16 conceptuses were analyzed by one-way ANOVA.

The qPCR data for normal tissues were analyzed for effects of day, pregnancy status, and their interaction for Days 9, 11, 13, 15 and 17 by 2-way ANOVA via the GLM procedures of SAS using the least significant difference (LSD) multiple testing method. The qPCR data were also subjected to a sliding time window linear regression analysis to determine if there was an effect of day of gestation on the expression of genes of interest throughout pregnancy (Days 9 to 85). The sliding time windows of the analysis were designed to detect effects of day on gene expression during three biologically relevant periods of time: peri-implantation period, period of placentation, and period of exponential fetal growth. Each window analyzed included a minimum of 3 days. Some windows contained greater than 3 days contingent on the regression model not detecting a decrease in significance in terms of r^2 and p-values of the F-statistics.

The data from the hormone therapy studies were analyzed using the Students t-test. All data are presented as means ± standard error of the means with significance set at $p<0.05$.

Results

Concentrations of Glucose Increase in Uterine Flushings during the Peri-Implantation Period of Pregnancy

Total recoverable glucose increased in the uterine flushings of both cyclic and pregnant gilts between Days 9 and 15 (Figure 1; $p<0.05$). Therefore, the free-floating blastocyst is exposed to increasing levels of glucose as the trophectoderm elongates and begins to attach to the uterine wall for implantation. There was no effect of pregnancy status or day by pregnancy interaction on total recoverable glucose (Figure 1; $p>0.05$).

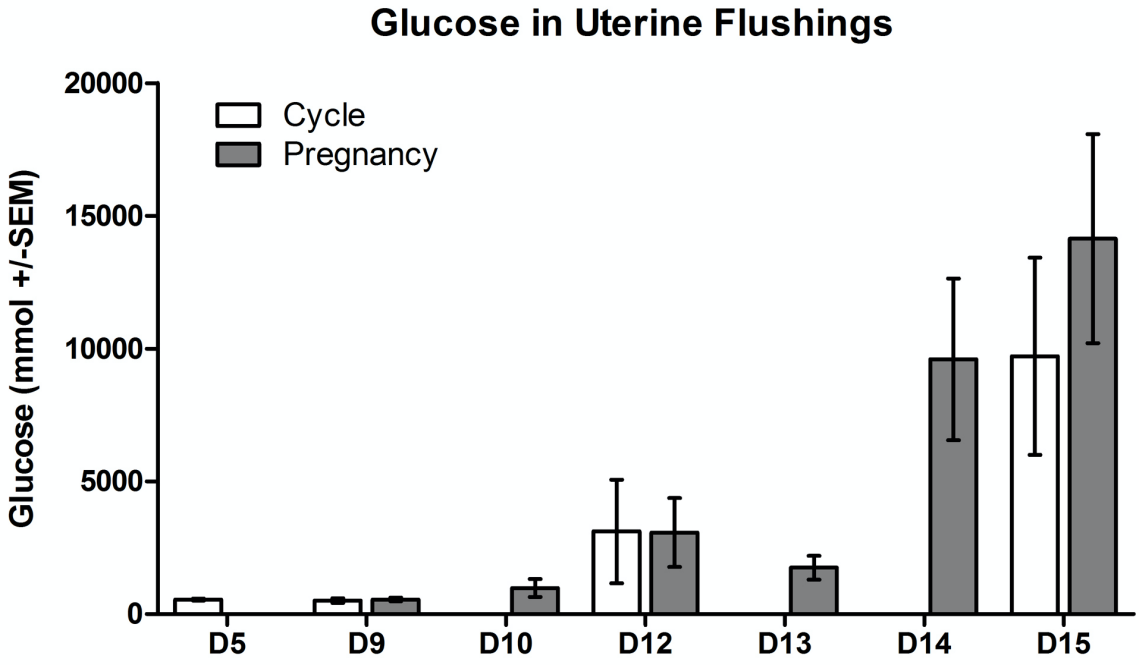

Figure 1. Total recoverable glucose in porcine uterine flushings.

Total recoverable glucose increased in uterine flushings between Day 9 and 15 of the estrous cycle and pregnancy ($p<0.01$). There was no interaction between Day and Status or effect of Status alone ($p>0.05$). Values are means ± SEM.

Glucose and Fructose are Metabolized by Elongating Conceptuses during the Peri-Implantation Period of Pigs

To determine if pig conceptuses metabolize glucose and fructose during the peri-implantation period, conceptus tissues from Day 14 and Day 16 of pregnancy were incubated with isotope-labeled glucose or fructose in medium containing either unlabeled glucose and/or fructose, and then oxidation of glucose and fructose was determined by measuring $^{14}CO_2$ released from conceptus tissues. Table 1 summarizes the production of $^{14}CO_2$ from [U-^{14}C]glucose and [U-^{14}C]fructose from conceptuses on Days 14 and 16 of pregnancy. Trophectoderm cells of Day 14 conceptus metabolized both glucose and fructose. However, in the presence of both glucose and fructose, the conceptuses preferentially metabolized glucose over fructose, but in the absence of glucose, the conceptuses actively metabolized fructose. At Day 16 of pregnancy, conceptuses metabolized glucose and fructose similar to that for conceptus from Day 14 of pregnancy. However, Day 16 conceptuses produce significantly more $^{14}CO_2$ than Day 14 conceptuses.

Day 14p Conceptus

	$^{14}CO_2$ production (nmol/ 60 min/mg of tissue)	
Media	[U-^{14}C]Glucose	[U-^{14}C]Fructose
Glucose and Fructose	18.73 ± 7.48[a]	1.43 ± 0.73[b]
Glucose	21.3 ± 11.38	---
Fructose	---	11.24 ± 4.44

Day 16p Conceptus

	$^{14}CO_2$ production (nmol/ 60 min/mg of tissue)	
Media	[U-^{14}C]Glucose	[U-^{14}C]Fructose
Glucose and Fructose	33.13 ± 4.59[a]	5.55 ± 1.25[b]
Glucose	41.69 ± 7.08	---
Fructose	---	30.38 ±6.16

Table 2. $^{14}CO_2$ Produced by Day 14 and Day 16 Conceptuses

Porcine conceptus tissues were cultured in KHB (7.4) containing glutamate and D-U-^{14}Cglucose or D-U-^{14}Cfructose at 37°C for 60 minutes. Data are the means ± SEM. (n = 4) and were analyzed

by one-way ANOVA. Values with different superscripted letters within each group are significantly different ($P < 0.05$) from each other.

SLC2A1 mRNA Localizes to Uterine LE during Pregnancy and Expression Is Upregulated by E2 and P4

Quantitative PCR was performed to determine steady-state levels of total *SLC2A1* mRNA in endometrial and placental tissues from the estrous cycle and pregnancy, and endometrial tissues from gilts treated with exogenous E2 or P4. Expression of *SLC2A1* mRNA increased from Days 11 to 15 in endometrial tissue from both cyclic and pregnant gilts; however, expression was greater for pregnant than cyclic gilts (Figure 2A; day x status, $p<0.001$). During pregnancy, expression of *SLC2A1* mRNA increased and was correlated to day between Days 9 and 17 ($r^2=0.864$; $p<0.05$), but then there was a day-associated decrease in expression between Days 17 and 25 ($r^2=0.764$; $p>0.05$) of pregnancy. Expression of *SLC2A1* mRNA was not affected by day of gestation between Days 30 and 85 ($r^2=0.016$; $p>0.05$) of pregnancy (Figure 2A). Expression of *SLC2A1* mRNA in the chorioallantois did not change between Days 30 and 85 of gestation (Figure 2B; $r^2=0.143$; $p>0.05$). Endometrial expression of *SLC2A1* mRNA was greater for gilts treated with E2 than CO (Figure 2C; $p<0.05$) and for gilts treated with P4 compared to CO ($p<0.05$; Figure 2D).

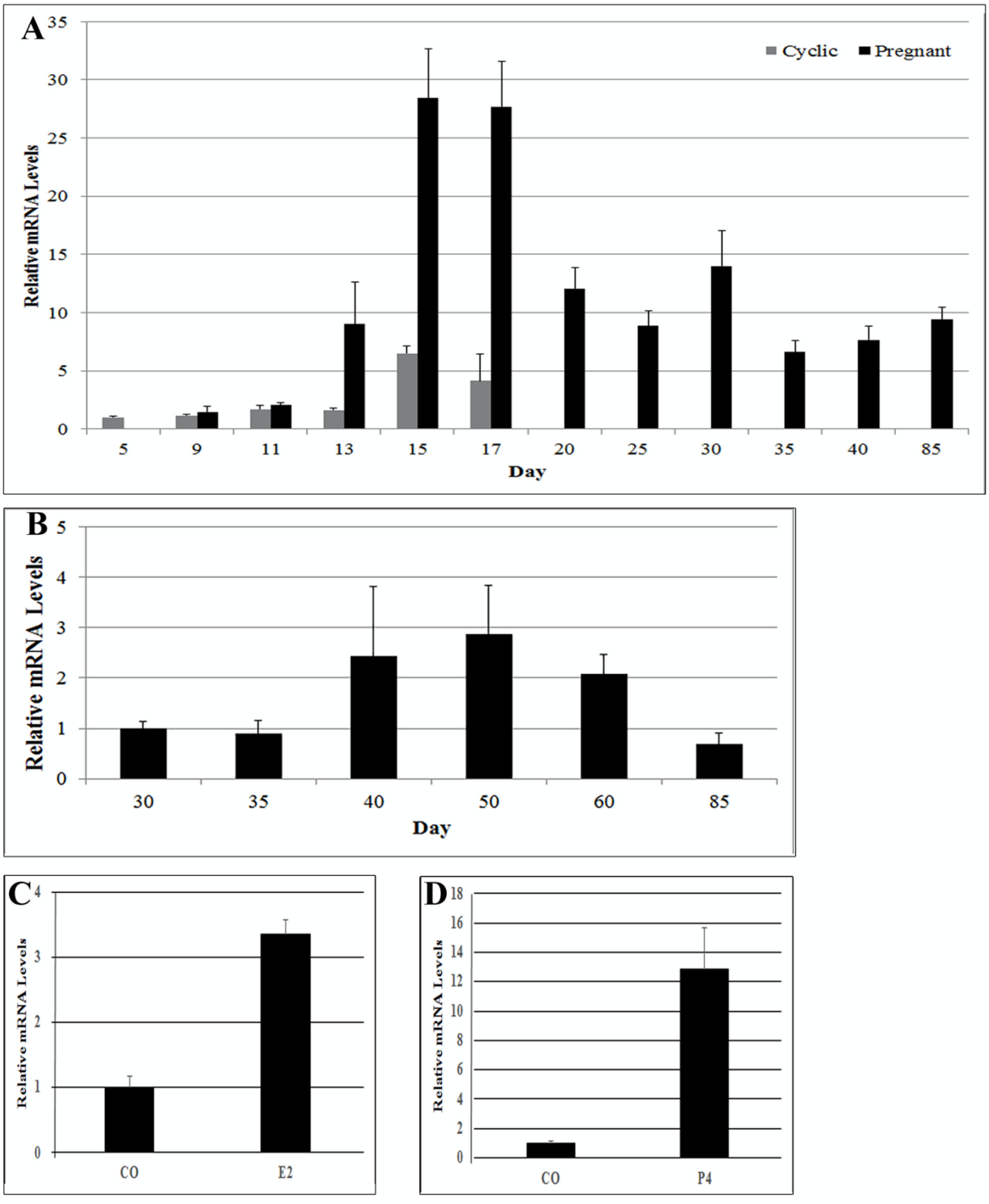

Figure 2. Expression of SLC2A1 mRNA in endometrial and placentae.

(A) Expression of *SLC2A1* mRNA increased between Days 11 and 15 in endometrial tissue from cycling and pregnant gilts, and expression was more abundant in endometrial tissue from pregnant than cyclic gilts (day x status, $p<0.001$); **(B)** Expression of *SLC2A1* mRNA in placenta did not change between Days 30 and 85 ($r^2=0.143$; $p>0.05$); **(C)** Exogenous E2 up-regulated expression of *SLC2A1* mRNA in endometria ($p<0.05$); **(D)** Exogenous P4 up-regulated expression of *SLC2A1* mRNA in endometria ($p<0.05$). Values are presented as means ± SEM and $p<0.05$ is significant.

I*n situ* hybridization analysis localized *SLC2A1* mRNA to the endometrial LE and GE on all days of the estrous cycle and pregnancy studied. On Day 15, expression of *SLC2A1* mRNA appeared to be greater in uterine LE from pregnant compared to cyclic gilts (Figure 3 and Supplemental Figure 1 (Kramer et al., 2020)). *SLC2A1* mRNA was also detected in conceptuses from Day 15 of pregnancy (Figure 3). Between Days 25 and 85 of pregnancy, expression of *SLC2A1* remained localized to the uterine LE with expression appearing to increase in the GE at Day 30, and then decrease by Day 85 (Figure 3). Expression of *SLC2A1* mRNA was also detected in the chorion on all days examined, although at lower levels than in uterine LE (Figure 3). *SLC2A1* mRNA appeared to increase in uterine LE of both E2- and P4-treated gilts over CO-treated control gilts (Figure 3).

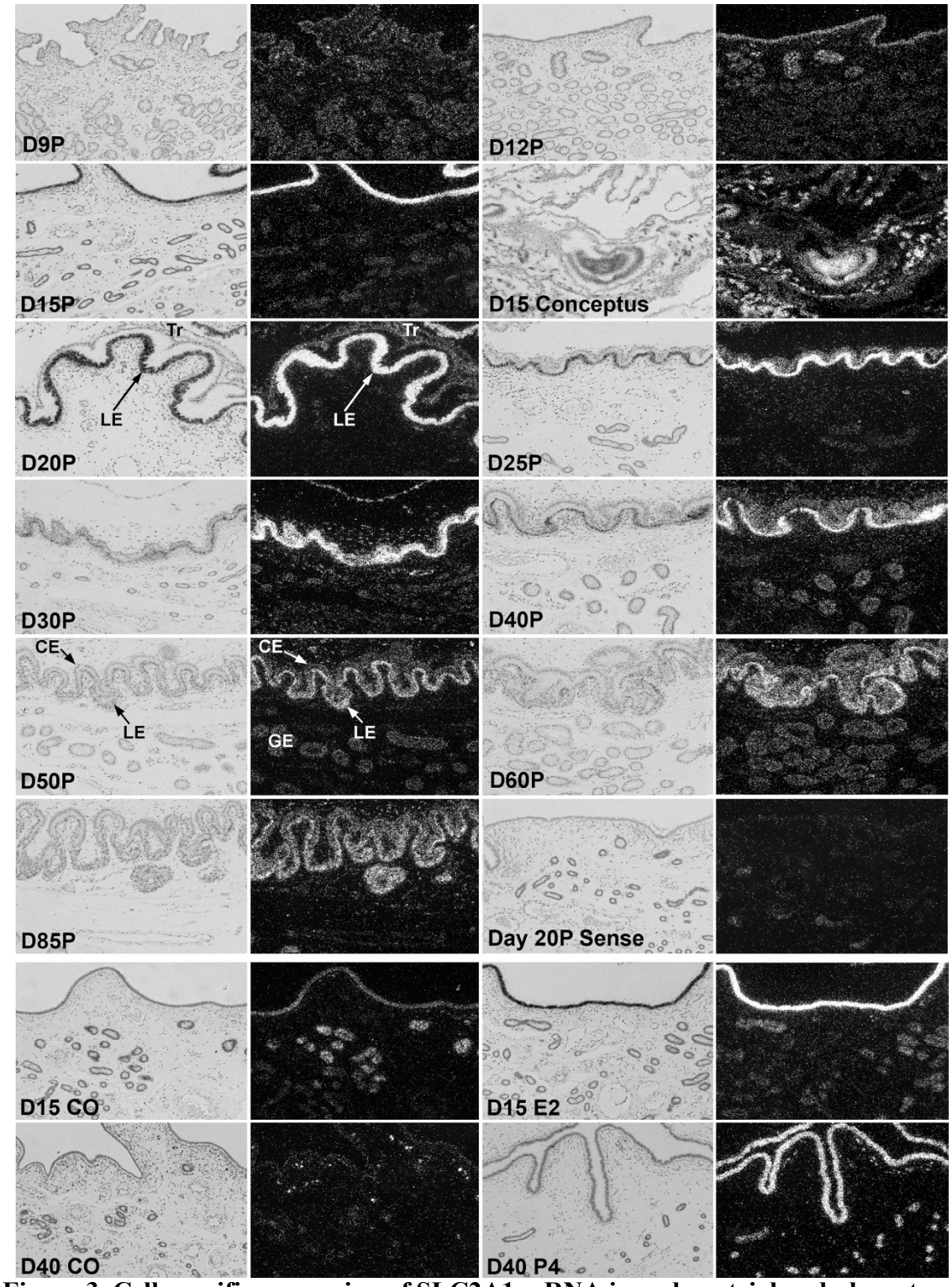

Figure 3. Cell-specific expression of SLC2A1 mRNA in endometrial and placentae.

Corresponding brightfield and darkfield images from *in situ* hybridization demonstrate that *SLC2A1* mRNA localizes predominantly to uterine LE during the estrous cycle and pregnancy with some expression in the uterine GE and trophectoderm/chorion. Exogenous E2 increased expression of *SLC2A1* mRNA in the LE, while exogenous P4 increased expression in the LE and GE. Width of fields is 870 µm. The Day 20P Sense panel is the negative control. Legend: D, Day; P, pregnancy; LE, luminal epithelium; GE, glandular epithelium; Tr, trophectoderm; CE, chorionic epithelium.

SLC2A2 mRNA Is Expressed During Late Pregnancy

Expression of *SLC2A2* mRNA in endometria was low during the estrous cycle and early pregnancy, compared to other *SLC2A* transporters studied, with no significant effect of day or pregnancy status during the peri-implantation period of pregnancy ($p>0.05$) (Supplemental Figure 2 (31). However, expression of *SLC2A2* mRNA increased in endometria between Days 9 and 85 of pregnancy ($r^2=0.774$; $p<0.001$), specifically between Days 25 and 60 ($r^2=0.847$; $p<0.001$), and in the placenta between Days 30 and 85 of pregnancy ($r^2=0.810$; $p<0.001$) (Supplemental Figure 2 (Kramer et al., 2020)).

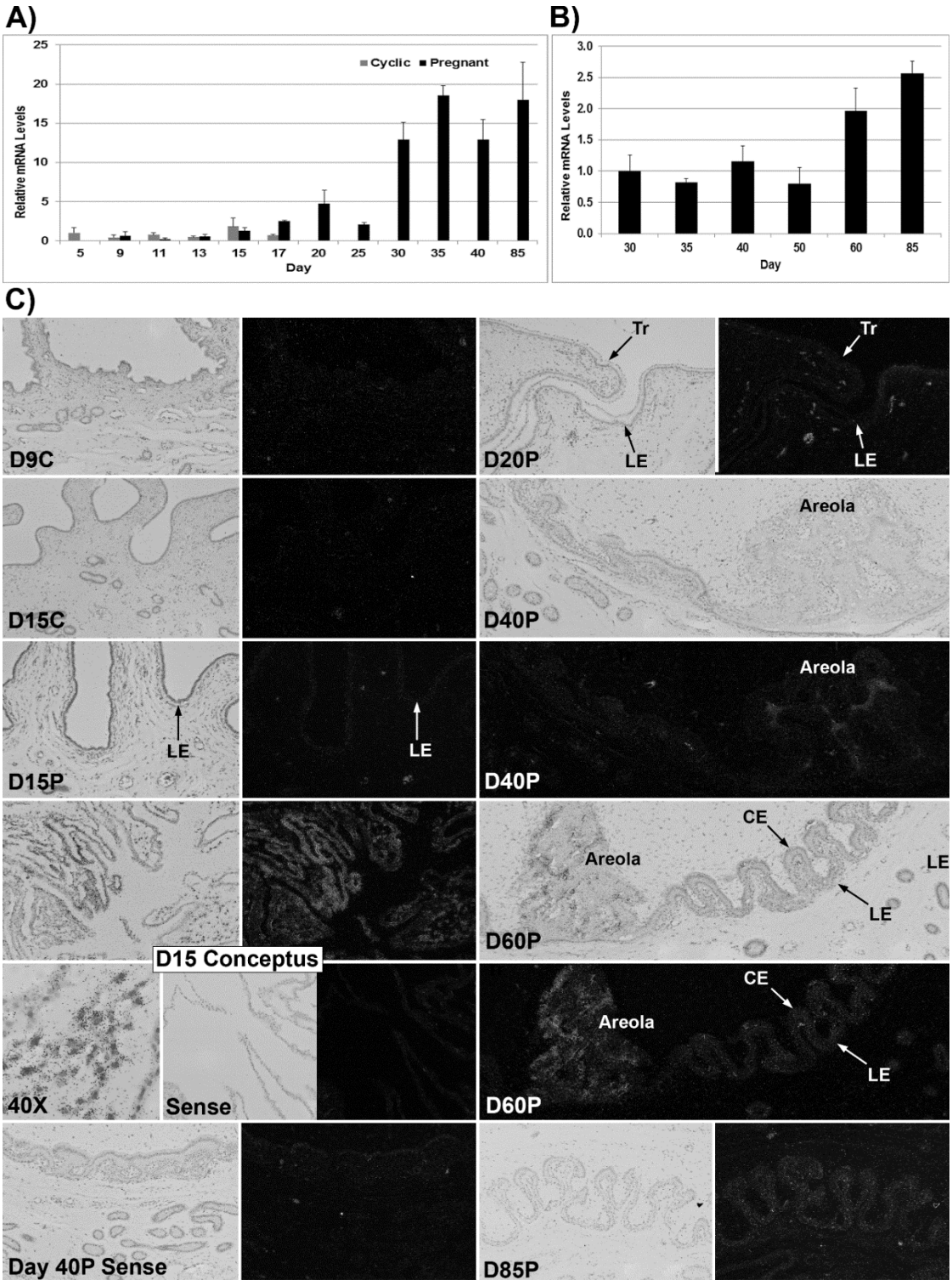
A)
B)
C)
Cyclic
Pregnant
Relative mRNA Levels
Day
Tr
LE
Areola
CE
D9C
D20P
D15C
D40P
D15P
D60P
D15 Conceptus
40X
Sense
Day 40P Sense
D85P

Figure 4. Expression of SLC2A2 mRNA in endometria and placentae.

(A) Endometrial expression of SLC2A2 mRNA increased between Days 9 and 85 of pregnancy (r2=0.774; p<0.001); (B) Placental expression of SLC2A2 mRNA increased between Days 30 and 85 of pregnancy (r2=0.810; p<0.001); (C) Corresponding brightfield and darkfield images demonstrate SLC2A2 mRNA in trophectoderm at Day 15 and in areolae, uterine LE, and CE on Days 60 to 85 of pregnancy. Values presented are means ± SEM and p<0.05 is significant. Width of fields is 870 μm except the D15 Conceptus 40X and Sense (580 μm) and D40P and D60P (1740 μm). The Day 40P Sense panel is the negative control. Legend: LE, luminal epithelium; Tr, trophectoderm; CE, chorion.

In situ hybridization detected *SLC2A2* mRNA in the trophectoderm of Day 15 conceptuses (Figure 4 (Kramer et al., 2020)). By Day 40, *SLC2A2* mRNA was detected in areolae and expression appeared to increase through Day 60. *SLC2A2* mRNA was barely detectable in inter-areolar regions of the chorioallantois between Days 60 and 85 of pregnancy.

There was no effect of E2 or P4 on expression of *SLC2A2* mRNA in uteri of pseudopregnant gilts or gilts on long-term P4 treatment (data not shown).

SLC2A3 mRNA Localizes Primarily to the Placenta throughout Pregnancy

Expression of *SLC2A3* mRNA in endometria decreased from Day 9 to Day 13 (p<0.001) in both pregnant and cycling gilts (Figure 5A; p>0.05). In pregnant gilts,

endometrial expression of *SLC2A3* mRNA decreased between Days 9 and 15 (r^2=0.686; p>0.05), but increased between Days 17 and 25 (r^2=0.790; p>0.05) and again between Days 30 and 85 (r^2=0.964; p<0.01) of gestation (Figure 5A). There was no change in expression of *SLC2A3* mRNA in the chorioallantois between Days 30 and 85 of pregnancy (Figure 5B; r^2=0.04; p>0.05). Endometrial expression of *SLC2A3* mRNA decreased in response to E2 (p<0.05; Figure 5C), whereas P4 had no effect on expression of *SLC2A3* mRNA (Figure 5D).

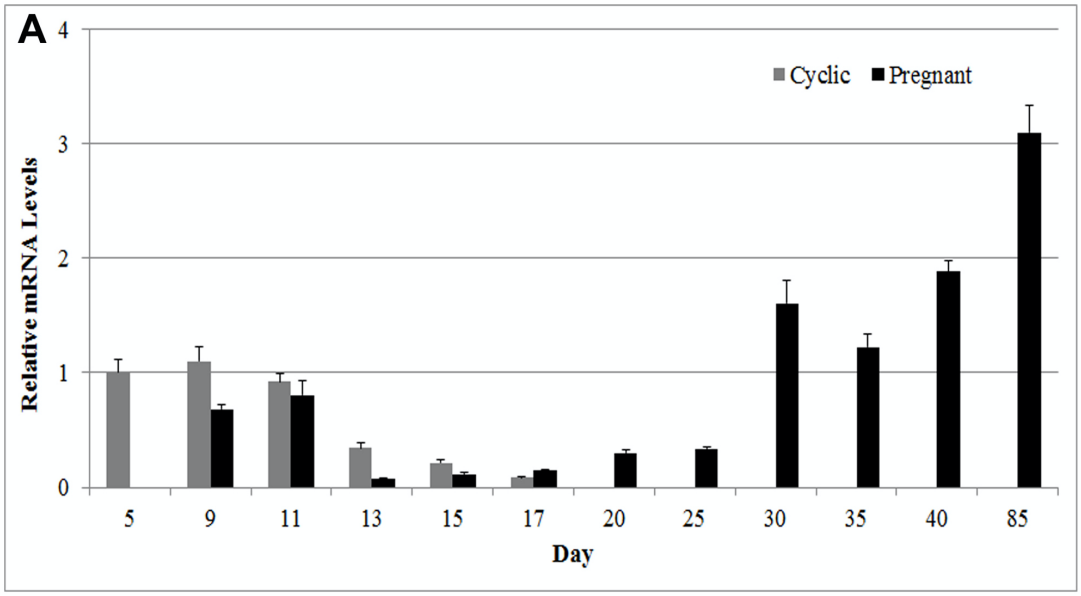
A
Cyclic
Pregnant
Relative mRNA Levels
0
1
2
3
4
5
9
11
13
15
17
20
25
30
35
40
85
Day

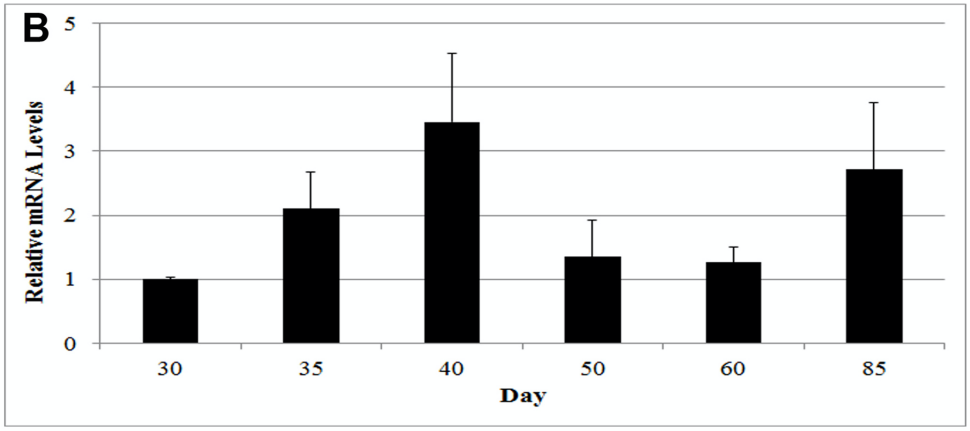
B
Relative mRNA Levels
0
1
2
3
4
5
30
35
40
50
60
85
Day

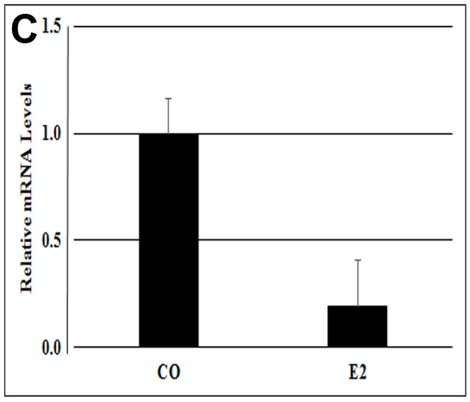
C
Relative mRNA Levels
0.0
0.5
1.0
1.5
CO
E2

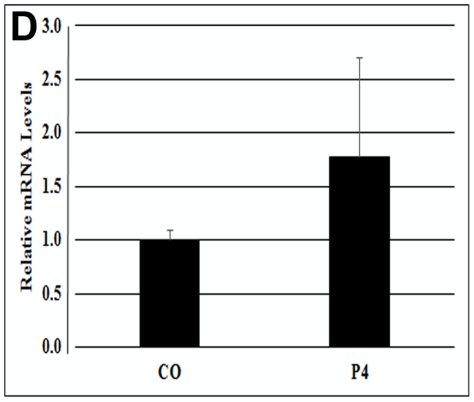
D
Relative mRNA Levels
0.0
0.5
1.0
1.5
2.0
2.5
3.0
CO
P4

Figure 5. Expression of SLC2A3 mRNA in endometria and placentae.

(A) Endometrial expression of *SLC2A3* mRNA was low during the estrous cycle and early pregnancy, then increased between Days 30 and 85 of pregnancy (r^2=0.964; $p<0.01$). **(B)** Placental expression of *SLC2A3* mRNA was not different between Days 30 and 85 (r^2=0.04; $p>0.05$). **(C)** Endometrial expression of *SLC2A3* mRNA decreased in response to E2 ($p<0.05$) and **(D)** was not affected by P4 ($p>0.05$). Values presented are means ± SEM and $p<0.05$ is significant.

SLC2A3 mRNA was barely detectable in the uterine LE and GE of cycling and pregnant gilts, however *SLC2A3* mRNA was very abundant in LE at the tips of the uterine villi on Day 60 of pregnancy (Figure 6 and Figure 2 (Kramer et al., 2020)). Expression of *SLC2A3* mRNA by trophectoderm was detected as early as Day 15 and expression was maintained in the chorion through Day 85 of pregnancy. Expression of *SLC2A3* mRNA was greater in the areolae than in inter-areolar regions of the chorion between Days 40 and 85 of pregnancy. Endometrial expression of *SLC2A3* mRNA was barely detectable in gilts treated with either E2 or P4 (Figure 6).

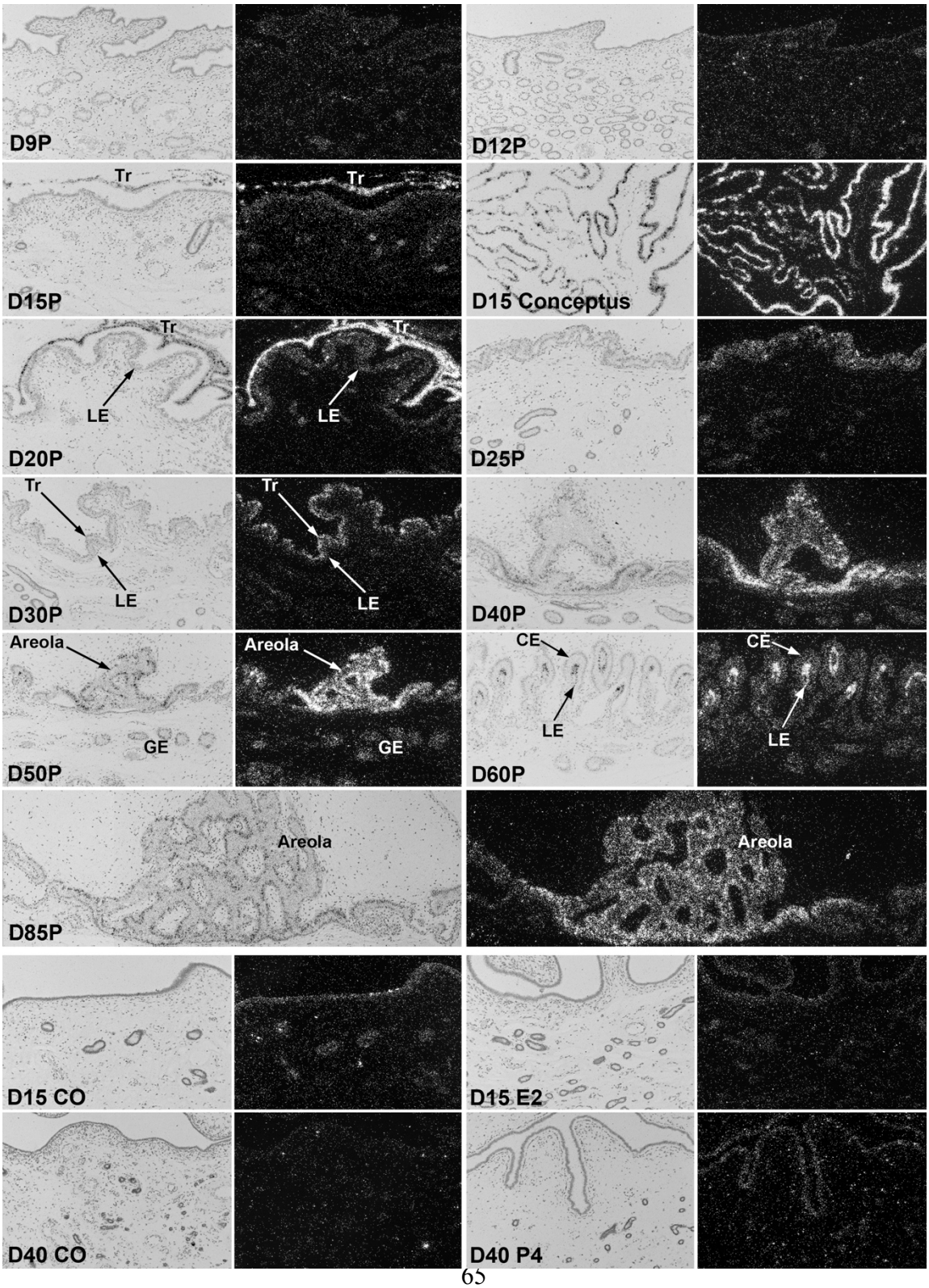
D9P
D12P
Tr
D15P
D15 Conceptus
LE
D20P
D25P
D30P
D40P
Areola
GE
D50P
CE
D60P
D85P
D15 CO
D15 E2
D40 CO
D40 P4

Figure 6. Cell-specific localization of SLC2A3 mRNA in endometria and placentae. Corresponding brightfield and darkfield images from *in situ* hybridization demonstrate low endometrial expression of *SLC2A3* mRNA in the endometrium during the estrous cycle and pregnancy. However, there was abundant expression of *SLC2A3* mRNA in the trophectoderm on Day 15 of pregnancy, which was maintained in the chorion and areolae through Day 85 of pregnancy. Width of fields is 870 μm. The D15 Conceptus Sense panel in Supplemental Figure 1 (Kramer et al., 2020) is the negative control. Legend: D, Day; P, pregnancy; LE, luminal epithelium; GE, glandular epithelium; Tr, trophectoderm; CE, chorionic epithelium.

SLC2A4 mRNA is Expressed Weakly in Endometria and Localizes to the Uterine LE

Endometrial expression of *SLC2A4* mRNA was less than for the other three *SLC2A* genes studied and was not affected by day, status, or day by status interaction during the estrous cycle or the peri-implantation period of pregnancy ($p>0.05$) (Figure 7 (Kramer et al., 2020)). Endometrial expression of *SLC2A4* mRNA was not different between Days 9 and 85 of pregnancy ($r^2=0.0014$; $p<0.05$) and placental expression of *SLC2A4* mRNA was not different between Days 30 and 85 of pregnancy ($r^2=0.019$; $p<0.05$) (Figure 7). Expression of *SLC2A4* mRNA decreased in endometria of gilts in response to both E2 and P4 ($p<0.05$) (Figure 7).

Endometrial expression of *SLC2A4* mRNA was barely detectable by *in situ* hybridization analysis between Days 9 and 12, but was detectable in uterine LE by Day

15 in cyclic and pregnant gilts (Figure 8). Expression of *SLC2A4* mRNA by uterine LE was maintained through Day 40 of gestation, and appeared to increase in expression in uterine GE on Day 30. Placental expression of *SLC2A4* mRNA was barely detectable by *in situ* hybridization analysis. There was an apparent increase of *SLC2A4* mRNA in uterine LE, but a decrease in expression in GE of both E2- and P4-treated gilts (Figure 8). Since the uterine GE represents a greater percentage of cells in endometrial tissue, the decrease in steady-state levels of endometrial *SLC2A4* mRNA in E2- and P4-treated gilts (Figure 8) is not surprising.

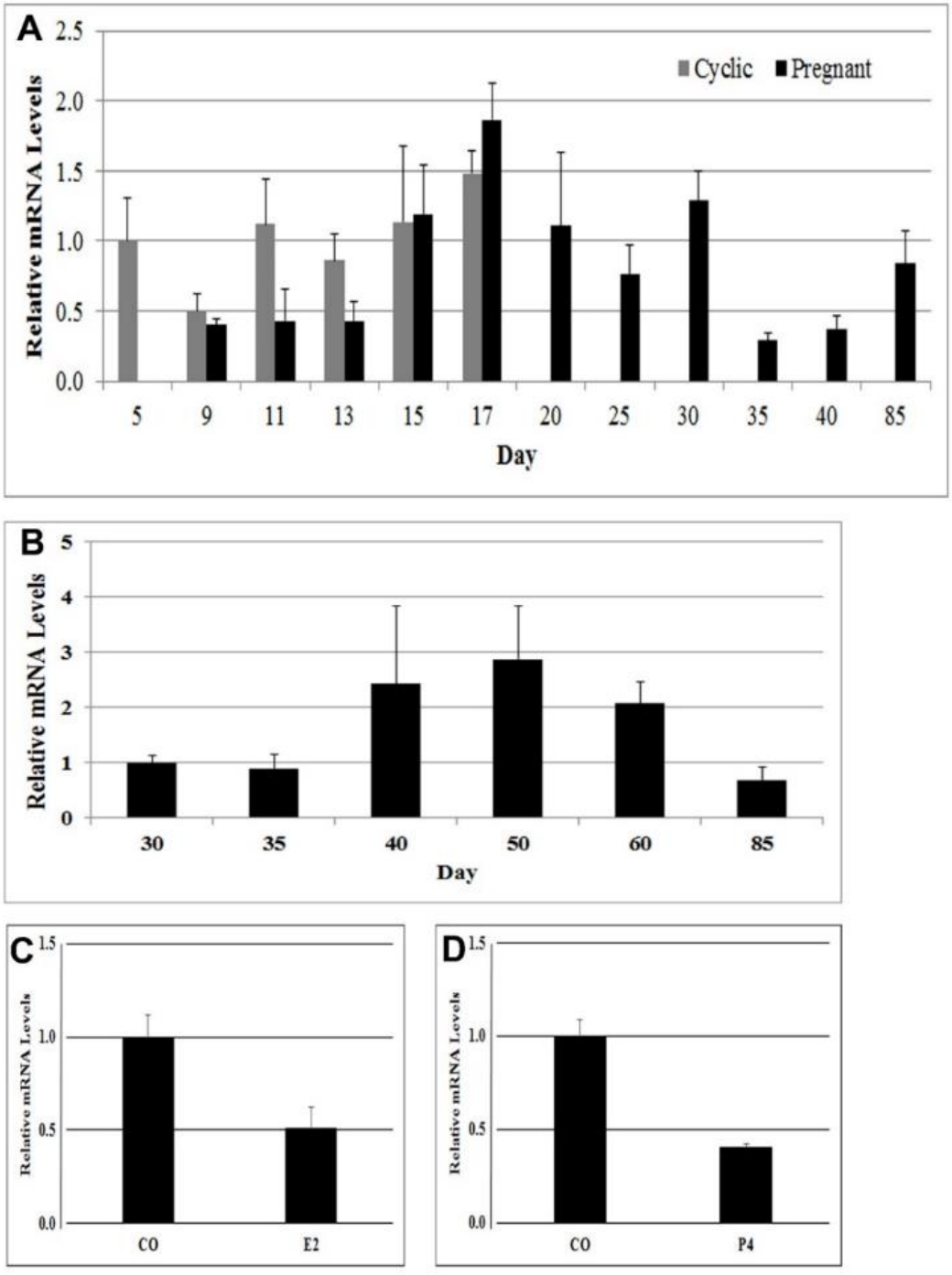

Figure 7. Expression of SLC2A4 mRNA in endometria and placentae. (A) Endometrial and (B) placental expression of SLC2A4 mRNA was not affected by day of

the estrous cycle or pregnancy ($p>0.05$). (C,D) Endometrial expression of SLC2A4 mRNA decreased in response to E2 and P4 ($p<0.05$). Values presented are means ± SEM and $p<0.05$ is significant.

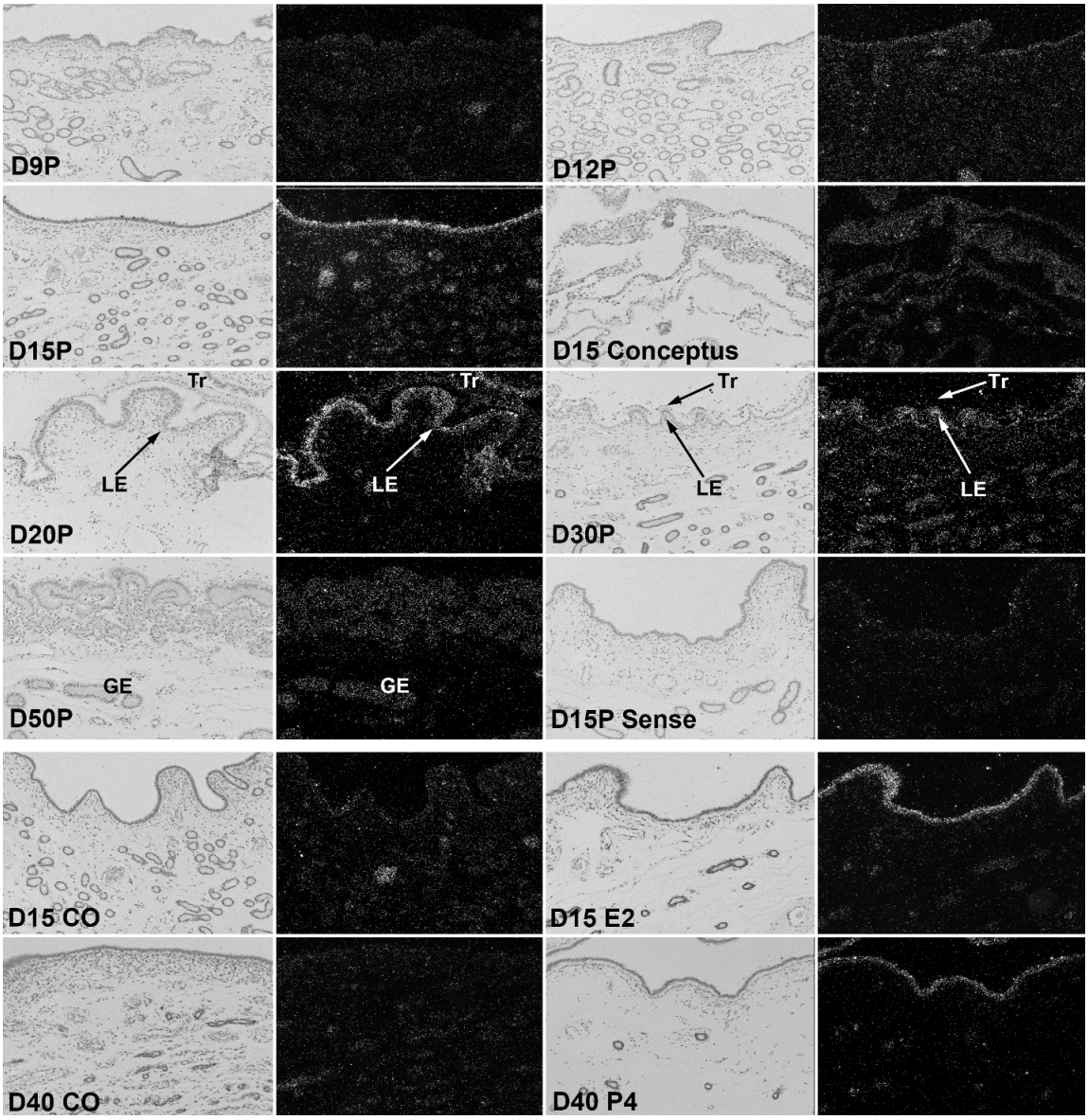

Figure 8. Cell-specific localization of SLC2A4 mRNA in endometria and placentae. Corresponding brightfield and darkfield images demonstrate SLC2A4 mRNA in uterine LE on Day 15 of the estrous cycle and pregnancy and in uterine LE through Day 50 of pregnancy. SLC2A4 mRNA localized to the uterine LE in response to both E2 and P4. Width of fields is 870 μm. The D15P Sense panel is the negative control. Legend: D, Day; P, pregnancy; CO, corn oil; E2, Estrogen; P4, progesterone; LE, luminal epithelium; Tr, trophectoderm.

SLC2A mRNAs Localize to Endometrial and Placental Endothelia

In addition to being expressed in epithelia at the uterine-placental interface, *SLC2A* transporter mRNAs were expressed in endothelial cells of blood vessels in both endometrial and placental tissues. The presence of *SLC2A* transporters in endothelial cells is important for movement of glucose out of and into the endometrial and placental vasculatures, respectively. *In situ* hybridization demonstrated that *SLC2A1* mRNA was expressed in both endometrial and placental endothelia (Figure 9). *SLC2A3* and *SLC2A4* mRNAs were also present in endometrial and placental endothelia, although expression was lower than for *SLC2A1*. *SLC2A4* mRNA appears to have greater expression in the placental endothelium than in the endometrial endothelium (Figure 9).

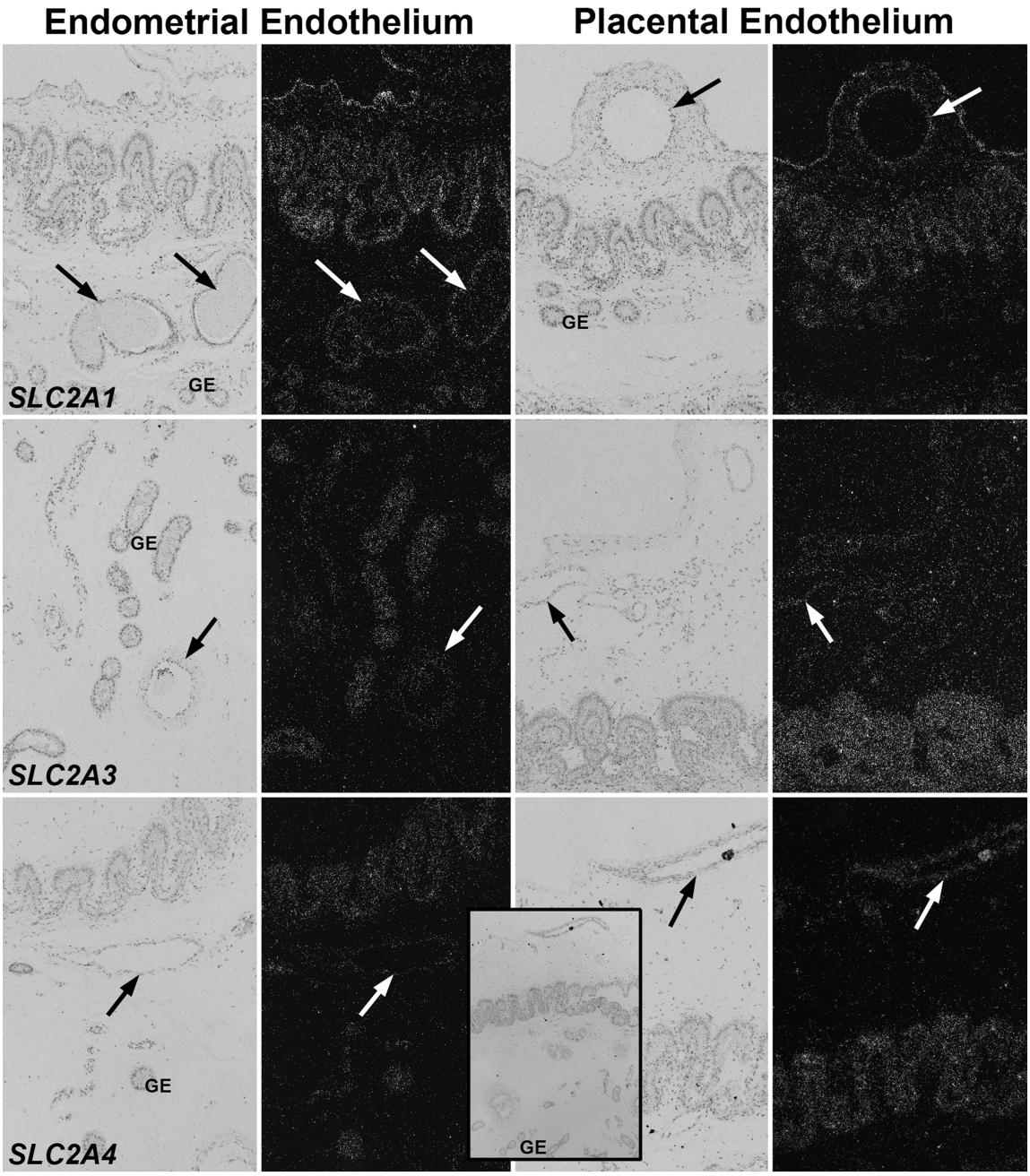

Figure 9. SLC2A transporter mRNAs localize to the endometrial and placental endothelial. Corresponding brightfield and darkfield images from *in situ* hybridization analyses demonstrate *SLC2A1*, *SLC2A3*, and *SLC2A4* mRNAs in endothelia of

endometrial and chorioallantoic blood vessels, which would allow movement of glucose out of and into the respective endometrial and placental vasculatures. All sections are oriented so that placental tissue is at the top and endometrial tissue is at the bottom of the panel. Note the typical folding of the interface between endometrial LE and chorion which is the demarcation between placental and endometrial tissue. Arrows indicate mRNA expression by blood vessels. Height of fields is 870 μm. Legend: LE, luminal epithelium; GE, glandular epithelium.

SLC2A mRNAs Localize to Areolae and the Allantoic Epithelium

In situ hybridization demonstrated that *SLC2A1*, *SLC2A3*, and *SLC2A4* mRNAs were expressed in areolae, but *SLC2A3* appeared to have the highest expression in areolae (Figure 10). The allantoic epithelium also expressed *SLC2A1*, *SLC2A3*, and *SLC2A4* mRNAs (Figure 10).

SLC2A1 Protein Localizes in a Complex Pattern Along the Uterine-Placental Interface by Mid-Pregnancy

Immunohistochemical analysis showed that SLC2A1 protein was not detected in endometrium from Day 11 of pregnancy, but SLC2A1 expression was observed in endometrial LE and blood vessels by Day 13. SLC2A1 protein continued to be expressed by LE in all regions of the uterine-placental interface except at sites of areolae through Day 60 of pregnancy (Figure 11). SLC2A1 protein was highly expressed in the chorionic

epithelium (CE) by Day 60 of pregnancy except at the tips of uterine-placental folds extending into the allantois and in areolae (Figure 11). SLC2A1 protein was also detected in the allantoic vasculature and allantoic epithelium (Figure 11).

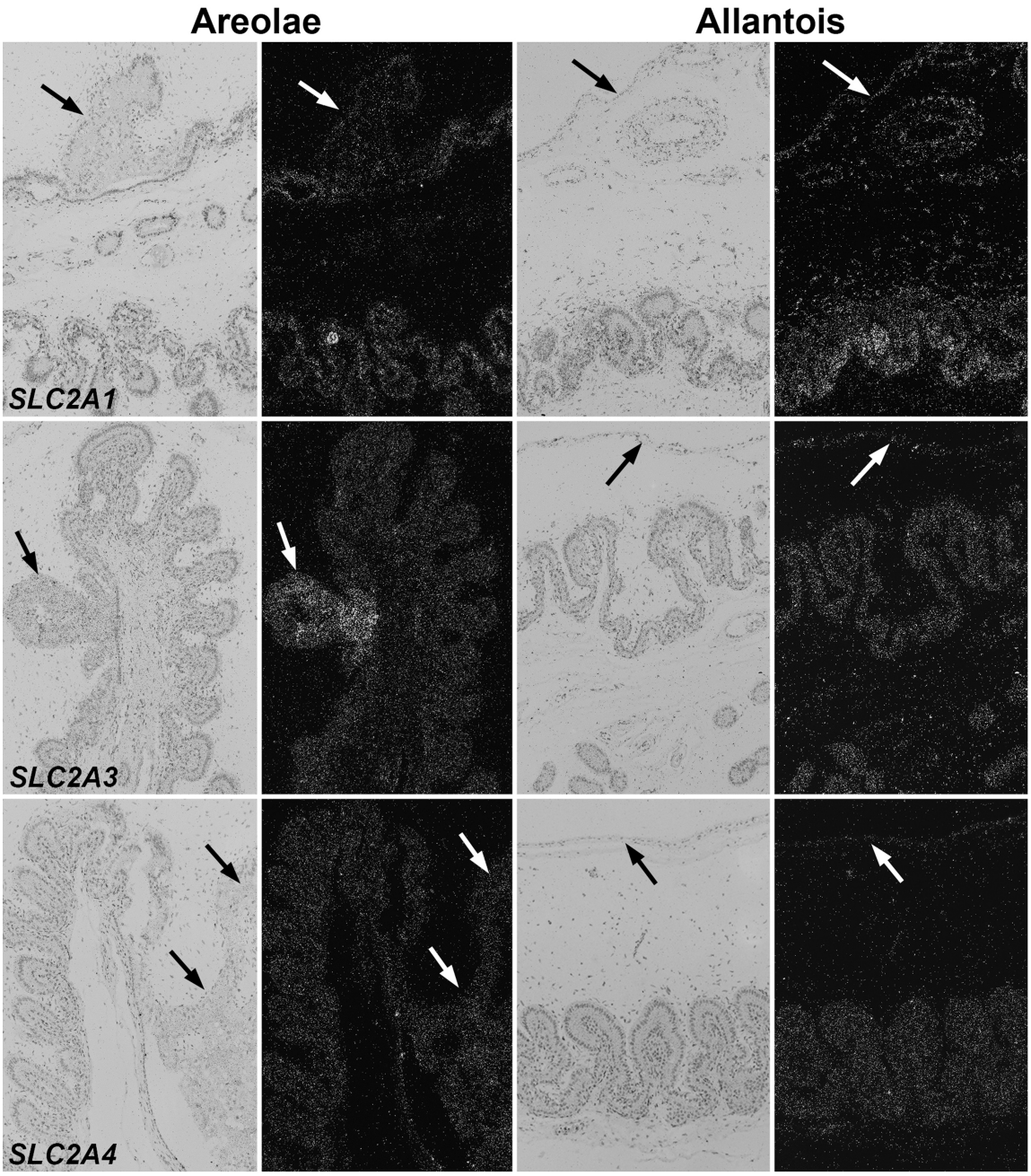
Areolae
Allantois
SLC2A1
SLC2A3
SLC2A4

Figure 10. SLC2A transporter mRNAs localize to areolae and allantoic epithelia. Corresponding brightfield and darkfield images from *in situ* hybridization analyses demonstrate *SLC2A1*, *SLC2A3*, and *SLC2A4* mRNAs in the chorionic epithelium of areolae and in the allantoic epithelium. Expression of *SLC2A3* mRNA was greater in areolar than in inter-areolar chorion. Arrows indicate areolae and allantoic epithelium. Note the typical folding of the interface between endometrial LE and chorion, which is the demarcation between placental and endometrial tissue. Height of fields is 870 μm.

Discussion

Results of this study indicate differential temporal and spatial expression, localization, and hormonal regulation of the facilitative diffusion glucose transporters SLC2A1, *SLC2A2*, *SLC2A3*, and *SLC2A4* at the uterine-placental interface of pigs during pregnancy (see Figure 9 and Figure 10). The localization of these transporters indicates that glucose can be transported from maternal blood across the endometrial epithelia by SLC2A1, and then through the chorioallantois to fetal-placental blood by SLC2A3. This is demonstrated by comparing the *in situ* hybridization panels representing Day 20 of pregnancy in Figures 3 and 5. The SLC2A transporters are necessary to transport glucose required for survival and development of the conceptus are upregulated by E2 from the conceptus trophectoderm, and P4 from the maternal ovary, indicating that glucose transport is dependent on steroid hormones during pregnancy in pigs. Once delivered to the conceptus, glucose and fructose are metabolized through glycolysis in support of

placental and fetal development during pregnancy in pigs. As placentation progresses, the individual temporal and spatial patterns of expression of the SLC2A transporters suggest that each SLC2A transporter, and the specific cell type that expresses each SLC2A transporter, have unique roles in glucose and fructose transport from the mother to the conceptus.

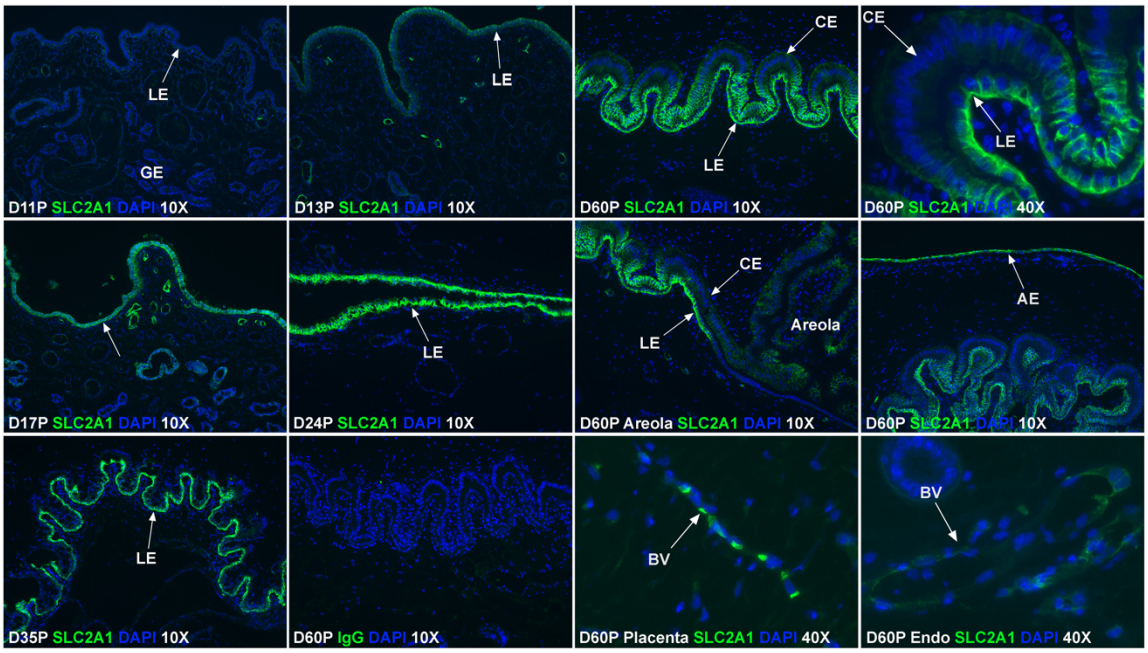

Figure 11. Cell-specific expression of SLC2A1 protein in endometria and placentae. Immunofluorescence microscopy for SLC2A1 protein in uterine and uterine-placental tissues from Day (D) 11 to Day 60 of pregnancy (P) illustrate localization of protein (green fluorescence) to the uterine LE, placental chorionic epithelium (CE), blood vessels (BV) and allantoic epithelium (AE). Note the lack of immunostaining in the tall columnar cells of the chorionic epithelium and areolae by Day 60 of gestation. Width of fields at 10X magnification is 870 μm and at 40X magnification is 230 μm. The nuclei are stained blue

with DAPI for histologic reference. A Day 60 section exposed to irrelevant rabbit IgG (bottom row, second panel is the negative control. Legend: Ge, glandular epithelium.

There is an abundance of information on glucose metabolism during late gestation in pigs and sheep, but little is known about the roles of glucose and fructose metabolism during the peri-implantation period of pregnancy in pigs. Preimplantation embryos/blastocysts of pigs, sheep, cattle, and mice metabolize glucose, and results of the present study indicate that conceptuses of pigs also metabolize glucose as they elongate and attach to the uterine LE for implantation (Ka, 2007; Ross 2007). This study is the first to demonstrate a functional role for the metabolism of fructose by porcine conceptuses. However, Kim et al. (2012) utilized an established porcine trophectoderm cell line to show that fructose stimulates cell proliferation by activating the mechanistic target of rapamycin (MTOR) cell signaling and glycosaminoglycans by way of the hexosamine biosynthetic pathway (Geisert et al., 1994). In addition, we reported that the fructose transporters SLC2A5 and SLC2A8 are present at the uterine-placental interface, and along with the present results, suggest that fructose plays a critical role in the growth and development of porcine conceptuses (Steinhauser et al., 2016). Our results also demonstrate that glucose is preferentially metabolized over fructose. However, fructose may still play a large role in supporting conceptus development due to the fact that fructose cannot be transported from the conceptus back to the mother and therefore is essentially sequestered within the intrauterine environment for access to conceptuses (Kim et al., 2012). This is important because fructose, in addition to glucose, can enter and be metabolized via the glycolytic

branching pathways when there is limited glucose availability (Park et al., 2017) or under hypoxic conditions (Park, 2017).

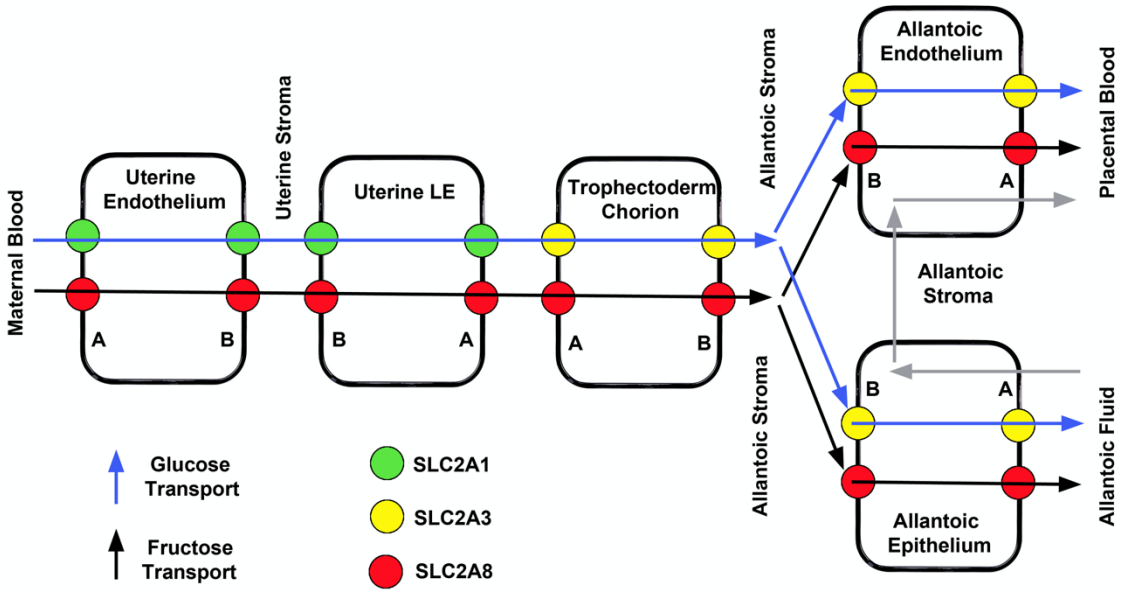

Figure 12. A model for glucose and fructose transport from maternal to placental vasculatures in pigs.

In an epitheliochorial placenta, glucose and fructose are transported from the maternal vasculature to the placental vasculature through multiple cell layers that comprise the uterine-placental interface. Movement of glucose fructose requires SLC2A transporters (ovals) on the apical (A) and basolateral (B) surfaces of each cell. Starting from the maternal blood, glucose and fructose are transported through an endothelium and into the uterine LE. The endothelial cells of the vasculature and the LE are in close proximity to facilitate this transport of glucose and fructose. Glucose and fructose then transported out

of the uterine LE and into the trophectoderm/chorion. Close proximity of the placental vasculature then facilitates movement of glucose and fructose from the trophectoderm/chorion, through the placental endothelium, and into the placental vasculature for use by the placenta and fetus. Glucose and fructose can also be transported into and out of the allantoic fluid through the allantoic epithelium. The arrows depict the direction of glucose and fructose movement.

Figure 12 is a model depicting the multiple cell layers at the uterine-placental interface in pigs where transporters are located in a cell-specific manner to effectively transport glucose and fructose from mother to conceptus. The present results, together with the previously published localization of the fructose transporter SLC2A8, indicate that the endometrial endothelium expresses SLC2A1, which can transport glucose out of the maternal vasculature (Steinhauser et al., 2016). The uterine LE expresses SLC2A1 and *SLC2A4*, although SLC2A1 expression is greatest. This is not surprising as *SLC2A4* is insulin dependent. The conceptus removes glucose from the maternal blood continually, not just after meals, so having SLC2A1 as the prominent isoform would result in a more continuous movement of glucose into the conceptus. Early in pregnancy, the trophectoderm expresses *SLC2A1* and *SLC2A3*, but as pregnancy progresses, *SLC2A3* becomes the predominant SLC2A transporter in the chorion. The placental allantoic endothelium expresses SLC2A1 for transport of glucose into the placental circulation. Finally, the allantoic epithelium expresses *SLC2A3,* which would allow for movement of

glucose either into or out of the glucose-rich allantoic fluid (Bazer et al., 1988). Previously published localization of the fructose transporter SLC2A8 has demonstrated that SLC2A8 is expressed by uterine endothelial cells, uterine LE, trophectoderm/chorion, allantoic endothelium and allantoic epithelium (Johnson et al., 2000).

SLC2A1 and *SLC2A3* are the prominent glucose transporters in the pig uterus and placenta, respectively, similar to that for mice and humans (Frolova and Moley, 2011a; Jansson et al., 1995). SLC2A1 is the most abundant glucose transporter in the endometrium of most mammals studied, but the cell-specific localization of the transporter differs (Frolova and Moley, 2011c; Gao et al., 2009a; Korgun et al., 2001; von Wolff et al., 2003). In mice and humans, *SLC2A1* is more abundant in uterine stromal cells than epithelia, especially as decidualization progresses, while in the pig, SLC2A1 localizes to the uterine LE. These differences in cell-specific localization of this glucose transporter may be explained by major differences in types of implantation and placentation among species. The invading mouse and human blastocysts are supported by the decidualizing stromal cells immediately surrounding them, while the free-floating pig conceptuses must rely on molecules secreted or transported by uterine LE and GE into the uterine lumen during the peri-implantation period of pregnancy. After firm attachment of the conceptus to the uterine LE, the pig placenta continues to rely on hemotrophic support relayed through the uterine LE and histotrophic support from uterine GE via the areolae. In both cases, it is the uterine epithelia that are directly associated with the chorionic epithelium of the placenta.

Pig conceptuses remain free-floating within the uterine lumen for a protracted period of time prior to implantation as compared to those in humans and rodents. Results of the present study indicate that expression of *SLC2A1* is up-regulated in uterine LE by E2 and P4 during this crucial period and the uterine LE is likely responsible for glucose transport into the uterine luminal fluid. In the pig, the corpora lutea can be maintained without any conceptuses present in the uterine horns, a state of pseudopregnancy, when injections of exogenous E2 are administered daily between Days 11 to 14 of the estrous cycle to mimic the maternal recognition of pregnancy signal (Geisert et al., 1987). However, when estrogen synthesis by the conceptus was ablated by targeting the aromatase (CYP19A1) gene utilizing CRISPR/Cas9 genome editing technology, the role of E2 was brought into question as to its role in support of pre-implantation conceptus development, conceptus elongation and CL maintenance. However, E2 was essential for maintenance of pregnancy beyond 30 days and its ablation disrupted a number of biological pathways (Meyer et al., 2019). Indeed, in addition to pregnancy recognition, conceptus estrogens modulate uterine gene expression (Geisert et al., 1994; Johnson et al., 2009; Waclawik et al., 2017). The present results clearly show that E2 upregulates expression of *SLC2A1* mRNA in the uterine LE of pseudopregnant gilts, suggesting that estrogens, secreted by conceptuses, increase expression of this key glucose transporter in the endometrium. Previous studies revealed that conceptus E2 upregulates multiple genes in the endometrial LE between Days 12 and 15 of pregnancy, as was *SLC2A1* mRNA in this study (Joyce et al., 2007; Ka et al., 2007; Ross et al., 2007; White et al., 2005).

When exogenous P4 was administered to ovariectomized gilts, there was upregulation of *SLC2A1* mRNA in the uterine LE and GE that respond to P4 yet do not express the nuclear P4 receptor (PGR) at this stage of gestation (Geisert et al., 1994; Steinhauser et al., 2017a). Therefore, it is reasonable to hypothesize that P4 induces *SLC2A1* mRNA expression in uterine LE, while E2 amplifies this expression. A similar physiology has been demonstrated for sheep as expression of *SLC2A1* mRNA is upregulated by P4 and enhanced by interferon tau (IFNT), the pregnancy recognition signal in sheep (Gao et al., 2009a). In both pigs and sheep P4 induces *SLC2A1* mRNA for glucose transport, and its expression is increased by a conceptus-secreted signal. Regardless of whether a steroid hormone (E2) or a cytokine (IFNT) enhances expression of *SLC2A1* mRNA, the finding that both species use this mechanism suggests that *SLC2A1* is a particularly important glucose transporter for conceptus growth and development in species with a protracted period of conceptus development prior to implantation. Interestingly, the expression of *SLC2A1* mRNA by GE was not upregulated by E2, but was increased by P4. This indicates a differential mechanism for regulation of *SLC2A1* expression by the two epithelia.

The trophoblast cells of most mammalian species studied predominantly express the glucose transporter *SLC2A3*. In rodents and humans, expression is high during the first trimester, but decreases with advancing stage of gestation, while in the pig, *SLC2A3* appears to be the predominant transporter of glucose by the trophectoderm/chorion throughout pregnancy (Brown et al., 2011; Ganguly et al., 2007; Hahn et al., 2001).

Similar to the endometrium, differences in expression of *SLC2A3* over time, and among species, can be attributed to different types of implantation and placentation. During the first trimester of pregnancy in the mouse and human, the conceptus establishes connections with the maternal vasculature, but until this is firmly established, glucose has to be efficiently accrued from the surrounding decidualized stroma. In contrast, the pig conceptus never develops an intimate contact with the maternal vasculature, since it develops an epitheliochorial placenta and, therefore, must maximize the efficiency of glucose transport throughout pregnancy.

By Day 24 of pregnancy in pigs, there is attachment between the apical surfaces of uterine LE and conceptus trophectoderm, and these adhered epithelia begin to fold around Day 30 to increase surface area for hemotrophic transport of nutrients (Friess et al., 1980). At the tops of the uterine folds that extend into the chorioallantois placenta, the chorionic epithelial cells are tall columnar, and the maternal and placental vasculatures are within 2 micrometers of each other, the closest that they are at any time during pregnancy (Friess et al., 1980). Additionally, the maternal and fetal capillaries are arranged in a cross-countercurrent manner on opposite sides of the adhered, folded epithelia. If the fetal side of the placenta is "up", then maternal blood enters at the top of the folds and exits at the bottom. In contrast, the placental blood enters at the bottom of the folds and exits at the top (Leiser and Dantzer, 1988). This arrangement allows for optimum transport of nutrients, especially those dependent on concentration gradients, such as glucose, from mother to fetus. It is noteworthy that SLC2A expression is unique

at the tops of these folds. By Day 60 of pregnancy: (1) *SLC2A3* mRNA is downregulated in the chorionic epithelium across the length of the folds; (2) *SLC2A3* mRNA, normally limited to expression in the placenta, is expressed in the uterine LE at the tops of the folds adjacent to the chorionic tall columnar cells; (3) SLC2A1 protein, although expressed by the remainder of the chorionic epithelium lining the folds, is not expressed by the tall columnar cells at the top of the folds; and (4) SLC2A8 protein, as previously reported (Geisert et al., 1994), is expressed by the chorionic epithelium, but only in the tall columnar cells at the top of the folds (see Figure 13).

A similar unique pattern of expression for the SLC2A transporters is observed in areolae. In the pig, beginning around Days 15-17, areolar structures form over the mouths of endometrial glands to transport large amounts of histotrophic nutrients from the uterine GE into the specialized microvasculature on the placental side of areolar chorion cells. The blood supply to the folds of the wall of the areolae form a ring towards the periphery and the areolar capillaries converge into one or two stem veins indicating facilitated external inflow of blood into the areola and outflow in a manner different from that of the inter-areolar regions. This anatomy allows areolae to transport glandular secretions such as macromolecules, particularly proteins, by fluid-phase pinocytosis across the placenta and into the fetal-placental circulation. The chorionic epithelium lining these areolae are tall columnar cells, and areolae are in optimal locations to move glucose from the uterine GE to the placental vasculature (Leiser and Dantzer, 1994; Renegar et al., 1982). By Day 60 of pregnancy: (1) *SLC2A3* mRNA, although downregulated in the chorionic epithelia

lining the uterine-placental folds, is expressed in the chorionic epithelial cells of the areolae; (2) SLC2A1 protein is not expressed by the tall columnar chorionic epithelial cells of the areolae; and (3) SLC2A8 protein, as previously reported (Johnson et al., 2000), is expressed by the chorionic epithelium of the areolae (see Figure 10).

SLC2A1 is a transporter responsible for the basal uptake of glucose into most cells, whereas SCL2A3 is a high affinity and high capacity glucose transporter, and SLC2A8 is a high affinity glucose transporter that can also transport fructose. Therefore, the results, summarized in the previous two paragraphs, provide evidence that expression of SLC2A1, *SLC2A3*, and SLC2A8 is precisely regulated in a spatial-temporal pattern along the uterine-placental interface of pigs, and that expression of SLC2A1 is replaced by *SLC2A3* and SLC2A8 at the tops of uterine folds and in areolae to maximize potential glucose and fructose transport to the pig conceptus (see Figure 10).

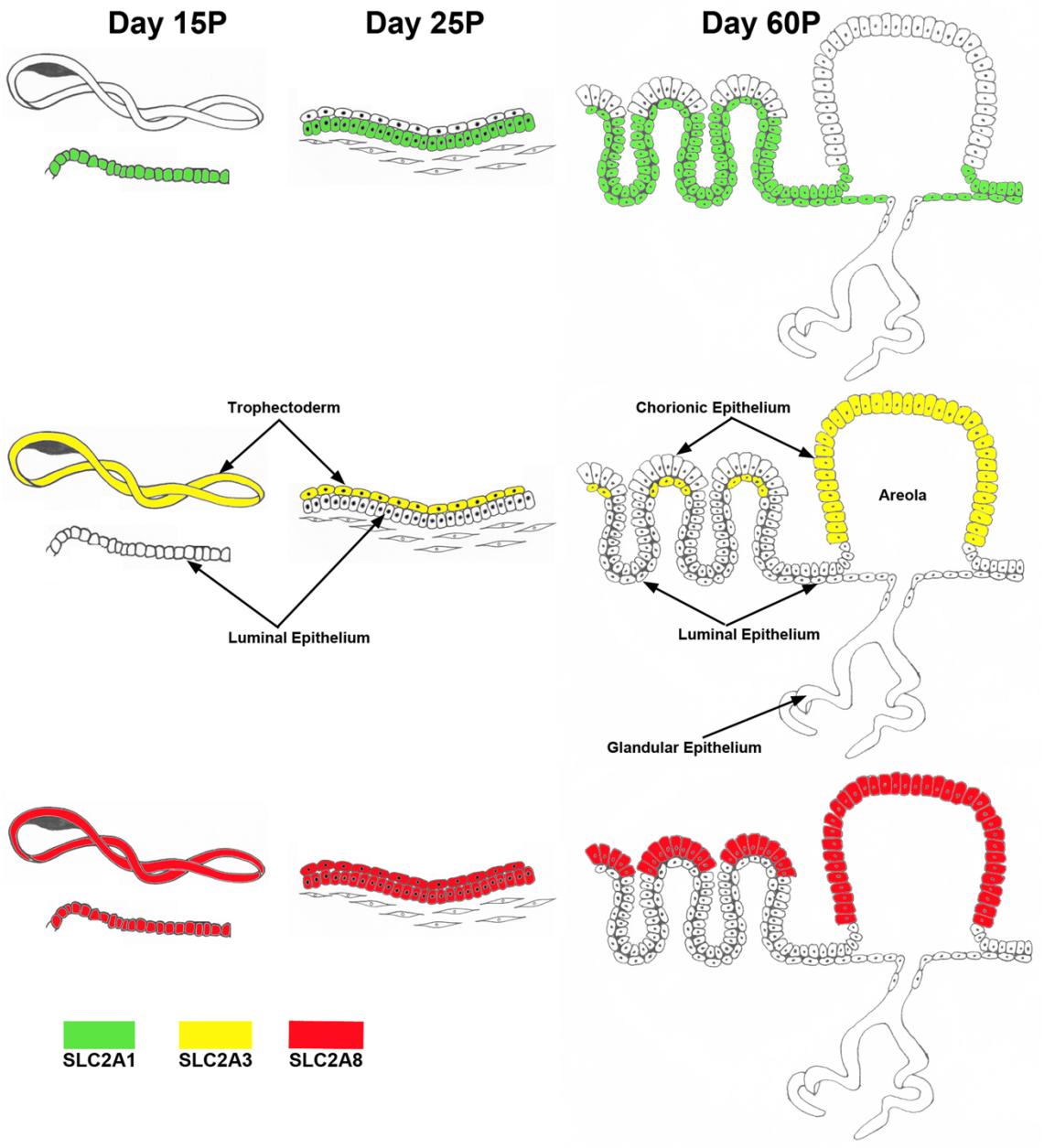

Figure 13. Model illustrating the spatial-temporal pattern of the transporters SLC2A1 (green), SLC2A3 (yellow), and SLC2A8 (red) along the uterine-placental interface of pigs at day 15, 25, and 60 of gestation.

SLC2A1 is a transporter responsible for the basal uptake of glucose into most cells, whereas SCL2A3 is a high affinity and high capacity glucose transporter, and SLC2A8 is a high affinity glucose transporter that can also transport fructose. Therefore, the results, summarized in the previous two paragraphs, provide evidence that expression of SLC2A1, *SLC2A3*, and SLC2A8 is precisely regulated in a spatial-temporal pattern along the uterine-placental interface of pigs, and that expression of SLC2A1 is replaced by *SLC2A3* and SLC2A8 at the tops of uterine folds and in areolae to maximize potential glucose and fructose transport to the pig conceptus

Once glucose is transported across the chorion by *SLC2A3*, transporters must be strategically placed to move glucose into the placental vasculature and into the allantoic cavity which is filled with a hypotonic solution composed of electrolytes, sugars, proteins, and water that are of maternal and fetal origin, and which provide a nutrient reservoir for the fetus (Aherne et al., 1969; Wu et al., 1995). Glucose and fructose are found in substantial amounts in allantoic fluid and, therefore, must be transported through the allantoic epithelium into the vascular system. Results of the present study indicate that SLC2A1 protein, and *SLC2A3* and *SLC2A4* mRNAs localize to the placental endothelium, although SLC2A1 appears to be the most abundant transporter in this cell type. Further, SLC2A1*, SLC2A3,* and *SLC2A4* have the potential to transport glucose through the allantoic epithelium.

CHAPTER IV

PORCINE CONCEPTUSES UTILIZE THE PENTOSE PHOSPHATE PATHWAY TO SUPPORT DEVELOPMENT DURING THE PERI-IMPLANTATION PERIOD OF PREGNANCY

Introduction

About 60% of all pig pregnancies result in pregnancy loss. During this time period, pig conceptuses (embryos and associated placental membranes) undergo extensive morphological changes, transforming from a spherical shape into a tubular and finally a filamentous form. Following elongation, the conceptus begins to attach to the uterine luminal epithelium (LE), initiating placentation (Bazer and Johnson, 2014). This rapid growth and remodeling of the free-floating pig conceptuses requires extensive proliferation, cellular remodeling, and migration of trophectoderm (Tr) cells. Because the conceptuses have not yet established a placental connection to the LE, they must rely on limited nutrients present within the uterine lumen to perform these cellular processes which require significant amounts of energy. In response, the uterine LE and glandular epithelium (GE) secrete histotroph, a complex mixture of sugars, amino acids, hormones, and cytokines, to support conceptus development (Bebington et al., 1999). Glucose and fructose are major components of histotroph that can potentially be utilized by multiple biosynthetic pathways for the production of ribose, hexosamines, amino acids, nucleotides, and ATP, all of which are required for early conceptus development and

survival. Previous studies have shown that glucose and fructose are present within the uterine lumen of pigs, fructose being the most abundant, with total recoverable hexose sugars increasing from days 12 to 18 of pregnancy. Glucose. These hexose sugars are likely major energy sources for conceptus growth and development (Pere, 2003; White et al., 1979b; Zavy et al., 1982).

Glucose and fructose can be transported by facilitated diffusion transporters of the solute carrier 2A (SLC2A; GLUT) family; and there are 14 members of the SLC2A family capable of transporting glucose and other hexose sugars. Our previous studies showed that SLC2A3 (a high affinity and high capacity glucose transporter) and SLC2A8 (a glucose and fructose transporter) are expressed by the porcine conceptus trophectoderm cells during the peri-implantation period, and that conceptuses are able to metabolize glucose and fructose (Kramer et al., 2020; Steinhauser et al., 2016). However, metabolic pathways activated in the trophectoderm of elongating conceptuses to utilize glucose and fructose remain unknown.

Cellular metabolism is a network of biochemical reactions that primarily occurs through the TCA cycle and oxidative phosphorylation, which are complex, but efficient processes for generating ATP (Wu, 2018). Cells maintaining homeostasis are metabolically distinct from cells undergoing proliferation and differentiation, such as tumor and immune cells. The metabolic demands of proliferating cells are higher than those of cells in homeostasis, requiring the cell to maintain adequate levels of energy stores to support survival, as well as to produce an abundance of biosynthetic intermediates to

support cellular growth and proliferation. Tumor and activated immune cells alter their metabolism by switching from utilization of the TCA cycle and oxidative phosphorylation to aerobic glycolysis. Aerobic glycolysis is a phenomenon also known as the Warburg effect, where glycolysis occurs even in the presence of oxygen (Warburg, 1956; Warburg et al., 1927). In normal tissues, glycolysis is a physiological response to hypoxia, however in the 1920s Otto Warburg first observed that cancer cells were utilizing more glucose than normal control cells and were producing lactate regardless of the oxygen availability (Warburg et al., 1927). The generation of lactate from pyruvate leads to the regeneration of NAD^+ allowing for glycolysis to be maintained through maintenance of the NAD^+/NADH redox balance. Since Warburg's observations of glycolysis in cancer cells, enhanced glycolysis has also been observed in rapidly proliferating cells such as immune cells (Brand, 1985; Hedeskov, 1968; Hume et al., 1978; Wang et al., 1976). One requirement of rapidly proliferating cells is energy. While glycolysis is an inefficient way to generate ATP compared to oxidative phosphorylation, ATP production through glycolysis is faster and preferentially used to meet the high ATP demands of proliferating cells (Pfeiffer et al., 2001). In addition to faster ATP production, glycolysis is able to maintain the production of glycolytic intermediates to support the metabolic demands of proliferating cells though the biosynthesis of nucleotides, amino acids, and fatty acids (Hume and Weidemann, 1979; Vander Heiden et al., 2010). Tumor and other proliferating cells appear to utilize glucose by shunting it into the branching pathways to provide glycolytic intermediates necessary to support their proliferation.

An important pathway that branches from glycolysis is the Pentose Phosphate Pathway (PPP), which converts the intermediate glucose-6-phosphate (G6P) to ribose-5-phosphate (R5P) and NADPH. These two metabolites are essential for the proliferation and survival of cells. R5P is a nucleotide building block and is involved in nucleotide synthesis. While NADPH is important for the synthesis of non-essential amino acids, fatty acids, sterols, and nucleotides (Patra and Hay, 2014; Wamelink et al., 2008). Therefore, we hypothesized that the Tr cells of porcine conceptuses utilize glucose and fructose within the uterine lumen via the glycolytic biosynthetic pathway, and accumulating glycolytic intermediates are shunted into the PPP for the *de novo* synthesis of nucleotides. In this study, we aimed to: (1) determine whether aerobic glycolysis occurs in the elongating conceptuses of pigs; (2) determine whether conceptus tissues express the enzymes required for entry into the PPP; and (3) use isotope-labeled glucose and fructose to determine the flux of these hexose sugars into the PPP.

Materials and Methods

Animals and tissue collection

Sexually mature, 8-month-old crossbred gilts were observed daily for estrus (day 0) and exhibited at least 2 estrous cycles of normal duration (18 to 21 days) before being used in these studies. All experimental and surgical procedures were in compliance with the Guide for Care and Use of Agricultural Animals in Teaching and Research, and approved by the institutional animal care and use committee of Texas A&M University.

To evaluate oxidation of glucose and fructose, gilts were bred naturally to boars with proven fertility, euthanized, and ovariohysterectomized on day 15 (n = 4 litters) and day 16 (n = 4 litters) of pregnancy, and conceptuses collected by flushing the uterine lumen with 40 mL physiological saline. The isolated conceptus tissues were washed 3 times with oxygenated (95% O_2 + 5% CO_2) Krebs-Henseleit bicarbonate buffer (119 mM NaCl, 4.8 mM KCl, 1.2 mM $MgSO_4$, 1.2 mM KH_2PO_4, and 25 mM $NaHCO_3$, pH 7.4) containing 20 mM Hepes (pH 7.4) and 1 mM glutamate, and then used immediately in the experiments.

To evaluate the effects of pregnancy on expression of G6PDH mRNA and protein, PCNA protein and LDHA protein in concepts trophectoderm. Gilts in the pregnant group were bred naturally to boars with proven fertility. Pregnant gilts were euthanized on either day 11, 13, 15, 16, or 17 of pregnancy (n = 3 or 4 gilts/days). The lumen of each uterine horn from days 11 through 17 of pregnancy were flushed with 20 ml physiological saline. Pregnancy was confirmed in the mated gilts by the presence of morphologically normal conceptuses. Tissue sections (uterus or uterus with attached placenta ~1 cm thick) from the middle of each uterine horn of all gilts were fixed in fresh 4% paraformaldehyde in phosphate-buffered saline (PBS) (pH 7.2) and embedded in Paraplast-Plus (Oxford Laboratory).

Oxidation of glucose and fructose in pig conceptuses

To evaluate oxidation of glucose and fructose, conceptus tissues (20 mg) were placed in polypropylene test tubes and incubated with either [1-^{14}C]glucose (0.1 μCi/ml; American Radiolabeled Chemicals Inc), [6-^{14}C]glucose (0.1 μCi/ml), [1-^{14}C]fructose (0.1 μCi/ ml) or [6-^{14}C]fructose (0.1 μCi/ ml) in 1 mL of Krebs-Henseleit bicarbonate buffer containing unlabeled glucose and/or fructose as follows: 1) [1-14C] glucose + 4 mM glucose; 2) [6-14C] glucose + 4 mM glucose; 3) [1-14C]glucose + 4 mM glucose and fructose; 4) [6-14C]glucose + 4 mM glucose and fructose; 5) [1-14C]fructose + 4 mM fructose; 6) [6-14C]fructose + 4 mM fructose; 7) [1-14C]fructose + 4 mM glucose and fructose; or 8) [6-14C] fructose + 4 mM glucose and fructose. After incubation for 2 hours at 37 °C, 0.2 mL of soluene (Perkin-Elmer) was injected through the rubber cap into a suspended cup inside the tube, and 0.2 mL of 1.5 M $HClO_4$ acid was injected into the medium to liberate $^{14}CO_2$. Following the 1-hour incubation, the suspended cups were transferred to scintillation vials containing 5 mL of cocktail. Radioactivity of $^{14}CO_2$ produced from oxidation of glucose and fructose by conceptus tissue were measured using liquid scintillation spectrometry (Perkin- Elmer) (Kim et al., 2012).

Calculation. The medium specific activities of [1-^{14}C]glucose, [6- ^{14}C]glucose, [1-^{14}C]fructose, and [6- ^{14}C]fructose were used to calculate rates of CO2 production. It is assumed that ^{14}CO2 is produced from [1-^{14}C]- glucose via both Krebs cycle and

pentose cycle or from [6-^{14}C]glucose via Krebs cycle, with the difference in $^{14}CO_2$ yield between [1-^{14}C]- glucose and [6-^{14}C]glucose due to pentose cycle activity (Larrabee, 1989, 1990). The difference in $^{14}CO_2$ production between [1-^{14}C]- glucose and [6-^{14}C]glucose was used to estimate the flux from glucose into pentose cycle (Larrabee, 1989, 1990; Wu and Marliss, 1993). The disappearance of unlabeled glucose or fructose from the incubation medium was taken to represent glucose or fructose utilization (Wu, 1996). The percentage of glucose utilized via pentose cycle was calculated by dividing glucose flux by glucose utilization.

RNA extraction, complementary DNA synthesis, and primer design

Total RNA was extracted from trophectoderm tissue samples using Trizol reagent (Life Technologies) according to the manufacturer's recommendations. First strand complementary DNA (cDNA) was synthesized using a Superscript III First Strand Kit (Life Technologies) according to the manufacturer's instructions. First-strand cDNA was diluted 10× in water for the quantitative polymerase chain reaction (qPCR) reaction. Primers for qPCR and in situ hybridization were designed using NCBI Genbank sequences and Primer-BLAST (http://www.ncbi.nlm.nih.gov/). Primers were submitted to BLAST to confirm specificity against the known porcine genome.

Quantitative PCR assays were performed using PerfeCta SYBR Green Mastermix (Quanta Biosciences) in 10-μL reactions with 2.5 μM of each specific primer, on a Roche

480 Lightcycler with approximately 60 ng cDNA per reaction. The PCR program began with 5 minutes at 95 °C followed by 40 cycles of 95 °C denaturation for 10 seconds and 60 °C annealing/extension for 30 seconds. A melt curve was produced with every run to verify a single gene-specific peak. Standard curves using pooled cDNA with 2-fold serial dilutions were run to determine primer efficiencies. All primer correlation coefficients were greater than 0.95 and efficiencies were 95% to 102%. The geometric mean of TATA-binding protein (*TBP*), succinate dehydrogenase complex subunit A flavoprotein (*SDHA*), and beta actin (*ACTB*) was used to normalize endometrial tissue, whereas the geometric mean of TBP, hypo- xanthine phosphoribosyl transferase 1 (*HPRT1*), and tubulin alpha 1B (*TUBA1B*) was used to normalize chorioallantoic tissue (Steinhauser et al., 2017b). The $2^{-\Delta\Delta Ct}$ method was used to normalize data, and fold-changes were subjected to statistical analyses. The primer sequences for G6PDH were, forward 5′-acctacggcaacagatacaagaac-3′ and reverse 5′- gtactggaaccccactctcttca-3′. The primer sequences for Rpl7 were, forward 5′ -aagccaagcactatcacaaggaatac-3′ and reverse 5′ -tgcaacacctttctgacctttgg-3′. The $2^{-\Delta\Delta Ct}$ method was used to normalize data, and fold-changes were subjected to statistical analyses.

Immunofluorescence analysis

Immunoreactive G6PDH protein was localized in paraffin-embedded samples from pregnant pigs using immunofluorescence microscopy. Antigen retrieval was performed using boiling citrate. These sections were then blocked in 10% normal goat

serum diluted in antibody dilution buffer for 1 hour at room temperature. Rabbit anti-G6PDH immunoglobulin G (IgG) (1:100; Abcam; AB76598) or mouse anti-PCNA immunoglobulin G (Abcam; AB29) was added and incubated over- night at 4 °C in a humidified chamber. Normal rabbit IgG (Sigma-Aldrich; I5006) was substituted for primary antibody and served as a negative control. Tissue sections were then washed 3 times for 5 minutes per wash in PBS. Goat anti-rabbit IgG Alexa 488 (Life Technologies; 1:250) was added and incubated for 1 hour at room temperature. Tissue sections were then washed 3 times for 5 minutes per wash in PBS. Slides were counterstained with Prolong Gold Antifade reagent containing DAPI (4′,6-diamidino-2-phenylindole) (Life Technologies) and coverslipped. Images were taken using an Axioplan 2 micro- scope (Carl Zeiss) interfaced with an Axioplan HR digital camera.

Western Blot Analyses

For protein extraction, porcine conceptus tissues were incubated in IP lysis buffer containing complete EDTA-free protease inhibitors (Roche Diagnostics) on ice for 30 min. Tissues were then sheared by pipetting multiple times, and cellular debris was cleared by centrifugation (12,000× *g*, 15 min, 4°C). Protein concentrations were determined using absorbance at 280 nm on a NanoDrop 1000 spectrophotometer (Thermo Scientific). Western blot analyses were performed as described previously (Joyce et al., 2005b). Briefly, proteins (100 μg) were denatured in Laemmli buffer, separated on 100% SDS-PAGE gels, and transferred to nitrocellulose. Blots were blocked in 5% nonfat

milk/TBST (Tris-buffered saline, 0.1% Tween-20) at room temperature for 1 h, incubated with either rabbit anti-G6PDH (Abcam, Waltham, MA, USA; AB76598; 1:2000) or rabbit anti-LDHA (R&D System, Minneapolis, MN, USA; MAB9158; 1:2000), mouse anti-PCNA (Abcam, Waltham, MA, USA; AB29; 1:4000) or normal rabbit IgG or normal mouse IgG (Sigma Aldrich, St. Louis, MO, USA; 1:1000) in 2% nonfat milk/TBST overnight at 4 °C. Blots were then rinsed three times for 10 min each with TBST at room temperature, incubated with goat anti-rabbit IgG horseradish peroxidase conjugate (1:20,000 dilution of 1 mg/mL stock; Kirkegaard & Perry Laboratories, Bethesda, MD, USA), and then rinsed three times for 10 min each with TBST. Immunoreactive proteins were detected using enhanced chemiluminescence (SuperSignal West Pico Luminol System, Pierce Chemical Co., Rockford, IL, USA) according to the manufacturer's recommendations using a FluorChem IS-8800 120 imager (Alpha Innotech, San Leandro, CA, USA). Blots were quantified using AlphaEase FC software (Alpha Innotech).

Statistical analyses

Data for concentrations of lactate and pyruvate were analyzed for effects of day of pregnancy were analyzed by one-way ANOVA. Data for $^{14}CO_2$ produced by day 15 and day 15 conceptuses were analyzed by one-way ANOVA. Data from qPCR for effect of days of pregnancy were subjected to the Students t-test using GraphPad Prism (GraphPad Software, La Jolla, CA). All data are presented as mean ± standard errors of the mean with significance at $P < 0.05$.

Results

Cell Proliferation

Localization of PCNA protein was assessed by immunofluorescence staining on paraffin-embedded uterine cross-sections. PCNA protein is localized to the conceptus Tr cells on day 13 and 15 of pregnancy (Figure 14A). The microvasculature underneath the luminal epithelium (LE) also expresses PCNA protein. Western blot analysis revealed that PCNA protein increases in the conceptus trophectoderm tissues from days 11 to 16 of pregnancy (Figure 14B).

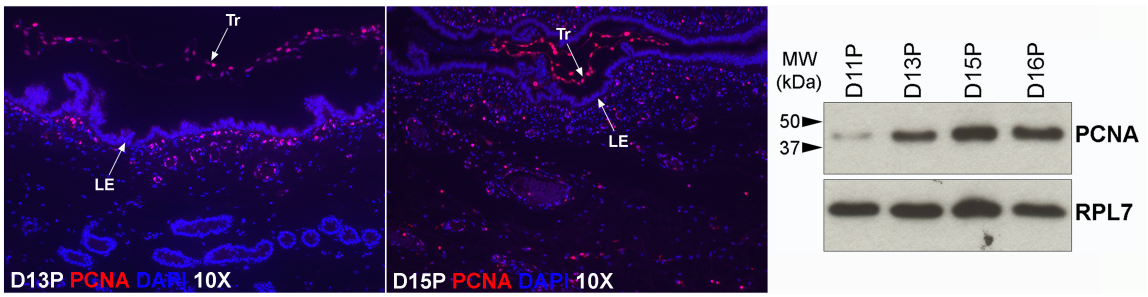

Figure 14. Proliferation of trophectoderm (Tr) cells during the peri-implantation period of pigs. (A) Immunofluorescence staining for proliferating cell nuclear antigen (PCNA; red) at implantation sites in pigs, and (B) Western blot analysis for PCNA in conceptuses of pigs. PCNA expression indicates proliferation of Tr cells in pigs. Nuclei are stained with DAPI for histologic reference. D, Day; P, pregnancy; LE, uterine luminal epithelium; RPL7, ribosomal protein l 7.

Lactate and pyruvate levels

Total recoverable lactate increased in the uterine flushings of pregnant gilts between days 13 and 15 of pregnancy and these levels were maintained from day 15 through 17 (Figure 15A; $P < 0.05$). In addition, lactate and pyruvate concentrations were measured in the medium of day 16 conceptuses cultured with glucose and/or fructose (Figure 15B). Pyruvate concentrations were 0.5 nmol/mg tissue/2h, 1 nmol/mg tissue/2h, and 0.25 nmol/mg tissue/2h when cultured in a medium containing glucose, fructose, and glucose with fructose, respectively. Lactate concentrations in the medium of conceptuses cultured in glucose, fructose, and glucose with fructose were 18 nmol/mg tissue/2h, 10 nmol/mg tissue/2h, and 12 nmol/mg tissue/2h, respectively. Therefore, lactate is increased in the uterine lumen of pig as the conceptuses are elongating, suggesting the presence of aerobic glycolysis.

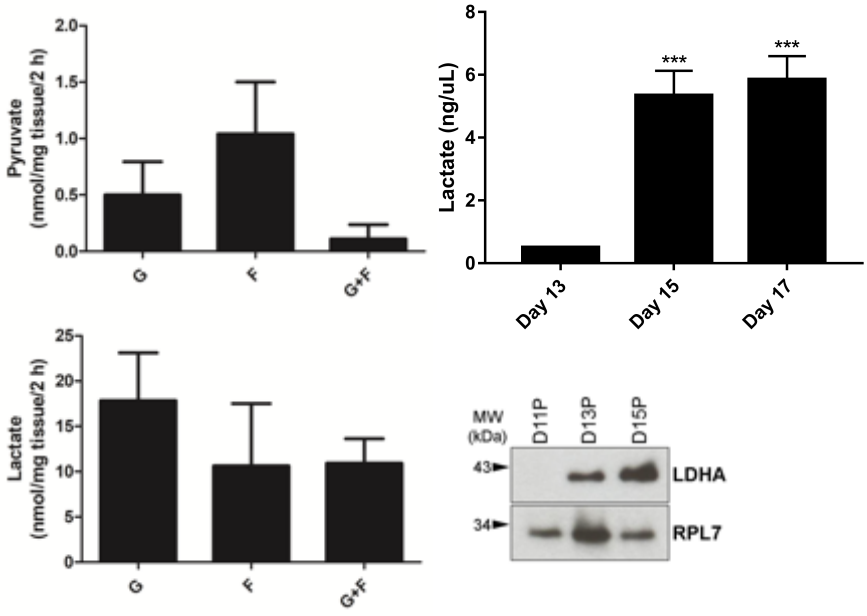

Figure 15. Lactate and pyruvate concentrations in uterine flushings and conceptus tissues.

Colormetric assay for levels of lactate in uterine flush on days 13, 15, and 17. Middle panel, Fluorometric assay for levels of lactate in conceptus tissues and culture media on day 16 of pregnancy. Right panel, Western blot for lactate dehydrogenase in conceptus tissues at days 11, 13 and 15. Fluorometric assay to determine the levels lactate in conceptus tissues and culture media on day 16 of pregnancy. Western blot for lactate dehydrogenase protein in conceptus tissues at days 11, 13 and 15 of pregnancy.

Glucose 6 Phosphate Dehydrogenase mRNA, protein and immunofluorescence

qPCR was performed to determine steady-state levels of total *G6PDH* mRNA in conceptus tissues from days 11, 13, 15, and 16 of pregnancy. Expression of *G6PDH* mRNA significantly increases from day 11 to 13 of pregnancy, then expression of *G6PDH* mRNA significantly decreases from day 13 to 16 of pregnancy (Figure 16A). Lactate dehydrogenase A (LDHA) protein, an enzyme that converts pyruvate into lactate, increases in the porcine conceptus as they elongate (Figure 16B). Immunofluorescence analysis showed that G6PDH protein was detected in the conceptus trophectoderm cells on days 15, 18, and 25 of pregnancy, and when G6PDH was colocalized with PCNA the majority of cells that were proliferating also expressed G6PDH (Figure 16C).

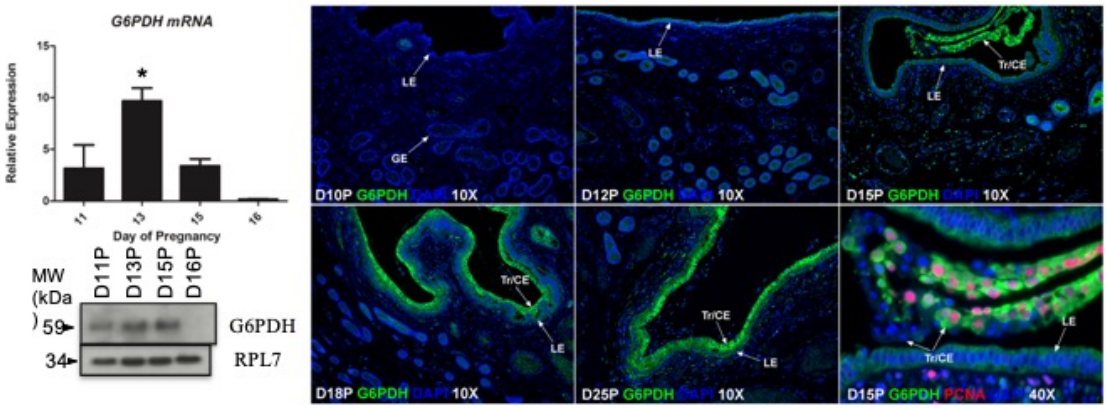

Figure 16. G6pdh an enzyme required for the pentose phosphate pathways is expressed by the conceptus trophectoderm.G6PDH an enzyme required for the pentose phosphate pathway is expressed by the conceptus trophectoderm (Tr) of pigs at sites of implantation. (A) Real-time PCR for mRNAs for G6PDH involved in the pentose phosphate pathway in the conceptus during the peri- implantation period of pregnancy. (B) Western blot for G6PDH protein in the conceptus during the peri-implantation period. (C) Immunofluorescence staining for G6PDH at sites of conceptus implantation. Nuclei are stained with DAPI for histologic reference. D, Day; P, pregnancy; LE, luminal epithelium.

Glucose and Fructose Flux into the Pentose Phosphate Pathway

To determine glucose and fructose metabolism via the PPP, conceptus tissues from days 15 and 16 of gestation were incubated with isotope-labeled glucose or fructose in a medium containing either unlabeled glucose and/or fructose, and then oxidation of glucose and fructose was determined by measuring $^{14}CO_2$ released from conceptus tissues. Figure

17 summarizes the production of $^{14}CO_2$ flux into the PPP from [1-^{14}C]glucose, [6-^{14}C]glucose, [1-^{14}C]fructose, and [6-^{14}C]fructose from conceptuses on day 15 and 16 of pregnancy. Trophectoderm cells from day 15 conceptuses metabolized glucose via the PPP at a significantly higher rate than fructose. Day 16 conceptuses utilized glucose and fructose via the PPP at similar rates. Similar rates of fructose flux into the PPP were observed at days 15 and 16 of pregnancy. However, day 15 conceptuses utilized more glucose for the PPP than day 16 conceptuses.

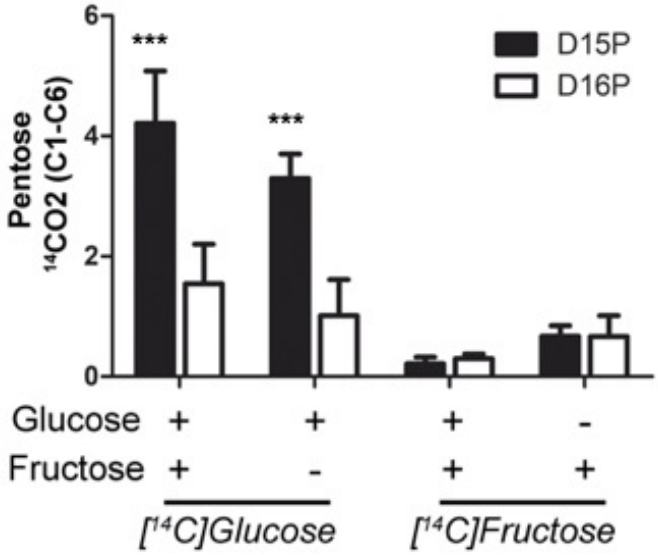

Figure 17. Porcine conceptus tissues from days 15 and 16 of pregnancy were cultured with isotope labeled glucose or fructose. Porcine conceptus tissues from day 15 and 16 of pregnancy were cultured in KHB (7.4) containing glutamate and D-[1-^{14}C]glucose, D-[6-^{14}C]glucose, D-[1-^{14}C]fructose or D-[6-^{14}C]fructose at 37°C for 60 minutes. Data are

the means ± SEM. (6 = 4) and were analyzed by two-way ANOVA. Values with * were significantly different ($P < 0.05$) from each other.

Discussion

Cells undergoing proliferation and differentiation, such as tumor and immune cells are metabolically distinct from cells of resting tissues, altering their metabolism from oxidative phosphorylation to enhanced glycolysis. During the peri-implantation period, porcine conceptuses are elongating, and this elongation is the result of rapid cell proliferation, tissue remodeling, and cell migration. As a result of these processes, conceptuses consume and deplete available nutrients within the uterine lumen, similar to tumor and immune cells (DeBerardinis et al., 2007). In our study, we observed that pig conceptuses began to proliferate after day 11, when conceptuses are transitioning from a spherical to a tubular shape. There was a further increase in proliferation of the Tr cells after day 13 of pregnancy when the conceptuses are transitioning from a tubular to filamentous form. Our data show that as conceptuses were proliferating, lactate concentrations increased within the uterine flushings from days 13 to 17 of pregnancy, suggesting that during the process of elongation conceptuses utilize enhanced glycolysis. Lactate is an important product of enhanced glycolysis because it is synthesized from pyruvate by lactate dehydrogenase, which regenerates NAD+. Regeneration of NAD+ is required for continued flux through glycolysis allowing for the maintenance of this pathway in the absence of ATP produced by oxidative phosphorylation. Increased

concentrations of lactate in the uterine flushings as conceptuses undergo elongation suggests that conceptus Tr cells are utilizing enhanced glycolysis in order to synthesize ATP more rapidly and increase production of glycolytic intermediates for use in the branching pathways of glycolysis.

In order to determine if pig conceptuses utilize glycolytic intermediates for the PPP, we next examined whether the rate limiting enzyme, G6PDH, was present. The enzyme G6PDH catalyzes the first reaction in the PPP, generating the first molecule of NADPH. G6PDH is tightly regulated, however its expression has been shown to be increased in cancer cells and normal proliferating tissues (Hilf et al., 1975; Jonas et al., 1992; Okano et al., 1965; Park et al., 2005; Rudack et al., 1971). Data from this study demonstrate that the proliferating Tr cells express G6PDH, with mRNA expression highest on day 13 of pregnancy, and protein expression increasing through day 15 of pregnancy and decreasing significantly by day 16 of pregnancy. These results suggest that conceptuses are able to utilize the PPP to produce ribose and NADPH for the *de novo* synthesis of nucleotides in order to provide the necessary building blocks for the developing conceptuses.

In normal physiology, fructose and glucose have been considered interchangeable monosaccharides that are oxidized equally by the TCA cycle and aerobic glycolysis (Gatenby and Gillies, 2004; Liu et al., 2010). In pig pregnancy, both glucose and fructose are present in the uterine flushings, but fructose is the most abundant hexose sugar in pig conceptuses, suggesting a potential discrepancy in the metabolism of these two sugars

(Zavy et al., 1982). It is known that glucose can serve directly as an energy source for cells (Chen et al., 2015), and there is data suggesting that pig conceptuses are able to convert glucose into fructose via the polyol pathway (Steinhauser et al., 2017a; White et al., 1979b). The large presence of fructose in the intrauterine environment of pigs has led to different hypotheses for the role of fructose in porcine pregnancy. First, the pig placenta is likely responsible for the conversion of glucose to fructose because glucose, but not fructose can be transported back into the mother's vasculature (White et al., 1982). A similar hypothesis is that because fructose can be sequestered in the conceptus and synthesized from glucose, it potentially serves as a "storage" form of carbohydrates for animals with little or no glycogen in their placenta (Goodwin, 1956). Later studies found that HeLa cells cultured in the presence of fructose only metabolized 4 to 5 percent of the fructose through glycolysis and almost all of the fructose was metabolized via the pentose phosphate pathway, producing ribose and NADPH (Reitzer et al., 1979). We have also previously shown that both glucose and fructose are able to be transported into the conceptuses, presumable into the Tr cells, and are metabolized by the conceptuses of pigs, with glucose being preferentially metabolized over fructose (Kramer et al., 2020; Steinhauser et al., 2017a). In our study, day 15 conceptuses had a greater flux of glucose carbons into the PPP when compared to fructose carbons. Suggesting that day 15 conceptuses are able to utilize the PPP for synthesis of ribose-5-phosphate and NADPH, while fructose carbons are likely being used by other metabolic pathways, including potentially the hexosamine biosynthetic pathway (Kim et al., 2012). Interestingly, day 15

conceptuses utilized greater amounts of via the PPP when compared to day 16 conceptuses. This could be due to pig conceptuses elongating to a filamentous shape by day 15 of pregnancy and by day 16 elongation is almost complete, so the conceptuses are no longer requiring the same amount of influx of glucose carbons for synthesis of ribose for nucleotide synthesis.

In summary, elongating and proliferating conceptuses require large amounts of energy and building blocks for DNA synthesis in order to develop into a fully functioning organism. One pathway necessary for the synthesis of nucleotides, required by proliferating cells, is the PPP. Results from this study demonstrate that pig conceptuses 1) generate lactate, and lactate increases in the uterine flushings during elongation, suggesting conceptuses are utilizing aerobic glycolysis; 2) express the enzyme G6PDH, which is necessary for entry into the PPP; and 3) metabolize glucose carbons for the production of ribose for nucleotide synthesis.

CHAPTER V

SPP1 EXPRESSION IN THE MOUSE UTERUS AND PLACENTA: IMPLICATIONS FOR IMPLANTATION*

Introduction

Secreted phosphoprotein 1 SPP1, also known as osteopontin (OPN is a secretory protein, that can be found in the extracellular matrix (ECM), as well as in biological fluids and luminal spaces. SPP1 binds to integrin receptors via its Gly-Arg-Gly-Asp-Ser (GRGDS) sequence to mediate cell-cell and cell-ECM interactions. SPP1 can undergo posttranslational modifications, including glycosylation, phosphorylation, cleavage into biologically active subunits, and formation of multimers by transglutaminase. The specific combination of posttranslational modifications that SPP1 undergoes is specific to the histological and physiological environment in which the SPP1 resides, and varies between species and within species. These posttranslational modifications of SPP1 alter its function and complicate detection of the SPP1 protein by immunohistochemistry and western blotting (Butler, 1996; Denhardt and Guo, 1993; Johnson et al., 2003; Sodek et al., 2000).

SPP1 expression is up-regulated in the endometrium and placenta of mice (Nomura et al., 1988), humans (Brown et al., 1992), sheep (Johnson et al., 1999b), pigs

---

* Kramer, A.C., Erikson, D.W., McLendon, B.A., Seo, H., Hayashi, K., Spencer, T.E., Bazer, F.W., Burghardt, R.C., and Johnson, G.A. (2021). SPP1 expression in the mouse uterus and placenta: implications for implantationdagger. Biol Reprod *105*, 892-904. By permission of Oxford University Press.

(Garlow et al., 2002), rabbits (Apparao et al., 2003), cattle (Kimmins et al., 2004), and goats (Joyce et al., 2005a), and SPP1 has received considerable interest as a key player during conceptus (embryo and associated placental membranes) implantation, and in the maintenance of pregnancy (Berneau et al., 2019; Frank et al., 2017; Johnson et al., 2014; Johnson et al., 2003; Kang et al., 2014; Seo et al., 2020a).

SPP1 was first described in endometrial tissue when *Spp1* mRNA was localized within the decidua and deciduoma of mice (Nomura et al., 1988; Waterhouse et al., 1992). It was later demonstrated that uterine natural killer (uNK) cells express SPP1 protein within the decidua and deciduoma (Herington and Bany, 2007a). Waterhouse et al. (1992) also detected *Spp1* mRNA in the endometrial luminal epithelium (LE), but not in the endometrial glandular epithelium (GE), of pregnant mice (Waterhouse et al., 1992), and it was later determined that expression of *Spp1* mRNA is upregulated in the endometrial LE of ovariectomized mice injected with estrogen (White et al., 2006). Once again, although both *Spp1* mRNA and protein were localized to the endometrial LE, expression of SPP1 was not observed in the endometrial GE (White et al., 2006). Disruption of the *Spp1* gene in mice results in increased early pregnancy loss, and pups that are born are significantly smaller than are pups born to wild-type counterparts (Weintraub et al., 2004). More recently, there have been three reports of SPP1 expression in the endometrium of pregnant mice. In one manuscript SPP1 protein was localized to the endometrial LE on Day 5 of gestation (Liu et al., 2013), whereas in the other two manuscripts SPP1 protein was localized to the endometrial GE, and SPP1 was demonstrated to mediate in vitro blastocyst adhesion in these studies (Chaen et al., 2012; Qi et al., 2014). Therefore, it is

not clear whether SPP1 is expressed by the endometrial LE and/or endometrial GE during the window of implantation in mice, and, while SPP1 has been implicated as an adhesion molecule for implantation, SPP1 expression has not been directly linked to the implantation chamber and in vivo implantation of the mouse blastocyst.

However, there is strong in vitro evidence that SPP1 has the potential to mediate trophoblast attachment and migration during the initial stages of implantation in mice. Kang et al. have shown that SPP1 is highly expressed by the trophoblast cells of cultured mouse blastocysts and by the monolayered human endometrial Ishikawa cells adjacent to these attaching blastocysts (Kang et al., 2014). SPP1 expression is predominantly localized to the apical surfaces of these cells, but is also associated with vesicular deposits, indicating likely secretion at the interface between trophoblast and endometrial cells. Interestingly, expression decreases in Ishikawa cells further away from the blastocyst. Additionally, knockdown of SPP1 suppresses mouse blastocyst attachment in vitro. Attachment of SPP1-coated beads to Ishikawa cells has been shown to be an αvβ3 integrin-dependent process, and knockdown of the αvβ3 integrin also suppresses the attachment of beads bearing SPP1, suggesting that SPP1 acts as a bridging ligand between the trophoblast and Ishikawa cells during blastocyst attachment in vitro (Kang et al., 2014).

Available evidence suggests that SPP1 is involved in implantation and placentation in the mouse, but the in vivo localization of SPP1 and in vivo mechanistic studies to support this idea remain incomplete and contradictory. Therefore, we performed temporal localization of *Spp1* mRNA and protein in the endometrium and placenta of mice

throughout gestation, and utilized a delayed implantation model to link SPP1 to the implantation chamber of murine pregnancy. Results of this study suggest that (1) implantation directly induces expression of SPP1 in mouse endometrium, (2) SPP1 is likely involved in the initial adhesion and invasion stages of implantation, and (3) SPP1 may be secreted from uNK cells to support vascular development within the decidua.

Materials and Methods

Animals and tissue preparation

All experimental and surgical procedures followed the Guide for Care and Use of Agriculture Animals and were approved by the Institutional Agricultural Animal Care and Use Committee of Texas A&M University. Temporal and spatial changes in *Spp1* mRNA and protein expression were evaluated in the uteri of adult virgin CD-1 female mice (6 to 8 weeks old) and obtained from Charles River Laboratories (Wilmington, MA). All mice were housed in a temperature-controlled room (21°C to 22°C) with a 12-hour light/12-hour dark cycle and allowed free access to food and water. In Study 1, female mice were mated with fertile males of the same strain to establish pregnancy and mating was confirmed by the presence of a vaginal plug (designated Day 0 of gestation). Uteri were collected at 0900 h on Days 1, 4, 4.5, 5, 8, 9, 10, 11, 12, 15, 16 and 17 after mating (n = 5/day). Segments of the uterus containing implanting blastocysts (implantation site) or not containing implanting blastocysts (nonimplantation site) were dissected and processed as outline below. In Study 2, delayed implantation was induced in pregnant mice using an established method (Paria et al., 1993). Briefly, pregnant mice were ovariectomized on

Day 4 of pregnancy and administered progesterone (2 mg per mouse in 1 ml of sesame oil, subcutaneously) on gestational Days 5, 6, and 7. Delayed implantation was terminated by injecting estradiol-17β (25 ng per mouse in 1 ml of sesame oil, subcutaneously) on Day 7 concomitant with administration of progesterone. Uteri were collected 24 h after termination of delayed implantation (Day 8; n = 8 each).

Uteri were fixed in fresh 4% paraformaldehyde in phosphate buffer saline (PBS) and embedded in Paraplast Plus (Oxford Laboratory, St Louis, MO) for in situ hybridization and immunofluorescence analysis or snap frozen in liquid nitrogen and stored at -80°C for RNA extraction and quantitative PCR (qPCR) analysis.

For generation of interleukin 15 (*Il15*)-null mice, outbred CD-1 mice and mice with a targeted deletion of the *Il15* (C57BL/6-IL15^{tm1Imx}) were mated and then sacrificed on gestational Day 10 (n=4/strain) (Gift from Dr. Anne Croy). Uteri were fixed in 4% paraformaldehyde and paraffin-embedded.

RNA Extraction, cDNA Synthesis, and quantitative PCR

Total RNA was isolated from frozen uteri using Trizol reagent (Life Technologies, Carlsbad, CA) according to the manufacturer's recommendations. First strand cDNA was synthesized using a Superscript III First Strand Kit (Life Technologies, Carlsbad, CA) according to the manufacturer's instructions. First strand cDNA was diluted 5x for the qPCR reaction. Primers for qPCR were designed using NCBI Genbank sequences and submitted to BLAST (http://www.ncbi.nlm.nih.gov/) to confirm specificity against the known mouse genome.

Quantitative PCR assays were performed using PerfeCta SYBR Green Master mix (Quanta Biosciences, Gaithersburg, MD) in 10 µl reactions with 2.5 mM of each specific primer, on a Roche 480 Lightcycler (Rochem Life Sciences) with approximately 60 ng cDNA per reaction. The PCR program began with 5 min at 95°C followed by 40 cycles of 95°C denaturation for 10 sec and 60°C annealing/extension for 30 sec. A melt curve was produced with every run to verify a single gene-specific peak. Standard curves using pooled cDNA with 2-fold serial dilutions were run to determine primer efficiencies. All primer correlation coefficients were greater than 0.95 and efficiencies were 92-100%. *Ribosomal protein l19* (*Rpl19*) was used to normalize data from endometrial tissues (Gao et al., 2009b). The primer sequences for *Spp1* were, forward 5'-tcaactaaagaagaggcaaaaacac-3'and reverse 5'-gcccaaaatattacctctctttctc-3'. The primer sequences for *Rpl19* were, forward 5'-atgagtatgctcaggctacaga-3' and reverse 5'-gcattggcgatttcattggtc-3'. The $2^{-\Delta\Delta Ct}$ method was used to normalize data, and fold-changes were subjected to statistical analyses.

In situ hybridization analysis

Spp1 mRNA was localized in paraffin-embedded mouse uterine tissue by in situ hybridization using methods previously described (Johnson et al., 1999b). Briefly, deparaffinized, rehydrated, and deproteinated uterine cross-sections (5 µm) were hybridized with radiolabeled antisense or sense mouse *Spp1* cRNA probes (Fisher et al., 1995) synthesized by in vitro transcription with [α-^{35}S]uridine 5-triphosphate (PerkinElmer Life Sciences, Wellesley, MA, USA). After hybridization, washes, and

RNase A digestion, autoradiography was performed using nuclear track material type NTB-2 liquid photographic emulsion (Eastman Kodak, Rochester, NY, USA). Slides were exposed at 4°C for 5 days, developed in Kodak D-19 developer, counterstained with Harris' modified hematoxylin (Fisher Scientific, Fairlawn, NJ, USA), dehydrated, and protected with cover slips.

Immunofluorescence analyses

Immunoreactive SPP1 and E-cadherin proteins were localized in paraffin-embedded samples from pregnant mice using immunofluorescence microscopy. Antigen retrieval was performed using boiling citrate. Sections were then blocked with 10% normal goat serum for 1 h at room temperature. These sections were incubated over night at 4°C with the following primary antibodies: rabbit anti-SPP1 polyclonal antibody (EMD Millipore; Billerica, MA, USA; AB10910; 1:200; this antibody detects proteins of 50 kDa and 30 kDa in endometrial tissue, see supplemental Figure 1C) and mouse anti-E-cadherin (CDH1) monoclonal antibody (BD Biosciences; San Jose, CA, USA; 610182; 1:200). Normal rabbit IgG (EMD Millipore; Billerica, MA, USA; 12-370) at the same concentration as used for the primary IgG, was used as the negative control. Immunoreactive proteins were detected using the appropriate Alexa Fluor 488- or Alexa Fluor 594-conjugated secondary antibodies (Life Technologies, Grand Island, NY, USA) for 1 h at room temperature at a dilution of 1:250. Tissue sections were then washed three times for 5 min/wash in PBS. Slides were counterstained with Prolong Gold Antifade reagent containing DAPI (Life Technologies) and coverslipped. Images were taken using

an Axioplan 2 microscope (Carl Zeiss; Thornwood, NY, USA) interfaced with an Axioplan HR digital camera.

For dual immunofluorescence staining (SPP1 + CDH1) the same procedures as described for normal immunofluorescence staining was used except that the two primary antibodies were added simultaneously on the first day and the two secondary antibodies (goat anti-rabbit-Alexa Fluor 488-conjugated and goat anti-mouse-Alexa Fluor 594-conjugated) were added simultaneously on the second day (Seo et al., 2019).

Dolichos biflorus (DBA) lectin staining

To localize SPP1 and uNK cells, tissue sections from pregnant mice were paraffin-embedded, and sections (5 μm thick) were deparaffinized and rehydrated in an alcohol gradient. Antigen retrieval was performed using boiling citrate. Sections were then blocked with 10% normal goat serum for 1 h at room temperature. These sections were incubated over night at 4°C with the rabbit anti-SPP1 polyclonal primary antibody (EMD Millipore; Billerica, MA, USA; AB10910; 1:200). Sections were then incubated with both Alexa Fluor 594-conjugated secondary antibody (Life Technologies, Grand Island, NY, USA; 1:250) and FITC-conjugated lectin from *Dolichos biflorus* (Sigma-Aldrich; St. Louis, MO, USA; L9142-1MG; 1:200) for 1 h at room temperature. Tissue sections were then washed three times for 5 min/wash in PBS. Slides were counterstained with Prolong Gold Antifade reagent containing DAPI (Life Technologies) and coverslipped. Images were taken using an Axioplan 2 microscope (Carl Zeiss; Thornwood, NY, USA) interfaced with an Axioplan HR digital camera.

Statistical analysis

Data from qPCR for effect of days of pregnancy were subjected to the Students t-test using GraphPad Prism (GraphPad Software, La Jolla, CA). All data are presented as mean ± standard errors of the mean with significance at $P < 0.05$.

Results

Spp1 mRNA and protein in the endometrium of pregnant mice

Localization of *Spp1* mRNA was assessed by in situ hybridization and SPP1 protein was assessed by immunofluorescence staining on paraffin embedded uterine cross-sections. SPP1 protein was localized to the apical surface of the endometrial LE on Day 1 of gestation (Figure 18A and 18B), but was not detected in the endometrial GE on Day 1 of gestation (Figure 18A and 18C). SPP1 was localized to cells scattered throughout the endometrial stroma on Day 4 (mRNA), and Days 4.5 and 5 (protein) of gestation (Figure 19A, 19B, and 19C). Many of these cells also bound to DBA lectin (Figure 19C). *Spp1* mRNA and protein were not detected in the endometrial LE or endometrial GE on Days 4, 4.5 and 5 of gestation (Figure 19A, 19B and 19C). *Spp1* mRNA was localized to the endometrial LE and cells within the decidua on Day 9 of gestation (Figure 20A, 20B, and 20C), and SPP1 protein was localized to cells in the decidua on Day 8 of gestation (Figure 20D and 3E). *Spp1* mRNA continued to be localized to the endometrial LE and cells within the decidua on Day 10 of gestation (Figure 21A and 21B), and SPP1 protein was localized to the endometrial LE and cells within the decidua on Day 11 of gestation (Figure 21C, 21D, 21E and 21F). *Spp1* mRNA continued to be localized to the endometrial LE and cells

within the decidua on Days 15 and 17 of gestation; however, the number of cells expressing SPP1 in the decidua appeared to decrease between Days 15 and 17 of pregnancy (Figure 22B and 22C). A comprehensive display of *in situ* hybridization of *Spp1* mRNA for Days 4, 5, 6, 10, 11, 15, 16 and 17 of gestation is presented in supplemental Figure 1A.

Temporal changes in the steady-state levels of *Spp1* mRNA in total mouse endometrial tissues were quantified by qPCR for Days 5 and 11 of pregnancy. Steady-state levels of *Spp1* mRNA expression significantly increased between Day 5 and Day 11 of gestation ($p < 0.05$) (Figure 22A).

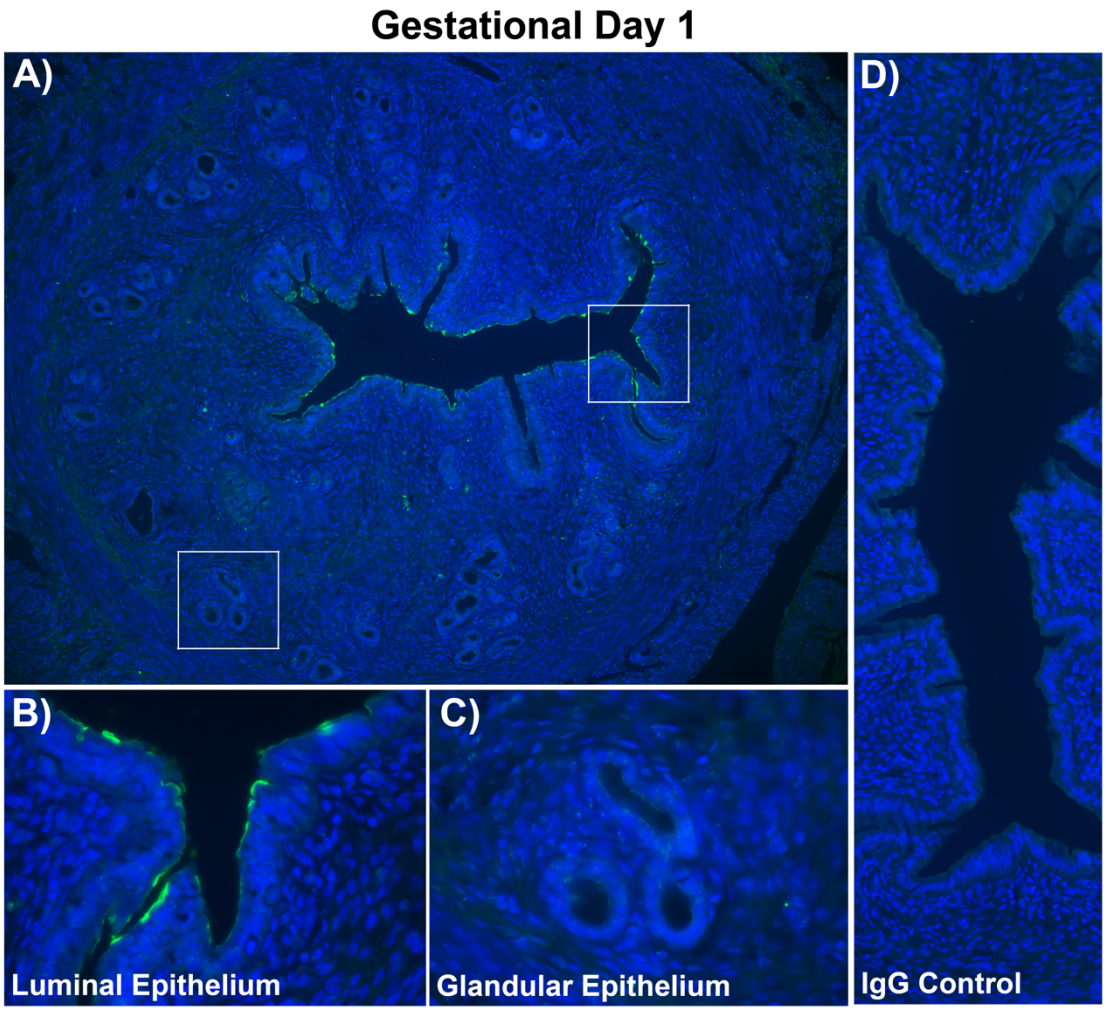

Figure 18. Immunofluorescence localization of SPP1 protein in paraffin embedded cross-sections of mouse uterus on Day 1 of gestation.

(A) Cross section of the entire mouse uterus. SPP1 immunoreactivity was primarily localized to the endometrial LE. (B) SPP1 protein was present on the apical surface of the endometrial LE. (C) SPP1 protein was not present in the endometrial GE. (D) Rabbit IgG served as a negative control. Nuclei were stained with DAPI for histological reference. Width of field for panel A is 870 um, for panels B and C is 220 um and for panel D is 500 um.

SPP1 mRNA in the developing bone of fetal mice

SPP1 is an extracellular matrix molecule associated with bone mineralization and development. *Spp1* mRNA was localized to developing bone of fetal mice on Day 16 of gestation (Figure 6).

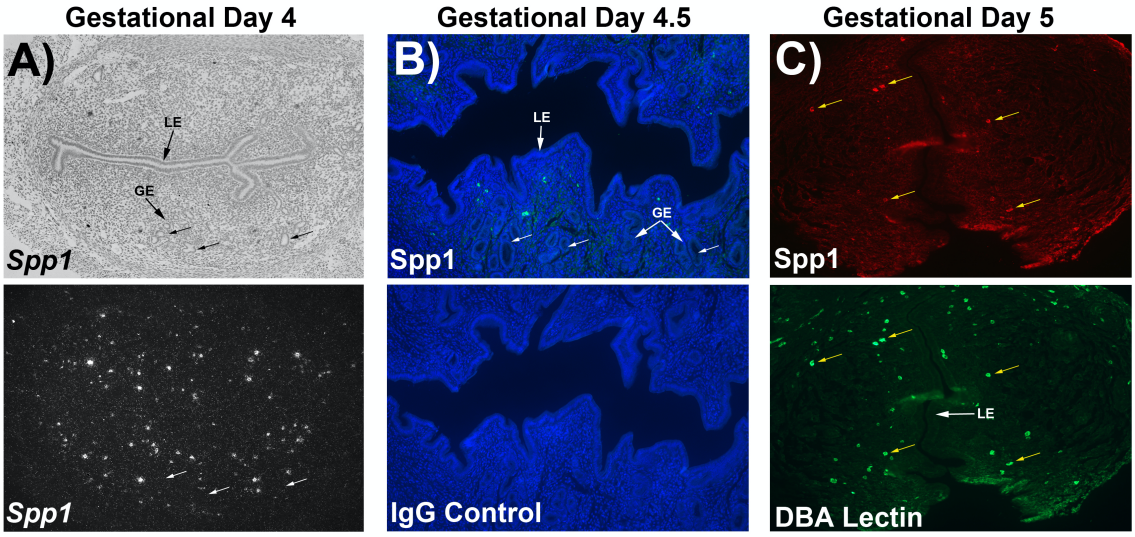

Figure 19. In situ hybridization and immunofluorescence analyses of *Spp1* mRNA and proteins, respectively, in cross-sections of uteri of mice on Days 4, 4.5, and 5 of gestation. (A) In situ hybridization revealed *Spp1* mRNA is present in cells scattered throughout the endometrial stroma on Day 4 of gestation. Corresponding brightfield and darkfield images of representative cross-sections of uterus are shown. (B) SPP1 protein is expressed in cells scattered throughout the endometrial stroma on gestational Day 4.5. The arrows point to endometrial GE that do not appear to express SPP1 protein. Nuclei are stained with DAPI for histological reference. Rabbit IgG serves as a negative control. (C) Many of the DBA lectin-positive stained cells also express SPP1 protein. The arrows

indicate representative cells that are positive for both SPP1 and DBA lectin. Legend: LE, luminal epithelium; GE, glandular epithelium. Width of field for panel A is 1500 um, for panel B is 870 um, and for panel C is 870 um.

Localization of SPP1 to uNK cells

Il15 is required for maturation of uNK cells (Barber and Pollard, 2003); therefore, we performed in situ hybridization for *Spp1* mRNA utilizing uterine cross-sections from *Il15*-null mice to determine the relationship between uNK cells and SPP1 during pregnancy. *Spp1* mRNA was not detected in cells within the decidua of *Il15*-null mice that lack uNK cells; however, *Spp1* mRNA was expressed in the endometrial LE of *Il15*-null mice (Figure 7A). uNK cells express N-acetylgalactosamine on their surface, which binds DBA lectin (Paffaro et al., 2003), therefore we utilized FITC-conjugated DBA lectin and immunofluorescence staining for SPP1 protein to further confirm that uNK cells express SPP1 protein. DBA lectin and SPP1 protein co-localized to individual cells within the decidua (Figure 7B). DBA lectin also co-localized with SPP1 protein in cells scattered throughout the endometrial stroma on Day 5 of gestation; however, not all of the cells that stained positive for DBA lectin expressed SPP1 protein (Figure 19C). DBA lectin was also localized the endometrial LE that expresses SPP1 (supplemental Figure 18B).

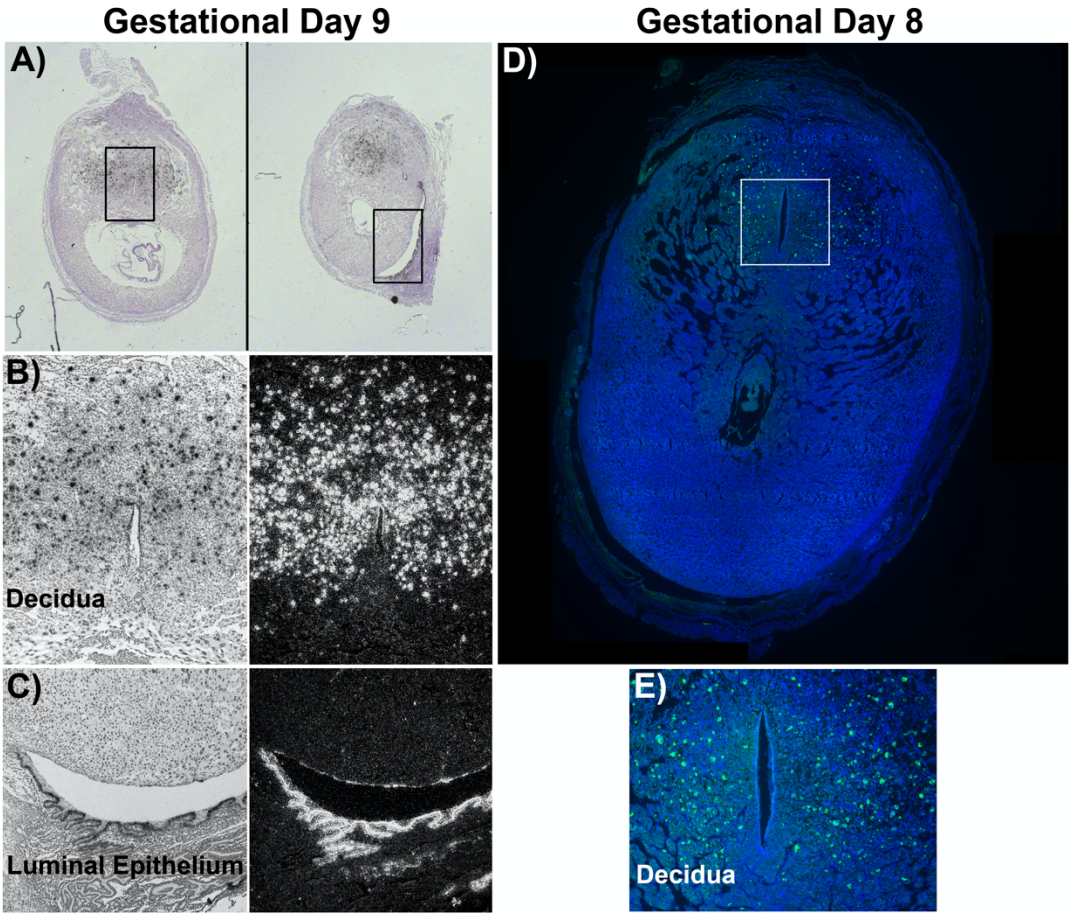

Figure 20. In situ hybridization and immunofluorescence staining for *Spp1* mRNA and protein, respectively, in cross-sections of uteri from mice on Days 8 and 9 of gestation.

(A-C) For in situ hybridization, corresponding brightfield and darkfield images of representative cross sections of endometrium from Day 9 of gestation are shown. (A) Low magnification brightfield overviews of Day 9 mouse uteri. (B) *Spp1* mRNA is expressed in the decidua. (C) *Spp1* mRNA is expressed in the endometrial LE. (D) Low magnification overview of a Day 8 uterus immunostained for SPP1 protein. (E) SPP1 protein is expressed by cells within the decidua. Nuclei are stained with DAPI for

histological reference. Width of fields for panels in A is 3940 um, for panels B and C are 750 um and for panel D is 4000 um, and for panel E is 850 um.

Localization of Spp1 mRNA and protein to the implantation chamber of mice

We utilized delayed implantation to identify the effect of nidatory estrogen on SPP1 expression in implantation chambers in the uteri of pregnant mice. *Spp1* mRNA was localized by in situ hybridization to the inner cell mass (ICM) of the conceptus and to focal extents of the endometrial LE monolayer of cells that directly contact the trophoblast cells of the blastocyst within the implantation chamber (Figure 25A). *Spp1* mRNA was also localized to cells scattered throughout the endometrial stroma (Figure 25A, 25B and 25C). In addition, *Spp1* mRNA was highly expressed in the endometrial LE of the interimplantation sites (Figure 25B and 25C). SPP1 protein was localized by immunofluorescence microscopy to the newly forming embryonic endoderm and to focal extents of the trophoblast cell layer directly contacting the endometrial LE within the implantation chamber (Figure 26). DBA lectin was localized in trophoblast cells that also expressed SPP1 (Figure 26).

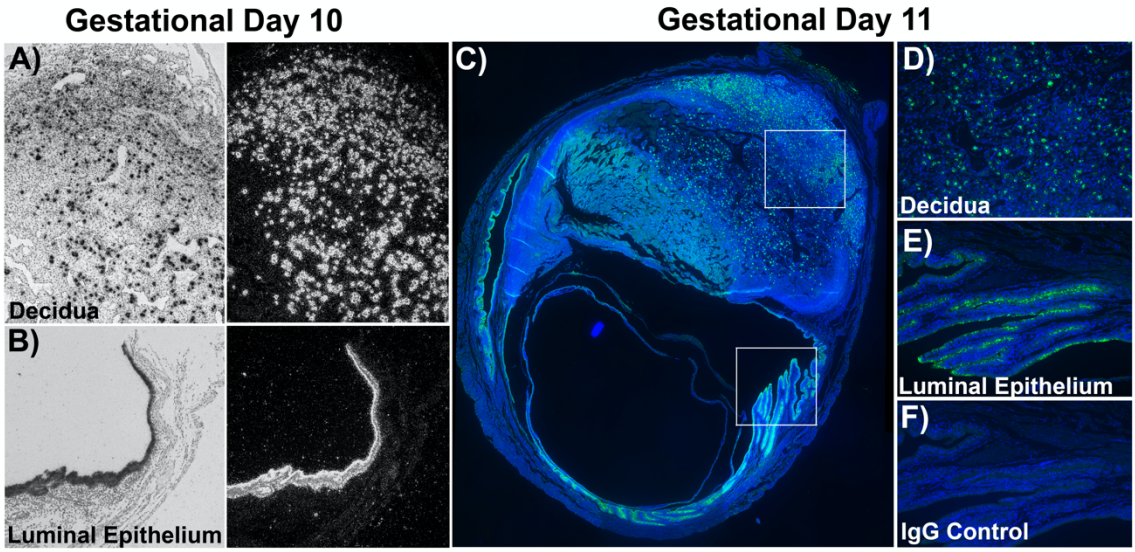

Figure 21. In situ hybridization and immunofluorescence staining for *Spp1* mRNA and protein, respectively, in cross-sections of uteri from mice on Days 10 and 11 of gestation.

(A and B) For in situ hybridization, corresponding brightfield and darkfield images of representative cross-sections of endometrium from Day 10 of gestation are shown. (A) *Spp1* mRNA is expressed by cells in the decidua. (B) *Spp1* mRNA is expressed by the endometrial LE. (C) Low magnification overview of a Day 11 uterus immunostained for SPP1 protein. (D) SPP1 protein is expressed by cells in the decidua. (E) SPP1 protein is expressed by the endometrial LE. (F) Rabbit IgG serves as a negative control. Nuclei are stained with DAPI for histological reference. Width of fields for panels in A and B is 750 um, for panel C is 4200 um, and for panel D-F is 520 um.

Discussion

Results from the present study suggest that secretory SPP1, and by conjecture, the integrin receptors which bind SPP1, may be important for murine implantation and placentation. Novel, and credible, concepts that arise from the present data include: 1) that SPP1 may be secreted by the endometrial LE at interimplantation sites to participate in closure of the uterine lumen to form the implantation chamber; 2) that SPP1 may be secreted by the endometrial LE adjacent to the attaching trophoblast cells to mediate attachment and invasion of the blastocyst during implantation; and 3) that SPP1 is likely not a component of histotroph secreted from the uterine GE, but is secreted from a subpopulation of uNK cells, as well as cells in the decidua that express SPP1 that are not uNK cells, perhaps to increase angiogenesis within the decidua to augment hemotrophic support of embryonic/fetal development.

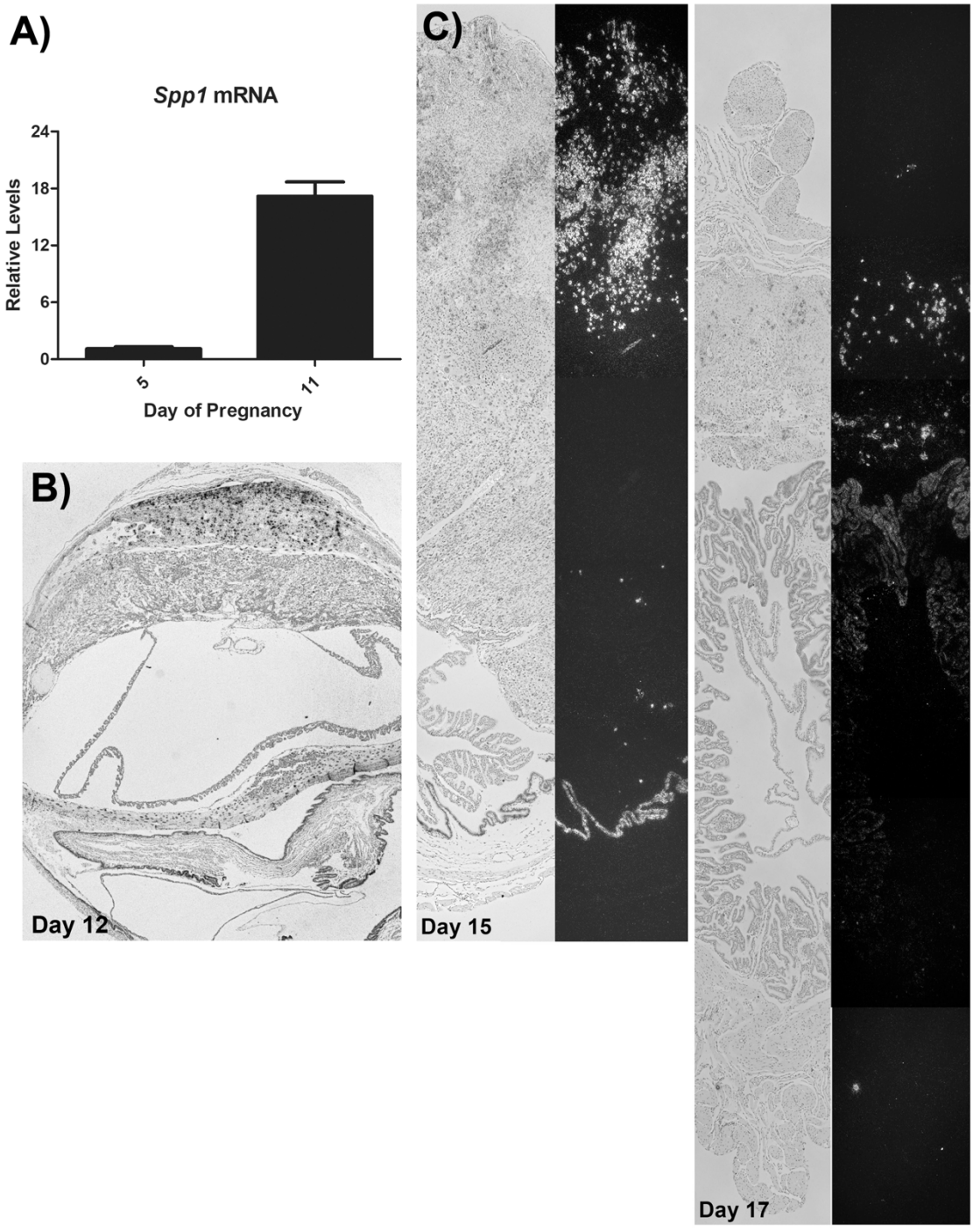

Figure 22. Quantitative real-time PCR and in situ hybridization analyses of *Spp1* mRNA in pregnant mouse uteri.

(A) Expression of *SPP1* mRNA increased between Day 5 and Day 11 of gestation ($p < 0.05$). (B) In situ hybridization for *Spp1* mRNA. A low magnification brightfield overview of a uterus from a mouse Day 12 pregnancy. (C) In situ hybridization, corresponding brightfield and darkfield images of representative cross sections of endometrium from Day 15 and Day 17 of gestation are shown. *Spp1* mRNA is expressed by cells within the decidua and by the endometrial LE on Day 15 of pregnancy; however, the number of cells expressing *Spp1* mRNA appears to decrease by Day 17 of gestation. Width of field for panel B is 4200 um, and for the panels in C is 750 um.

Although SPP1 is expressed by the endometrial GE of sheep and pigs (Garlow et al., 2002; Johnson et al., 1999a; Johnson et al., 1999b; White et al., 2005), in the present study neither *Spp1* mRNA nor SPP1 protein were detected in the endometrial GE of mice. These results agree with the findings of two previous studies by Waterhouse and co-workers (Waterhouse et al., 1992) and White and coworkers (White et al., 2006). In contrast, there are two reports of SPP1 expression by the endometrial GE of mice. In the first of these studies, *Spp1* mRNA was localized to Day 4 mouse endometrial GE by in situ hybridization, and SPP1 protein was localized to Day 4 GE by immunohistochemistry (Chaen et al., 2012). Further, expression of SPP1 by endometrial GE was disrupted by treatment of mice with both Tamoxifen and ICI 182780. Interestingly, Tamoxifen did not alter amounts of *Spp1* mRNA or SPP1 protein expression in endometria as measured by RT-PCR or Western blotting, respectively. The authors proposed that whole tissue

measures for *Spp1* mRNA and protein were confounded by mononuclear cells that express SPP1 within the endometrium (Chaen et al., 2012). In the second study, SPP1 protein was localized to the endometrial GE on Days 1 and 4, but not on Day 5 of gestation (Qi et al., 2014). Detection of SPP1 protein is made complex due to the fact that the SPP1 protein can be differentially post-translationally modified in individual cell types, and these multiple forms of SPP1 can be recognized by different SPP1 antisera (Kazanecki et al., 2007). Recently, at least seven SPP1 forms were identified in the human endometrial Ishikawa cell line. This caused the authors to note that investigation of endometrial-specific SPP1 forms is warranted (Berneau et al., 2019). Discrepancies among studies regarding localization of SPP1 mRNA to the endometrial GE are more difficult to explain, but may reflect variations associated with different in situ hybridization procedures.

Gestational Day 16

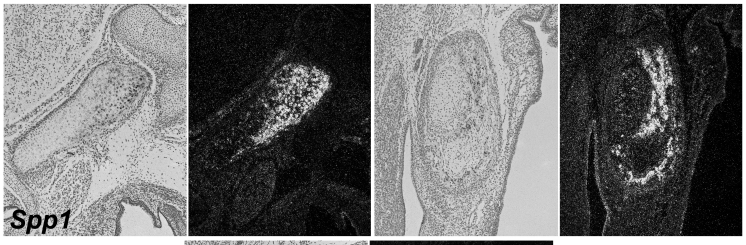

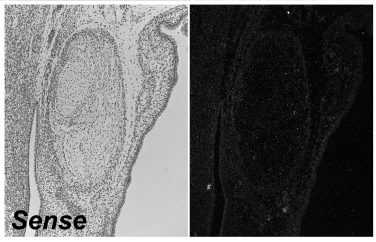

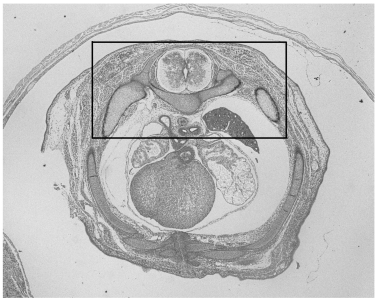

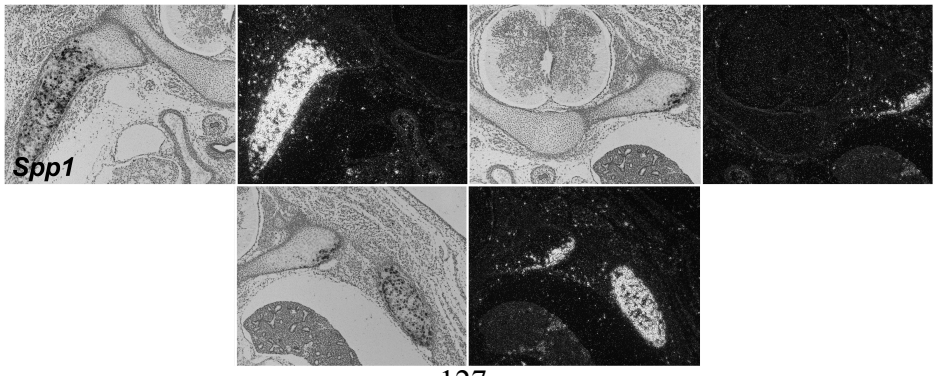

Figure 23. In situ hybridization for *Spp1* mRNA in Day 16 mouse embryos is shown. (A and B) The top panels are low magnification brightfield overviews of Day 16 mouse embryos. The lower panels are corresponding brightfield and darkfield images of representative cross sections of Day 16 embryos. *Spp1* mRNA is present in the developing bones of the embryos. Width of field for the top panels in A and B is 5500 um and 4000 um respectively, for second and third panels in A is 870 um, and for the second and third panels in B is 870 um.

During the attachment phase of implantation in mice, the blastocyst is confined to a limited space within the uterine lumen called the implantation chamber. The tight space formed by the implantation chamber restricts blastocyst movement and facilitates close apposition of the apical surfaces of trophoblast cells to endometrial LE cells. The integrity of the implantation chamber is maintained via closure of the lumen surrounding the chamber. The mechanisms involved in closure of the uterine lumen at interimplantation sites in mice are not completely understood, but almost certainly involve absorption of fluid within the uterine lumen by the endometrium mediated by aquaporins (Beall et al., 2007; Chan et al., 2009; de Oliveira et al., 2020; Richard et al., 2003). However, fluid transport alone may not explain closure of the uterine lumen at interimplantation sites. It is reasonable to propose that transient adhesion complexes, such as those that form between cells and the ECM, may help to keep the apposing endometrial LE surfaces in close contact at interimplantation sites. Results of the current study are the first, to our knowledge, to show that estrogen induced termination of delayed implantation results in

a dramatic increase in expression of SPP1 within the endometrial LE of interimplantation sites, but not within the implantation chamber itself. These results conflict with two previous reports (Mangale and Reddy, 2007; Qi et al., 2014) that there is no expression of SPP1 protein in the interimplantation sites of mice. However, these studies did not report on localization of *Spp1* mRNA, which is a strength of the present study. The complications of detecting SPP1 protein with its multiple post-translational modifications were previously discussed in the text. Mangale and Reddy (Mangale and Reddy, 2007) did report expression of the ECM proteins fibronectin and vitronectin, and the integrin subunits alpha 5 (α5), α6, and beta 3 (β3) in the endometrial LE of interimplantation sites of mice. Integrin subunits α5 and β3 assemble to form the integrin receptors α5β1 and αvβ3 which both bind to SPP1. We hypothesize that fluid is transported out of the uterine lumen at the same time the endometrial LE at interimplantation sites is secreting SPP1 into the lumen. This allows SPP1 to interact with integrin receptors expressed by the endometrial LE (Aplin, 1997) to maintain closure of the uterine lumen at interimplantation sites and create the implantation chamber for the developing conceptus.

During implantation, the initial interactions between the apical surfaces of the endometrial LE cells and the conceptus trophoblast begin with the sequential phases of non-adhesion or pre-contact, apposition, and adhesion. For conceptus attachment to occur adhesive molecules, expressed at the apical surface of the conceptus trophoblast, bind to adhesive molecules at the apical surface of the endometrial LE, in a juxtacrine manner (Aplin, 1997; Burghardt et al., 2002; Carson et al., 2000; Johnson et al., 2001). Murine implantation is invasive, where the trophoblast cells rapidly invade though the endometrial

LE and migrate into the differentiated stromal decidua (Carson et al., 2000). Therefore, as trophoblast cells attach to the endometrial LE, they are almost simultaneously migrating through the LE barrier to the underlying stroma. In the present study, *Spp1* mRNA was localized to endometrial LE cells along limited focal extents of close interaction between the endometrial LE and the conceptus trophoblast. In contrast, SPP1 protein was localized to individual conceptus trophoblast cells. *Spp1* mRNA was not detected in trophoblast cells, and SPP1 protein was not detected in endometrial LE cells within the implantation chamber. A similar pattern of expression is observed in the endometrial LE and conceptus trophoblast of sheep, where SPP1 is secreted by the endometrial LE and binds to the surface of the conceptus (Johnson et al., 1999a; Johnson et al., 1999b). These results agree, in part, with a previous report showing SPP1 protein expression increased in the blastocysts of mice activated by estrogen during delayed implantation. The increase in SPP1 expression was greater than we report here, but it is noteworthy that the same robust upregulation of SPP1 could not be replicated in vitro, and it was proposed that blastocyst expression of SPP1 required the blastocyst be present within the microenvironment of the implantation chamber (Xie et al., 2013). We propose that in mice, SPP1 is synthesized and secreted by endometrial LE cells within the implantation chamber, and then binds to integrins on adjacent conceptus trophoblast cells.

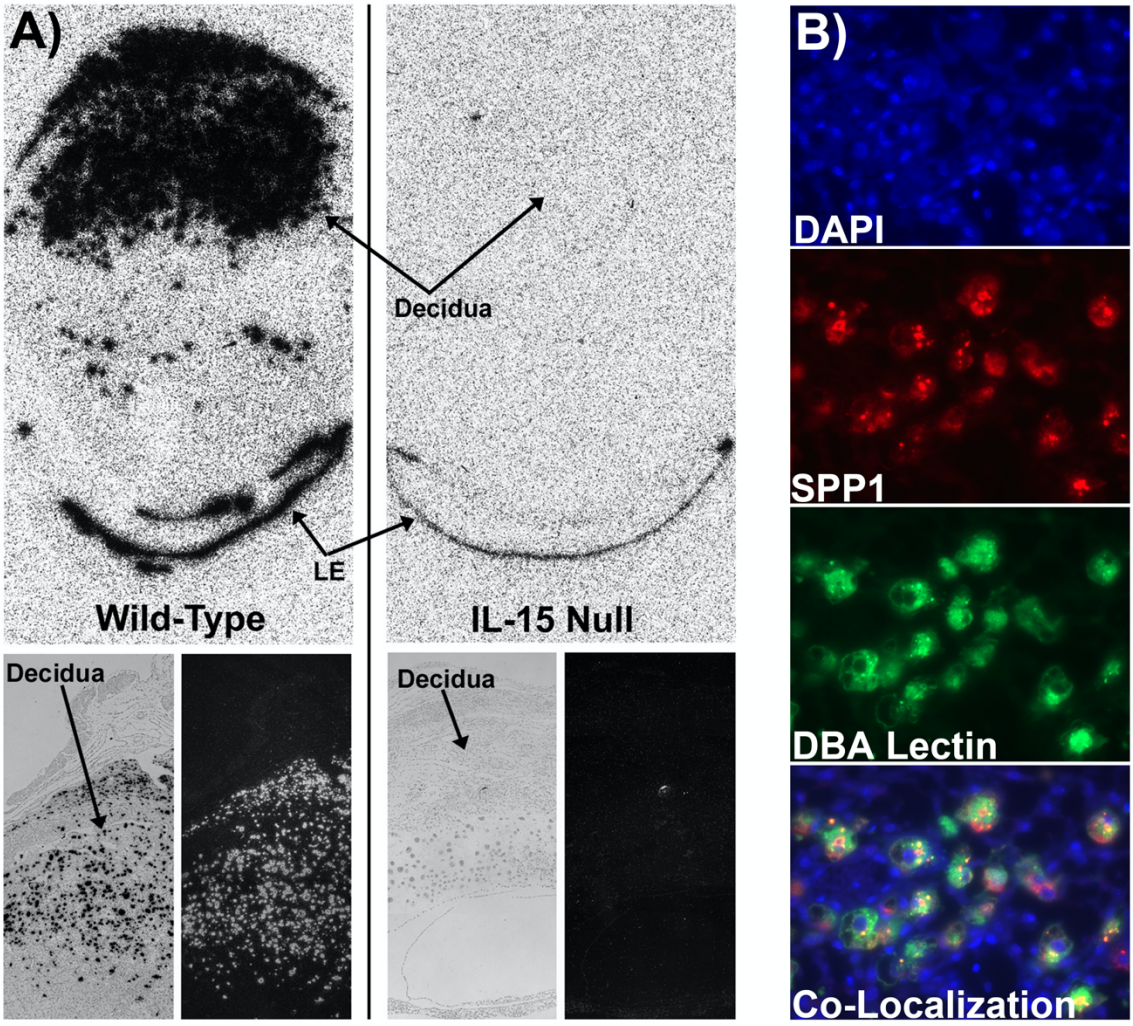

Figure 24. Spp1 is expressed by uterine natural killer (uNK) cells.

(A) In situ hybridization for *Spp1* mRNA in the uteri of wild-type and *Il15*-null mice. The top panels are low magnification brightfield overviews of mouse uteri. The lower panels are corresponding brightfield and darkfield images of in situ hybridization. The decidua of *Il15*-null mice lack uNK cells and SPP1 is not detectable in the decidua of *Il15*-null mice. (B) Immunofluorescence staining for SPP1 protein (red) and staining for DBA lectin

(green) in the decidua of wild-type mice. SPP1 and DBA lectin are co-localized to cells within the decidua. Nuclei were stained with DAPI for histological reference. Legend: LE, luminal epithelium. Width of field for the top panels in A is 1500 um, for the bottom panels in A is 870 um, and for the panels in B 220 um.

The role(s) for SPP1 in the implantation chamber of mice remains to be determined. The current consensus is that SPP1 binds integrin receptors to mediate attachment of the conceptus to endometrial LE during the attachment phase of implantation in species that have epitheliochorial/synepitheliochorial placentation in which the conceptus does not invade into the uterine wall (Johnson et al., 2014). In support of this consensus, human Ishikawa cells require expression of SPP1 for stable embryo attachment in vitro (Kang et al., 2014). However, a role for SPP1 in mediating trophoblast migration of trophoblast cells cannot be ruled out. Both ovine and porcine trophoblast cells adhere to SPP1-coated culture plates and migrate through SPP1-coated transwell insert filters in culture (Frank et al., 2017). Further, it has been proposed that in sheep, which exhibit synepitheliochorial placentation and transient destruction of the endometrial LE in interplacentomal regions of the uterus, SPP1 is secreted from the endometrial LE and binds to integrins expressed by the proliferating shallow GE. SPP1 then mediates migration of the shallow GE cells to repopulate the endometrial LE and maintain epitheliochorial placentation in interplacentomal regions (Seo et al., 2020a). The role(s) of SPP1 in the mouse implantation chamber is potentially complex, but it may be directly involved in initial attachment and migration of the mouse conceptus. Berneau and co-

workers suggest that SPP1 plays a role in the transition from attachment to invasion by mouse blastocysts (Berneau et al., 2019). In that recent study, when exogenous SPP1 was added to mouse blastocyst–Ishikawa cell co-cultures, initial attachment and invasion of the conceptus was weakened, but not delayed. Perhaps more importantly, exogenous SPP1 altered conceptus trophoblast expression of transcription factors involved with differentiation into invasive trophoblast cells. Therefore, SPP1 secreted by the adjacent endometrial LE may bind to integrins on conceptus trophoblast cells to mediate the transition from an adhesive to an invasive phenotype capable of breaching the endometrial LE barrier to the underlying uterine stroma (Berneau et al., 2019). The limited and focal pattern of expression of SPP1 we observed in the implantation chamber of mice supports this idea.

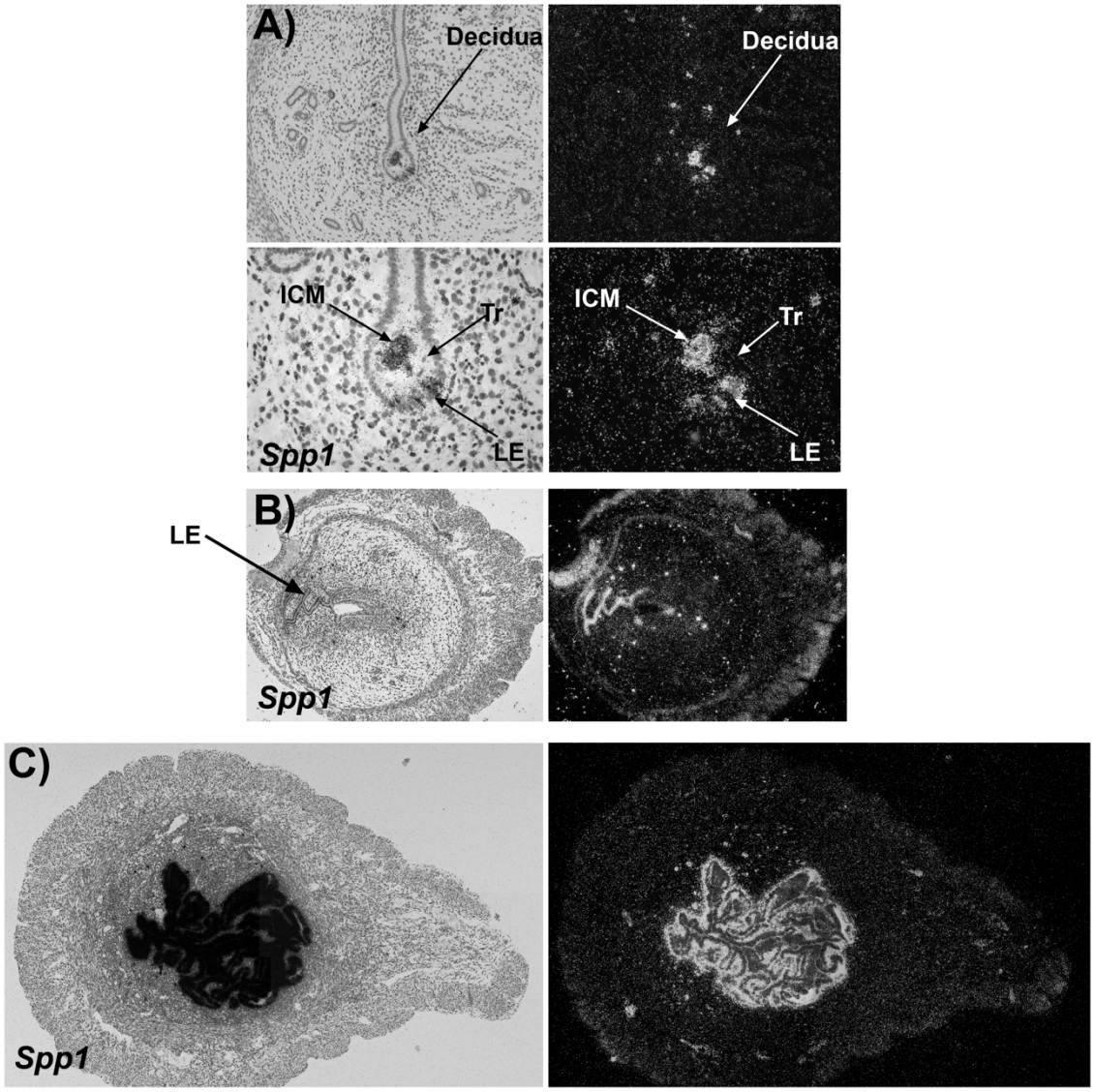

Figure 25. In situ hybridization of *Spp1* mRNA in the implantation chamber and interimplantation sites within the uteri of pregnancy mice.

The mice underwent a delayed implantation procedure. Corresponding brightfield and darkfield images of representative cross sections of endometrium are shown. (A) *Spp1* mRNA is localized to the inner cell mass (ICM) of the blastocyst, to focal extents of the endometrial luminal epithelium (LE) lining the implantation chamber, and to cells

scattered within the endometrial stroma (B). (C) *Spp1* mRNA is universally and highly expressed in the endometrial LE of the interimplantation sites. Legend: Tr, trophoblast. Width of field for the top panels in A is 650 um, for the bottom panels in A is 255 um, for B is 1400 um, and for C is 2500 um.

This distinct local pattern of SPP1 expression could also be explained by a phenomenon of cell invasion observed in cancer cells called entosis (Overholtzer et al., 2007). Entosis is defined as the invasion of a living cell into another cell's cytoplasm. Conceptus trophoblast cells directly attach to endometrial LE during the initial stages of implantation. In mice those endometrial LE cells are eliminated, allowing trophoblast cells to make direct physical contact with the underlying stroma to provide an unencumbered path to invasion of the uterine stroma for successful implantation. Until recently, the consensus has been that trophoblast cells invade through the endometrial LE by initiating apoptosis of the LE followed by phagocytosis of the LE by the trophoblast cells (Parr et al., 1987). However, entosis is similar to phagocytosis, wherein one cell will engulf another, the difference being that phagocytosis engulfs dying or dead cells, while entosis internalizes live cells. Li and coworkers reported that entosis may occur during mouse implantation (Liu et al., 2009). The trophoblast cells actively engulf the endometrial LE cells to remove the LE barrier to trophoblast invasion. As evidence that this is an active process initiated by the trophoblast cells, entosis does not occur when oil is infused into a steroid-primed uterus to induce decidualization (Li et al., 2015). Although the mechanism for elimination of endometrial LE cells is debated we suggest that if entosis takes place in the implantation chamber of mice, SPP1 may have an important role in embryo invasion

into the uterine stroma by maintaining attachment of the trophoblast cells to the endometrial LE, allowing the trophoblast cells to engulf the LE cells.

The embryonic endoderm is one of the first cell types to differentiate from the ICM and is a progenitor tissue responsible for forming the internal organ systems (Liu et al., 2009; Nowotschin et al., 2019). On Day 3.5, the ICM is a homogeneous population of cells, but as the blastocyst expands by Day 4.5, a heterogenous distribution of two distinct cell populations arises, the primitive endoderm and the epiblast (White et al., 2018). Primitive endoderm cells then migrate from the ICM to encapsulate the epiblast and face the blastocyst cavity. By Day 5, the time of embryo implantation, the primitive endoderm cells begin to differentiate into the parietal endoderm cells that then migrate along the trophoblast (Hermitte and Chazaud, 2014). Botquin et al. reported that *Spp1* mRNA was detectable within the ICM from Day 3.5 to Day 4.5 (Botquin et al., 1998). By Day 5.5 SPP1 was no longer detectable in the ICM (Botquin et al., 1998). Using the delayed implantation model in the present study, we confirm that *Spp1* mRNA is present in the ICM during the attachment phase of implantation. It is noteworthy however, that we did not detect SPP1 protein in the ICM, but SPP1 localized to the newly forming parietal endoderm, a cell type in which *Spp1* mRNA was not detected. We hypothesize that SPP1 is synthesized and secreted by cells of the ICM to bind integrins on differentiating and migrating endoderm cells. Accordingly, SPP1 has potential to then mediate endoderm cell functions including adhesion, differentiation and migration.

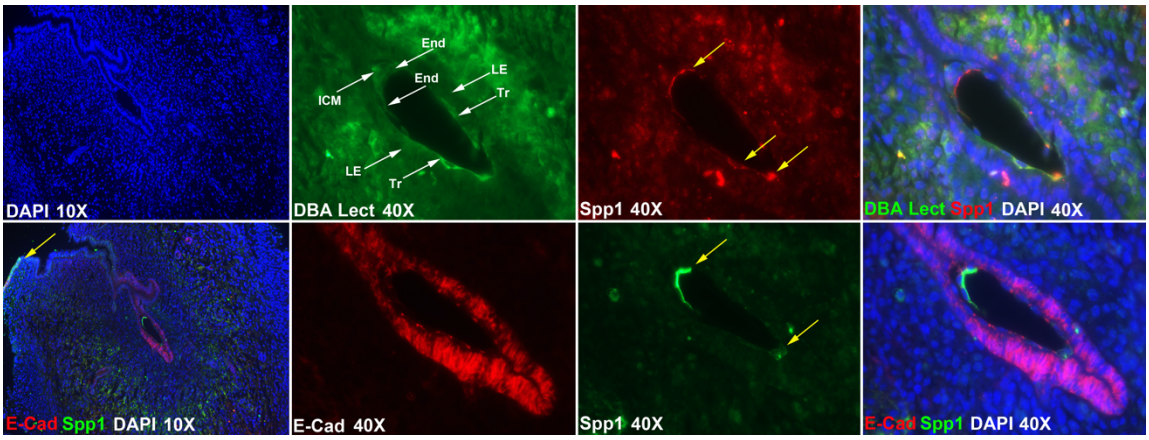

Figure 26. Immunofluorescence localization for Spp1 and E-cadherin (E-Cad), and fluorescence staining for DBA lectin in the implantation chamber of a mouse uterus at Day 5 of pregnancy.

(Top panels) Fluorescence stating for DBA lectin (green) and SPP1 (red) proteins. SPP1 is expressed by extra-embryonic endoderm (End) and some trophoblast [21] cells directly contacting the endometrial luminal epithelium (LE) within the implantation chamber, while DBA lectin is expressed in the same Tr cells as SPP1. (Bottom panels) Immunofluorescence staining for E-cad (red) and SPP1 (green) proteins. SPP1 protein is expressed by the endoderm (End). Legend: ICM, inner cell mass. Width of field for the far-left panels is 870 um, and the right 3 the panels is 220 um.

Nomura and co-workers (Nomura et al., 1988) and Waterhouse and co-workers (Waterhouse et al., 1992) were the first to observe the expression of SPP1 in granulated metrial gland cells (GMC) of decidual and deciduoma tissues, and speculated that SPP1 localized to immune cells. Decidual expression was again reported by Mangale and Reddy (Mangale and Reddy, 2007), and the cells expressing SPP1 were confirmed to be uNK

cells (Herington and Bany, 2007a). Results of the present study support those findings. However, this is the first study to localize both *Spp1* mRNA and SPP1 protein in decidual tissues throughout pregnancy. Our results demonstrate that SPP1 increases as the decidua continues to grow, then appears to decrease between Days 15 and 17 of gestation. In addition, as shown previously (Herington and Bany, 2007a), cells stained positive for SPP1 in the decidua also bind DBA lectin, a marker for uNK cells. As further evidence that uNK cells express SPP1, we examined the expression of SPP1 in the decidua of *Il15*-null mice. Il15 is required for the differentiation of precursor NK cells into lineage-committed uNK cells (Kennedy et al., 2000). *Il15*-null mice lack decidual expression of SPP1, further establishing that it is uNK cells that express SPP1.

The role of SPP1 within the decidua remains unknown, but uNK cells are believed to be involved with vascular changes and maintaining decidual integrity throughout pregnancy (Croy et al., 2003; Herington and Bany, 2007b). SPP1 has been shown to be involved with, or linked to, angiogenesis in other tissues (Chakraborty et al., 2008; Cook et al., 2005; Dai et al., 2009; Denhardt and Guo, 1993; Prols et al., 1998; Shijubo et al., 2000; Takano et al., 2000), including the placentae of sheep and pigs(Frank et al., 2021; Wing et al., 2020). One of the major roles of the decidual vasculature is to provide maternal nutrients to the developing placenta and embryo/fetus. When Weintraub et al. performed studies in mice to determine the effects of SPP1 on pregnancies in vivo, they determined that the pups of *Spp1*-null mice were growth-restricted (Weintraub et al., 2004). It is important to note that four strains of mice that lack decidual NK cells, including *Il15*-null mice, have anomalies of the decidua that result in fetuses with significantly lower

birthweights, similar to the outcome for mice with *Spp1*-null fetuses (Barber and Pollard, 2003; Croy et al., 2003; Greenwood et al., 2000; Weintraub et al., 2004). Taken together, it is likely that uNK cells synthesize and secrete SPP1 into the decidua to aid in remodeling of the decidual spiral arteries and the decidual bed to provide for transport of nutrients and gases across the maternal-conceptus interface to support development of the conceptuses.

We also report expression of *Spp1* mRNA in the fetal bone on Day 16 of gestation. This was expected because SPP1 is a major non-collagenous glycoprotein in the bone matrix and was first discovered in bone in 1985 when Franzen and Heinegard isolated two different sialoproteins from bovine bone; fraction 1 being osteopontin and fraction 2 being osteonectin (Franzen and Heinegard, 1985). Our results are consistent with previous reports for the spatial expression of SPP1 in the developing bone of rat and mouse fetuses (Chen et al., 1992; Hultenby et al., 1994; Nakase et al., 1994).

Collectively, results of the present study highlight the complex biological functions of secretory SPP1 and suggest likely roles in modifying the uterine-placental environment to support pregnancy in mice. Specifically, SPP1 appears to aid in the closure of interimplantation sites within the pregnant uterus, creating the implantation chamber necessary for proper apposition of trophoblast and endometrial LE. SPP1 may facilitate the initial attachment and early invasion of the blastocyst influencing or inducing the transition of trophoblast cells from an adhesive to an invasive phenotype necessary for successful conceptus implantation. SPP1 may also mediate differentiation and migration of the primitive parietal endoderm of the embryo. And, SPP1 may be secreted by uNK

cells within the decidua to aid in angiogenesis and vascular remodeling to provide hemotrophic support to the developing placenta and embryo/fetus.

REFERENCES

Abrams, R.M. (1979). Energy metabolism. Semin Perinatol *3*, 109-119.

Aghayan, M., Rao, L.V., Smith, R.M., Jarett, L., Charron, M.J., Thorens, B., and Heyner, S. (1992). Developmental expression and cellular localization of glucose transporter molecules during mouse preimplantation development. Development *115*, 305-312.

Aherne, F., Hays, V.W., Ewan, R.C., and Speer, V.C. (1969). Absorption and utilization of sugars by the baby pigs. J Anim Sci *29*, 444-450.

Akram, M. (2013). Mini-review on glycolysis and cancer. J Cancer Educ *28*, 454-457.

Albelda, S.M., and Buck, C.A. (1990). Integrins and other cell adhesion molecules. FASEB J *4*, 2868-2880.

Alexander, D.P., Huggett, A.S., Nixon, D.A., and Widdas, W.F. (1955). The placental transfer of sugars in the sheep: the influence of concentration gradient upon the rates of hexose formation as shown in umbilical perfusion of the placenta. J Physiol *129*, 367-383.

Amoroso, E.C. (1955). [Significance of the placenta in the development of pregnancy in viviparous animals]. Ann Endocrinol (Paris) *16*, 435-447.

Angulo, C., Rauch, M.C., Droppelmann, A., Reyes, A.M., Slebe, J.C., Delgado-Lopez, F., Guaiquil, V.H., Vera, J.C., and Concha, II (1998). Hexose transporter expression and function in mammalian spermatozoa: cellular localization and transport of hexoses and vitamin C. J Cell Biochem *71*, 189-203.

Aplin, J.D. (1997). Adhesion molecules in implantation. Rev Reprod *2*, 84-93.

Apparao, K.B., Illera, M.J., Beyler, S.A., Olson, G.E., Osteen, K.G., Corjay, M.H., Boggess, K., and Lessey, B.A. (2003). Regulated expression of osteopontin in the peri-implantation rabbit uterus. Biol Reprod *68*, 1484-1490.

Au, S.W., Gover, S., Lam, V.M., and Adams, M.J. (2000). Human glucose-6-phosphate dehydrogenase: the crystal structure reveals a structural NADP(+) molecule and provides insights into enzyme deficiency. Structure *8*, 293-303.

Augustin, R. (2010). The protein family of glucose transport facilitators: It's not only about glucose after all. IUBMB Life *62*, 315-333.

Augustin, R., Pocar, P., Navarrete-Santos, A., Wrenzycki, C., Gandolfi, F., Niemann, H., and Fischer, B. (2001). Glucose transporter expression is developmentally regulated in in vitro derived bovine preimplantation embryos. Mol Reprod Dev *60*, 370-376.

Augustin, R., Riley, J., and Moley, K.H. (2005). GLUT8 contains a [DE]XXXL[LI] sorting motif and localizes to a late endosomal/lysosomal compartment. Traffic *6*, 1196-1212.

Ayala, A., Fabregat, I., and Machado, A. (1991). The role of NADPH in the regulation of glucose-6-phosphate and 6-phosphogluconate dehydrogenases in rat adipose tissue. Mol Cell Biochem *105*, 1-5.

Bacon, J.S., and Bell, D.J. (1948). Fructose and glucose in the blood of the foetal sheep. Biochem J *42*, 397-405.

Baldwin, S.A. (1993). Mammalian passive glucose transporters: members of an ubiquitous family of active and passive transport proteins. Biochim Biophys Acta *1154*, 17-49.

Barber, E.M., and Pollard, J.W. (2003). The uterine NK cell population requires IL-15 but these cells are not required for pregnancy nor the resolution of a Listeria monocytogenes infection. J Immunol *171*, 37-46.

Bartrons, R., and Caro, J. (2007). Hypoxia, glucose metabolism and the Warburg's effect. J Bioenerg Biomembr *39*, 223-229.

Battaglia, F.C., and Meschia, G. (1981). Foetal and placental metabolisms: their interrelationship and impact upon maternal metabolism. Proc Nutr Soc *40*, 99-113.

Bazer, F.W., and Johnson, G.A. (2014). Pig blastocyst-uterine interactions. Differentiation *87*, 52-65.

Bazer, F.W., Song, G., Kim, J., Dunlap, K.A., Satterfield, M.C., Johnson, G.A., Burghardt, R.C., and Wu, G. (2012). Uterine biology in pigs and sheep. J Anim Sci Biotechnol *3*, 23.

Bazer, F.W., and Thatcher, W.W. (1977). Theory of maternal recognition of pregnancy in swine based on estrogen controlled endocrine versus exocrine secretion of prostaglandin F2alpha by the uterine endometrium. Prostaglandins *14*, 397-400.

Bazer, F.W., Thatcher, W.W., Martinat-Botte, F., and Terqui, M. (1988). Conceptus development in large white and prolific Chinese Meishan pigs. J Reprod Fertil *84*, 37-42.

Beall, M.H., Wang, S., Yang, B., Chaudhri, N., Amidi, F., and Ross, M.G. (2007). Placental and membrane aquaporin water channels: correlation with amniotic fluid volume and composition. Placenta *28*, 421-428.

Bebington, C., Bell, S.C., Doherty, F.J., Fazleabas, A.T., and Fleming, S.D. (1999). Localization of ubiquitin and ubiquitin cross-reactive protein in human and baboon endometrium and decidua during the menstrual cycle and early pregnancy. Biol Reprod *60*, 920-928.

Bell, A.W., and Ehrhardt, R.A. (2002). Regulation of placental nutrient transport and implications for fetal growth. Nutr Res Rev *15*, 211-230.

Bell, G.I., Burant, C.F., Takeda, J., and Gould, G.W. (1993). Structure and function of mammalian facilitative sugar transporters. J Biol Chem *268*, 19161-19164.

Berneau, S.C., Ruane, P.T., Brison, D.R., Kimber, S.J., Westwood, M., and Aplin, J.D. (2019). Characterisation of Osteopontin in an In Vitro Model of Embryo Implantation. Cells *8*.

Bertout, J.A., Patel, S.A., and Simon, M.C. (2008). The impact of O2 availability on human cancer. Nat Rev Cancer *8*, 967-975.

Blomberg, L., Hashizume, K., and Viebahn, C. (2008). Blastocyst elongation, trophoblastic differentiation, and embryonic pattern formation. Reproduction *135*, 181-195.

Boros, L.G., Brandes, J.L., Yusuf, F.I., Cascante, M., Williams, R.D., and Schirmer, W.J. (1998a). Inhibition of the oxidative and nonoxidative pentose phosphate pathways by somatostatin: a possible mechanism of antitumor action. Med Hypotheses *50*, 501-506.

Boros, L.G., Lee, P.W., Brandes, J.L., Cascante, M., Muscarella, P., Schirmer, W.J., Melvin, W.S., and Ellison, E.C. (1998b). Nonoxidative pentose phosphate pathways and their direct role in ribose synthesis in tumors: is cancer a disease of cellular glucose metabolism? Med Hypotheses *50*, 55-59.

Botquin, V., Hess, H., Fuhrmann, G., Anastassiadis, C., Gross, M.K., Vriend, G., and Scholer, H.R. (1998). New POU dimer configuration mediates antagonistic control of an osteopontin preimplantation enhancer by Oct-4 and Sox-2. Genes Dev *12*, 2073-2090.

Bowen, J.A., Bazer, F.W., and Burghardt, R.C. (1996). Spatial and temporal analyses of

integrin and Muc-1 expression in porcine uterine epithelium and trophectoderm in vivo. Biol Reprod *55*, 1098-1106.

Brand, K. (1985). Glutamine and glucose metabolism during thymocyte proliferation. Pathways of glutamine and glutamate metabolism. Biochem J *228*, 353-361.

Bremer, J.L. (1916). The interrelations of the mesonephros, kidney and placenta in development of classes of animals. Am J Anat *19*, 179-210.

Brown, K., Heller, D.S., Zamudio, S., and Illsley, N.P. (2011). Glucose transporter 3 (GLUT3) protein expression in human placenta across gestation. Placenta *32*, 1041-1049.

Brown, L.F., Berse, B., Van de Water, L., Papadopoulos-Sergiou, A., Perruzzi, C.A., Manseau, E.J., Dvorak, H.F., and Senger, D.R. (1992). Expression and distribution of osteopontin in human tissues: widespread association with luminal epithelial surfaces. Mol Biol Cell *3*, 1169-1180.

Burant, C.F., Takeda, J., Brot-Laroche, E., Bell, G.I., and Davidson, N.O. (1992). Fructose transporter in human spermatozoa and small intestine is GLUT5. J Biol Chem *267*, 14523-14526.

Burghardt, R.C., Bowen, J.A., Newton, G.R., and Bazer, F.W. (1997). Extracellular matrix and the implantation cascade in pigs. J Reprod Fertil Suppl *52*, 151-164.

Burghardt, R.C., Burghardt, J.R., Taylor, J.D., 2nd, Reeder, A.T., Nguen, B.T., Spencer, T.E., Bayless, K.J., and Johnson, G.A. (2009). Enhanced focal adhesion assembly reflects increased mechanosensation and mechanotransduction at maternal-conceptus interface and uterine wall during ovine pregnancy. Reproduction *137*, 567-582.

Burghardt, R.C., Johnson, G.A., Jaeger, L.A., Ka, H., Garlow, J.E., Spencer, T.E., and Bazer, F.W. (2002). Integrins and extracellular matrix proteins at the maternal-fetal interface in domestic animals. Cells Tissues Organs *172*, 202-217.

Butler, W.T., Ridall, A.L., and McKee, M.D. (1996). Osteopontin (Academic Press).

Carson, D.D., Bagchi, I., Dey, S.K., Enders, A.C., Fazleabas, A.T., Lessey, B.A., and Yoshinaga, K. (2000). Embryo implantation. Dev Biol *223*, 217-237.

Chaen, T., Konno, T., Egashira, M., Bai, R., Nomura, N., Nomura, S., Hirota, Y., Sakurai, T., and Imakawa, K. (2012). Estrogen-dependent uterine secretion of osteopontin activates blastocyst adhesion competence. PLoS One *7*, e48933.

Chakraborty, G., Jain, S., and Kundu, G.C. (2008). Osteopontin promotes vascular endothelial growth factor-dependent breast tumor growth and angiogenesis via autocrine and paracrine mechanisms. Cancer Res *68*, 152-161.

Chan, H.C., Ruan, Y.C., He, Q., Chen, M.H., Chen, H., Xu, W.M., Chen, W.Y., Xie, C., Zhang, X.H., and Zhou, Z. (2009). The cystic fibrosis transmembrane conductance regulator in reproductive health and disease. J Physiol *587*, 2187-2195.

Chen, J., Shapiro, H.S., and Sodek, J. (1992). Development expression of bone sialoprotein mRNA in rat mineralized connective tissues. J Bone Miner Res *7*, 987-997.

Chen, L.Q., Cheung, L.S., Feng, L., Tanner, W., and Frommer, W.B. (2015). Transport of sugars. Annu Rev Biochem *84*, 865-894.

Cohen, P., and Rosemeyer, M.A. (1969). Subunit interactions of glucose-6-phosphate dehydrogenase from human erythrocytes. Eur J Biochem *8*, 8-15.

Cole, S.W., and Hitchcock, M.W. (1946). Sugars in the foetal and maternal bloods of sheep. Biochem J *40*, li.

Cook, A.C., Tuck, A.B., McCarthy, S., Turner, J.G., Irby, R.B., Bloom, G.C., Yeatman, T.J., and Chambers, A.F. (2005). Osteopontin induces multiple changes in gene expression that reflect the six "hallmarks of cancer" in a model of breast cancer progression. Mol Carcinog *43*, 225-236.

Cooke, P.S., Buchanan, D.L., Young, P., Setiawan, T., Brody, J., Korach, K.S., Taylor, J., Lubahn, D.B., and Cunha, G.R. (1997). Stromal estrogen receptors mediate mitogenic effects of estradiol on uterine epithelium. Proc Natl Acad Sci U S A *94*, 6535-6540.

Cori, C. (1925). The fate of sugar in the animal body. I. The rate of absorption of hexoses and pentoses from the intestinal tract. J Biol Chem *66*, 691-715.

Cori, C. (1926). The rate of absorption of a mixture of glucose and galactose. Proc Soc Exp Biol Med *23*, 290-291.

Crane, R.K. (1965). Na+ -dependent transport in the intestine and other animal tissues. Fed Proc *24*, 1000-1006.

Croy, B.A., He, H., Esadeg, S., Wei, Q., McCartney, D., Zhang, J., Borzychowski, A., Ashkar, A.A., Black, G.P., Evans, S.S*., et al.* (2003). Uterine natural killer cells: insights into their cellular and molecular biology from mouse modelling. Reproduction *126*, 149-160.

Cura, A.J., and Carruthers, A. (2012). Role of monosaccharide transport proteins in carbohydrate assimilation, distribution, metabolism, and homeostasis. Compr Physiol *2*, 863-914.

Currie, M.J., Bassett, N.S., and Gluckman, P.D. (1997). Ovine glucose transporter-1 and -3: cDNA partial sequences and developmental gene expression in the placenta. Placenta *18*, 393-401.

Dai, J., Peng, L., Fan, K., Wang, H., Wei, R., Ji, G., Cai, J., Lu, B., Li, B., Zhang, D.*, et al.* (2009). Osteopontin induces angiogenesis through activation of PI3K/AKT and ERK1/2 in endothelial cells. Oncogene *28*, 3412-3422.

Dantzer, V. (1984). Scanning electron microscopy of exposed surfaces of the porcine placenta. Acta Anat (Basel) *118*, 96-106.

Dantzer, V. (1985). Electron microscopy of the initial stages of placentation in the pig. Anat Embryol (Berl) *172*, 281-293.

Davies, J. (1952). Correlated anatomical and histochemical studies on the mesonephros and placenta of the sheep. Am J Anat *91*, 263-299.

de Oliveira, V., Schaefer, J., Abu-Rafea, B., Vilos, G.A., Vilos, A.G., Bhattacharya, M., Radovick, S., and Babwah, A.V. (2020). Uterine aquaporin expression is dynamically regulated by estradiol and progesterone and ovarian stimulation disrupts embryo implantation without affecting luminal closure. Mol Hum Reprod *26*, 154-166.

De Vos, M., Che, L., Huygelen, V., Willemen, S., Michiels, J., Van Cruchten, S., and Van Ginneken, C. (2014). Nutritional interventions to prevent and rear low-birthweight piglets. J Anim Physiol Anim Nutr (Berl) *98*, 609-619.

DeBerardinis, R.J., Mancuso, A., Daikhin, E., Nissim, I., Yudkoff, M., Wehrli, S., and Thompson, C.B. (2007). Beyond aerobic glycolysis: transformed cells can engage in glutamine metabolism that exceeds the requirement for protein and nucleotide synthesis. Proc Natl Acad Sci U S A *104*, 19345-19350.

DeBosch, B.J., Chen, Z., Saben, J.L., Finck, B.N., and Moley, K.H. (2014). Glucose transporter 8 (GLUT8) mediates fructose-induced de novo lipogenesis and macrosteatosis. J Biol Chem *289*, 10989-10998.

Denhardt, D.T., and Guo, X. (1993). Osteopontin: a protein with diverse functions. FASEB J *7*, 1475-1482.

Douard, V., and Ferraris, R.P. (2008). Regulation of the fructose transporter GLUT5 in health and disease. Am J Physiol Endocrinol Metab *295*, E227-237.

Eggleston, L.V., and Krebs, H.A. (1974). Regulation of the pentose phosphate cycle. Biochem J *138*, 425-435.

Erikson, D.W., Burghardt, R.C., Bayless, K.J., and Johnson, G.A. (2009). Secreted phosphoprotein 1 (SPP1, osteopontin) binds to integrin alpha v beta 6 on porcine trophectoderm cells and integrin alpha v beta 3 on uterine luminal epithelial cells, and promotes trophectoderm cell adhesion and migration. Biol Reprod *81*, 814-825.

Farina, A.R., Cappabianca, L., Sebastiano, M., Zelli, V., Guadagni, S., and Mackay, A.R. (2020). Hypoxia-induced alternative splicing: the 11th Hallmark of Cancer. J Exp Clin Cancer Res *39*, 110.

Feng, L., and Frommer, W.B. (2015). Structure and function of SemiSWEET and SWEET sugar transporters. Trends Biochem Sci *40*, 480-486.

Fisher, L.W., Stubbs, J.T., 3rd, and Young, M.F. (1995). Antisera and cDNA probes to human and certain animal model bone matrix noncollagenous proteins. Acta Orthop Scand Suppl *266*, 61-65.

Fowden, A.L., Forhead, A.J., Silver, M., and MacDonald, A.A. (1997). Glucose, lactate and oxygen metabolism in the fetal pig during late gestation. Exp Physiol *82*, 171-182.

Fox, C.F., and Kennedy, E.P. (1965). Specific labeling and partial purification of the M protein, a component of the beta-galactoside transport system of Escherichia coli. Proc Natl Acad Sci U S A *54*, 891-899.

Frank, J.W., Seo, H., Burghardt, R.C., Bayless, K.J., and Johnson, G.A. (2017). ITGAV (alpha v integrins) bind SPP1 (osteopontin) to support trophoblast cell adhesion. Reproduction *153*, 695-706.

Frank, J.W., Steinhauser, C.B., Wang, X., Burghardt, R.C., Bazer, F.W., and Johnson, G.A. (2021). Loss of ITGB3 in ovine conceptuses decreases conceptus expression of NOS3 and SPP1: implications for the developing placental vasculaturedagger. Biol Reprod *104*, 657-668.

Franzen, A., and Heinegard, D. (1985). Isolation and characterization of two sialoproteins present only in bone calcified matrix. Biochem J *232*, 715-724.

Friess, A.E., Sinowatz, F., Skolek-Winnisch, R., and Traautner, W. (1980). The placenta of the pig. I. Finestructural changes of the placental barrier during pregnancy. Anat Embryol (Berl) *158*, 179-191.

Friess, A.E., Sinowatz, F., Skolek-Winnisch, R., and Trautner, W. (1981). The placenta of the pig. II. The ultrastructure of the areolae. Anat Embryol (Berl) *163*, 43-53.

Frolova, A., Flessner, L., Chi, M., Kim, S.T., Foyouzi-Yousefi, N., and Moley, K.H. (2009). Facilitative glucose transporter type 1 is differentially regulated by progesterone and estrogen in murine and human endometrial stromal cells. Endocrinology *150*, 1512-1520.

Frolova, A.I., and Moley, K.H. (2011a). Glucose transporters in the uterus: an analysis of tissue distribution and proposed physiological roles. Reproduction *142*, 211-220.

Frolova, A.I., and Moley, K.H. (2011b). Glucose transporters in the uterus: an analysis of tissue distribution and proposed physiological roles. Reproduction *142*, 211-220.

Frolova, A.I., and Moley, K.H. (2011c). Quantitative analysis of glucose transporter mRNAs in endometrial stromal cells reveals critical role of GLUT1 in uterine receptivity. Endocrinology *152*, 2123-2128.

Ganguly, A., McKnight, R.A., Raychaudhuri, S., Shin, B.C., Ma, Z., Moley, K., and Devaskar, S.U. (2007). Glucose transporter isoform-3 mutations cause early pregnancy loss and fetal growth restriction. Am J Physiol Endocrinol Metab *292*, E1241-1255.

Gao, H., Wu, G., Spencer, T.E., Johnson, G.A., and Bazer, F.W. (2009a). Select Nutrients in the Ovine Uterine Lumen. II. Glucose Transporters in the Uterus and Peri-Implantation Conceptuses. Biol Reprod *80*, 94-104.

Gao, H., Wu, G., Spencer, T.E., Johnson, G.A., and Bazer, F.W. (2009b). Select nutrients in the ovine uterine lumen. ii. glucose transporters in the uterus and peri-implantation conceptuses. Biol Reprod *80*, 94-104.

Gao, H., Wu, G., Spencer, T.E., Johnson, G.A., and Bazer, F.W. (2009c). Select nutrients in the ovine uterine lumen. III. Cationic amino acid transporters in the ovine uterus and peri-implantation conceptuses. Biol Reprod *80*, 602-609.

Garlow, J.E., Ka, H., Johnson, G.A., Burghardt, R.C., Jaeger, L.A., and Bazer, F.W. (2002). Analysis of osteopontin at the maternal-placental interface in pigs. Biol Reprod *66*, 718-725.

Gatenby, R.A., and Gillies, R.J. (2004). Why do cancers have high aerobic glycolysis? Nat Rev Cancer *4*, 891-899.

Geisert, R.D., Brenner, R.M., Moffatt, R.J., Harney, J.P., Yellin, T., and Bazer, F.W. (1993). Changes in oestrogen receptor protein, mRNA expression and localization in the endometrium of cyclic and pregnant gilts. Reprod Fertil Dev *5*, 247-260.

Geisert, R.D., Brookbank, J.W., Roberts, R.M., and Bazer, F.W. (1982a). Establishment of pregnancy in the pig: II. Cellular remodeling of the porcine blastocyst during elongation on day 12 of pregnancy. Biol Reprod *27*, 941-955.

Geisert, R.D., Pratt, T.N., Bazer, F.W., Mayes, J.S., and Watson, G.H. (1994). Immunocytochemical localization and changes in endometrial progestin receptor protein during the porcine oestrous cycle and early pregnancy. Reprod Fertil Dev *6*, 749-760.

Geisert, R.D., Thatcher, W.W., Roberts, R.M., and Bazer, F.W. (1982b). Establishment of pregnancy in the pig: III. Endometrial secretory response to estradiol valerate administered on day 11 of the estrous cycle. Biol Reprod *27*, 957-965.

Geisert, R.D., Zavy, M.T., Wettemann, R.P., and Biggers, B.G. (1987). Length of pseudopregnancy and pattern of uterine protein release as influenced by time and duration of oestrogen administration in the pig. J Reprod Fertil *79*, 163-172.

Giancotti, F.G., and Ruoslahti, E. (1999). Integrin signaling. Science *285*, 1028-1032.

Gingras, A.C., Raught, B., and Sonenberg, N. (2004). mTOR signaling to translation. Curr Top Microbiol Immunol *279*, 169-197.

Goldstein, M.H., Bazer, F.W., and Barron, D.H. (1980). Characterization of changes in volume, osmolarity and electrolyte composition of porcine fetal fluids during gestation. Biol Reprod *22*, 1168-1180.

Goodwin, R.F. (1956). Division of the common mammals into two groups according to the concentration of fructose in the blood of the foetus. J Physiol *132*, 146-156.

Greenwood, J.D., Minhas, K., di Santo, J.P., Makita, M., Kiso, Y., and Croy, B.A. (2000). Ultrastructural studies of implantation sites from mice deficient in uterine natural killer cells. Placenta *21*, 693-702.

Griffith, J.K., Baker, M.E., Rouch, D.A., Page, M.G., Skurray, R.A., Paulsen, I.T., Chater, K.F., Baldwin, S.A., and Henderson, P.J. (1992). Membrane transport proteins: implications of sequence comparisons. Curr Opin Cell Biol *4*, 684-695.

Hahn, D., Blaschitz, A., Korgun, E.T., Lang, I., Desoye, G., Skofitsch, G., and Dohr, G. (2001). From maternal glucose to fetal glycogen: expression of key regulators in the human placenta. Mol Hum Reprod *7*, 1173-1178.

Harrell, C.S., Burgado, J., Kelly, S.D., and Neigh, G.N. (2014). Ovarian steroids influence cerebral glucose transporter expression in a region- and isoform-specific pattern. J Neuroendocrinol *26*, 217-225.

Harris, A.L. (2002). Hypoxia--a key regulatory factor in tumour growth. Nat Rev Cancer *2*, 38-47.

Hedeskov, C.J. (1968). Early effects of phytohaemagglutinin on glucose metabolism of normal human lymphocytes. Biochem J *110*, 373-380.

Heimberg, H., De Vos, A., Pipeleers, D., Thorens, B., and Schuit, F. (1995). Differences in glucose transporter gene expression between rat pancreatic alpha- and beta-cells are correlated to differences in glucose transport but not in glucose utilization. J Biol Chem *270*, 8971-8975.

Henderson, A.R. (1969). Biochemistry of hypoxia: current concepts. I. An introduction to biochemical pathways and their control. Br J Anaesth *41*, 245-250.

Herington, J.L., and Bany, B.M. (2007a). The conceptus increases secreted phosphoprotein 1 gene expression in the mouse uterus during the progression of decidualization mainly due to its effects on uterine natural killer cells. Reproduction *133*, 1213-1221.

Herington, J.L., and Bany, B.M. (2007b). Effect of the conceptus on uterine natural killer cell numbers and function in the mouse uterus during decidualization. Biol Reprod *76*, 579-588.

Hermitte, S., and Chazaud, C. (2014). Primitive endoderm differentiation: from specification to epithelium formation. Philos Trans R Soc Lond B Biol Sci *369*.

Hilf, R., Ickowicz, R., Bartley, J.C., and Abraham, S. (1975). Multiple molecular forms of glucose-6-phosphate dehydrogenase in normal, preneoplastic, and neoplastic mammary tissues of mice. Cancer Res *35*, 2109-2116.

Huang, S., and Czech, M.P. (2007). The GLUT4 glucose transporter. Cell Metab *5*, 237-252.

Huggett, A.S., Warren, F.L., and Warren, N.V. (1951). The origin of the blood fructose of the foetal sheep. J Physiol *113*, 258-275.

Hultenby, K., Reinholt, F.P., Norgard, M., Oldberg, A., Wendel, M., and Heinegard, D. (1994). Distribution and synthesis of bone sialoprotein in metaphyseal bone of young rats show a distinctly different pattern from that of osteopontin. Eur J Cell Biol *63*, 230-239.

Hume, D.A., Radik, J.L., Ferber, E., and Weidemann, M.J. (1978). Aerobic glycolysis and lymphocyte transformation. Biochem J *174*, 703-709.

Hume, D.A., and Weidemann, M.J. (1979). Role and regulation of glucose metabolism in proliferating cells. J Natl Cancer Inst *62*, 3-8.

Ibberson, M., Uldry, M., and Thorens, B. (2000). GLUTX1, a novel mammalian glucose transporter expressed in the central nervous system and insulin-sensitive tissues. J Biol Chem *275*, 4607-4612.

James, D.E., Brown, R., Navarro, J., and Pilch, P.F. (1988). Insulin-regulatable tissues express a unique insulin-sensitive glucose transport protein. Nature *333*, 183-185.

Jansson, T., Cowley, E.A., and Illsley, N.P. (1995). Cellular localization of glucose transporter messenger RNA in human placenta. Reprod Fertil Dev *7*, 1425-1430.

Jansson, T., Wennergren, M., and Illsley, N.P. (1993). Glucose transporter protein expression in human placenta throughout gestation and in intrauterine growth retardation. J Clin Endocrinol Metab *77*, 1554-1562.

Johnson, G.A., Bazer, F.W., Burghardt, R.C., Spencer, T.E., Wu, G., and Bayless, K.J. (2009). Conceptus-uterus interactions in pigs: endometrial gene expression in response to estrogens and interferons from conceptuses. Soc Reprod Fertil Suppl *66*, 321-332.

Johnson, G.A., Bazer, F.W., Jaeger, L.A., Ka, H., Garlow, J.E., Pfarrer, C., Spencer, T.E., and Burghardt, R.C. (2001). Muc-1, integrin, and osteopontin expression during the implantation cascade in sheep. Biol Reprod *65*, 820-828.

Johnson, G.A., Burghardt, R.C., and Bazer, F.W. (2014). Osteopontin: a leading candidate adhesion molecule for implantation in pigs and sheep. J Anim Sci Biotechnol *5*, 56.

Johnson, G.A., Burghardt, R.C., Joyce, M.M., Spencer, T.E., Bazer, F.W., Pfarrer, C., and Gray, C.A. (2003). Osteopontin expression in uterine stroma indicates a decidualization-like differentiation during ovine pregnancy. Biol Reprod *68*, 1951-1958.

Johnson, G.A., Burghardt, R.C., Spencer, T.E., Newton, G.R., Ott, T.L., and Bazer, F.W. (1999a). Ovine osteopontin: II. Osteopontin and alpha(v)beta(3) integrin expression in the uterus and conceptus during the periimplantation period. Biol Reprod *61*, 892-899.

Johnson, G.A., Spencer, T.E., Burghardt, R.C., and Bazer, F.W. (1999b). Ovine osteopontin: I. Cloning and expression of messenger ribonucleic acid in the uterus during the periimplantation period. Biol Reprod *61*, 884-891.

Johnson, G.A., Spencer, T.E., Burghardt, R.C., Taylor, K.M., Gray, C.A., and Bazer, F.W. (2000). Progesterone modulation of osteopontin gene expression in the ovine uterus. Biol Reprod *62*, 1315-1321.

Jonas, S.K., Benedetto, C., Flatman, A., Hammond, R.H., Micheletti, L., Riley, C., Riley, P.A., Spargo, D.J., Zonca, M., and Slater, T.F. (1992). Increased activity of 6-phosphogluconate dehydrogenase and glucose-6-phosphate dehydrogenase in purified cell suspensions and single cells from the uterine cervix in cervical intraepithelial neoplasia. Br J Cancer *66*, 185-191.

Joyce, M.M., Burghardt, R.C., Geisert, R.D., Burghardt, J.R., Hooper, R.N., Ross, J.W., Ashworth, M.D., and Johnson, G.A. (2007). Pig conceptuses secrete estrogen and interferons to differentially regulate uterine STAT1 in a temporal and cell type-specific manner. Endocrinology *148*, 4420-4431.

Joyce, M.M., Gonzalez, J.F., Lewis, S., Woldesenbet, S., Burghardt, R.C., Newton, G.R., and Johnson, G.A. (2005a). Caprine uterine and placental osteopontin expression is distinct among epitheliochorial implanting species. Placenta *26*, 160-170.

Joyce, M.M., White, F.J., Burghardt, R.C., Muniz, J.J., Spencer, T.E., Bazer, F.W., and Johnson, G.A. (2005b). Interferon stimulated gene 15 conjugates to endometrial cytosolic proteins and is expressed at the uterine-placental interface throughout pregnancy in sheep. Endocrinology *146*, 675-684.

Judge, A., and Dodd, M.S. (2020). Metabolism. Essays Biochem *64*, 607-647.

Ka, H., Al-Ramadan, S., Erikson, D.W., Johnson, G.A., Burghardt, R.C., Spencer, T.E., Jaeger, L.A., and Bazer, F.W. (2007). Regulation of expression of fibroblast growth factor 7 in the pig uterus by progesterone and estradiol. Biol Reprod *77*, 172-180.

Kang, Y.J., Forbes, K., Carver, J., and Aplin, J.D. (2014). The role of the osteopontin-integrin alphavbeta3 interaction at implantation: functional analysis using three different in vitro models. Hum Reprod *29*, 739-749.

Kayano, T., Burant, C.F., Fukumoto, H., Gould, G.W., Fan, Y.S., Eddy, R.L., Byers, M.G., Shows, T.B., Seino, S., and Bell, G.I. (1990). Human facilitative glucose transporters. Isolation, functional characterization, and gene localization of cDNAs encoding an isoform (GLUT5) expressed in small intestine, kidney, muscle, and adipose tissue and an unusual glucose transporter pseudogene-like sequence (GLUT6). J Biol Chem *265*, 13276-13282.

Kayano, T., Fukumoto, H., Eddy, R.L., Fan, Y.S., Byers, M.G., Shows, T.B., and Bell, G.I. (1988). Evidence for a family of human glucose transporter-like proteins. Sequence and gene localization of a protein expressed in fetal skeletal muscle and other tissues. J Biol Chem *263*, 15245-15248.

Kazanecki, C.C., Uzwiak, D.J., and Denhardt, D.T. (2007). Control of osteopontin signaling and function by post-translational phosphorylation and protein folding. J Cell Biochem *102*, 912-924.

Kennedy, M.K., Glaccum, M., Brown, S.N., Butz, E.A., Viney, J.L., Embers, M., Matsuki, N., Charrier, K., Sedger, L., Willis, C.R.*, et al.* (2000). Reversible defects in natural killer and memory CD8 T cell lineages in interleukin 15-deficient mice. J Exp Med *191*, 771-780.

Kierans, S.J., and Taylor, C.T. (2021). Regulation of glycolysis by the hypoxia-inducible factor (HIF): implications for cellular physiology. J Physiol *599*, 23-37.

Kim, J., Song, G., Wu, G., and Bazer, F.W. (2012). Functional roles of fructose. Proc Natl Acad Sci U S A *109*, E1619-1628.

Kim, S.T., and Moley, K.H. (2009). Regulation of facilitative glucose transporters and AKT/MAPK/PRKAA signaling via estradiol and progesterone in the mouse uterine epithelium. Biol Reprod *81*, 188-198.

Kimmins, S., Lim, H.C., and MacLaren, L.A. (2004). Immunohistochemical localization of integrin alpha V beta 3 and osteopontin suggests that they do not interact during embryo implantation in ruminants. Reprod Biol Endocrinol *2*, 19.

Kling, D., Fingerle, J., and Harlan, J.M. (1992). Inhibition of leukocyte extravasation with a monoclonal antibody to CD18 during formation of experimental intimal thickening in rabbit carotid arteries. Arterioscler Thromb *12*, 997-1007.

Knapczyk-Stwora, K., Durlej, M., Duda, M., Czernichowska-Ferreira, K., Tabecka-Lonczynska, A., and Slomczynska, M. (2011). Expression of oestrogen receptor alpha and oestrogen receptor beta in the uterus of the pregnant swine. Reprod Domest Anim *46*, 1-7.

Knight, J.W., Bazer, F.W., Thatcher, W.W., Franke, D.E., and Wallace, H.D. (1977). Conceptus development in intact and unilaterally hysterectomized-ovariectomized gilts: interrelations among hormonal status, placental development, fetal fluids and fetal growth. J Anim Sci *44*, 620-637.

Komor, E., and Tanner, W. (1971). Characterization of the active hexose transport system of Chlorella vulgaris. Biochim Biophys Acta *241*, 170-179.

Korgun, E.T., Celik-Ozenci, C., Seval, Y., Desoye, G., and Demir, R. (2005). Do glucose transporters have other roles in addition to placental glucose transport during early pregnancy? Histochem Cell Biol *123*, 621-629.

Korgun, E.T., Demir, R., Hammer, A., Dohr, G., Desoye, G., Skofitsch, G., and Hahn, T. (2001). Glucose transporter expression in rat embryo and uterus during decidualization, implantation, and early postimplantation. Biol Reprod *65*, 1364-1370.

Kramer, A.C., Steinhauser, C.B., Gao, H., Seo, H., McLendon, B.A., Burghardt, R.C., Wu, G., Bazer, F.W., and Johnson, G.A. (2020). Steroids Regulate SLC2A1 and SLC2A3 to Deliver Glucose Into Trophectoderm for Metabolism via Glycolysis. Endocrinology *161*.

Kuehne, A., Emmert, H., Soehle, J., Winnefeld, M., Fischer, F., Wenck, H., Gallinat, S., Terstegen, L., Lucius, R., Hildebrand, J.*, et al.* (2015). Acute Activation of Oxidative Pentose Phosphate Pathway as First-Line Response to Oxidative Stress in Human Skin Cells. Mol Cell *59*, 359-371.

Larrabee, M.G. (1989). The pentose cycle (hexose monophosphate shunt). Rigorous evaluation of limits to the flux from glucose using 14CO2 data, with applications to peripheral ganglia of chicken embryos. J Biol Chem *264*, 15875-15879.

Larrabee, M.G. (1990). Evaluation of the pentose phosphate pathway from 14CO2 data. Fallibility of a classic equation when applied to non-homogeneous tissues. Biochem J *272*, 127-132.

Leino, R.L., Gerhart, D.Z., van Bueren, A.M., McCall, A.L., and Drewes, L.R. (1997). Ultrastructural localization of GLUT 1 and GLUT 3 glucose transporters in rat brain. J Neurosci Res *49*, 617-626.

Leiser, R., and Dantzer, V. (1988). Structural and functional aspects of porcine placental microvasculature. Anat Embryol (Berl) *177*, 409-419.

Leiser, R., and Dantzer, V. (1994). Initial vascularisation in the pig placenta: II. Demonstration of gland and areola-gland subunits by histology and corrosion casts. Anat Rec *238*, 326-334.

Lessey, B.A. (2002). Adhesion molecules and implantation. J Reprod Immunol *55*, 101-112.

Li, Y., Sun, X., and Dey, S.K. (2015). Entosis allows timely elimination of the luminal epithelial barrier for embryo implantation. Cell Rep *11*, 358-365.

Lisinski, I., Schurmann, A., Joost, H.G., Cushman, S.W., and Al-Hasani, H. (2001). Targeting of GLUT6 (formerly GLUT9) and GLUT8 in rat adipose cells. Biochem J *358*, 517-522.

Liu, H., Huang, D., McArthur, D.L., Boros, L.G., Nissen, N., and Heaney, A.P. (2010). Fructose induces transketolase flux to promote pancreatic cancer growth. Cancer Res *70*, 6368-6376.

Liu, J., He, X., Corbett, S.A., Lowry, S.F., Graham, A.M., Fassler, R., and Li, S. (2009). Integrins are required for the differentiation of visceral endoderm. J Cell Sci *122*, 233-242.

Liu, N., Zhou, C., Chen, Y., and Zhao, J. (2013). The involvement of osteopontin and beta3 integrin in implantation and endometrial receptivity in an early mouse pregnancy model. Eur J Obstet Gynecol Reprod Biol *170*, 171-176.

Mangale, S.S., and Reddy, K.V. (2007). Expression pattern of integrins and their ligands in mouse feto-maternal tissues during pregnancy. Reprod Fertil Dev *19*, 452-460.

Manolescu, A.R., Witkowska, K., Kinnaird, A., Cessford, T., and Cheeseman, C. (2007). Facilitated hexose transporters: new perspectives on form and function. Physiology (Bethesda) *22*, 234-240.

Mattson, B.A., Overstrom, E.W., and Albertini, D.F. (1990). Transitions in trophectoderm cellular shape and cytoskeletal organization in the elongating pig blastocyst. Biol Reprod *42*, 195-205.

McNamee, E.N., Korns Johnson, D., Homann, D., and Clambey, E.T. (2013). Hypoxia and hypoxia-inducible factors as regulators of T cell development, differentiation, and function. Immunol Res *55*, 58-70.

McPherson, R.L., Ji, F., Wu, G., Blanton, J.R., Jr., and Kim, S.W. (2004). Growth and compositional changes of fetal tissues in pigs. J Anim Sci *82*, 2534-2540.

Meyer, A.E., Pfeiffer, C.A., Brooks, K.E., Spate, L.D., Benne, J.A., Cecil, R., Samuel, M.S., Murphy, C.N., Behura, S., McLean, M.K., *et al.* (2019). New perspective on conceptus estrogens in maternal recognition and pregnancy establishment in the pigdagger. Biol Reprod *101*, 148-161.

Meznarich, H.K., Hay, W.W., Jr., Sparks, J.W., Meschia, G., and Battaglia, F.C. (1987). Fructose disposal and oxidation rates in the ovine fetus. Q J Exp Physiol *72*, 617-625.

Mossman, H.W. (1974). Structural changes in vertebrate fetal membranes associated with the adoption of viviparity. Obstet Gynecol Annu *3*, 7-32.

Mueckler, M., and Thorens, B. (2013). The SLC2 (GLUT) family of membrane transporters. Mol Aspects Med *34*, 121-138.

Muhr, J., and Ackerman, K.M. (2021). Embryology, Gastrulation. In StatPearls (Treasure Island (FL).

Mulukutla, B.C., Yongky, A., Le, T., Mashek, D.G., and Hu, W.S. (2016). Regulation of Glucose Metabolism - A Perspective From Cell Bioprocessing. Trends Biotechnol *34*, 638-651.

Munyon, W.H., and Merchant, D.J. (1959). The relation between glucose utilization, lactic acid production and utilization and the growth cycle of L strain fibroblasts. Exp Cell Res *17*, 490-498.

Nakase, T., Takaoka, K., Hirakawa, K., Hirota, S., Takemura, T., Onoue, H., Takebayashi, K., Kitamura, Y., and Nomura, S. (1994). Alterations in the expression of osteonectin, osteopontin and osteocalcin mRNAs during the development of skeletal tissues in vivo. Bone Miner *26*, 109-122.

Nishimura, M., and Naito, S. (2005). Tissue-specific mRNA expression profiles of human ATP-binding cassette and solute carrier transporter superfamilies. Drug Metab Pharmacokinet *20*, 452-477.

Nomura, S., Wills, A.J., Edwards, D.R., Heath, J.K., and Hogan, B.L. (1988). Developmental expression of 2ar (osteopontin) and SPARC (osteonectin) RNA as revealed by in situ hybridization. J Cell Biol *106*, 441-450.

Nowotschin, S., Hadjantonakis, A.K., and Campbell, K. (2019). The endoderm: a divergent cell lineage with many commonalities. Development *146*.

O'Neill, L.A., Kishton, R.J., and Rathmell, J. (2016). A guide to immunometabolism for immunologists. Nat Rev Immunol *16*, 553-565.

Oestrup, O., Hall, V., Petkov, S.G., Wolf, X.A., Hyldig, S., and Hyttel, P. (2009). From zygote to implantation: morphological and molecular dynamics during embryo development in the pig. Reprod Domest Anim *44 Suppl 3*, 39-49.

Okano, K., Matsumoto, K., Koizumi, T., Mizushima, T., and Mori, M. (1965). Histochemical comparison of oxidative enzymes in adrenal glands of mammals. Histochemie *4*, 494-501.

Olson, A.L., and Pessin, J.E. (1996). Structure, function, and regulation of the mammalian facilitative glucose transporter gene family. Annu Rev Nutr *16*, 235-256.

Overholtzer, M., Mailleux, A.A., Mouneimne, G., Normand, G., Schnitt, S.J., King, R.W., Cibas, E.S., and Brugge, J.S. (2007). A nonapoptotic cell death process, entosis, that occurs by cell-in-cell invasion. Cell *131*, 966-979.

Paffaro, V.A., Jr., Bizinotto, M.C., Joazeiro, P.P., and Yamada, A.T. (2003). Subset classification of mouse uterine natural killer cells by DBA lectin reactivity. Placenta *24*, 479-488.

Pantaleon, M., Harvey, M.B., Pascoe, W.S., James, D.E., and Kaye, P.L. (1997). Glucose transporter GLUT3: ontogeny, targeting, and role in the mouse blastocyst. Proc Natl Acad Sci U S A *94*, 3795-3800.

Pao, S.S., Paulsen, I.T., and Saier, M.H., Jr. (1998). Major facilitator superfamily. Microbiol Mol Biol Rev *62*, 1-34.

Paria, B.C., Das, S.K., Andrews, G.K., and Dey, S.K. (1993). Expression of the epidermal growth factor receptor gene is regulated in mouse blastocysts during delayed implantation. Proc Natl Acad Sci U S A *90*, 55-59.

Park, J., Rho, H.K., Kim, K.H., Choe, S.S., Lee, Y.S., and Kim, J.B. (2005). Overexpression of glucose-6-phosphate dehydrogenase is associated with lipid dysregulation and insulin resistance in obesity. Mol Cell Biol *25*, 5146-5157.

Park, T.J., Reznick, J., Peterson, B.L., Blass, G., Omerbasic, D., Bennett, N.C., Kuich, P., Zasada, C., Browe, B.M., Hamann, W.*, et al.* (2017). Fructose-driven glycolysis supports anoxia resistance in the naked mole-rat. Science *356*, 307-311.

Parr, E.L., Tung, H.N., and Parr, M.B. (1987). Apoptosis as the mode of uterine epithelial cell death during embryo implantation in mice and rats. Biol Reprod *36*, 211-225.

Patra, K.C., and Hay, N. (2014). The pentose phosphate pathway and cancer. Trends Biochem Sci *39*, 347-354.

Patten, B. (1948). Embryology of the Pig (McGraw-Hil Book Company).

Pere, M.C. (1995). Maternal and fetal blood levels of glucose, lactate, fructose, and insulin in the conscious pig. J Anim Sci *73*, 2994-2999.

Pere, M.C. (2003). Materno-foetal exchanges and utilisation of nutrients by the foetus: comparison between species. Reprod Nutr Dev *43*, 1-15.

Perry, J.S. (1981). The mammalian fetal membranes. J Reprod Fertil *62*, 321-335.

Persico, M.G., Viglietto, G., Martini, G., Toniolo, D., Paonessa, G., Moscatelli, C., Dono, R., Vulliamy, T., Luzzatto, L., and D'Urso, M. (1986). Isolation of human glucose-6-phosphate dehydrogenase (G6PD) cDNA clones: primary structure of the protein and unusual 5' non-coding region. Nucleic Acids Res *14*, 2511-2522.

Pfeiffer, T., Schuster, S., and Bonhoeffer, S. (2001). Cooperation and competition in the evolution of ATP-producing pathways. Science *292*, 504-507.

Prols, F., Loser, B., and Marx, M. (1998). Differential expression of osteopontin, PC4, and CEC5, a novel mRNA species, during in vitro angiogenesis. Exp Cell Res *239*, 1-10.

Qi, Q.R., Xie, Q.Z., Liu, X.L., and Zhou, Y. (2014). Osteopontin is expressed in the mouse uterus during early pregnancy and promotes mouse blastocyst attachment and invasion in vitro. PLoS One *9*, e104955.

Quick, M., Tomasevic, J., and Wright, E.M. (2003). Functional asymmetry of the human Na+/glucose transporter (hSGLT1) in bacterial membrane vesicles. Biochemistry *42*, 9147-9152.

Rais, B., Comin, B., Puigjaner, J., Brandes, J.L., Creppy, E., Saboureau, D., Ennamany, R., Lee, W.N., Boros, L.G., and Cascante, M. (1999). Oxythiamine and dehydroepiandrosterone induce a G1 phase cycle arrest in Ehrlich's tumor cells through inhibition of the pentose cycle. FEBS Lett *456*, 113-118.

Randall, G.C. (1977). Daily changes in the blood of conscious pigs with catheters in foetal and uterine vessels during late gestation. J Physiol *270*, 719-731.

Reitzer, L.J., Wice, B.M., and Kennell, D. (1979). Evidence that glutamine, not sugar, is the major energy source for cultured HeLa cells. J Biol Chem *254*, 2669-2676.

Renegar, R.H., Bazer, F.W., and Roberts, R.M. (1982). Placental transport and distribution of uteroferrin in the fetal pig. Biol Reprod *27*, 1247-1260.

Richard, C., Gao, J., Brown, N., and Reese, J. (2003). Aquaporin water channel genes are differentially expressed and regulated by ovarian steroids during the periimplantation period in the mouse. Endocrinology *144*, 1533-1541.

Riganti, C., Gazzano, E., Polimeni, M., Aldieri, E., and Ghigo, D. (2012). The pentose phosphate pathway: an antioxidant defense and a crossroad in tumor cell fate. Free Radic Biol Med *53*, 421-436.

Ritacco, G., Radecki, S.V., and Schoknecht, P.A. (1997). Compensatory growth in runt pigs is not mediated by insulin-like growth factor I. J Anim Sci *75*, 1237-1243.

Ross, J.W., Ashworth, M.D., White, F.J., Johnson, G.A., Ayoubi, P.J., DeSilva, U., Whitworth, K.M., Prather, R.S., and Geisert, R.D. (2007). Premature estrogen exposure alters endometrial gene expression to disrupt pregnancy in the pig. Endocrinology *148*, 4761-4773.

Rudack, D., Chisholm, E.M., and Holten, D. (1971). Rat liver glucose 6-phosphate dehydrogenase. Regulation by carbohydrate diet and insulin. J Biol Chem *246*, 1249-1254.

Sancho, S., Casas, I., Ekwall, H., Saravia, F., Rodriguez-Martinez, H., Rodriguez-Gil, J.E., Flores, E., Pinart, E., Briz, M., Garcia-Gil, N.*, et al.* (2007). Effects of cryopreservation on semen quality and the expression of sperm membrane hexose transporters in the spermatozoa of Iberian pigs. Reproduction *134*, 111-121.

Scott, T.W., Setchell, B.P., and Bassett, J.M. (1967). Characterization and metabolism of ovine foetal lipids. Biochem J *104*, 1040-1047.

Semenza, G.L. (2001). HIF-1 and mechanisms of hypoxia sensing. Curr Opin Cell Biol *13*, 167-171.

Seo, H., Bazer, F.W., Burghardt, R.C., and Johnson, G.A. (2019). Immunohistochemical Examination of Trophoblast Syncytialization during Early Placentation in Sheep. Int J Mol Sci *20*.

Seo, H., Frank, J.W., Burghardt, R.C., Bazer, F.W., and Johnson, G.A. (2020a). Integrins and OPN localize to adhesion complexes during placentation in sheep. Reproduction *160*, 521-532.

Seo, H., Li, X., Wu, G., Bazer, F.W., Burghardt, R.C., Bayless, K.J., and Johnson, G.A. (2020b). Mechanotransduction drives morphogenesis to develop folding during placental development in pigs. Placenta *90*, 62-70.

Shelley, H.J. (1960). Blood sugars and tissue carbohydrate in foetal and infant lambs and rhesus monkeys. J Physiol *153*, 527-552.

Shelley, H.J., and Dawes, G.S. (1962). Fate of fructose in the newly delivered foetal lamb. Nature *194*, 296-297.

Shijubo, N., Uede, T., Kon, S., Nagata, M., and Abe, S. (2000). Vascular endothelial growth factor and osteopontin in tumor biology. Crit Rev Oncog *11*, 135-146

Sistrom, W.R. (1958). On the physical state of the intracellularly accumulates substrates of beta-galactoside-permease in Escherichia coli. Biochim Biophys Acta *29*, 579-587.

Sodek, J., Ganss, B., and McKee, M.D. (2000). Osteopontin. Crit Rev Oral Biol Med *11*, 279-303.

Soede, N.M., Langendijk, P., and Kemp, B. (2011). Reproductive cycles in pigs. Anim Reprod Sci *124*, 251-258.

Song, G., Bailey, D.W., Dunlap, K.A., Burghardt, R.C., Spencer, T.E., Bazer, F.W., and Johnson, G.A. (2010). Cathepsin B, cathepsin L, and cystatin C in the porcine uterus and placenta: potential roles in endometrial/placental remodeling and in fluid-phase transport of proteins secreted by uterine epithelia across placental areolae. Biol Reprod *82*, 854-864.

Spencer, T.E., Burghardt, R.C., Johnson, G.A., and Bazer, F.W. (2004). Conceptus signals for establishment and maintenance of pregnancy. Anim Reprod Sci *82-83*, 537-550.

Steele, N.C., Frobish, L.T., Miller, L.R., and Young, E.P. (1971). Certain aspects on the utilization of carbohydrates by the neonatal pig. J Anim Sci *33*, 983-991.

Steinhauser, C.B., Bazer, F.W., Burghardt, R.C., and Johnson, G.A. (2017a). Expression of progesterone receptor in the porcine uterus and placenta throughout gestation: correlation with expression of uteroferrin and osteopontin. Domest Anim Endocrinol *58*, 19-29.

Steinhauser, C.B., Landers, M., Myatt, L., Burghardt, R.C., Vallet, J.L., Bazer, F.W., and Johnson, G.A. (2016). Fructose Synthesis and Transport at the Uterine-Placental Interface of Pigs: Cell-Specific Localization of SLC2A5, SLC2A8, and Components of the Polyol Pathway. Biol Reprod *95*, 108.

Steinhauser, C.B., Wing, T.T., Gao, H., Li, X., Burghardt, R.C., Wu, G., Bazer, F.W., and Johnson, G.A. (2017b). Identification of appropriate reference genes for qPCR analyses of placental expression of SLC7A3 and induction of SLC5A1 in porcine endometrium. Placenta *52*, 1-9.

Steven, D.H. (1975). Comparative Placentation. Essays in Structure and Function. Academic Press, 215.

Takano, S., Tsuboi, K., Tomono, Y., Mitsui, Y., and Nose, T. (2000). Tissue factor, osteopontin, alphavbeta3 integrin expression in microvasculature of gliomas associated with vascular endothelial growth factor expression. Br J Cancer *82*, 1967-1973.

Tam, P.P., Williams, E.A., and Chan, W.Y. (1993). Gastrulation in the mouse embryo: ultrastructural and molecular aspects of germ layer morphogenesis. Microsc Res Tech *26*, 301-328.

Tao, Y., Cheung, L.S., Li, S., Eom, J.S., Chen, L.Q., Xu, Y., Perry, K., Frommer, W.B., and Feng, L. (2015). Structure of a eukaryotic SWEET transporter in a homotrimeric complex. Nature *527*, 259-263.

Thorens, B., and Mueckler, M. (2010). Glucose transporters in the 21st Century. Am J Physiol Endocrinol Metab *298*, E141-145.

Tilley, R.E., McNeil, C.J., Ashworth, C.J., Page, K.R., and McArdle, H.J. (2007). Altered muscle development and expression of the insulin-like growth factor system in growth retarded fetal pigs. Domest Anim Endocrinol *32*, 167-177.

Ullrey, D.E., Sprague, J.I., Becker, D.E., and Miller, E.R. (1965). Growth of the Swine Fetus. J Anim Sci *24*, 711-717.

Urner, F., and Sakkas, D. (1999). Characterization of glycolysis and pentose phosphate pathway activity during sperm entry into the mouse oocyte. Biol Reprod *60*, 973-978.

Vallet, J.L., and Freking, B.A. (2007). Differences in placental structure during gestation associated with large and small pig fetuses. J Anim Sci *85*, 3267-3275.

Vander Heiden, M.G., Locasale, J.W., Swanson, K.D., Sharfi, H., Heffron, G.J., Amador-Noguez, D., Christofk, H.R., Wagner, G., Rabinowitz, J.D., Asara, J.M*., et al.* (2010). Evidence for an alternative glycolytic pathway in rapidly proliferating cells. Science *329*, 1492-1499.

von Wolff, M., Ursel, S., Hahn, U., Steldinger, R., and Strowitzki, T. (2003). Glucose transporter proteins (GLUT) in human endometrium: expression, regulation, and function throughout the menstrual cycle and in early pregnancy. J Clin Endocrinol Metab *88*, 3885-3892.

Waclawik, A., Kaczmarek, M.M., Blitek, A., Kaczynski, P., and Ziecik, A.J. (2017). Embryo-maternal dialogue during pregnancy establishment and implantation in the pig. Mol Reprod Dev *84*, 842-855.

Wamelink, M.M., Struys, E.A., and Jakobs, C. (2008). The biochemistry, metabolism and inherited defects of the pentose phosphate pathway: a review. J Inherit Metab Dis *31*, 703-717.

Wang, T., Marquardt, C., and Foker, J. (1976). Aerobic glycolysis during lymphocyte proliferation. Nature *261*, 702-705.

Warburg, O. (1956). On the origin of cancer cells. Science *123*, 309-314.

Warburg, O., Wind, F., and Negelein, E. (1927). The Metabolism of Tumors in the Body. J Gen Physiol *8*, 519-530.

Waterhouse, P., Parhar, R.S., Guo, X., Lala, P.K., and Denhardt, D.T. (1992). Regulated temporal and spatial expression of the calcium-binding proteins calcyclin and OPN (osteopontin) in mouse tissues during pregnancy. Mol Reprod Dev *32*, 315-323.

Waugh, E.E., and Wales, R.G. (1993). Oxidative utilization of glucose, acetate and lactate by early preimplantation sheep, mouse and cattle embryos. Reprod Fertil Dev *5*, 123-133.

Weintraub, A.S., Lin, X., Itskovich, V.V., Aguinaldo, J.G., Chaplin, W.F., Denhardt, D.T., and Fayad, Z.A. (2004). Prenatal detection of embryo resorption in osteopontin-deficient mice using serial noninvasive magnetic resonance microscopy. Pediatr Res *55*, 419-424.

Wen, H.Y., Abbasi, S., Kellems, R.E., and Xia, Y. (2005). mTOR: a placental growth signaling sensor. Placenta *26 Suppl A*, S63-69.

White, C.E., Piper, E.L., and Noland, P.R. (1979a). Conversion of Glucose to Fructose in the Fetal Pig. J Anim Sci *48*, 585-590.

White, C.E., Piper, E.L., and Noland, P.R. (1979b). Conversion of glucose to fructose in the fetal pig. J Anim Sci *48*, 585-590.

White, C.E., Piper, E.L., Noland, P.R., and Daniels, L.B. (1982). Fructose utilization for nucleic acid synthesis in the fetal pig. J Anim Sci *55*, 73-76.

White, F.J., Burghardt, R.C., Hu, J., Joyce, M.M., Spencer, T.E., and Johnson, G.A. (2006). Secreted phosphoprotein 1 (osteopontin) is expressed by stromal macrophages in cyclic and pregnant endometrium of mice, but is induced by estrogen in luminal epithelium during conceptus attachment for implantation. Reproduction *132*, 919-929.

White, F.J., Ross, J.W., Joyce, M.M., Geisert, R.D., Burghardt, R.C., and Johnson, G.A. (2005). Steroid regulation of cell specific secreted phosphoprotein 1 (osteopontin) expression in the pregnant porcine uterus. Biol Reprod *73*, 1294-1301.

White, M.D., Zenker, J., Bissiere, S., and Plachta, N. (2018). Instructions for Assembling the Early Mammalian Embryo. Dev Cell *45*, 667-679.

Widdowson, E.M. (1971). Intra-uterine growth retardation in the pig. I. Organ size and cellular development at birth and after growth to maturity. Biol Neonate *19*, 329-340.

Wing, T.T., Erikson, D.W., Burghardt, R.C., Bazer, F.W., Bayless, K.J., and Johnson, G.A. (2020). OPN binds alpha V integrin to promote endothelial progenitor cell incorporation into vasculature. Reproduction *159*, 465-478.

Wislocki, G.B., and Dempsey, E.W. (1946). Histochemical reactions of the placenta of the pig. Am J Anat *78*, 181-225.

Wright, E.M., Loo, D.D., and Hirayama, B.A. (2011). Biology of human sodium glucose transporters. Physiol Rev *91*, 733-794.

Wu, G. (1996). An important role for pentose cycle in the synthesis of citrulline and proline from glutamine in porcine enterocytes. Arch Biochem Biophys *336*, 224-230.

Wu, G., Bazer, F.W., Satterfield, M.C., Li, X., Wang, X., Johnson, G.A., Burghardt, R.C., Dai, Z., Wang, J., and Wu, Z. (2013). Impacts of arginine nutrition on embryonic and fetal development in mammals. Amino Acids *45*, 241-256.

Wu, G., Bazer, F.W., and Tou, W. (1995). Developmental changes of free amino acid concentrations in fetal fluids of pigs. J Nutr *125*, 2859-2868.

Wu, G., and Marliss, E.B. (1993). Enhanced glucose metabolism and respiratory burst in peritoneal macrophages from spontaneously diabetic BB rats. Diabetes *42*, 520-529.

Xie, Q.Z., Qi, Q.R., Chen, Y.X., Xu, W.M., Liu, Q., and Yang, J. (2013). Uterine micro-environment and estrogen-dependent regulation of osteopontin expression in mouse blastocyst. Int J Mol Sci *14*, 14504-14517.

Yamaguchi, M., Sakata, M., Ogura, K., and Miyake, A. (1996). Gestational changes of glucose transporter gene expression in the mouse placenta and decidua. J Endocrinol Invest *19*, 567-569.

Yen, W.C., Wu, Y.H., Wu, C.C., Lin, H.R., Stern, A., Chen, S.H., Shu, J.C., and Tsun-Yee Chiu, D. (2020). Impaired inflammasome activation and bacterial clearance in G6PD deficiency due to defective NOX/p38 MAPK/AP-1 redox signaling. Redox Biol *28*, 101363.

Zavy, M.T., Clark, W.R., Sharp, D.C., Roberts, R.M., and Bazer, F.W. (1982). Comparison of glucose, fructose, ascorbic acid and glucosephosphate isomerase enzymatic activity in uterine flushings from nonpregnant and pregnant gilts and pony mares. Biol Reprod *27*, 1147-1158.

Zhao, F.Q., and Keating, A.F. (2007). Functional properties and genomics of glucose transporters. Curr Genomics *8*, 113-128.

APPENDIX A

INTEGRINE ADHESION COMPLEX ORGANIZATION IN SHEEP MYOMETRIUM REFLECTS CHANGING MECHANICAL FORCES DURING PREGNANCY AND POSTPARTUM[*]

Introduction

Throughout pregnancy the myometrium undergoes hypertrophy in response to the developing fetus and associated placental membranes (Shynlova et al., 2007). This includes cell proliferation, increased ECM production and remodeling of integrin-focal adhesion (FA) contacts (Williams et al., 2005). FAs, a type of integrin adhesion complex (IAC), are consistently seen in cultured cells (Burridge and Chrzanowska-Wodnicka, 1996; Humphries et al., 2006), although are less obvious *in vivo*.

The onset of parturition is initiated by the fetus and relies on both endocrine and mechanical signaling pathways caused by uterine stretch in the myometrium. In sheep, the endocrine signaling pathway involves a change in the ratio of estrogen to progesterone secretion that primes the uterus for myometrial activation critical for delivery of the fetus (Challis et al., 2000). The simultaneous increase of estrogen and decrease of progesterone increases the contractility of the myometrium, in part, by increasing contraction associated proteins (including gap junctions, comprised of connexin 43 (Cx43), oxytocin receptor,

---

[*] McLendon, B.A., Kramer, A.C., Seo, H., Bazer, F.W., Burghardt, R.C., and Johnson, G.A. (2021). Integrin Adhesion Complex Organization in Sheep Myometrium Reflects Changing Mechanical Forces during Pregnancy and Postpartum. Biology (Basel) *10*.

and others) which allow for direct electrical and chemical communication between the muscle fibers [6]. In addition to endocrine signaling, mechanotransduction by integrins plays an important role in parturition, with mechanical stretch promoting extensive uterine hypertrophy and remodeling in pregnant and postpartum animals (Csapo et al., 1965; Cullen and Harkness, 1968; Goldspink and Douglas, 1988).

Integrin activation through binding with the ECM leads to assembly of IACs that relay a variety of signals involved in many cellular processes such as cellular adhesion, migration, and stimulation of numerous signal transduction pathways (Wozniak et al., 2004). Each integrin is a heterodimer that includes an alpha and beta subunit, and the alpha/beta heterodimers specify the ligand-binding abilities of the integrin. For example, the alpha 5 integrin subunit (ITGA5) partners exclusively with the beta 1 integrin subunit (ITGB1) forming the ITGA5/ITGB1 (ITGA5B1) integrin receptor (Robinson et al., 2004). This is a classic mechanosensory receptor for the matricellular protein fibronectin (FN1). FN1 is a multimodular force-bearing ECM protein that can exhibit a wide range of conformations in the ECM based upon substrate rigidity(Vogel, 2006). It is secreted by cells and assembled into a matrix that binds to cell surface integrin receptors, which under tension, can lead to conformational changes of FN1 into different functional signaling states. Binding of FN1 to ITGA5B1 can promote FN1 fibrillogenesis to provide a dense meshwork of interconnected ECM supporting strong intercellular cohesion(Robinson et al., 2004; Vogel, 2006; Wierzbicka-Patynowski and Schwarzbauer, 2003). Talin (TLN1) and vinculin (VCL) are interacting cytoplasmic adaptor proteins that connect the ITGA5B1 integrin receptor to the actin cytoskeleton, allowing for communication and

mechanotransduction between cells and/or cell-ECM contacts (Larsen et al., 2006; Sastry and Burridge, 2000; Vogel, 2006).

In vitro studies revealed that size, as well as specific protein components, of IACs are dependent on the rigidity of the ECM and internal or external mechanical forces applied to the integrin-ECM complex (Galbraith et al., 2002; Katz et al., 2000). IACs organize into linear strands called dense plaques within the smooth muscle cells of hollow organs (Eddinger et al., 2007; Gabella, 1984). Smooth muscle IACs are present in many organs, including the smooth muscle surrounding blood vessels, to create a cohesive functional syncytium that can coordinate contractility of the organ or vessel wall (Williams et al., 2005). Studies in rats showed that ITGA5 integrin gene and protein expression increase within the myometrium and incorporate into IACs during late pregnancy and labor (Williams et al., 2005). Similar observations have been made for multiple integrins in the nonlaboring and laboring myometrium of women (Burkin et al., 2013). The ITGA5 integrin and multiple adaptor proteins have been localized in myometrium of sheep during gestation (Burghardt et al., 2009). However, less is known about IACs located within the sheep myometrium during the pre- and post-partum periods.

Fetal size is similar between sheep and humans. The uterus of both species undergoes significant growth during late pregnancy resulting in uterine stretch and parturition requires similar coordinated smooth muscle contractions. Procurement of myometrial tissues from women over the course of pregnancy is problematic for ethical reasons. The temporal assembly of IACs within the myometrium throughout pregnancy has only been reported for the rat, a species with far smaller fetuses and proportionately

less stretch of the uterine wall (Williams et al., 2005). We hypothesized that the uterus of sheep develops the mechanical strength to expel the fetus and placenta at parturition by assembling highly ordered IACs between myometrial cells during late pregnancy. These IACs subsequently disassemble after parturition. Therefore, we examined the spatial expression of ITGA5, ITGB1, FN1, TLN1 and VCL proteins, all components of IACs, in the myometrium of sheep throughout gestation and after parturition. We also examined the same IAC components in myometrial cells grown on either uncoated or FN1-coated rigid substrates. Results of the present study indicate that sheep are similar to humans regarding the assembly of IACs in the pregnant myometrium, and suggest that IACs may form much earlier in human gestation than was previously implied by the rat model. Results highlight the continued value of the sheep model as a flagship gynecological model for understanding parturition in humans (Challis et al., 2000).

Materials and Methods

Animals and tissue collection

All animal experiments complied with the Guide for Care and Use of Agricultural Animals and were approved by the Institutional Agricultural Animal Care and Use Committee of Texas A&M University. Ewes (*Ovis aries*) were observed daily for estrus in the presence of vasectomized rams. Cyclic ewes were ovariohysterectomized on Day 15 of the estrous cycle (n=4). Ewes were mated to intact rams three times at 12 h intervals beginning at onset of estrus (Day 0). Pregnant ewes were ovariohysterectomized on either Day 15, 40, 80, 120, or 140 of pregnancy and on Day 1, 7, or 14 postpartum (n=4

ewes/day). Myometrial tissue was dissected from the endometrium and stored at −80°C until processed for western blot analyses. In addition, several sections (~ 1.5 cm) from the middle of each uterine horn were embedded in Tissue-Tek Optimal Cutting Temperature (OCT) Compound (Miles, Oneonta, NY), frozen in liquid nitrogen vapor, and stored at −80°C until processed for immunofluorescence analyses.

Cell culture

For *in vitro* studies we utilized the human myometrial cell line PHM1-41, which was derived from term-pregnant human myometrium (patients not in labor) and immortalized using a vector expressing human papillomavirus E6 and E7 proteins (Monga et al., 1996). Cells were cultured in DMEM-F12 plus 10% fetal calf serum.

Western blot analyses

Myometrial samples were homogenized in lysis buffer (1% Triton X-100, 0.5% Nonidet P-40, 150 mM NaCl, 10 mM Tris, 1 mM EDTA, 0.1 mM EGTA, 0.2 mM Na_3VO_4, 0.2 mM phenylmethylsulfonyl fluoride, 50 mM NaF, 30 mM $Na_4P_2O_7$, 1 mg/ml leupeptin, 1 mg/ml pepstatin) at a ratio of 1 g tissue per 5 ml buffer. Cellular debris was cleared by centrifugation (12,000 ×*g*, 15 min, 4°C). The protein concentration of the supernatant was determined using a Bradford protein assay (Bio-Rad Laboratories, Hercules, CA) with BSA as the standard. Western blot analyses were performed as described previously [24]. Briefly, proteins (10 μg) were denatured in Laemmli buffer, separated on 8% SDS-PAGE gels, and transferred to nitrocellulose. Blots were blocked in

5% nonfat milk/TBST (Tris-buffered saline, 0.1% Tween-20) at room temperature for 1 h, incubated with either rabbit anti-ITGA5 (#AB1928; 1:1000) or rabbit anti-ITGB1 (#AB1952; 1:1000) from Chemicon (Temecula, CA, USA) [22], or normal rabbit IgG (Sigma Aldrich, St. Louis, MO; 1:1000) in 2% nonfat milk/TBST overnight at 4°C. Blots were then rinsed three times for 10 min each with TBST at room temperature, incubated with goat anti-rabbit IgG horseradish peroxidase conjugate (1:20,000 dilution of 1 mg/ml stock; Kirkegaard & Perry Laboratories, Bethesda, MD), and then rinsed three times for 10 min each with TBST. Immunoreactive proteins were detected using enhanced chemiluminescence (SuperSignal West Pico Luminol System, Pierce Chemical Co., Rockford, IL) according to the manufacturer's recommendations using a FluorChem IS-8800 120 imager (Alpha Innotech, San Leandro, CA). Blots were quantified using AlphaEase FC software (Alpha Innotech).

Immunofluorescence analyses

For immunofluorescence staining, primary antibodies included rabbit anti-ITGA5 (#AB1928; 1:200), rabbit anti-ITGB1 (#AB1952; 1:200), and mouse anti-FN1 (#MAB88916; 1:200) from Chemicon (Temecula, CA), and mouse anti-talin clone 8d4 (#T3287; 1:100), mouse anti-vinculin clone hVN-1 (#V9131; 1:200), normal rabbit IgG (#15006; 1:200) and normal mouse IgG (#15381; 1:100 or 1:200) from Sigma Aldrich (St. Louis, MO). The secondary antibodies included fluorescein-conjugated goat anti-rabbit IgG (Chemicon; 1:250), fluorescein-conjugated goat anti-mouse IgG (Zymed, San

Francisco, CA, USA; 1:250), as well as Texas Red-conjugated goat anti-rabbit IgG (Molecular Probes, Eugene, OR, USA).

Immunostaining of frozen sections of myometrium allowed for localization of ITGA5, ITGB1, FN1, TLN1, and VCL proteins as previously described [25]. Briefly, frozen sections (~ 10 μm) of uterine wall, including the myometrium, were cut with a cryostat (Hacker-BrightOTF, Hacker Instruments, Inc., Winnsboro, SC, USA) and mounted on Superfrost/Plus microscope slides (Fisher Scientific, Pittsburgh, PA, USA). Sections were fixed in −20°C methanol for 10 min, permeabilized at room temperature with 0.3% Tween-20 in 0.02 M PBS (rinse solution), and blocked in 10% normal goat serum for 1 h at room temperature. Sections were then dipped in rinse solution at room temperature and incubated overnight at 4°C with each primary antibody, and detected with fluorescein-conjugated secondary antibody. Slides were then overlaid with a cover-glass and Prolong antifade mounting reagent (Molecular Probes). Negative controls included the appropriate normal rabbit or mouse IgG at the same concentration as primary antibodies. For co-localization of proteins, frozen sections were prepared as described above.

Immunostaining of cultured human myometrial PHM1-41 cells involved seeding cells on Lab-Tek glass chambered slides that were either untreated or pretreated overnight with 50 μg/ml of human fibronectin 120 kDa α chymotryptic fragment containing the cell attachment region (Sigma Aldrich, St. Louis, MO). Myometrial cells were then added and allowed to attach in DMEM-F12 plus 10% fetal calf serum. Cells were then washed in PBS, chambers were removed leaving a silicone gasket surrounding each well, and fixed

in -20°C methanol for 10 min. Immunofluorescence co-localization of proteins was then performed as described previously (Muniz et al., 2006). After washing with PBS containing 0.3% (vol/vol) Tween-20, slides were incubated overnight at 4°C with initial primary antibody (either anti-ITGA5, -ITGB1, -FN1, or -VCL IgG at dilutions described above). Following three washes in 4°C rinsing solution for 10 min each, slides were incubated with initial secondary antibody (either FITC- or Texas Red-conjugated anti-mouse IgG at dilutions described above) for 4 h at room temperature and washed in 4°C rinsing solution 6 times for 10 min each. Slides were then incubated overnight at 4°C with the second primary antibody (either anti-ITGA5, -ITGB1, -FN1, or -VCL IgG at dilutions described above). Following six washes in 4°C rinsing solution for 10 min each, slides were incubated with 2 μg/ml of the second secondary antibody (either FITC- or Texas Red-conjugated anti-rabbit IgG at the dilutions described above) for 2 h at 4°C, washed 6 times in 4°C rinsing solution for 10 min each, and dipped in distilled-deionized H_2O. Gaskets were removed and antifade mounting reagent was added prior to overlaying a coverslip. Immunofluorescence images were acquired using an Axioplan 2 microscope (Carl Zeiss, Thornwood, NY, USA) interfaced with an Axioplan HR digital camera.

Statistical Analyses

Data were subjected to least-squares ANOVA using the general linear models procedures of the Statistical Analysis System (SAS, Cary, NC). The abundances of ITGA5 and ITGB1 proteins were determined by western blotting and evaluated within each blot to control for any differences in exposure times. All tests of significance were performed

using the appropriate error terms according to the expectation of the mean squares for error. Data are presented as least-squares means with overall standard errors.

Results

ITGA5 and ITGB1 proteins increase in the myometrium during mid-gestation and are maintained postpartum

Temporal changes in the expression of ITGA5 and ITGB1 proteins in the myometrium of pregnant and postpartum ewes were determined using Western blotting (Figures 27 and 28). ITGA5 migrated to ~130 kDa on all Days examined, whereas ITGB5 migrated to ~128 kDa on all Days examined, however a lower MW band was also observed on Day 80 of gestation. The lower molecular weight form has not been reported in the literature, but is observed for the product quality control Western blots for the anti-ITGB5 IgGs from some companies. At present we do not speculate on the identity of this immunoreactive protein. On Day 15 of gestation, ITGA5 and ITGB1 proteins were expressed at low levels. However, on Day 80, abundance of ITGA5 and ITGB1 proteins in the myometrium increased significantly compared with Day 15, and abundant levels of

ITGA5 and ITGB1 proteins were maintained for the remainder of pregnancy and through Day 14 postpartum (Figures 27 and 28).

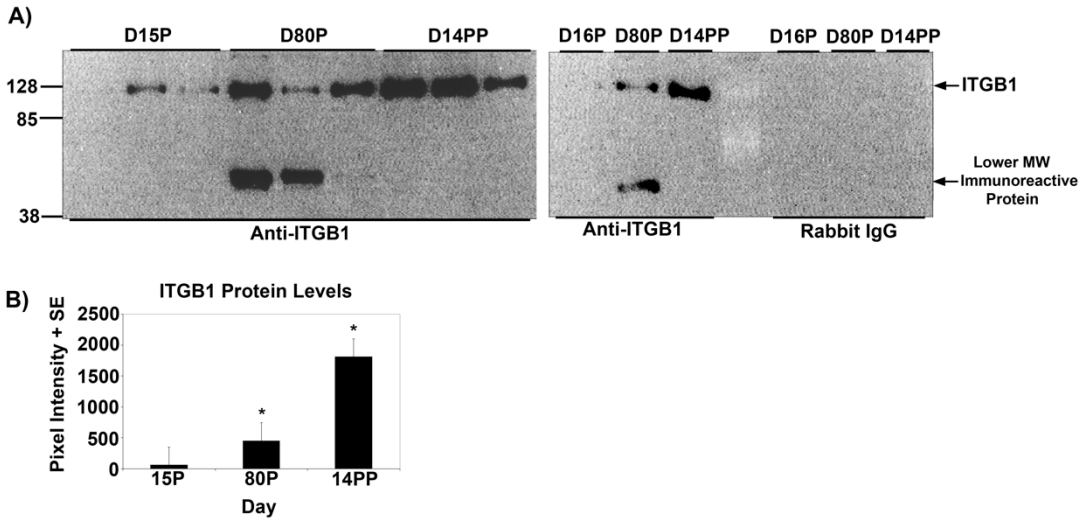

Figure 27. Western blot detection of alpha 5 integrin.

A) Western blot detection of the alpha 5 integrin (ITGA5, 8% 1D-PAGE) in ovine myometrial extracts (10 μg/lane) from different Days of pregnancy (P) or postpartum (PP). Each lane represents a sample from a different ewe. Immunoreactive proteins were detected using a rabbit anti-ITGA5 IgG or irrelevant rabbit IgG. The positions of pre-stained molecular weight standards are indicated on the left of the gels. B) Quantification of total ITGA5 protein in myometrial tissue as detected by Western blotting. ITGA5 protein increased on Day 80 of gestation, and expression remained elevated through Day 14 postpartum.

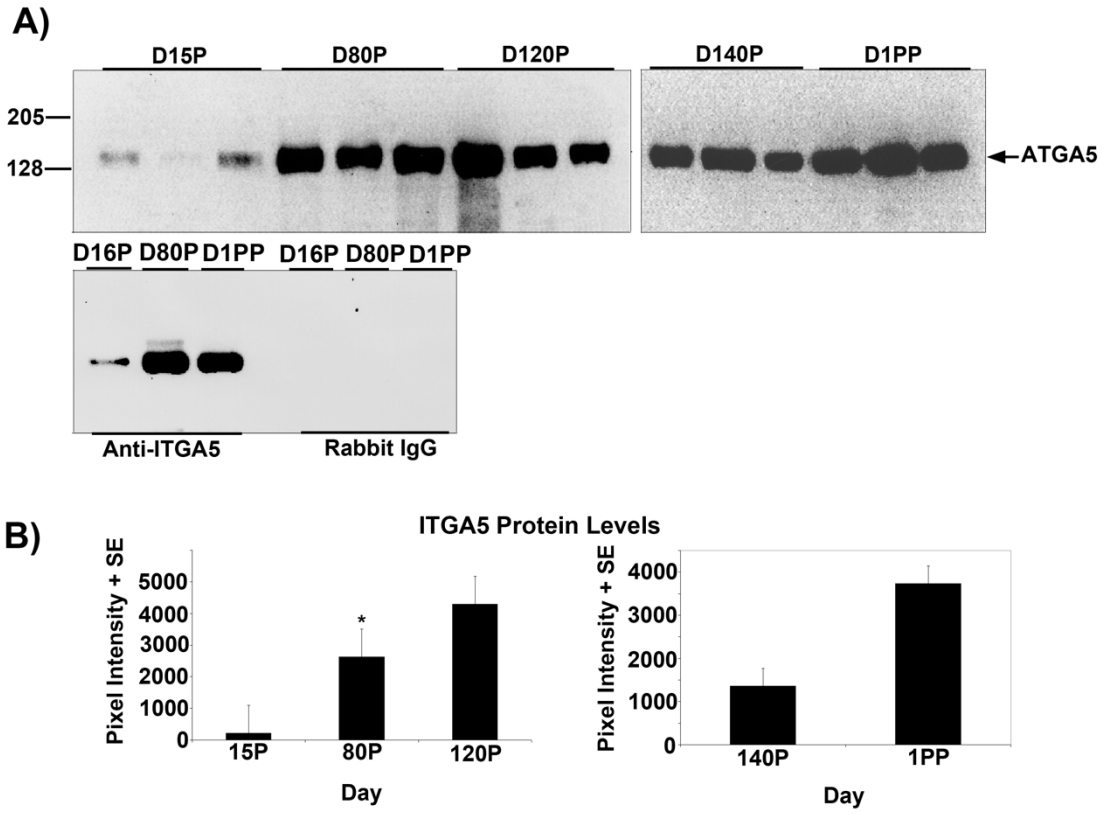

Figure 28. Western blot detection of beta 1 integrin.

A) Western blot detection of the beta 1 integrin (ITGB1, 8% 1D-PAGE) in ovine myometrial extracts (10 μg/lane) from different Days of pregnancy (P) or postpartum (PP). Each lane represents a sample from a different ewe. Immunoreactive proteins were detected using a rabbit anti-ITGB1 IgG or irrelevant rabbit IgG. The positions of pre-stained molecular weight standards are indicated on the left of the gels. B) Quantification of total ITGB1 protein in myometrial tissue as detected by Western blotting. ITGB1 protein increased on Day 80 of gestation, and expression remained elevated through Day 14 postpartum.

ITGA5 and ITGB1 proteins assemble into longitudinally oriented IACs at the surface of myometrial cells during late pregnancy that disperse postpartum

The temporal and spatial localization of ITGA5 and ITGB1 in the myometrium of pregnant and postpartum sheep were determined by immunofluorescence staining (Figures 29 and 30). Scattered punctate immunostaining for ITGA5 and ITGB1 was detected at the surface of myometrial cells in both longitudinal and circular layers of Day 15 cyclic (shown for ITGB1, Figure 30) and pregnant sheep myometrium (Figures 29 and 30). The punctate staining was more obvious in the Day 15 pregnant myometrium. Longitudinal strands of IACs developed at the surface of the myometrial cells by Day 40 of pregnancy; and increasingly ordered IACs were present in Day 80, Day 120, and Day 140 myometrium (Figures 29 and 30). ITGA5 and ITGB1 continued to be highly expressed in postpartum myometrium although they were no longer organized into longitudinal IACs at the surface of myometrial cells on postpartum Day 1, Day 7, or Day 14 (Figures 29 and 30).

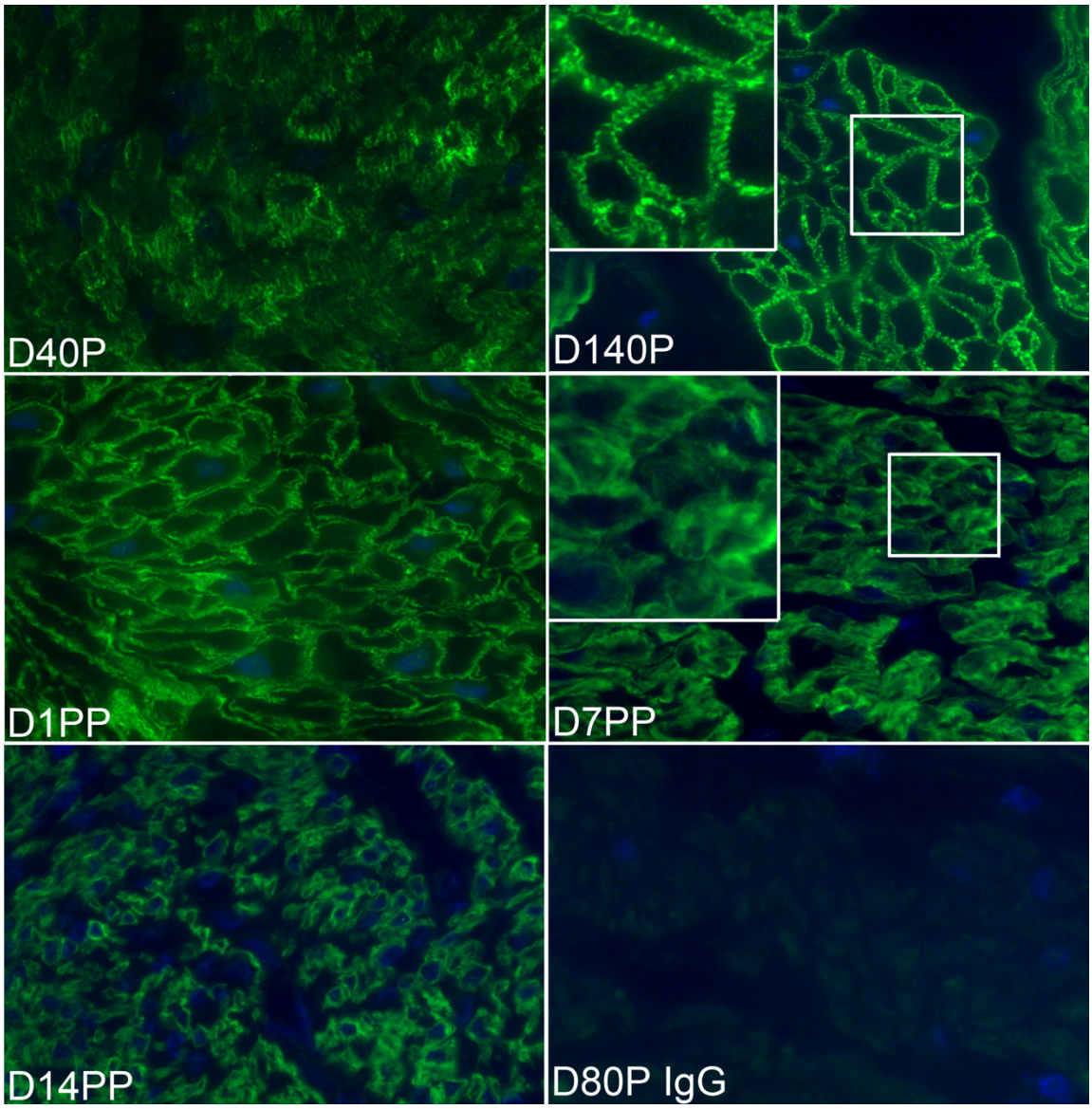

Figure 29. Immunostaining for alpha 5 integrin in myometrium of ewes

Immunostaining for the alpha 5 integrin (ITGA5) in the myometrium of ewes on Days (D) 40 and 140 of pregnancy (P) and Days 1, 7, and 14 postpartum (PP). Note the linear strands of IACs that appear as regularly distributed spots at the myometrial cell surface present in some cells on Day 40, which are present and highly ordered on all myometrial cells by Day 140 of pregnancy. These highly ordered IACs are no longer present in the

myometrium of postpartum ewes. Insets provide for comparison surface views of myometrial cells during late pregnancy and postpartum. An irrelevant rabbit IgG serves as a negative control. Width of each field is 140 μm; inset is 25 μm.

The ITGA5 subunit partners exclusively with the ITGB1 subunit forming the ITGA5B1 receptor (Shynlova et al., 2007), and the spatial pattern of expression of ITGA5 and ITGB1 precisely overlapped in the myometrium of Day 80 pregnant ewes, confirming the presence of the ITGA5B1 integrin receptor at the surface of myometrial cells (Figure 5). Further similar spatial immunostaining patterns were observed for the mechanosensory ECM protein FN1 and ITGA5, and for ITGA5 and the intracellular mechanosensory cytoskeletal protein VCL in the myometrium of Day 80 pregnant ewes, confirming the assembly of IACs at the surface of myometrial cells (Figure 32). It is noteworthy that the overlap of expression for ITGA5 with FN1 and VCL was not as exact as the overlap of expression for ITGA5 and ITGB1. ITGA5 and ITGB1 both span the cell membrane. However, FN1 is present external to the cell in the ECM, and VCL is located about 40-60 nm deep within the cytoplasm of the cell (Kanchanawong et al., 2010). Therefore, the expression of FN1 and VCL do not precisely overlap spatially with the expression of ITGA5, and a yellow immunofluorescence signal is not observed. FN1, VCL, and the intracellular mechanosensory cytoskeletal protein TLN1 no longer assembled into IACs in the myometrium of postpartum ewes (Figure 33).

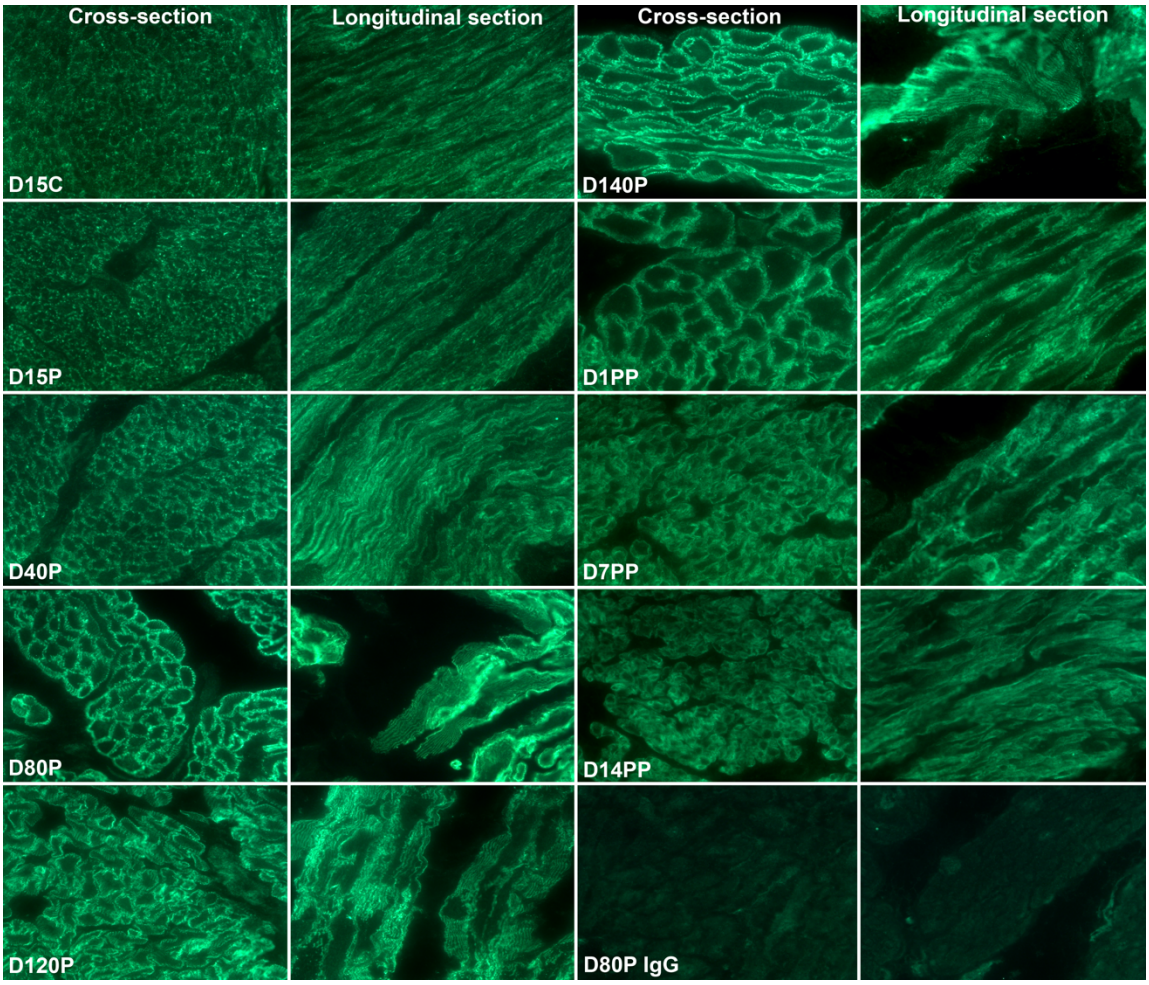

Figure 30. Immunostaining for beta 1 integrin in the myometrium of ewes

Immunostaining for beta 1 integrin (ITGB1) in the myometrium of ewes on Day (D) 15 of the estrous cycle (C), Days 15, 40, 80, 120, and 140 of pregnancy (P), and Days 1, 7, and 14 postpartum (PP) is shown. Note the linear strands of IACs that appear as regularly distributed spots at the myometrial cell surface present in some cells on Day 40, which are present and highly ordered on all myometrial cells on Days 80, 120, and 140 of pregnancy. These highly ordered IACs are not present on the myometiral cells on Day 15 of the estrous cycle or pregnancy and are not present in the myometrium of postpartum ewes.

Views of myometrial cells cut in cross-section and in longitudinal section are shown. An irrelevant rabbit IgG serves as a negative control. Width of each field is 140 μm.

FN1 stimulates activation of ITGA5, ITGB1, and TLN1 to rapidly form IACs

As a corollary to the increasing order of IACs during expansion of the uterine wall and greater forces applied between FN1, the fibronectin receptor, and cytoskeletal adaptor protein TLN1, we compared the attachment of human myometrial cells to uncoated and FN1-coated culture dishes following seeding of cells into culture medium containing fetal bovine serum. While serum contains growth and attachment factors and cultured cells secrete ECM, there was an increased spreading of cells, plus the number and size of IACs in cells attaching to FN1-coated slides compared with non-coated slides (Figure 34). Immunostaining of ITGB1 and TLN1 at the basal surface of the cells indicated that rapid *in vitro* assembly of IACs on a FN1 rigid substrate was occurring (data not shown). Comparable results showing co-distribution of ITGA5 with TLN1 at the basal surface of the cells confirms the rapid *in vitro* assembly of IACs to FN1 on a rigid substrate (Figure 34).

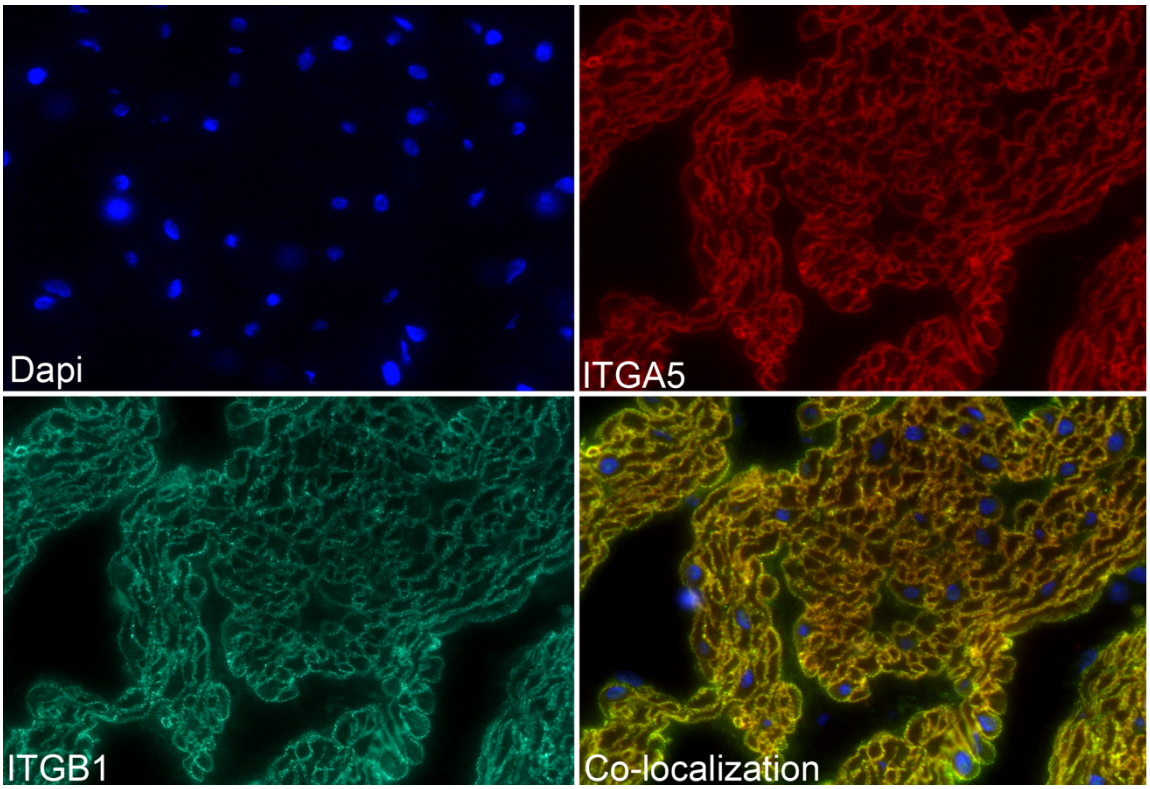

Figure 31. Double-immunostaining for alpha 5 integrin and beta 1 integrin in the myometrium of ewes

Double-immunostaining for alpha 5 integrin (ITGA5, red color) and beta 1 integrin (ITGB1, green color) in the myometrium of ewes on Day 80 of pregnancy is shown. ITGA5 and ITGB1 precisely co-localized to the same regions on the surface of the myometrial cells (yellow color), confirming the presence of the ITGA5B1 integrin receptor. DAPI was used to stain nuclei for histological reference. Width of each field is 220 μm.

Discussion

Constant changes in the lumen diameter of hollow organs generate forces that strain the intercellular connections between smooth muscle cells within the muscularis externa (Bershadsky et al., 2006). Cells within tissue-level compartments respond to extracellular mechanical forces by integrin-activated assembly of IACs that dynamically respond to those forces (Chen, 2008; Zhang et al., 1999). IACs are complex structures composed of transmembrane integrins activated by attachment to ECM proteins that connect to the cytoskeleton and serve as signaling centers that can regulate numerous physiological processes (Humphries et al., 2019). As external forces sensed through integrins increase, IACs grow and mature, which leads to actin remodeling that transduces intracellular forces necessary to balance changing external forces (Chen, 2008; Zhang et al., 1999). The myometrium of the pregnant uterus is exposed to external forces that differ over the course of pregnancy from those forces applied to the smooth muscle cells of blood vessels or tubal organs that undergo peristalsis. As pregnancy progresses in women, the uterus can increase 500- to 1000-fold in volume and 24-fold in weight. Therefore, the uterine wall must adapt to increases in fetal growth, placental fluid volumes, blood flow, and hormonal profiles in order to transform it into an organ that can forcefully expel the fetus and placental membranes during parturition (Ono et al., 2007).

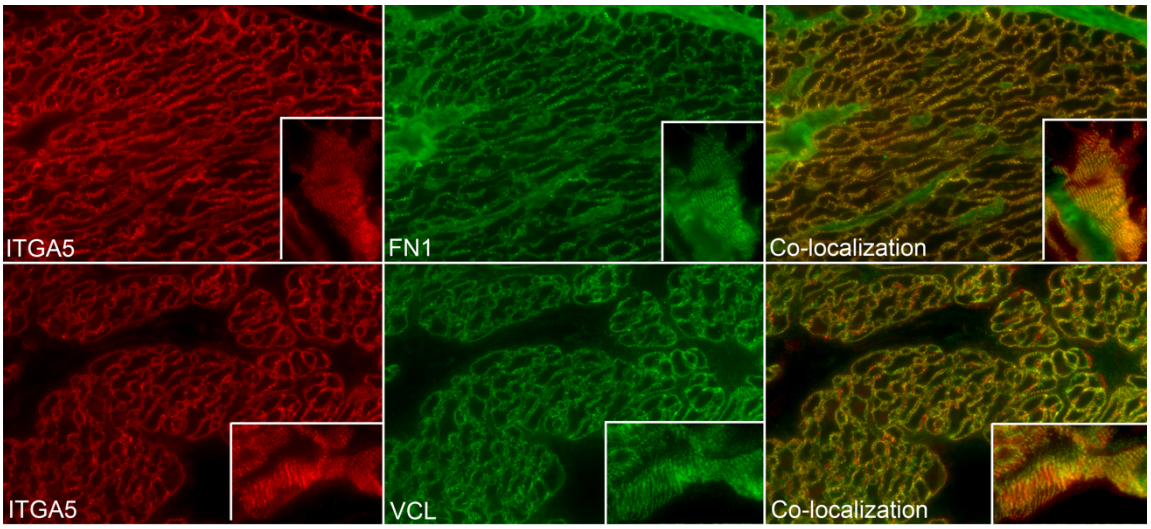

Figure 32. Assembly of integrin adhesion complexes (IACs) in sheep myometrium

Immunostaining for alpha 5 integrin (ITGA5, red color), fibronectin (FN1, green color), and vinculin (VCL, green color) in the myometrium of ewes on Day 80 of pregnancy is shown. ITGA5 and FN1, and ITGA5 and VCL co-distributed to the same regions on the surface of the myometrial cells (note), confirming the presence of IACs. Note that while ITGA5 and VCL are co-localized, VCL is located deeper within the cytoplasm therefore fluorophores do not always overlap. Width of each field is 220 μm; inserts are between 20-30 μm wide.

In response to these unique forces in rodents, myometrial cells assemble IACs, but these IACs develop during late pregnancy. Both the hormones of pregnancy and mechanical stretch upregulate the expression of FN1, the integrin receptor ITGA5B1, and other IAC constituents, including the cytoskeletal mechanosensor TLN1 (Shynlova et al., 2004; Shynlova et al., 2007; Williams et al., 2005). Both TLN1 and vinculin (VCL) are

recognized as cytoplasmic tension-transducing proteins whose signaling activity is modulated by force-induced conformational changes in IACs (Hytonen and Vogel, 2008; Mykuliak et al., 2018). FN1 is a multimodular force-bearing ECM protein that can exhibit a wide range of conformations in the ECM based upon substrate rigidity (Vogel, 2006). It is secreted by cells and assembled into a matrix that binds to cell surface integrin receptors, which under tension can lead to conformational changes of FN1 into different functional signaling states (Robinson et al., 2004; Vogel, 2006; Wierzbicka-Patynowski and Schwarzbauer, 2003). FN1-mediated focal adhesion kinase activation through the FN1 receptor is dependent on mechanical tension which, in contrast to the collagen I receptor, is decoupled from substrate rigidity or mechanical tension (MacPhee et al., 2001; Seong et al., 2013). The growth of myometrial IACs is sensitive to rigidity and strength of adhesion to the ECM (Nicolas et al., 2004) and the IAC linkage to the ECM and the myometrial actomyosin complex provides sufficient force to expel the fetus at term (Macphee and Lye, 2000).

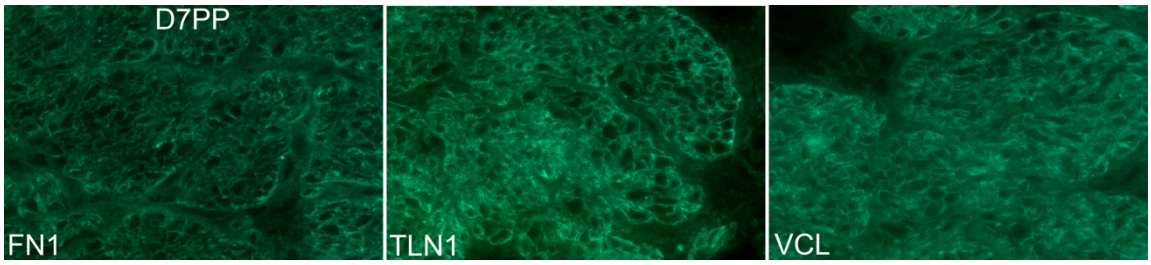

Figure 33. Integrin adhesion complexes (IACs) in sheep myometrium disassemble postpartum

Immunostaining for fibronectin (FN1), talin (TLN1), and vinculin (VCL) in the myometrium of ewes on Day 7 postpartum (D7PP) is shown. Similar to results for the alpha 5 integrin (ITGA5) and the beta 1 integrin (ITGB1) shown in Figures 3 and 4, the

multimodular, mechanosensory ECM protein FN1 and intracellular mechanosensory cytoskeletal proteins TLN1 and VCL no longer assemble into IACs in the myometrium of postpartum ewes. Width of each field is 220 μm.

Human fetuses are larger than those of rats and, therefore, in women, mRNA and protein for the alpha 1 (ITGA1), alpha 3 (ITGA3), ITGA5, alpha 7 (ITGA7), alpha v (ITGAV), ITGB1, beta 2 (ITGB2), beta 3 (ITGB3), and beta 5 (ITGB5) are significantly higher in term myometrial samples than in nonpregnant control samples (Burkin et al., 2013). Therefore, it is likely that their presence within the uterus generates more significant mechanical stretch of the uterine wall than rats. The present study is the first to comprehensively examine, across the extent of pregnancy, IAC assembly within the myometrium of a species larger than rats, where the stretch forces applied to the myometrium during gestation are expected to be amplified. Results of the present study indicate that a similar process of IAC assembly takes place in sheep myometrium as occurs in rodents and humans during pregnancy. Interestingly, punctate staining of ITGA5 and ITGB1 subunits was detected in cyclic ewes on Day 15, but punctate staining of these integrin subunits was greater in Day 15 pregnant animals. This punctate staining in cyclic animals has not been reported in rodents. Immunostaining of the integrin subunits increased and was co-distributed with FN1, VCL, and TLN1 on the surface of myometrial cells by Day 40 of pregnancy, indicating the assembly of IACs. Therefore, well-defined IACs begin to assemble in the myometrium of sheep during the first trimester, which is significantly earlier than IACs assemble during pregnancy in rodents. The magnitude and

organization of these IACs continue to increase concurrently with the increasing accumulation of fluids in the allantois and amnion and growth of the fetus, suggesting that mechanical stretch of the uterine wall contributes sufficient continuous local force by Day 40 of pregnancy to initiate the development of ordered IACs in the myometrial cells of sheep. Because sheep have a fetus near the size of the human fetus, first trimester assembly of IACs in the myometrium of women may occur in a manner similar to described here for the sheep. This highlights the continued value of the sheep model as a flagship gynecological model for understanding parturition in humans (Challis et al., 2000). Further, these IACs disassemble by Day 1 postpartum although expression of the proteins was maintained for at least 14 days, presumably due to the size of the gravid uterus and duration of uterine involution.

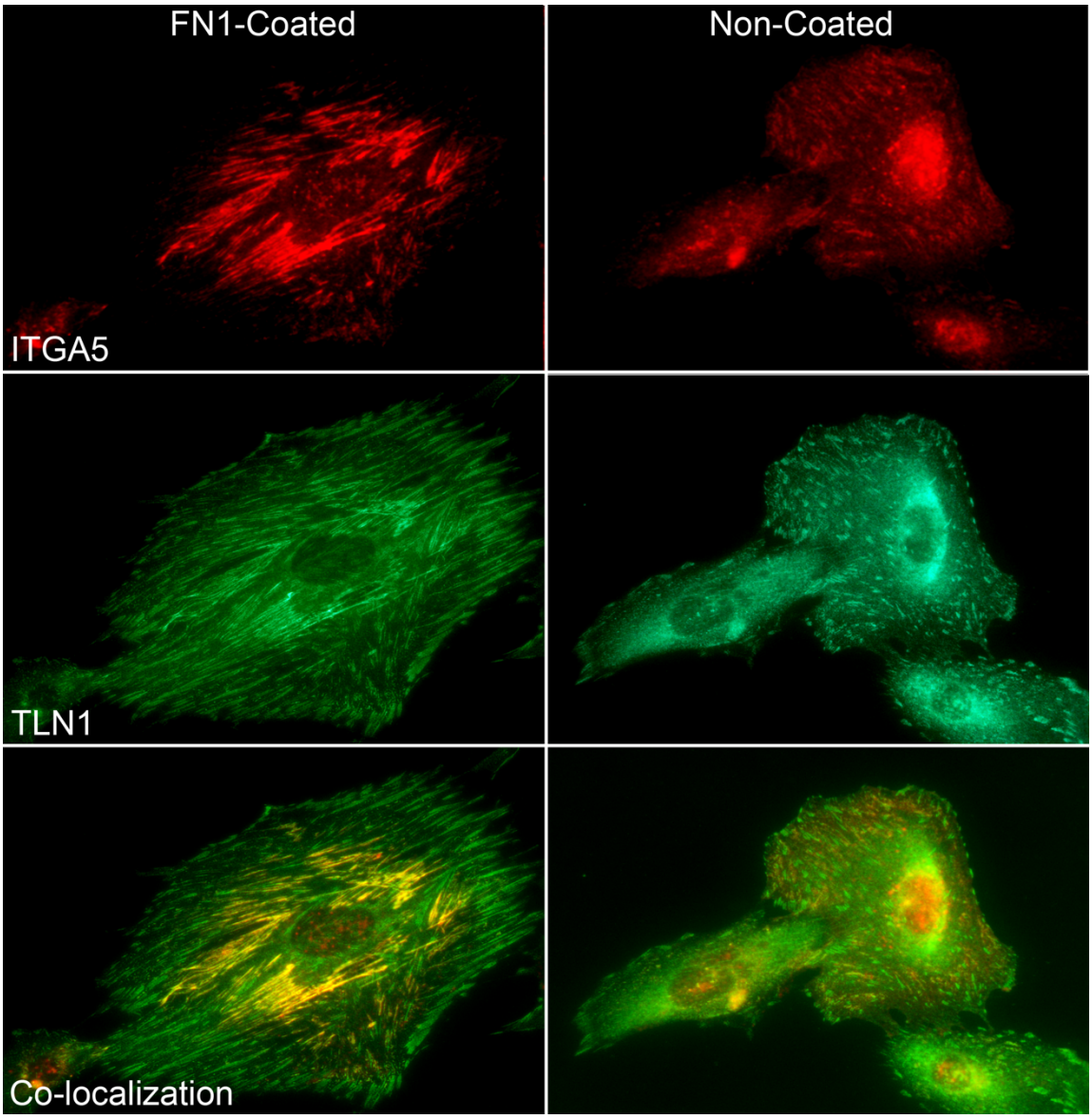

Figure 34. Immunofluorescence localization of the alpha 5 integrin and talin on human myometrial cells bound to fibronectin.

Cells were seeded on coverglass chambered slides coated with FN1 and immunostained with antibodies to ITGA5 and TLN1. Both ITGA5 and TLN1 were observed in large aggregates as components of integrin adhesion complexes (IACs) at the basal surface of myometrial cells as they attach to the FN1-coated slides. Although cultured cells secrete

ECM and bind to that ECM at their basal surface while attaching to slides, note the increased number of IACs for cells attaching to FN1-coated versus non-coated slides. Width of each field is 140 μm.

Earlier studies have shown that other tissue compartments within the uteri of domestic species exhibit tissue-specific organization of IACs during pregnancy. First, the subepithelial uterine stromal cells of sheep and pigs differentiate into a myofibroblast phenotype associated with the upregulation of the cytoskeletal proteins desmin, vimentin, and alpha smooth muscle actin to augment the contractility of fibroblasts (Johnson et al., 2003; Seo et al., 2020b). These stromal cells also express ITGAV and ITGB3 integrins, as well as the ECM proteins secreted phosphoprotein 1 [SPP1, also known as osteopontin (OPN)], FN1, and vitronectin (VTN). The stromal ITGAVB3 receptor binds VTN, FN1, and SPP1 to form IACs, and the diffuse spatial pattern of localization of these proteins within the stroma suggests they are organized into 3D matrix adhesions that developed in a mechanically stressed but more strain-shielded environment (Burghardt et al., 2009). Second, in pigs it is hypothesized that folding at the interface between the uterine luminal epithelium (LE) and the non-invasive placental chorionic epithelium (CE) is driven by external forces delivered to this interface. Subepithelial endometrial blood vessels deliver increased blood flow that pushes upward on the interface between the uterine LE and the placental CE to trigger focal IAC assembly, and endometrial fibroblasts differentiate into contractile myofibroblasts that pull connective tissue downward and inward to sculpt folds at the uterine-placental interface (Seo et al., 2020b). Third, it is proposed that SPP1 binds

integrin receptors expressed by the uterine LE and placental trophectoderm of both sheep and pigs to form IACs that adhere the uterus to the placenta during the attachment phase of implantation and the development of synepitheliochorial and epitheliochorial placentation, respectively (Erikson et al., 2009; Frank et al., 2017; Kim et al., 2010).

In the present study, the ability of myometrial cells to dynamically adapt to changes in extracellular force was also illustrated by the formation of IACs in human myometrial cells on FN1-coated glass chambered slides. Results showed that the ITGA5 integrin subunit was abundantly expressed at the basal surface of cultured myometrial cells and aggregated to IACs at sites of cell anchorage to the substrate. Pre-coating of the substrate with the cell attachment fragment of FN1 enhanced the size and length of *in vitro* IACs compared to the untreated substrate, illustrating the dynamic ability of cells to respond to ECM stiffness through the FN1 receptor.

In summary, IACs begin to assemble within the sheep myometrium during early-to-mid gestation in response to increased stretch of the uterine wall and continue to increase as pregnancy progresses. FN1 is essential for IAC assembly and these IACs contribute to a mechanical syncytium that allows for the sensing of mechanical forces from both inside and outside of the cell in order to sustain powerful contractions during labor. After parturition, IACs are disassembled, but the integrin subunits ITGA5 and ITGB1 remain expressed at the protein level at least two weeks postpartum, indicating that turnover of these proteins is much slower than their synthesis and suggesting that integrins may contribute to the involution process of an organ capable of remarkable myometrial hypertrophy and hyperplasia. Results of the present study indicate that sheep

are similar to humans regarding the assembly of IACs in the pregnant myometrium, and suggest that IACs may form much earlier in human gestation than was previously implied by the rat model. Results highlight the continued value of the sheep model as a flagship gynecological model for understanding parturition in humans (Challis et al., 2000).

REFERENCES

Bershadsky, A., Kozlov, M., and Geiger, B. (2006). Adhesion-mediated mechanosensitivity: a time to experiment, and a time to theorize. Curr Opin Cell Biol *18*, 472-481.

Burghardt, R.C., Burghardt, J.R., Taylor, J.D., 2nd, Reeder, A.T., Nguen, B.T., Spencer, T.E., Bayless, K.J., and Johnson, G.A. (2009). Enhanced focal adhesion assembly reflects increased mechanosensation and mechanotransduction at maternal-conceptus interface and uterine wall during ovine pregnancy. Reproduction *137*, 567-582.

Burkin, H.R., Rice, M., Sarathy, A., Thompson, S., Singer, C.A., and Buxton, I.L. (2013). Integrin upregulation and localization to focal adhesion sites in pregnant human myometrium. Reprod Sci *20*, 804-812.

Burridge, K., and Chrzanowska-Wodnicka, M. (1996). Focal adhesions, contractility, and signaling. Annu Rev Cell Dev Biol *12*, 463-518.

Challis, J.R.G., Matthews, S.G., Gibb, W., and Lye, S.J. (2000). Endocrine and paracrine regulation of birth at term and preterm. Endocr Rev *21*, 514-550.

Chen, C.S. (2008). Mechanotransduction - a field pulling together? J Cell Sci *121*, 3285-3292.

Csapo, A., Erdos, T., De Mattos, C.R., Gramss, E., and Moscowitz, C. (1965). Stretch-induced uterine growth, protein synthesis and function. Nature *207*, 1378-1379.

Cullen, B.M., and Harkness, R.D. (1968). Collagen formation and changes in cell population in the rat's uterus after distension with wax. Q J Exp Physiol Cogn Med Sci *53*, 33-42.

Eddinger, T.J., Schiebout, J.D., and Swartz, D.R. (2007). Adherens junction-associated protein distribution differs in smooth muscle tissue and acutely isolated cells. Am J Physiol Gastrointest Liver Physiol *292*, G684-697.

Erikson, D.W., Burghardt, R.C., Bayless, K.J., and Johnson, G.A. (2009). Secreted phosphoprotein 1 (SPP1, osteopontin) binds to integrin alpha v beta 6 on porcine trophectoderm cells and integrin alpha v beta 3 on uterine luminal epithelial cells, and promotes trophectoderm cell adhesion and migration. Biol Reprod *81*, 814-825.

Frank, J.W., Seo, H., Burghardt, R.C., Bayless, K.J., and Johnson, G.A. (2017). ITGAV (alpha v integrins) bind SPP1 (osteopontin) to support trophoblast cell adhesion. Reproduction *153*, 695-706.

Gabella, G. (1984). Structural apparatus for force transmission in smooth muscles. Physiol Rev *64*, 455-477.

Galbraith, C.G., Yamada, K.M., and Sheetz, M.P. (2002). The relationship between force and focal complex development. J Cell Biol *159*, 695-705.

Goldspink, D.F., and Douglas, A.J. (1988). Protein turnover in gravid and nongravid horns of uterus in pregnant rats. Am J Physiol *254*, E549-554.

Humphries, J.D., Byron, A., and Humphries, M.J. (2006). Integrin ligands at a glance. J Cell Sci *119*, 3901-3903.

Humphries, J.D., Chastney, M.R., Askari, J.A., and Humphries, M.J. (2019). Signal transduction via integrin adhesion complexes. Curr Opin Cell Biol *56*, 14-21.

Hytonen, V.P., and Vogel, V. (2008). How force might activate talin's vinculin binding sites: SMD reveals a structural mechanism. PLoS Comput Biol *4*, e24.

Johnson, G.A., Burghardt, R.C., Joyce, M.M., Spencer, T.E., Bazer, F.W., Pfarrer, C., and Gray, C.A. (2003). Osteopontin expression in uterine stroma indicates a decidualization-like differentiation during ovine pregnancy. Biol Reprod *68*, 1951-1958.

Kanchanawong, P., Shtengel, G., Pasapera, A.M., Ramko, E.B., Davidson, M.W., Hess, H.F., and Waterman, C.M. (2010). Nanoscale architecture of integrin-based cell adhesions. Nature *468*, 580-584.

Katz, B.Z., Zamir, E., Bershadsky, A., Kam, Z., Yamada, K.M., and Geiger, B. (2000). Physical state of the extracellular matrix regulates the structure and molecular composition of cell-matrix adhesions. Mol Biol Cell *11*, 1047-1060.

Kim, J., Erikson, D.W., Burghardt, R.C., Spencer, T.E., Wu, G., Bayless, K.J., Johnson, G.A., and Bazer, F.W. (2010). Secreted phosphoprotein 1 binds integrins to initiate multiple cell signaling pathways, including FRAP1/mTOR, to support attachment and force-generated migration of trophectoderm cells. Matrix Biol *29*, 369-382.

Larsen, M., Artym, V.V., Green, J.A., and Yamada, K.M. (2006). The matrix reorganized: extracellular matrix remodeling and integrin signaling. Curr Opin Cell Biol *18*, 463-471.

Macphee, D.J., and Lye, S.J. (2000). Focal adhesion signaling in the rat myometrium is abruptly terminated with the onset of labor. Endocrinology *141*, 274-283.

MacPhee, D.J., Mostachfi, H., Han, R., Lye, S.J., Post, M., and Caniggia, I. (2001). Focal adhesion kinase is a key mediator of human trophoblast development. Lab Invest *81*, 1469-1483.

Monga, M., Ku, C.Y., Dodge, K., and Sanborn, B.M. (1996). Oxytocin-stimulated responses in a pregnant human immortalized myometrial cell line. Biol Reprod *55*, 427-432.

Muniz, J.J., Joyce, M.M., Taylor, J.D., 2nd, Burghardt, J.R., Burghardt, R.C., and Johnson, G.A. (2006). Glycosylation dependent cell adhesion molecule 1-like protein and L-selectin expression in sheep interplacentomal and placentomal endometrium. Reproduction *131*, 751-761.

Mykuliak, V.V., Haining, A.W.M., von Essen, M., Del Rio Hernandez, A., and Hytonen, V.P. (2018). Mechanical unfolding reveals stable 3-helix intermediates in talin and alpha-catenin. PLoS Comput Biol *14*, e1006126.

Nicolas, A., Geiger, B., and Safran, S.A. (2004). Cell mechanosensitivity controls the anisotropy of focal adhesions. Proc Natl Acad Sci U S A *101*, 12520-12525.

Ono, M., Maruyama, T., Masuda, H., Kajitani, T., Nagashima, T., Arase, T., Ito, M., Ohta, K., Uchida, H., Asada, H.*, et al.* (2007). Side population in human uterine myometrium displays phenotypic and functional characteristics of myometrial stem cells. Proc Natl Acad Sci U S A *104*, 18700-18705.

Robinson, E.E., Foty, R.A., and Corbett, S.A. (2004). Fibronectin matrix assembly regulates alpha5beta1-mediated cell cohesion. Mol Biol Cell *15*, 973-981.

Sastry, S.K., and Burridge, K. (2000). Focal adhesions: a nexus for intracellular signaling and cytoskeletal dynamics. Exp Cell Res *261*, 25-36.

Seo, H., Li, X., Wu, G., Bazer, F.W., Burghardt, R.C., Bayless, K.J., and Johnson, G.A. (2020). Mechanotransduction drives morphogenesis to develop folding during placental development in pigs. Placenta *90*, 62-70.

Seong, J., Tajik, A., Sun, J., Guan, J.L., Humphries, M.J., Craig, S.E., Shekaran, A., Garcia, A.J., Lu, S., Lin, M.Z.*, et al.* (2013). Distinct biophysical mechanisms of focal adhesion kinase mechanoactivation by different extracellular matrix proteins. Proc Natl Acad Sci U S A *110*, 19372-19377.

Shynlova, O., Mitchell, J.A., Tsampalieros, A., Langille, B.L., and Lye, S.J. (2004). Progesterone and gravidity differentially regulate expression of extracellular matrix components in the pregnant rat myometrium. Biol Reprod *70*, 986-992.

Shynlova, O., Williams, S.J., Draper, H., White, B.G., MacPhee, D.J., and Lye, S.J. (2007). Uterine stretch regulates temporal and spatial expression of fibronectin protein and its alpha 5 integrin receptor in myometrium of unilaterally pregnant rats. Biol Reprod *77*, 880-888.

Vogel, V. (2006). Mechanotransduction involving multimodular proteins: converting force into biochemical signals. Annu Rev Biophys Biomol Struct *35*, 459-488.

Wierzbicka-Patynowski, I., and Schwarzbauer, J.E. (2003). The ins and outs of fibronectin matrix assembly. J Cell Sci *116*, 3269-3276.

Williams, S.J., White, B.G., and MacPhee, D.J. (2005). Expression of alpha5 integrin (Itga5) is elevated in the rat myometrium during late pregnancy and labor: implications for development of a mechanical syncytium. Biol Reprod *72*, 1114-1124.

Zhang, J.Z., Behrooz, A., and Ismail-Beigi, F. (1999). Regulation of glucose transport by hypoxia. Am J Kidney Dis *34*, 189-202.

APPENDIX B

TEMPORAL AND SPATIAL EXPRESSION OF AQUAPORINS 1, 5, 8, AND 9 WITHIN THE PORCINE UTERUS AND PLACENTA DURING GESTATION

Introduction

The volumes of allantoic and amniotic fluids in mammalian conceptuses are rapidly changing during gestation to support embryonic/fetal growth and development (Bazer 1989). Aquaporins (AQPs) are water-selective channels that function as pores for water transport through the plasma membrane (Agre et al., 2002). To date, 13 isoforms of AQPs have been found in mammals, with some AQPs transporting other molecules in addition to water. In the current study, we focused on three aquaporins and one aquaglyceroporin, which is known to transport other molecules including glycerol and lactate. The movement of water and nutrients across cell membranes is crucial for reproduction and is likely influenced by the expression of AQPs in tissues of the reproductive tract (Zhu et al., 2015). 2015). The placenta and uterus are the major organs responsible for supporting embryonic/fetal development, and thus play essential roles in assuring survival and growth of the conceptus (embryo/fetus and associated placental membranes and fluids). Key roles of the uterus and placenta are to regulate the transport of nutrients and water across the uterine-placental interface during pregnancy recognition, conceptus implantation, and placental development/placentation (Wilson 2002). Expression of AQPs in the uteri of different species, including humans (Li et al., 1994), mice (Richard et al., 2003), rats (Lindsay and Murphy, 2006, 2007), dogs (Aralla et al., 2012), and pigs (Skowronski,

2010) has been reported. Further, mice lacking AQP5 and AQP8 have an abnormal accumulation of intrauterine luminal fluid and aberrant implantation of conceptuses (Zhang et al., 2015). At present, there is a paucity of information regarding the expression of AQPs at the uterine-placental interface of mammals, including pigs. Therefore, the current study was conducted to determine the temporal cell-type specific expression of AQPs 1, 5, 8, and 9 at the uterine-placental interface of gilts during gestation.

Materials and Methods

Chemicals and reagents

Primary antibodies of AQPs 1 (Millipore), 5 (Sigma Chemicals), 8 (Sigma Chemicals), and 9 (GeneTex) were purchased. Mouse and rabbit IgG (Millipore) antibodies were used as negative controls for immunofluorescence analyses. Other reagents were obtained from Sigma Chemicals.

Animals and tissue collection

This study was approved by the Texas A&M University's Animal use and Care Committee. Twenty gilts (Yorkshire × Landrace) were fed daily 2 kg of a corn- and soybean meal-based diet (Li et al. 2014) and bred to boars of known fertility during the second period of estrus. The day of breeding was designated as day 0 of gestation. Hysterectomy was performed on Days 9, 12, and 15 of the cycle and Days 10, 12, 15, 20, 25, 30, 35, 40, 60, 85, and 90 of gestation (5 gilts/Day), as described previously (Li et al. 2014). Tissue sections (~1 cm thick) from the middle of each uterine horn of gilts on Days

9, 10, 12, and 15, and from implantation sites beginning Day 20, were fixed in fresh 4% paraformaldehyde in PBS (pH 7.2) and embedded in Paraplast-Plus (Oxford Laboratory, St. Louis, MO).

Progesterone and Estrogen Models

To evaluate effects of estrogen (E2) and E2-induced pseudopregnancy on expression of AQPs 1, 5, 8, and 9 mRNAs in endometria, gilts were detected in estrus (Day 0) and assigned randomly to receive daily intramuscular injections of either estradiol benzoate (E2 in corn oil (E2); n = 4) or corn oil alone (CO; n = 4) on Days 11, 12, 13, and 14 of the estrous cycle to induce pseudopregnancy (Frolova et al. 2009). All gilts were euthanized and then ovariohysterectomized on Day 15. Endometrial tissues were collected as previously described.

To evaluate effects of long-term treatment with progesterone (P4) on expression of AQPs 1, 5, 8, and 9 mRNAs in endometria, gilts were ovariectomized on Day 12 of the estrous cycle and assigned randomly to receive daily intramuscular injections of either CO (4 ml) or P4 (200 mg in 4 ml CO) on Days 12 through 39 post-estrus (n = 3/treatment) (Waugh and Wales 1993). All gilts were hysterectomized on Day 40 post-estrus and endometrial tissues collected as previously described.

Immunofluorescence Microscopy

Paraffin embedded sections (5 μm) of the uterine-placental interface were adhered to slides, deparaffinized and rehydrated in CitriSolv, ethanol, and water. For antigen

unmasking, the sections were brought to a boil in a 10mM Sodium Citrate Buffer solution. The sections were then washed in PBS 3 times for 5 min each, blocked with 10% normal goat serum, and then the sections were incubated with either rabbit anti-AQP1 (2.5 μg/ml), rabbit anti-AQP5 (2 μg/ml), mouse anti-AQP8 (5 μg/ml), or rabbit anti-AQP9 (2.5 μg/ml) overnight at 4°C in a humidified chamber. Normal rabbit or mouse IgG was substituted for a primary antibody and served as a negative control. Expression was detected with either fluorescein-conjugated goat anti-rabbit IgG or goat anti-mouse IgG (1:250) for one hour (Chemicon International). Slides were then overlaid with Prolong Gold Anti-fade mounting reagent containing DAPI (Molecular Probes) and a coverslip. Images were taken using an Axioplan 2 microscope and a Zeiss Imager.M2, (Carl Zeiss, Thornwood, NY) interfaced with an Axioplan HR and an AxioCam HRm digital camera, respectively. Photographic plates were assembled using Adobe Photoshop (version 6.0, Adobe Systems Inc., San Jose, CA).

RNA Extraction, cDNA Synthesis, and Primer Design

Total RNA was isolated from frozen endometrium using Trizol reagent (Life Technologies, Carlsbad, CA) according to the manufacturer's recommendations. First strand cDNA was synthesized using a Superscript III First Strand Kit (Life Technologies, Carlsbad, CA) according to the manufacturer's instructions. First strand cDNA was diluted 5x for the qPCR reaction. Primers for qPCR were designed using NCBI Genbank sequences and submitted to BLAST (http://www.ncbi.nlm.nih.gov/) to confirm specificity against the known porcine genome.

Quantitative PCR assays were performed using PerfeCta SYBR Green Master mix (Quanta Biosciences, Gaithersburg, MD) in 10 µl reactions with 2.5 mM of each specific primer, on a Roche 480 Lightcycler (Rochem Life Sciences) with approximately 60 ng cDNA per reaction. The PCR program began with 5 min at 95°C followed by 40 cycles of 95°C denaturation for 10 sec and 60°C annealing/extension for 30 sec. A melt curve was produced with every run to verify a single gene-specific peak. Standard curves using pooled cDNA with 2-fold serial dilutions were run to determine primer efficiencies. All primer correlation coefficients were greater than 0.95 and efficiencies were 100-112%. Ribosomal protein 7 (Rpl7) was used to normalize data from endometrial tissues (Seo et al., 2012). The primer sequences for AQP1 were, forward 5'-tcaactaaagaagaggcaaaaacac-3'and reverse 5'-gcccaaaatattacctctctttctc-3'. The primer sequences for AQP5 were, forward 5'- ccatcctctacttctacctgctc-3' and reverse 5'- ttcgctgtcatctgttttccttctt-3'. The primer sequences for AQP8 were, forward 5'- attctccatcggcttctctgt-3' and reverse 5'- tccctttagaattaggcgagttttc-3'. The primer sequences for AQP9 were, forward 5'- tcattatagtcttcgctgtttttga-3' and reverse 5'- ctacaggaatccaccagaagttatt-3'. The 2-ΔΔCt method was used to normalize data, and fold-changes were subjected to statistical analyses.

Statistical analysis

All statistical analyses were performed using GraphPad Prism (GraphPad Software, La Jolla, CA). Data from quantitative PCR for effect of days of pregnancy were subjected to one-way ANOVA followed by a post-hoc Tukey analysis. Data from

quantitative PCR analyses for effect of P4 and E2 treatments were analyzed using the Students t-test. All data are presented as mean ± SEM with significance set at $P < 0.05$.

Results

AQP1 mRNA and protein expression increase at the uterine-placental interface throughout the estrous cycle and gestation

AQP1 protein was highly expressed in all endothelial cells of both the uterine and placental vasculatures from Day 15 to Day 90 of pregnancy (Figure 35). AQP1 protein expression was also observed in red blood cells (RBCs) and the smooth muscle cells of the myometrium. Interestingly, only the smooth muscle cells in the myometrium showed expression of AQP1, as there was no expression of AQP1 protein in the smooth muscle cells of the tunica media of blood vessels. AQP1 mRNA expression showed a significant increase in both the cycle and throughout gestation.

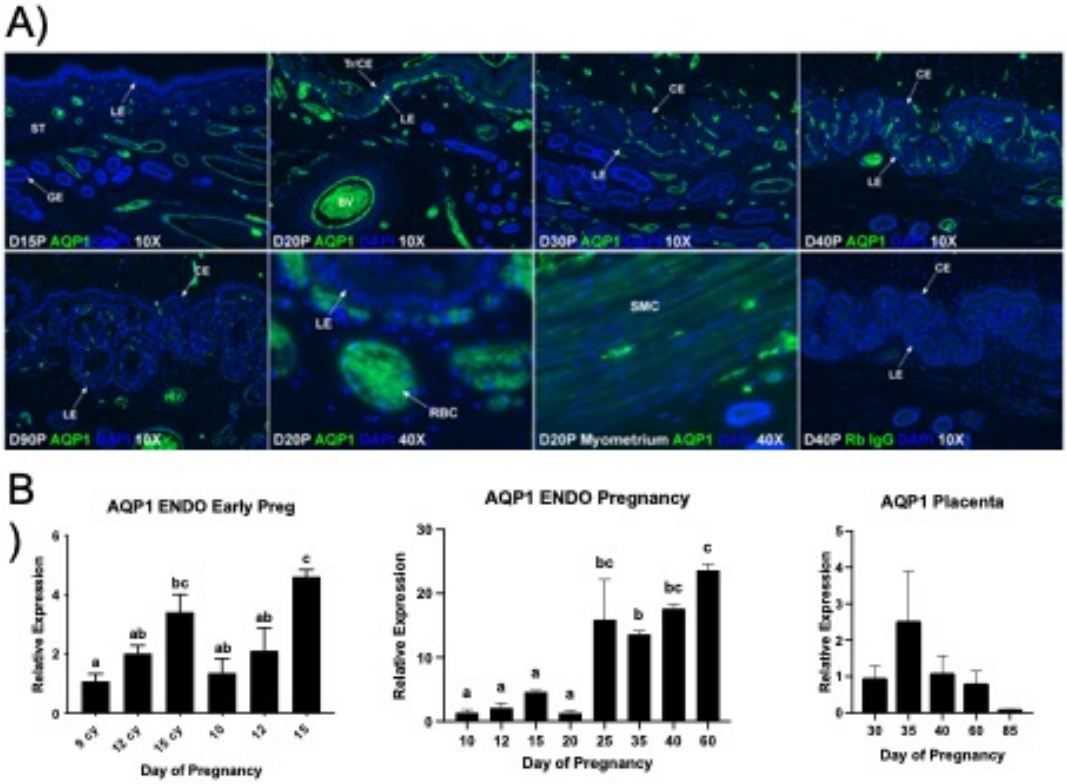

Figure 35. Expression of aquaporin 1 at the uterine-placental interface of gilts

Immunofluorescence microscopy for aquaporin 1 (AQP1; green) at the uterine-placental interface of gilts on Days 15 (D15), 20, 30, 40, and 90 of pregnancy. AQP1 protein is localized to all endothelial cells within both uterine and placental tissues, to the myometrium and within red blood cells. Nuclei are stained with DAPI for histologic reference. The D40 rabbit IgG (Rb IgG) panel serves as the negative control. Width of fields for microscopic images captured at 10X is 940 μm. Width of fields for microscopic images captured at 40X is 230 μm. Legend: D, day; P, pregnancy; LE, luminal epithelium; GE, glandular epithelium; ST, stroma; BV, blood vessel; Tr, trophectoderm; CE, chorionic epithelium; RBC, red blood cells; SMC, smooth muscle cells.

AQP5 is expressed in the placental areolae throughout gestation

AQP 5 protein was expressed in small sections of the chorionic epithelium beginning on Day 20 of gestation. By Day 25, it was apparent that AQP5 was being localized to the chorionic epithelium of areolae and this expression continued through Day 90 of pregnancy (Figure 36). AQP5 mRNA showed no change in expression levels throughout pregnancy.

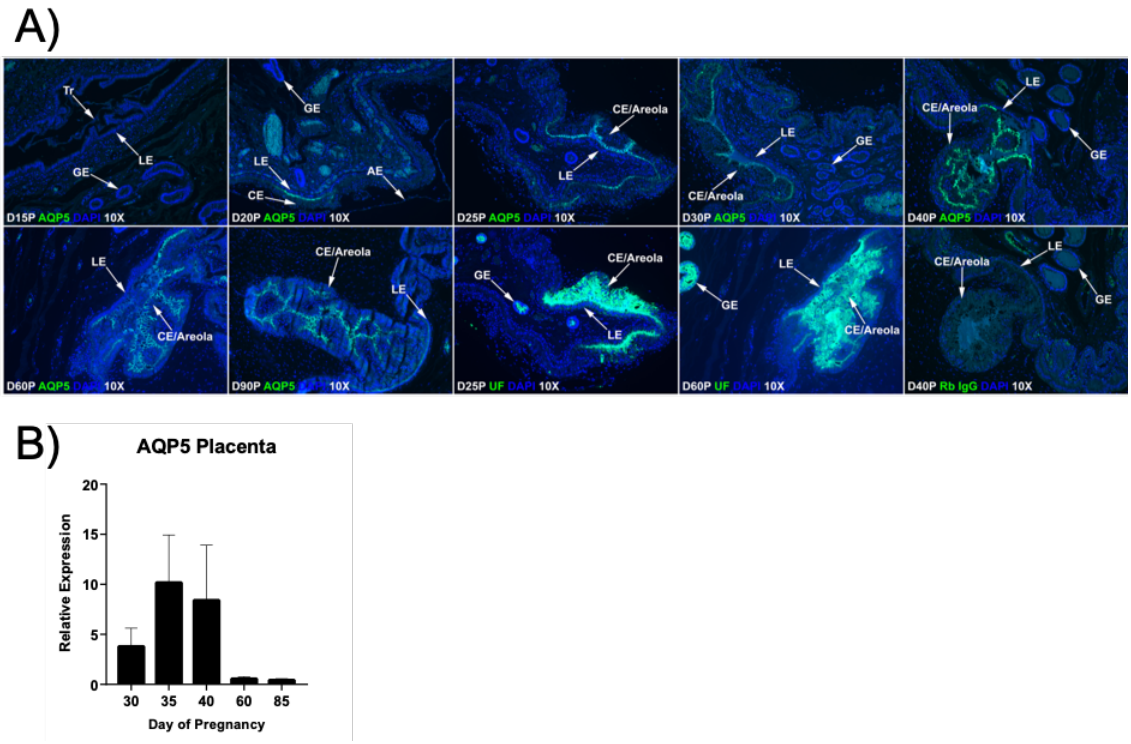

Figure 36. Expression of aquaporin 5 at the uterine-placental interface of gilts

Immunofluorescence microscopy for aquaporin 5 (AQP5; green) at the uterine-placental interface of gilts on Days 15 (D15), 20, 25, 30, 40, 60, and 90 of pregnancy. AQP5 protein is localized to the chorionic epithelium on Day 20 and this expression is maintained through Day 90 in the areolae. Day 25 and Day 60 have serial sections stained with

uteroferrin to confirm areolae. Nuclei are stained with DAPI for histologic reference. The D40 rabbit IgG (Rb IgG) panel serves as the negative control. Width of fields for microscopic images captured at 10X is 895 μm. Legend: D, day; P, pregnancy; LE, luminal epithelium; GE, glandular epithelium; Tr, trophectoderm; CE, chorionic epithelium; AE, allantoic epithelium.

AQP8 mRNA and protein expression increase at the uterine-placental interface throughout gestation

Endometrial expression (Figure 37A and 37B). AQP8 protein was expressed by the endometrial glands and glandular epithelium (GE), and in the tunica media and adventitia of blood vessels beginning on Day 25 of pregnancy and continued to be expressed through Day 60. AQP8 expression also localized to the stroma adjacent to the luminal epithelium beginning on Day 30 of gestation. There appeared to be a decrease in AQP8 expression on Days 35 and 40 of gestation but an increase on Day 60. Although there was no expression in the smooth muscle cells of the myometrium, AQP8 staining was expressed in the connective tissue of the myometrium (Figure 3D).

Conceptus expression (Figure 37A and 37C). AQP8 protein expression was localized to the conceptus trophectoderm on Days 15 and 20 of pregnancy, but by Day 25 its expression was limited to the placental areolae. AQP8 was also expressed in the tunica media and adventitia of placental blood vessels and within the stroma by Day 30 of gestation and appeared to decrease on Days 35 and 40, but expression increased on Day 60 of gestation.

mRNA expression levels (Figure 37D). AQP8 mRNA expression showed no significant changes during the cycle or in the placenta throughout gestation. However, endometrial mRNA expression increased starting at day 15 of pregnancy and continued until day 40 where it remained until day 60 of pregnancy.

A) AQP8 Expression throughout Gestation

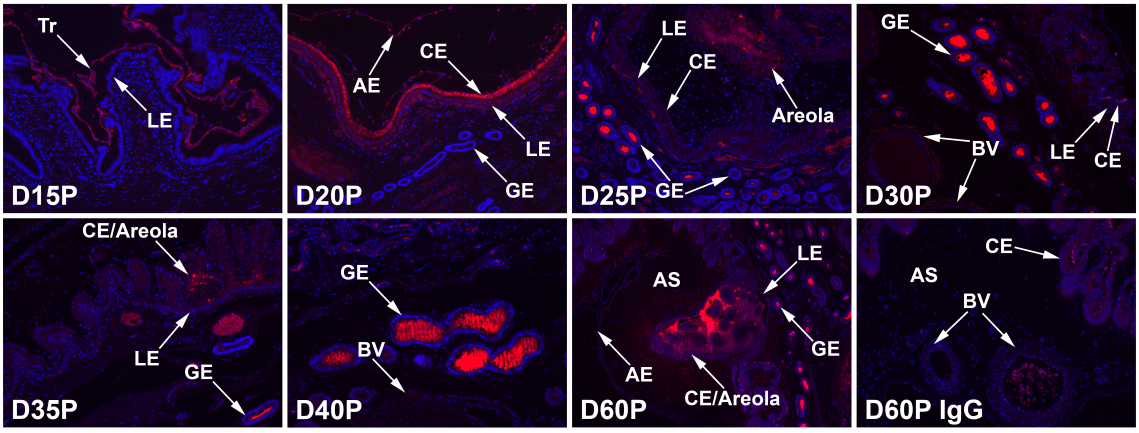

B) AQP8 Endometrial Blood Vessel and Stromal Expression

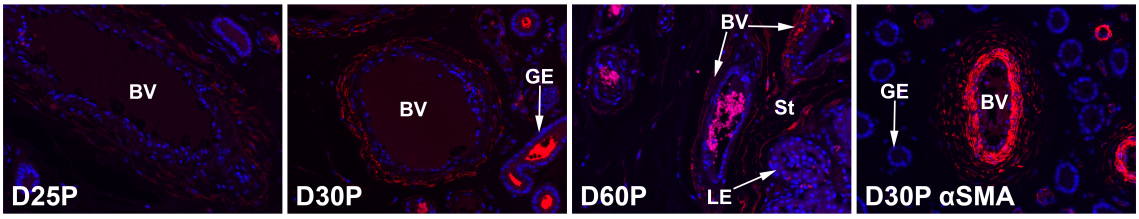

C) AQP8 Placental Blood Vessel and Stromal Expression

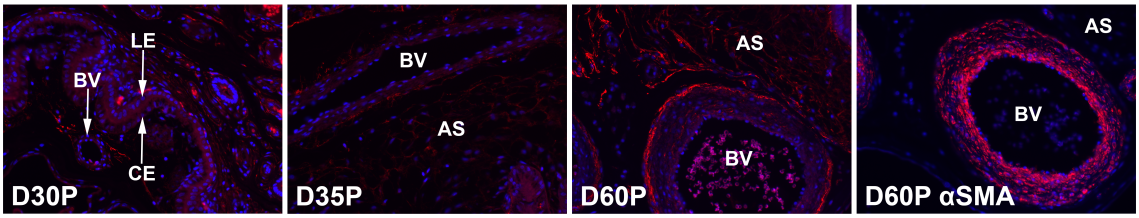

D) AQP8 Myometrial Expression

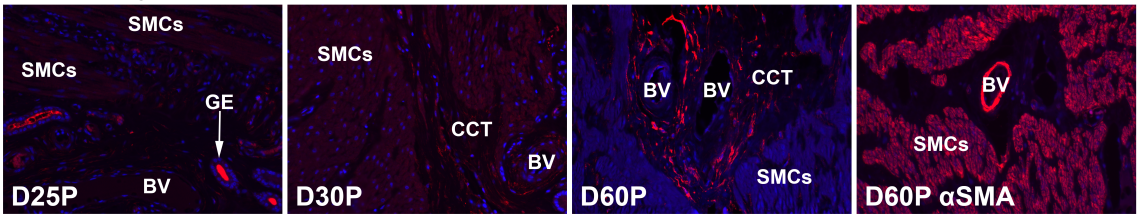

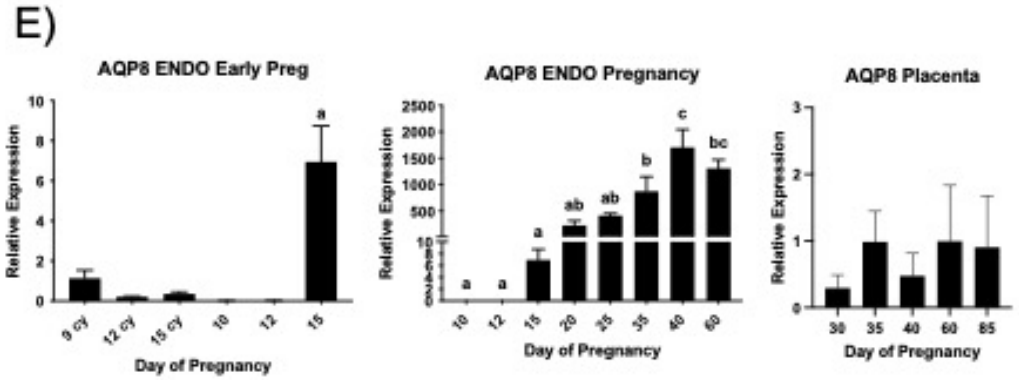

Figure 37. Expression of aquaporin 8 at the uterine-placental interface of gilts.

Immunofluorescence microscopy for aquaporin 8 (AQP8; red) at the uterine-placental interface of gilts on Days 15 (D15), 20, 25, 30, 35, 40, and 60 of pregnancy. AQP8 protein is localized to the trophectoderm on Days 15 and 20, the areolae, endometrial glands, and glandular epithelium beginning on Day 25, the tunica media and tunica adventitia of blood vessels within both uterine and placental tissues, and stromal cells within the allantois and endometrium beginning on Day 30 of gestation. The connective tissue within the myometrium also expressed AQP8 protein beginning on Day 25 of pregnancy. Alpha smooth muscle actin was shown to denote the smooth muscle cells within the myometrium and blood vessel walls. Nuclei are stained with DAPI for histological reference. The Day 60 mouse IgG (Ms IgG) panel serves as the negative control. Width of fields for microscopic images captured at 10X is 895 μm. Width of fields for microscopic images captured at 20X is 448 μm. Legend: D, day; P, pregnancy; LE, luminal epithelium; AE, allantoic epithelium; GE, glandular epithelium; BV, blood vessel; Tr, trophectoderm; CE, chorionic epithelium; AS, allantoic stroma; St, stroma; SMCs, smooth muscle cells; CCT, collagenous connective tissue.

AQP9 protein expression is localized to the endometrial LE and placental allantoic epithelium and mRNA expression increases in the placenta

AQP9 protein was expressed in the uterine luminal epithelium (LE), GE, and areolae throughout pregnancy (Figure 38). In the uterine LE, AQP9 was localized to the apical surface of the cells during early pregnancy, with a shift in expression towards the basal surface of the cells by Day 40. Expression within the uterine GE was low throughout gestation and the allantoic epithelium showed AQP9 protein expression on Day 20 of gestation. AQP9 mRNA expression decreased during the cycle and increased in the placenta during gestation.

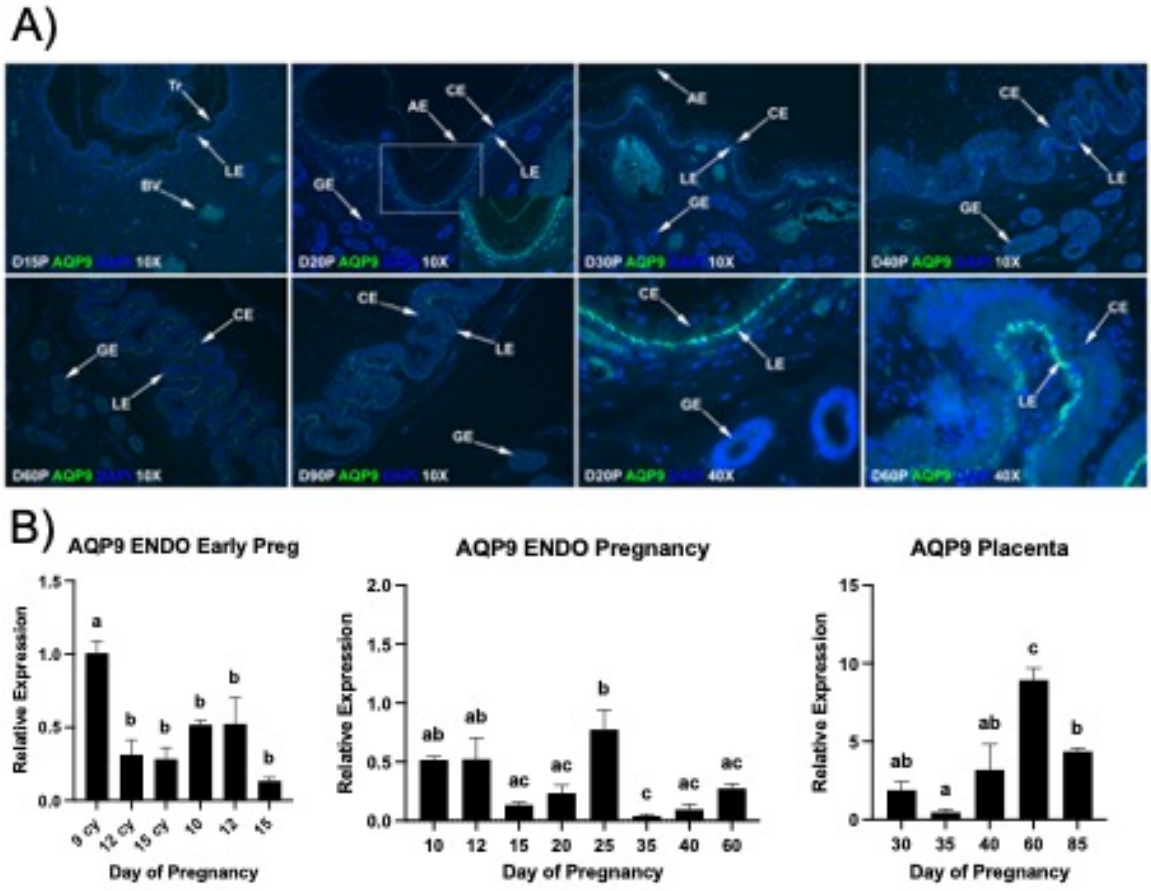

Figure 38. Expression of aquaporin 9 at the uterine-placental interface of gilts

Immunofluorescence microscopy for aquaporin 9 (AQP9; green) at the uterine-placental interface of gilts on Days 15 (D15), 20, 30, 40, 60 and 90 of pregnancy. AQP9 protein is localized primarily to the uterine luminal epithelium (LE) throughout gestation, changing from an apical expression at the beginning of gestation to a more basal expression around Day 40. AQP9 is also expressed in the allantoic epithelium on Day 20 and decreases thereafter. It is also localized to the glandular epithelium starting on Day 20 and maintains low expression throughout gestation. Nuclei are stained with DAPI for histologic reference. The D60 rabbit IgG (Rb IgG) panel serves as the negative control. Width of

fields for microscopic images captured at 10X is 895 μm. Width of fields for microscopic images captured at 20X is 448 μm. Width of fields for microscopic images captured at 40X is 224 μm. Legend: D, day; P, pregnancy; LE, luminal epithelium; GE, glandular epithelium; Tr, trophectoderm; BV, blood vessel; CE, chorionic epithelium; AE, allantoic epithelium.

Discussion

Placentation in pigs initially involves rapid expansion and development of the chorion (trophectoderm) and allantois between Days 18 and 30 of gestation in pigs due to the accumulation of water within membranes (Bazer and Johnson, 2014). The driving force for expansion of the allantois, and in turn the chorioallantois, is the rapid accumulation of water from about 1 ml on Day 18 to 200-250 ml on Day 30 of gestation. Allantoic fluid volume increases from Day 20 (3.7 ml) to Day 30 (189 ml), decreases to Day 45 (75 ml), and then increases again to Day 58 (451 ml). Thereafter, it decreases to Day 112 (24 ml). AQPs play an important role in the transport of water from mother to fetus. The uterus is the site of implantation and development of the conceptus in mammals, and there is evidence for the expression of AQPs in the uteri of humans, rats, mice, dogs, sheep, horse, and pigs (Ducza et al., 2017). For example, AQP1, 5, 7, 8, and 9 transcripts were detected in the uterine GE of the rat uterus (Lindsay and Murphy, 2007). There is also evidence for the expression of AQP1, AQP5, and AQP9 in the ovary, oviduct, and uterus of gilts on days 17 and 19 of the estrous cycle (Skowronski et al., 2009). We have previously shown that AQPs 1, 3, 5, and 9 were expressed in the uterine endometrium, as

well as the placenta of gilts at both mRNA and protein levels on day 25 of gestation (Zhu et al., 2015). The current work identified the cell-specific expression of AQPs 1, 5, 8, and 9 mRNA and protein at the porcine uterine-placental interface during gestation.

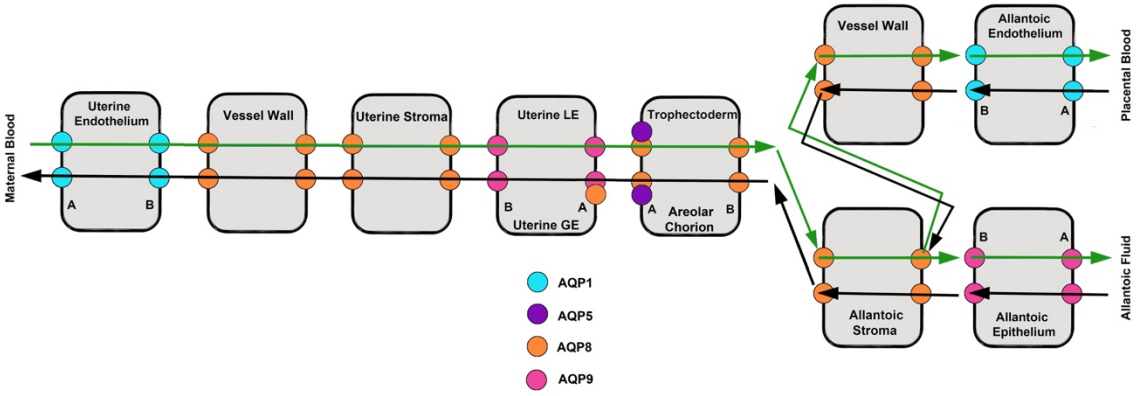

Figure 39. Image depicting the different cell layers in epitheliochorial placentation and where each aquaporin is located

The expression of AQP1 in the porcine endothelium (Figure 1) was expected because it was initially discovered in erythrocytes and later found in endothelial cells throughout the human body (Agre et al., 1987; Mobasheri and Marples, 2004). This also explains why the mRNA expression increased because as pregnancy progresses, there is a higher requirement for nutrients to be transported to the fetus, resulting in increased angiogenesis. AQP1 is responsible for the high water permeability of the endothelium to maintain water and ion homeostasis for numerous functions, including cell differentiation, proliferation, secretion, and apoptosis (Ishibashi et al., 2011). Expression of AQP1 in the RBCs (Figure 1) of pigs was not unprecedented. There are two hypotheses about the function of AQP1 in the membranes of RBCs. The first suggests that AQP1 contributes to undulations or "flickering" of the cell membrane, which helps in moving the RBCs through capillaries.

The second suggests that the high permeability of RBC membranes allows for concomitant displacement of water molecules when rapid exchange of ions and solutes occurs (Benga, 2012). We also observed AQP1 expression in the myometrium of pigs (Figure 1). Lindsay and Murphy (2004) have shown AQP1 in the myometrium of rats and this expression is believed play a role in decreasing the size of the uterine lumen to assist in positioning of the blastocyst during implantation (Lindsay and Murphy, 2004). In rodents, the uterine lumen closes down to form an implantation chamber and previous reports have speculated that AQP1 in the myometrium could allow water into the cells, leading to swelling of the smooth muscle and closing of the lumen (Gannon et al., 2000). Increased expression of AQP1 in the mesometrial smooth muscle rather than the antimesometrial myometrium could initiate contraction or cause swelling, which could contribute to the antimesometrial location of the implanting blastocyst (Lindsay and Murphy, 2004). Although AQP1 mRNA and protein have been previously reported to be expressed in the myometrium of pigs in explant cultures by real-time PCR and Western blot analyses, respectively (Skowronska et al., 2015; Skowronski et al., 2009), the localization of AQP1 protein in the smooth muscle cells of the porcine myometrium (Figure 1) is a novel finding. AQP1 in the smooth muscle cells of the myometrium could act similarly to rodents and allow swelling of the myometrium in order to increase contact with the conceptuses or to displace them throughout the lumen. Pope et al. (1986) found that porcine embryos migrated through the uterus in response to uterine contractions and in vitro studies with rat smooth muscle cells have shown that AQP1 transports hydrogen peroxide into smooth muscle cells, which then leads to hypertrophy of those cells (Al Ghouleh et al., 2013).

Additionally, AQP1 has been shown to upregulate beta-catenin protein levels, which promotes smooth muscle cell proliferation in vitro (Yun et al., 2017). These data suggest potential roles of AQP1 in the myometrium of pigs, but further studies are necessary to determine the effects of AQP1.

AQP5 has been described throughout the human body and, along with water, it has been proposed to transport gases and ions (Boassa et al., 2006; Direito et al., 2016; Wang and Tajkhorshid, 2010; Yool and Weinstein, 2002). AQP5-null mice show decreased water permeability across the alveolar membranes (Ma et al., 2000), suggesting an important role in water transport across membranes. Interestingly, AQP5 expression is upregulated in numerous cancers throughout the body and it is has been shown that downregulation of AQP5 leads to a higher susceptibility of apoptosis in cancer cells (Chae et al., 2008; Direito et al., 2016). In the current study, we found that AQP5 was expressed solely in the chorionic epithelium where areolae were located (Figure 2). This expression is important because areolae allow for large amounts of histotroph to be transported from mother to fetus. Because there is significant transport of water and nutrients through the areolae during gestation, it is likely that AQP5 plays a crucial role in providing the fetus with water and other nutrients necessary for growth and survival.

Based on quantitative real-time PCR data, ovine conceptuses express AQP8 mRNA beginning on Day 27 of gestation and its expression is maintained throughout the remainder of gestation (Liu et al., 2004). Expression of AQP8 mRNA in the endometrium of mares on Day 14 of pregnancy has also been reported (Klein et al., 2013). However, the present results are the first to reveal the cell-specific localization of AQP8 in the uteri

and conceptuses of pigs. In addition to water, AQP8 has been shown to transport ions and ammonia, both of which are important nutrients for cell homeostasis and growth (Saparov et al., 2007). It has been proposed that AQP8 in the rodent uterus is responsible for shuttling water between the myometrium and stroma of the endometrium (Kobayashi and Yasui, 2010), and that AQP8 in the sheep conceptus is partially responsible for the high water permeability of the placenta (Liu et al., 2004). Our novel results suggest that AQP8 in the porcine uterus, specifically the trophectoderm cells of the early conceptus, cells of blood vessel walls, endometrial glands, placental areolae, endometrial and allantoic stromal cells, and the allantoic epithelium may play a role similar to that in the rat uterus and sheep conceptus for the transport of water from the maternal circulation to the chorioallantois during pregnancy. In addition, the localization of AQP8 protein in epithelial cells of the amnion and allantois of canines has been suggested to mediate fluid transfer across fetal membranes (Aralla et al., 2012). There are also dynamic changes in allantoic fluid volume in pigs throughout pregnancy and those changes may be responsible for expanding the chorioallantoic membranes and allowing them to establish intimate contact with a maximum amount of endometrial surface area (Knight et al., 1977). This agrees with our immunofluorescence results showing AQP8 protein in the allantois of pigs during later pregnancy (Figure 2) and suggests that it is involved in water and ammonia transport within the placenta. The increase in mRNA expression supports this idea that AQP8 is involved in water and nutrient transport because the expression increased as pregnancy progressed. Lastly, the localization of AQP8 protein in the placental areolae associated with the openings of the uterine glands in the pig endometrium is novel and

important because there is substantial transport of water and other nutrients through the areolae throughout pregnancy(Bazer et al., 2012). We propose that AQP8 is at least partly responsible for the transport of water and other nutrients through the chorionic epithelium of the areolae.

Aquaporin 9 has been investigated in a number of species for multiple roles (Ducza et al., 2017; Prat et al., 2012). Here, we focus primarily on the expression of AQP9 protein at the porcine uterine-placental interface and its novel localization within the endometrial LE, GE, and allantoic epithelium. The expression of AQP9 protein in the uterine GE is important because the GE is responsible for the secretion of histotroph, which is critical for the developing conceptus (Bazer et al., 2012). Because the uterine GE expresses AQP9 protein, certain solutes like glycerol (a product of lipolysis) and lactate (a product of glycolysis) are able to be transported from the maternal endometrium to the conceptus which is able to utilize these nutrients due to its expression in the allantoic epithelium. Glycerol and lactate are important for many biological processes and along with water provide essential nutrients for the growth and development of the conceptus (Maciolek et al., 2014; Xue et al., 2017). It has been reported that, in pigs, there are two periods of fluid accumulation in the allantoic sac, the first being between Days 20 and 30 of gestation, and the second between Days 40 and 60. This is accompanied with an increase in protein within the allantoic sac, followed by a decline in both protein and fluid volume to Day 100 (Knight et al., 1977). Interestingly, we observed a spatial-temporal localization of AQP9 protein in the uterine LE that suggests AQP9 may play a role in the accumulation and subsequent decrease in fluid volume at these time points. The mRNA data agrees with the

idea of changing the expression pattern because there is an increase in expression from day 20 to 25 in the endometrium when fluid accumulation in the conceptus is increasing and a subsequent decrease in mRNA expression on day 35, when there is a corresponding decrease in fluid accumulation within the conceptus (Bazer and Johnson, 2014). During the period of fluid accumulation within the allantoic sac, AQP9 protein is expressed at the apical surface of the uterine LE, typical of a secretory phenotype. As the allantoic fluid volume decreases, the location of the expression of AQP9 protein changes to the basal surface of the uterine LE, consistent with an epithelium that absorbs fluid from the lumen. This novel localization may provide a mechanism to explain the transportation of water and other nutrients from the porcine maternal endometrium to the conceptus, and then back from the conceptus to the endometrium. This is also supported by our AQP1, AQP5, and AQP8 results. Therefore, using AQP1, AQP5, AQP8, and AQP9, cells can potentially transport water and other nutrients from the uterine vasculature, through the tunica intima, tunica media, and tunica adventitia, across the uterine LE and chorion, and either through the tunica adventitia, tunica media, and tunica intima of placental blood vessels or across the allantoic stroma and into the allantois, via the allantoic epithelium, for utilization within the stromal compartment of the placenta (Figure 4). Indeed, the reverse is also possible, and may explain the changing volumes of allantoic fluid and hydration of placental connective tissues during pregnancy in pigs (Knight et al., 1977).

In conclusion, our results reveal the temporal cell-type specific expression of AQP 1, 5, 8, and 9 proteins within the porcine uterus and placenta during gestation. The expression of these AQPs in the endometrium and myometrium of the uterus, and the chorioallantois

is likely key to the rapid changes in volumes of the fetal fluids that are critical for implantation and placentation in pigs. These findings provide new knowledge and insight about the transport of water and other nutrients from mother to fetus in support of conceptus growth, development, and survival in mammals in general, and pigs in particular.

REFERENCES

Agre, P., King, L.S., Yasui, M., Guggino, W.B., Ottersen, O.P., Fujiyoshi, Y., Engel, A., and Nielsen, S. (2002). Aquaporin water channels--from atomic structure to clinical medicine. J Physiol *542*, 3-16.

Agre, P., Saboori, A.M., Asimos, A., and Smith, B.L. (1987). Purification and partial characterization of the Mr 30,000 integral membrane protein associated with the erythrocyte Rh(D) antigen. J Biol Chem *262*, 17497-17503.

Al Ghouleh, I., Frazziano, G., Rodriguez, A.I., Csanyi, G., Maniar, S., St Croix, C.M., Kelley, E.E., Egana, L.A., Song, G.J., Bisello, A.*, et al.* (2013). Aquaporin 1, Nox1, and Ask1 mediate oxidant-induced smooth muscle cell hypertrophy. Cardiovasc Res *97*, 134-142.

Aralla, M., Mobasheri, A., Groppetti, D., Cremonesi, F., and Arrighi, S. (2012). Expression of aquaporin water channels in canine fetal adnexa in respect to the regulation of amniotic fluid production and absorption. Placenta *33*, 502-510.

Bazer, F.W., and Johnson, G.A. (2014). Pig blastocyst-uterine interactions. Differentiation *87*, 52-65.

Bazer, F.W., Song, G., Kim, J., Dunlap, K.A., Satterfield, M.C., Johnson, G.A., Burghardt, R.C., and Wu, G. (2012). Uterine biology in pigs and sheep. J Anim Sci Biotechnol *3*, 23.

Benga, G. (2012). The first discovered water channel protein, later called aquaporin 1: molecular characteristics, functions and medical implications. Mol Aspects Med *33*, 518-534.

Boassa, D., Stamer, W.D., and Yool, A.J. (2006). Ion channel function of aquaporin-1 natively expressed in choroid plexus. J Neurosci *26*, 7811-7819.

Chae, Y.K., Woo, J., Kim, M.J., Kang, S.K., Kim, M.S., Lee, J., Lee, S.K., Gong, G., Kim, Y.H., Soria, J.C.*, et al.* (2008). Expression of aquaporin 5 (AQP5) promotes tumor invasion in human non small cell lung cancer. PLoS One *3*, e2162.

Direito, I., Madeira, A., Brito, M.A., and Soveral, G. (2016). Aquaporin-5: from structure to function and dysfunction in cancer. Cell Mol Life Sci *73*, 1623-1640.

Ducza, E., Csanyi, A., and Gaspar, R. (2017). Aquaporins during Pregnancy: Their Function and Significance. Int J Mol Sci *18*.

Gannon, B.J., Warnes, G.M., Carati, C.J., and Verco, C.J. (2000). Aquaporin-1 expression in visceral smooth muscle cells of female rat reproductive tract. J Smooth Muscle Res *36*, 155-167.

Ishibashi, K., Kondo, S., Hara, S., and Morishita, Y. (2011). The evolutionary aspects of aquaporin family. Am J Physiol Regul Integr Comp Physiol *300*, R566-576.

Klein, C., Troedsson, M.H., and Rutllant, J. (2013). Expression of aquaporin water channels in equine endometrium is differentially regulated during the oestrous cycle and early pregnancy. Reprod Domest Anim *48*, 529-537.

Knight, J.W., Bazer, F.W., Thatcher, W.W., Franke, D.E., and Wallace, H.D. (1977). Conceptus development in intact and unilaterally hysterectomized-ovariectomized gilts: interrelations among hormonal status, placental development, fetal fluids and fetal growth. J Anim Sci *44*, 620-637.

Kobayashi, K., and Yasui, M. (2010). Cellular and subcellular localization of aquaporins 1, 3, 8, and 9 in amniotic membranes during pregnancy in mice. Cell Tissue Res *342*, 307-316.

Li, X., Yu, H., and Koide, S.S. (1994). The water channel gene in human uterus. Biochem Mol Biol Int *32*, 371-377.

Lindsay, L.A., and Murphy, C.R. (2004). Aquaporin-1 increases in the rat myometrium during early pregnancy. J Mol Histol *35*, 75-79.

Lindsay, L.A., and Murphy, C.R. (2006). Redistribution of aquaporins 1 and 5 in the rat uterus is dependent on progesterone: a study with light and electron microscopy. Reproduction *131*, 369-378.

Lindsay, L.A., and Murphy, C.R. (2007). Aquaporins are upregulated in glandular epithelium at the time of implantation in the rat. J Mol Histol *38*, 87-95.

Liu, H., Koukoulas, I., Ross, M.C., Wang, S., and Wintour, E.M. (2004). Quantitative comparison of placental expression of three aquaporin genes. Placenta *25*, 475-478.

Ma, T., Fukuda, N., Song, Y., Matthay, M.A., and Verkman, A.S. (2000). Lung fluid transport in aquaporin-5 knockout mice. J Clin Invest *105*, 93-100.

Maciolek, J.A., Pasternak, J.A., and Wilson, H.L. (2014). Metabolism of activated T lymphocytes. Curr Opin Immunol *27*, 60-74.

Mobasheri, A., and Marples, D. (2004). Expression of the AQP-1 water channel in normal human tissues: a semiquantitative study using tissue microarray technology. Am J Physiol Cell Physiol *286*, C529-537.

Prat, C., Blanchon, L., Borel, V., Gallot, D., Herbet, A., Bouvier, D., Marceau, G., and Sapin, V. (2012). Ontogeny of aquaporins in human fetal membranes. Biol Reprod *86*, 48.

Richard, C., Gao, J., Brown, N., and Reese, J. (2003). Aquaporin water channel genes are differentially expressed and regulated by ovarian steroids during the periimplantation period in the mouse. Endocrinology *144*, 1533-1541.

Saparov, S.M., Liu, K., Agre, P., and Pohl, P. (2007). Fast and selective ammonia transport by aquaporin-8. J Biol Chem *282*, 5296-5301.

Skowronska, A., Mlotkowska, P., Nielsen, S., and Skowronski, M.T. (2015). Difference in expression between AQP1 and AQP5 in porcine endometrium and myometrium in response to steroid hormones, oxytocin, arachidonic acid, forskolin and cAMP during the mid-luteal phase of the estrous cycle and luteolysis. Reprod Biol Endocrinol *13*, 131.

Skowronski, M.T. (2010). Distribution and quantitative changes in amounts of aquaporin 1, 5 and 9 in the pig uterus during the estrous cycle and early pregnancy. Reprod Biol Endocrinol *8*, 109.

Skowronski, M.T., Kwon, T.H., and Nielsen, S. (2009). Immunolocalization of aquaporin 1, 5, and 9 in the female pig reproductive system. J Histochem Cytochem *57*, 61-67.

Wang X, Johnson, G.A., Burghardt, R.C., Wu G., Bazer, F.W., (2015a) Functional roles of arginine during the peri-implantation period of pregnancy. III Arginine stimulates proliferation and interferon tau production by ovine trophectoderm cells via nitric oxide and polyamines-TSC2-MTOR signaling. Biol Reprod *92*, 75.

Wang X, Johnson, G.A., Burghardt, R.C., Wu G., Bazer, F.W., (2015b) Uterine histotroph and cocneptus development. I. cooperative effects of arginine and secreted phosphoprotein 1 on proliferation of ovine triphectoderm cells via acitivation of PDK1-Akt/PKB-TSC20MTORC1 signaling Cascade. Biol Reprod *92,*51.

Wang, Y., and Tajkhorshid, E. (2010). Nitric oxide conduction by the brain aquaporin AQP4. Proteins *78*, 661-670.

Xue, L.L., Chen, H.H., and Jiang, J.G. (2017). Implications of glycerol metabolism for lipid production. Prog Lipid Res *68*, 12-25.

Yool, A.J., and Weinstein, A.M. (2002). New roles for old holes: ion channel function in aquaporin-1. News Physiol Sci *17*, 68-72.

Yun, X., Jiang, H., Lai, N., Wang, J., and Shimoda, L.A. (2017). Aquaporin 1-mediated changes in pulmonary arterial smooth muscle cell migration and proliferation involve beta-catenin. Am J Physiol Lung Cell Mol Physiol *313*, L889-L898.

Zhang, Y., Chen, Q., Zhang, H., Wang, Q., Li, R., Jin, Y., Wang, H., Ma, T., Qiao, J., and Duan, E. (2015). Aquaporin-dependent excessive intrauterine fluid accumulation is a major contributor in hyper-estrogen induced aberrant embryo implantation. Cell Res *25*, 139-142.

Zhu, C., Jiang, Z., Bazer, F.W., Johnson, G.A., Burghardt, R.C., and Wu, G. (2015). Aquaporins in the female reproductive system of mammals. Front Biosci (Landmark Ed) *20*, 838-871.